Fall 2009 | Winter 2010 | Spring 2010 | Summer 2010 | Volume XXXVIII, Number 3

JNMM Journal of Nuclear Materials Management

Non-Profit Organization
U.S. POSTAGE
PAID
Permit No. 2066
Eau Claire, WI

INMM
INSTITUTE OF NUCLEAR MATERIALS MANAGEMENT

Published by the Institute of Nuclear Materials Management

"This new RFID technology for the management of nuclear materials has many applications in nuclear industries, and as the technology is further developed, the need for talent to advance its growth is essential."
Dr. James Shuler, Manager DOE Packaging Certification Program, Office of Packaging and Transportation.
http://rampac.energy.gov/RFID/RFID.htm

Argonne NATIONAL LABORATORY

U.S. DEPARTMENT OF ENERGY

Environmental Management
DOE Packaging Certification Program

To learn more about science and engineering opportunities at Argonne, please visit www.anl.gov.

Argonne is an equal opportunity employer and values diversity in the workforce.

JNMM Journal of Nuclear Materials Management

JNMM (ISSN 0893-6188) is published four times a year by the Institute of Nuclear Materials Management Inc., a not-for-profit membership organization with the purpose of advancing and promoting efficient management of nuclear materials.

SUBSCRIPTION RATES: Annual (United States, Canada, and Mexico) $200; annual (other countries) $270 (shipped via air mail printed matter); single copy regular issues (United States and other countries) $55; single copy of the proceedings of the Annual Meeting (United States and other countries) $175. Mail subscription requests to *JNMM*, 111 Deer Lake Road, Suite 100, Deerfield, IL 60015 U.S.A. Make checks payable to INMM.

DISTRIBUTION and delivery inquiries should be directed to *JNMM*, 111 Deer Lake Road, Suite 100, Deerfield, IL 60015 U.S.A., or contact Jodi Metzgar at +1-847-480-9573; fax, +1-847-480-9282; or E-mail, inmm@inmm.org. Allow eight weeks for a change of address to be implemented.

JNMM Journal of Nuclear Materials Management

Topical Papers

Institute News

Departments

INMM
INSTITUTE OF NUCLEAR MATERIALS MANAGEMENT

Storing Excess Plutonium

By Steve Ortiz
INMM President

The winter edition of the *Journal* focused around safe storage of plutonium-bearing materials. The spring issue does as well. If you read the winter issue you realize that the articles are centered around DOE-STD-3013, which assures that excess plutonium materials within the U.S. Department of Energy (DOE) complex are stored in a safe and environmentally friendly manner. The Obama administration's recently released Nuclear Posture Review could increase the need for safe storage of excess plutonium materials in the United States. Countries with growing nuclear power programs will have similar technical issues to deal with. Even though the winter issue was focused around a U.S. standard for excess plutonium storage, the problem is a worldwide one. The winter and spring issues demonstrate the great work being done by professionals in nuclear materials management.

Nuclear materials management continues to grow as a profession. An article in the August 14, 2008, issue of *U.S. News and World Report* stated the following: 'Nuclear Help Desperately Wanted' could be the sign in front of dozens of engineering colleges across the country. With worldwide interest in nuclear energy and technology skyrocketing, engineers with a nuclear background are feeling very popular these days. It's welcome news for a field that has been long stifled by negative public opinion. The challenge the discipline faces is how to meet this new demand after years of shrinking interest."

We, as a professional society, have begun to feel the growth occurring in the industry the last couple of years. Our 2009 annual meeting broke records for attendance and the number of technical papers and sessions. This year we surpassed the number of abstracts submitted last year. When I became president of the Institute of Nuclear Materials Management in 2008, I stated a goal of having ten student chapters by the end of my tenure. At the time we only had one, the Texas A&M Student Chapter. Today we have eight student chapters and are in the process of developing another. Many universities are resurrecting their nuclear engineering schools. This was also noted in the *U.S. News and World Report* article. "Students appear to be eager to fill the gap. Even without recruiting, some university departments are seeing as much growth as they can handle: "There are more than three times as many nuclear engineering students now as there were just five years ago. …Not only are the existing programs growing near capacity, but departments that shuttered years ago are finding new life."

This continues to be an exciting time for our profession. We have many technical challenges ahead in nuclear material management. The *Journal* and the INMM Annual Meeting will continue to be the primary vehicles for us to share technological advances and best practices with our membership. I hope that you continue to contribute so that the Institute of Nuclear Materials Management can continue to serve our industry.

And the March Goes On

By Dennis Mangan
INMM *Technical Editor*

This issue of the *Journal* focuses on the remaining articles on the efforts put forth to address the safe storage of plutonium, and complements our winter 2010 issue. My technical editor's note in that issue provides the background of having all these articles on the safe storage of plutonium published in these two issues of our *Journal*. The team of folks who have participated in these various efforts have accomplished a great deal regarding the safe storage of plutonium, and the picture they paint is definitely pretty. If one asked if any work was done addressing the safe storage of plutonium, these two issues provide an impressive answer. As was the case with the winter issue, Kerry Dunn, an advisory engineer at Savannah River National Laboratory (SRNL), served as an excellent point of contact and again accomplished her mission quite effectively and efficiently, and we express our appreciation to her and all the authors for a job well done.

Also in this issue is an article by Caroline Jorant of AREVA, Paris, France, titled, *International Safeguards in Nuclear Weapons States and a Look at the Future.* This article is timely from the viewpoint of the upcoming NPT (Nuclear Nonproliferation Treaty) Review Conference, coupled with the potential nuclear energy growth through the nuclear initiatives and the upcoming (at the time I'm writing this) Nuclear Security Summit meeting in Washington, DC USA.

It will be interesting over the next several years to observe changes in the international (and national) attitude about nuclear energy. As many of us have opined, nuclear energy is not the only source of energy to address the carbon emission problems of much of our energy sources, but it should definitely be a significant part of the solution. And recently I've observed a more favorable potential acceptance of nuclear energy, which is encouraging.

I hope to see you in Baltimore in July for our Annual Meeting. I participated in the technical program meeting in early March. The number of abstracts submitted exceeded any previous meeting, approaching 600. With this large a response and with the venue being Baltimore, this year's meeting could be the largest ever.

JNMM *Technical Editor Dennis L. Mangan can be reached at dennismangan@comcast.net*

Relative Humidity and the Susceptibility of Austenitic Stainless Steel to Stress-corrosion Cracking in an Impure Plutonium Oxide Environment

Philip E. Zapp, Jonathan M. Duffey, Poh Sang Lam, and Kerry A. Dunn
Savannah River National Laboratory, Aiken, South Carolina USA

D. Kirk Veirs, Laura A. Worl, and John M. Berg
Los Alamos National Laboratory, Los Alamos, New Mexico USA

Abstract

Laboratory tests to investigate the corrosivity of moist plutonium oxide/chloride salt mixtures on 304L and 316L stainless steel coupons showed that corrosion occurred in selected samples. The tests exposed flat coupons for pitting evaluation and "teardrop" stressed coupons for stress-corrosion cracking (SCC) evaluation at room temperature to various mixtures of PuO_2 and chloride-bearing salts for periods up to 500 days. The exposures were conducted in sealed containers in which the oxide-salt mixtures were loaded with about 0.6 wt percent water from a humidified helium atmosphere. Observations of corrosion ranged from superficial staining to pitting and SCC. The extent of corrosion depended on the total salt concentration, the composition of the salt and the moisture present in the test environment. The most significant corrosion was found in coupons that were exposed to 98 wt percent PuO_2, 2 wt percent chloride salt mixtures that contained calcium chloride and 0.6 wt percent water. SCC was observed in two 304L stainless steel teardrop coupons exposed in solid contact to a mixture of 98 wt percent PuO_2, 0.9 wt percent NaCl, 0.9 wt percent KCl, and 0.2 wt percent $CaCl_2$. The cracking was associated with the heat-affected zone of an autogenous weld that ran across the center of the coupon. Cracking was not observed in coupons exposed to the headspace gas above the solid mixture, or in coupons exposed to other mixtures with either no $CaCl_2$ or 0.92 wt percent $CaCl_2$. SCC was present where the 0.6 wt percent water content exceeded the value needed to fully hydrate the available $CaCl_2$, but was absent where the water content was insufficient.

These results reveal the significance of the relative humidity in the austenitic stainless steels' environment to their susceptibility to corrosion. The relative humidity in the test environment was controlled by the water loading and the concentration of the hydrating salts such as $CaCl_2$. For each salt or salt mixture there is a threshold relative humidity below which the necessary liquid electrolyte cannot exist, and therefore below which the SCC risk is very low. This threshold is a thermodynamic quantity known as the deliquescence relative humidity that is dependent on the identity of the salt but is independent of the quantity of salt. Below the deliquescence RH there should be low corrosion risk, and above it the corrosion risk increases rapidly as a liquid phase, which is initially saturated with salt, grows and becomes more widespread in the container.

Introduction

The stress-corrosion cracking (SCC) of austenitic stainless steels has been extensively studied, especially in acidic aqueous chloride solutions, and is described in a large body of literature.[1] Although SCC is most frequently investigated in a wide variety of bulk liquid phase environments, there has been interest in exploring the phenomenon where the corrosive electrolyte derives from humid atmospheres. Stress-corrosion cracking in such instances is of particular interest in the safe containment and storage of impure plutonium oxides in austenitic stainless steel vessels, where the impurities include hydrophilic chloride salts.

As discussed in the previous issue of this journal,[2] the U.S. Department of Energy (DOE) Standard DOE-STD-3013-2004 Stabilization, Packaging and Storage of Plutonium-Bearing Materials (the '3013' standard) specifies the processing steps and storage vessel attributes that are required for the storage of plutonium metal and oxides. These include the heat treatment of the oxide mixtures to reduce water content and the use of at least two nested, welded containers fabricated from corrosion resistant alloy(s). In practice the inner of the two containers has been fabricated from either 304L or 316L stainless steel, and the outer has been fabricated of 316L stainless steel. The Pu-oxide heat-treatment requires heating to 950°C for at least two hours in an oxidizing atmosphere. The heat-treated material shall contain less than 0.5 percent by weight water, and that limit must be maintained through the packaging and sealing of the material within the two containers. Both inner and outer containers are sealed by welding, and the 3013 standard specifies leak-tightness limits.

A portion of the plutonium oxide inventory may contain chloride salts in significant concentration, so that there is the

potential of an aqueous electrolyte containing chloride ions in contact with the stainless steel containers, if there is sufficient moisture in the sealed 3013 container to exceed the deliquescence relative humidity of the salts in the container. For austenitic stainless steels, such an electrolyte can induce localized modes of corrosion such as pitting and stress-corrosion cracking, as well as crevice corrosion. Ninety days of exposure to PuO_2/Cl^- salt mixtures can produce pitting in small-scale 304L stainless steel vessels.[3] Pitting depths up to 100 µm were observed on the metal surface in contact with the solid oxide and up to 25 µm on metal exposed to the vapor space above the solid. Testing of flat coupons showed that 304L stainless steel exposed at 55°C to salt mixtures with approximately 0.5 wt percent moisture suffers pitting corrosion to a maximum depth of 30 µm in an area in contact with the solid mixture.[4] The flat coupons were exposed for 150 days. Additionally, a 316L coupon exposed to similar conditions had a small area (2 by 4 mm) of pitting of about 10 µm in depth. Coupons of both 304L and 316L stainless steel exposed at room temperature were either not corroded or had barely detectable attack. Specimens under tensile stress were not investigated in those early tests.

This paper describes the results of coupon immersion tests that investigated stress-corrosion cracking as well as pitting in moist plutonium oxide/chloride salt mixtures. The objective was to determine the effects of chloride salt composition and radiation on the corrosion of 304L and 316L austenitic stainless steel and to refine the understanding of the relative importance of the concentrations of NaCl, KCl, $MgCl_2$, and $CaCl_2$, water content, and radiation dose to the corrosion-cracking process.

The small-scale test program included the following five test series (Table 1):

Series 1 included one test container (series 1a) with a PuO_2 sample with no chloride salts as an experimental control. The two other containers in this series (series 1b) contain a composition of PuO_2 with 28 wt percent chloride salts composed largely of non-hydrating NaCl and KCl with some $CaCl_2$ and $MgCl_2$.

Series 2a tests contained PuO_2 with 5 wt percent NaCl and 5 wt percent KCl.

Series 3 tests evaluated the impact of the hydrating salt $MgCl_2$ on the corrosion of stainless steel using a laboratory-prepared surrogate of PuO_2 and salts intended to be representative of salts produced by the electrorefining process (termed 'ER' salt). Three compositions of the PuO_2/ER salt mixture that contained equal weight NaCl/KCl and $MgCl_2$ equal to one tenth of the total salt content were tested:

Series 3a) 90 wt percent PuO_2 + 10 wt percent ER salt
Series 3b) 95 wt percent PuO_2 + 5 wt percent ER salt
Series 3c) 98 wt percent PuO_2 + 2 wt percent ER salt

Series 4 tests assessed the role of $CaCl_2$, another hydrating salt, versus that of $MgCl_2$ in the overall salt composition. The total salt concentration was 2 wt percent in the series 4 tests, with two variants containing different concentrations of $CaCl_2$. Series 4a contained 0.2 wt percent $CaCl_2$, and series 4b 0.92 wt percent $CaCl_2$.

Series 5a tests evaluated the impact of increased α-dose on corrosion during exposure to the series 3b oxide/salt composition. Series 5a used a 5 wt percent $MgCl_2$-rich ER salt with the mixture's specific radioactivity increased by the addition of ^{238}Pu and ^{241}Am to the standard ^{239}Pu isotope used in the preparation of the oxide. The addition of ^{238}Pu and ^{241}Am increased the thermal power of this isotopic mixture from 2.26 W/kg Pu for the weapons grade mixture used in the series 1 through 4 tests to 5.09 W/kg Pu in the series 5a tests.

Table 1. Test series solid mixture compositions (weight percent)

Series	Description	PuO_2	NaCl	KCl	$MgCl_2$	$CaCl_2$
1a	Control, 0 percent salt	100	–	–	–	–
1b	master blend	72	11.7	14.8	1.1	0.4
2a	10 percent NaCl/KCl	90	5.0	5.0	–	–
3a	10 percent ER Salt	90	4.5	4.5	1.0	–
3b	5 percent ER Salt	95	2.25	2.25	0.50	–
3c	2 percent ER Salt	98	0.90	0.90	0.20	–
4a	2 percent Ca Salt	98	0.90	0.90	–	0.20
4b	2 percent 11589 Salt	98	0.54	0.54	–	0.92
5a	5 percent ER Salt	95	2.25	2.25	0.5	–

Role of Relative Humidity

The risk of SCC in stressed stainless steel is very low in the absence of direct contact of the metal with a liquid phase that can serve as an electrolyte for the corrosion process. Therefore, a major goal of this test plan is to better define whether a liquid phase could be present in any 3013 containers given current knowledge about packaging conditions, container contents, and storage conditions.

Internal relative humidity (RH) is a useful indicator of the potential existence of an aqueous liquid phase anywhere in a container. For each salt or salt mixture there is a threshold RH below which a liquid cannot exist and, therefore, below which the SCC risk is very low. This threshold is a thermodynamic quantity known as the deliquescence RH and is dependent on the identity of the salt but is independent of the quantity of salt. Below the deliquescence RH there should be low corrosion risk, while above

the deliquescence RH the corrosion risk increases rapidly as the liquid phase forms and becomes more widespread in the container. At extremely high relative humidity the risk may fall due to the formation of less corrosive dilute salt solutions. However, the RH at which the risk falls is dependent on the quantity of salt in the container. (Note that the concept of a maximum safe chloride concentration is problematic due to possible concentrating mechanisms such as thermal cycling.)

Figure 1. Conceptual plot of corrosion risk as a function of relative humidity within a container. Curves are shown for alkali chlorides (NaCl, KCl) [Dotted line] and for a representative collection of alkaline earth chlorides (labeled AECs) [Solid lines]. Risk is shown as increasing rapidly beginning at the threshold for liquid formation (deliquescence). The range of relative humidity to which material was exposed during packaging is shown for comparison.

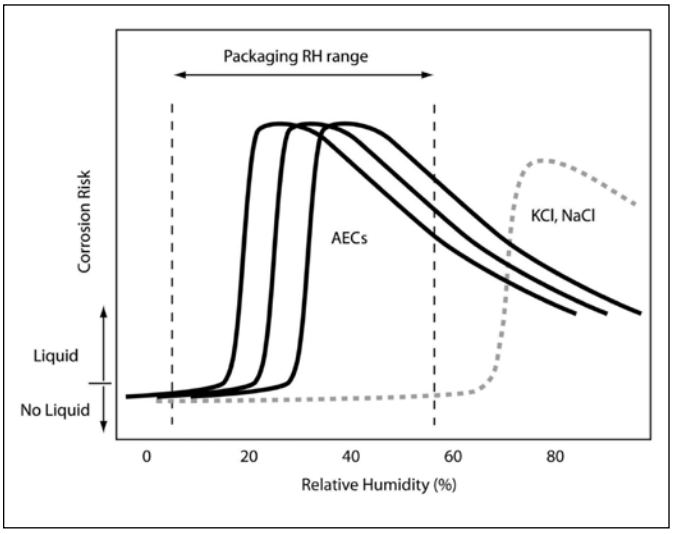

Figure 1 shows a conceptual plot of how SCC risk might vary with the container internal relative humidity for two general categories of impurity phases. The first category (dotted line in Figure 1) contains only alkali chloride salts (NaCl, KCl) and is expected to represent little risk within the range of packaging relative humidities because an aqueous salt solution will not form. The second category (solid lines in Figure 1) includes alkaline earth chloride (AEC) materials with pure alkaline earth chlorides ($MgCl_2$, $CaCl_2$) and mixed salts containing alkaline earths ($KMgCl_3$, $KCaCl_3$, etc.), which are known to form aqueous chloride solutions within the range of packaging relative humidities. These materials represent the greatest risk for SCC within the range of packaging relative humidities. Figure 1 and subsequent plots are based on published thermodynamic studies of chloride salts and water, and on corrosion studies conducted in Japan which observed stainless steel SCC in contact with alkaline earth chloride salts at room temperature.[5]

The range of relative humidity experienced during packaging spans the known deliquescence relative humidity values of all the calcium and magnesium chloride salts likely to be present in packaged material. Therefore SCC must be considered as possible within existing containers based on this simple thermodynamic picture. Several mitigating factors may effect actual 3013 packages, including the potential decline in the internal relative humidity, due to radiolysis of water after container closure, to values substantially below the packaging relative humidity and perhaps below the deliquescence relative humidity of any impurity salts. Establishing reliable methods to estimate this reduction in relative humidity, as well as better defining the range of plausible deliquescence thresholds of real stored material is the most promising approach to reducing the overall concern and, through knowledge of the package contents, limiting the concern to the fewest possible number of specific containers.

Relative humidity within a container is controlled by an affinity and capacity for water that is characteristic of each of the solid constituents in the package. Figure 2 shows simplified examples where $CaCl_2$ is the only solid constituent that interacts with water. As moisture is added to the system the dry salt is converted into solid hydrates, with stepwise increases in RH evident as each formation step is completed. Once the salt is fully hydrated, further moisture addition begins to form a saturated salt solution at a constant RH characteristic of the deliquescence RH of the salt. Eventually the salt will be fully dissolved and further moisture addition will be characterized by a smooth increase in RH as the solution becomes more dilute.

Comparison of the two curves in Figure 2 illustrates the difficulty of attempting to use total moisture content to estimate SCC risk. At a moisture content of 0.34 percent, indicated by the vertical dashed line in Figure 2, the 0.2 percent $CaCl_2$ material would contain an aqueous salt solution phase while all the H_2O will be tied up in solid hydrates of the 0.4 percent $CaCl_2$ material,

Figure 2. Relative humidity vs. moisture content for two mixtures of $CaCl_2$ with an inert matrix

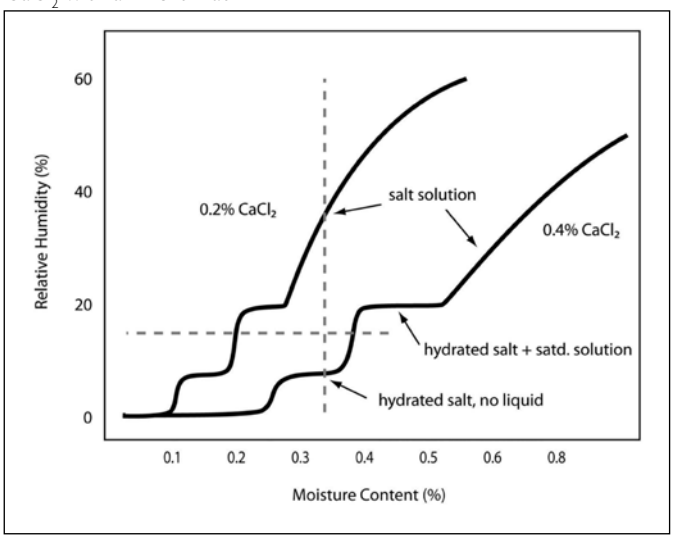

so the corrosion risk would be very different in these two cases. An analogous plot for a real packaged batch of material would be more complex due to multiple impurity phases but the conclusion would be the same. To relate the existence or absence of a liquid phase to overall moisture content, one must also know the quantities of those impurity phases that interact most strongly with H_2O, not just their identities. Since there is little prospect of adequately quantifying important impurity phases in individual containers from existing data, moisture content alone is not a promising predictor of the potential for liquid formation, and therefore the SCC risk will also be difficult to predict.

Bounding estimates of internal RH, in contrast, would be good predictors of the potential for existence of an aqueous liquid phase even without knowledge of the quantities of the impurity phases. For example, at or below the RH indicated by the horizontal dashed line in Figure 2 no solution could exist regardless of how much or how little $CaCl_2$ is present in these hypothetical material mixtures. The added complexity of actual packaged material will not alter the basic premise as long as the identities of the phases can be reasonably constrained by existing information. As long as the upper bound for potential internal RH does not exceed the deliquescence RH of any plausible impurity phases, an aqueous liquid phase will not exist in the container. This approach avoids what would be a highly problematic effort to quantify minor impurity phases in individual containers.

Figure 3 shows a conceptual model of SCC risk versus moisture content for the same two hypothetical material compositions shown in Figure 2. The main change in risk occurs due to liquid formation and is seen to occur at dramatically different moisture loadings for the two mixtures. An analogous plot versus internal relative humidity, as in Figure 1, would show the rise in risk occurring at the same RH for both mixtures.

Figure 3. Conceptual plot of relative corrosion risk as a function of total moisture content for two batches with different loading of $CaCl_2$ and no other active salt. Note that corrosion risk is strongly dependent on the amount of active salt and can be significant well below 0.5 wt % moisture. The dashed vertical lines indicate the approximate moisture loadings above which solution exists in the two cases.

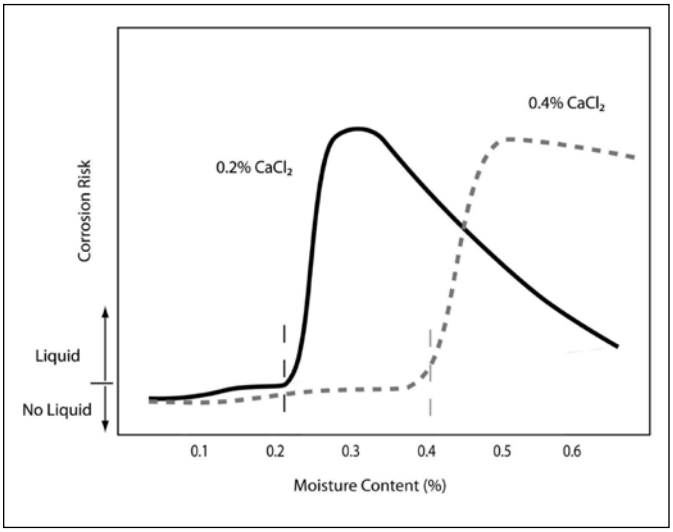

Experimental Procedure

The corrosion tests used 304L and 316L stainless steel coupons purchased from Metal Samples Inc., Munford, Alabama USA. Pitting corrosion was evaluated with 1-inch by 2-inch by 0.06-inch flat coupons with a longitudinally centered autogenous weld (ground flat to the coupon surface with a 600-grit finish). The weld penetration was approximately 0.03 inches or half way through the plate sample. SCC was evaluated with a teardrop specimen, a type of compact U-bend specimen with its ends

Figure 4. Flat and teardrop coupons in glass inserts, open test container, and sealed container

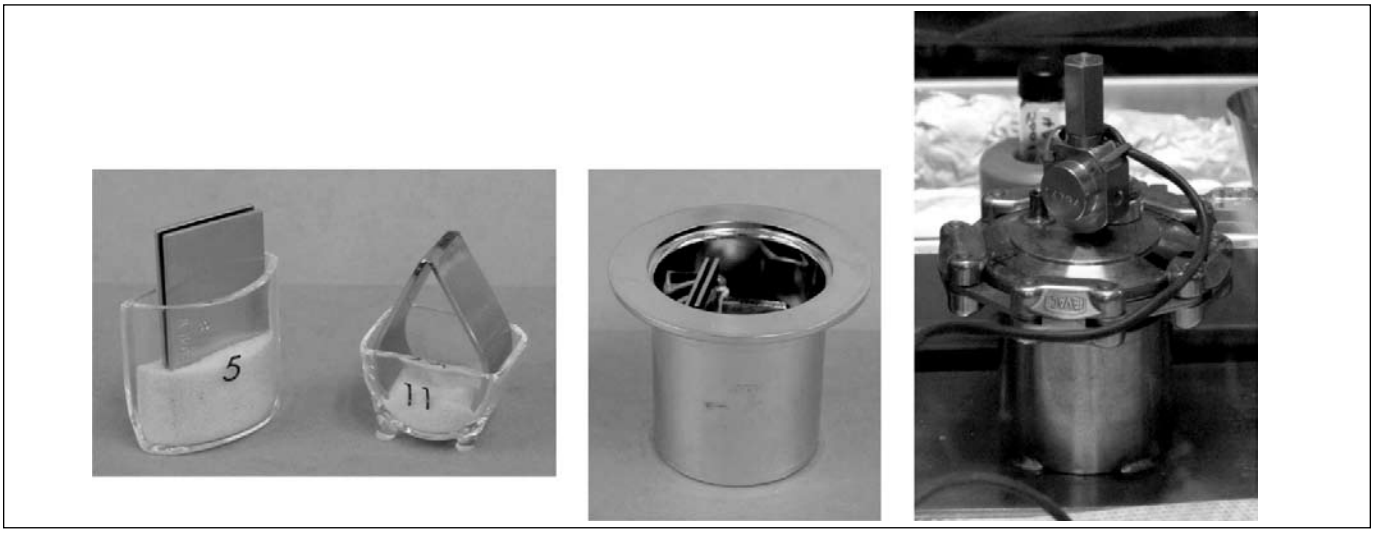

welded together to hold the stressed bend. The metal was plastically deformed during bending around a mandrel. An analysis of the stresses within the specimen is discussed below. The *teardrop* specimens had a transverse autogenous weld at the center of curvature.

The test container for the small-scale tests was a 5-cm (2-inch) diameter, 6.5-cm (2.5-inch) tall stainless steel can sealed with a metal gasket. The container was equipped with a pressure transducer for continuous pressure monitoring during an exposure and a valve for acquiring gas samples periodically (Figure 4). Glass inserts were used to hold the small (several cubic-centimeter) volumes of oxide/salt mixture (allowed under limits on the fissile material mass) to maximize the surface area of contact with the test coupons.

Figure 4 shows the coupons in their glass boats or inserts and an open test container with coupons. One 304L flat coupon and one 316L flat coupon were placed side by side in one glass insert. Enough oxide/salt mixture was added between and around the coupons to cover the lower half of each coupon. Several grams of oxide/salt mixture were added to a second glass insert, and one teardrop coupon was placed in this second glass insert on top of the oxide/salt mixture. Several more grams of oxide/salt mixture were added inside the closed loop of the teardrop coupon. The two glass inserts were placed side by side in the vessel. A second teardrop coupon was then placed on top of the first such that it rested in the headspace position without contacting the oxide/salt mixtures.

PuO_2 was prepared by anion exchange purification, oxalate precipitation, and calcination in a dry air purge for two hours at 950°C. Various salt mixtures having the desired ratios of NaCl, KCl, $MgCl_2$, and $CaCl_2$ were prepared by combining the required amounts of each salt in a glovebox with a dry argon atmosphere. The dry salt mixtures were then removed from the glovebox in a desiccator and heated in a static air atmosphere to between 820°C and 850°C for two hours to melt the salts together. While still warm, the fused salts were placed back in the desiccator and transferred back to the dry glovebox where they were ground and pre-weighed into screw-cap glass vials. The pre-weighed salt mixtures were transferred to a plutonium glovebox where they were combined with pre-weighed amounts of PuO_2 in screw-cap jars, mixed briefly while the jars were capped, then transferred to a crucible and placed directly in a warm furnace. The PuO_2/salt mixtures were heated in a static air atmosphere at 850°C for two hours, cooled to approximately 300°C, and transferred to screw-cap glass jars.

A helium-purged glove bag deployed inside a plutonium glovebox was used to provide a helium atmosphere for loading PuO_2/salt mixtures and corrosion test coupons into the test containers. The glove bag was first purged with helium until the relative humidity (RH) was below 10 percent. PuO_2/salt mixtures were then weighed into glass inserts containing the corrosion test coupons as previously described. The two glass inserts in each sample set were placed in small stainless steel pans for ease of handling. The RH in the glove bag was gradually increased by bubbling helium through a container of distilled water and/or by moistening absorbent wipes with water and spreading them out in a large stainless steel pan to speed evaporation of water. The small stainless steel pans holding the sample sets were weighed periodically in the humidified helium atmosphere until the weight gain of each sample set corresponded to uptake of about 0.6 wt percent water. This moisture content was selected because it was slightly above the allowable moisture in the 3013 containers. A *blank* consisting of pan, glass inserts, and test coupons with no PuO_2/salt mixture was weighed along with each set of exposed samples to estimate the amount of water adsorbed by the container and coupons surfaces. The maximum RH required for samples to reach the target moisture loading in a nominal eight-hour shift was between 58 percent and 94 percent. The containers, with their moisture loadings, were closed and transferred to air atmosphere gloveboxes for ambient temperature staging.

Results

Corrosion observations and an analysis of the water content of the test containers that have completed their exposures were made after the containers were opened. These containers had been at ambient glovebox temperature for between 150 and 506 days. Prior to opening each container, the headspace gas in the container was diluted with helium and sampled for analysis. The post-exposure water content of samples of the PuO_2/salt mixtures was measured by thermogravimetric analysis coupled with mass spectrometric detection (TGA-MS), typically within one to three days after opening the container. During this interval the samples were in screw-lid sealed glass vials.

Upon completion of their exposures, the stainless steel coupons were examined visually and photographed. The coupons were lightly brushed to remove oxide/salt mixture, and cleaned of corrosion product with 0.1 M nitric acid. Observations of corrosion are summarized in Table 2 below. Corrosion ranged from slight, superficial staining in the series 1 tests to pitting with measurable depth and SCC in the 304L coupons in the series 4a containers. There was no significant qualitative difference in the pitting attack on the 304L and 316L stainless steels, and the depth of attack measured on all the flat coupons was comparable. The only extensive pitting was in coupons exposed to PuO_2/Cl^- salt mixtures with 2 wt percent total salt that included $CaCl_2$ (the 4a and 4b series tests). Although not quantified, pitting was observed on the teardrop coupons in containers whose flat coupons were pitted.

Stress-corrosion Cracking Observations

Teardrop coupons were used to assess the susceptibility of 304L stainless steel to SCC induced by the moist oxide/salt mixture. Two teardrop coupons, one from container 4a-3 and one from container 4a-2, were found to have undergone SCC after 166 and

Table 2. Summary of corrosion observations

Test Container	Salt Content	Days Sealed	Corrosion Observations of Tear Drop Coupons
1a-1	None	325	no cracking (304L)
1b-1	28 percent Salt	489	no cracking (304L)
1b-2		150	no cracking (304L)
3c-1	2 percent ER Salt	274	no cracking (304L)
4a-1	2 percent Salt with 0.2 percent $CaCl_2$	506	no cracking (316L), pitting
4a-2		335	cracking (304L) in solid contact region, pitting
4a-3		166	cracking (304L) in solid contact region, pitting
4b-1	2 percent Salt with 0.9 percent $CaCl_2$	193	no cracking (304L), pitting
4b-2		340	no cracking (304L), pitting
4b-3		496	no cracking (304L), pitting
5a-1	5 percent ER Salt with increased α-dose	352	no cracking (304L), pitting
5a-2		168	no cracking (304L), pitting
5a-3		470	no cracking (304L), pitting

335 days of exposure, respectively, in the solid contact position. Cracking was not observed in coupons from any other container opened to date, nor was cracking seen in any headspace-position coupon, even in the coupons exposed in containers 4a-3 and 4a-2. Cracking was not observed in the 316L teardrop coupons exposed to mixture 4a-1.

In general, all teardrop coupons had staining and pitting similar in extent to that seen in their companion flat coupons. Some teardrop coupons had general staining or corrosion in the heat-affected zones of their closure weld. Figures 5 and 6 show examples of the pitting and staining in teardrop coupons exposed in the solid contact positions in containers 4a-3 and 4b-1. These images were made before acid cleaning of the coupons. Pitting is visible on the outer and inner curved surfaces of the coupons as well as at edges.

SCC was initially revealed in the container 4a-3 solid contact teardrop coupon 304L – 23, through dye penetrant testing.[6] Optical microscopy, scanning electron microscopy, and optical metallography were used to examine the path and nature of the

Figure 5. Container 4a-3 teardrop coupon 304L – 23 showing pitting in the metal in contact with the oxide/salt mixture. Corrosion is also evident in the heat-affected zone of the closure weld at the coupon tip, which was not in contact with the solid mixture.

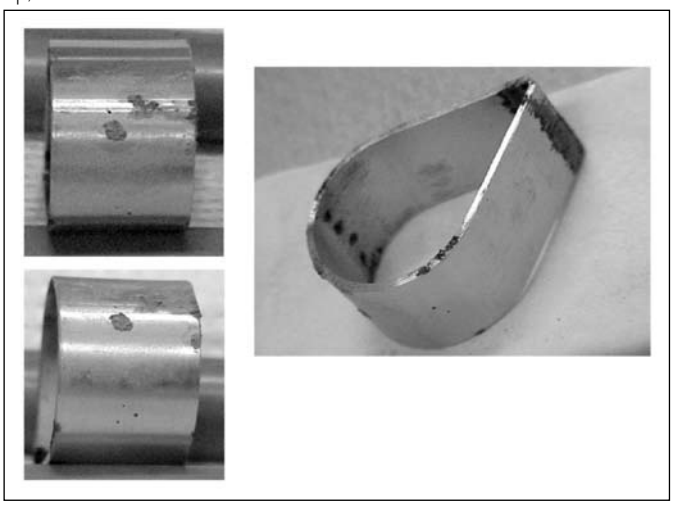

Figure 6. Container 4b-1 teardrop coupon 304L – 02 showing pitting inside and outside in metal in solid contact; no evidence of cracking; staining near closure weld

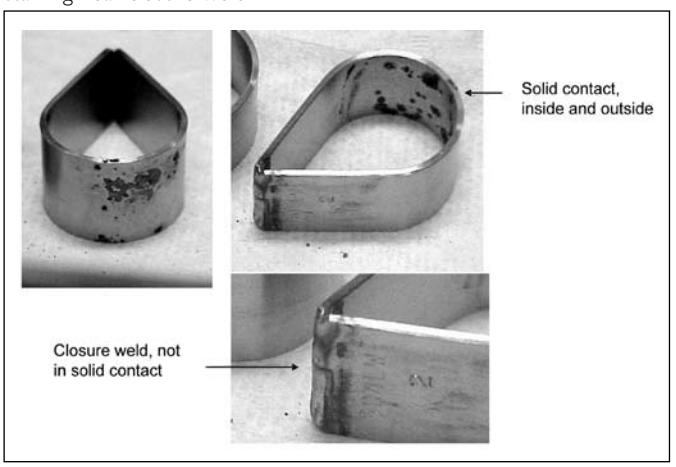

cracking.[7] The cracking extended across more than half the width of the coupon and was associated with the transverse autogenous weld. Figure 7 is an optical micrograph that shows the cracking starting at the edge of the coupon in a localized area of general corrosion and propagating along the interface between the weld and the parent metal, that is, in the weld heat-affected zone. Figure 8 shows the entire crack path on the coupon surface in a composite scanning electron micrograph. The crack was highly branched as it crossed through weld metal and continued its path along the opposite weld/parent metal interface. Optical metallography of one cross-section of the coupon reveals the propagation of the crack along the interface (Figure 9) and, in a second cross-section, propagation through the weld metal into the parent metal (Figures 10 and 11). The enlargement in Figure 10 shows what appears to be intergranular cracking around grains in

Figure 7. Photomicrograph of teardrop coupon 304L–23, showing branched cracking near and within the autogenous weld; possible crack initiation site in area of localized corrosion at right edge of coupon. Approximately 10X magnification.

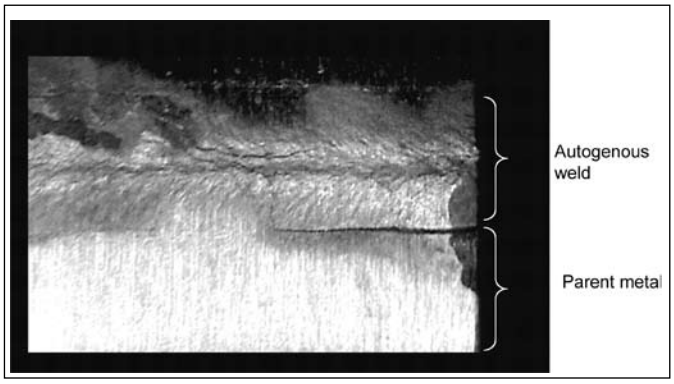

Figure 8. Composite scanning electron micrographs of coupon 304L-23 showing full extent of cracking on outside (convex) surface

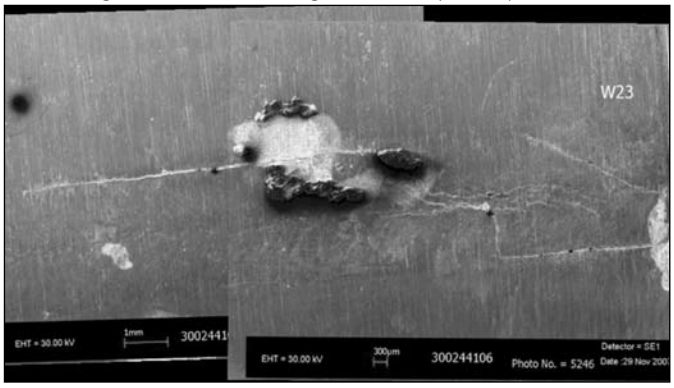

Figure 9. Scanning electron micrograph of edge of coupon 304L-23 showing cracking along weld/parent metal interface

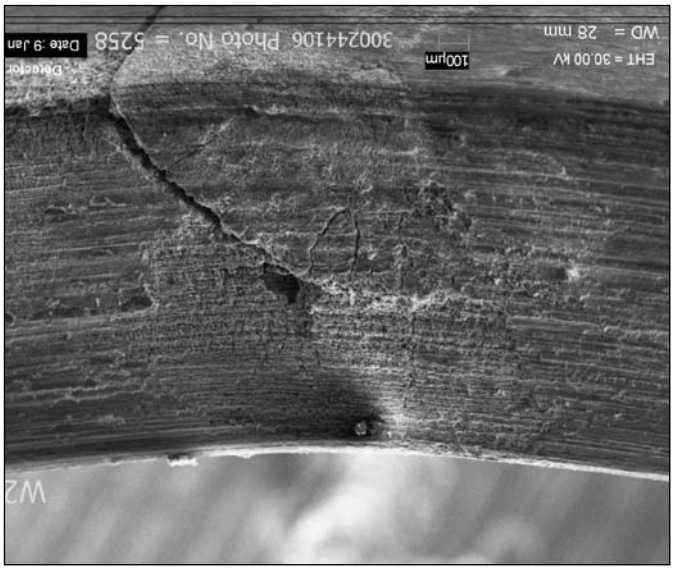

Figure 10. Optical micrographs of a reversed cross-section through teardrop coupon 304L-23 showing cracking along the weld/parent metal interface

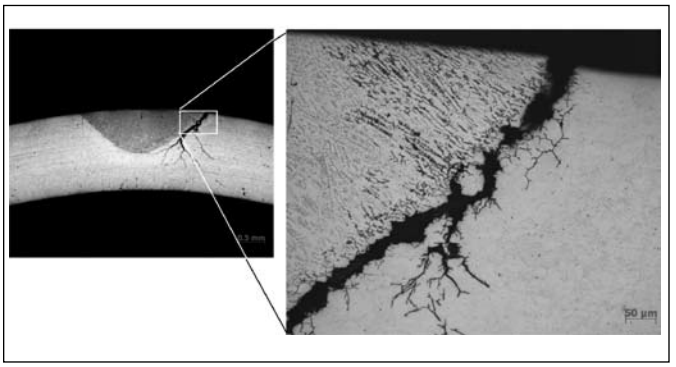

Figure 11. Optical micrograph of a second cross-section of coupon 304L–23, showing propagation of multiple cracks through the weld metal into the parent metal

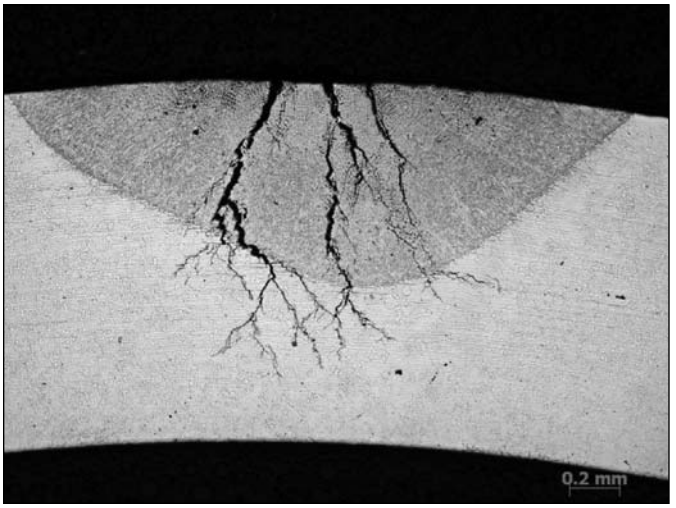

Figure 12. Optical micrograph showing transgranular nature of the cracking

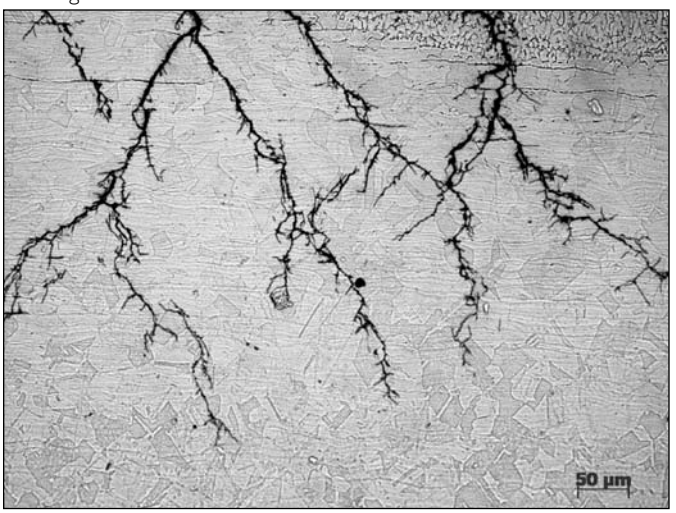

the weld heat-affected zone. This possible intergranular cracking can result from the sensitization of the 304L stainless steel by the welding heat input. Sensitization is the phenomenon of the depletion of the protective chromium content of the alloy matrix by concentrating the chromium in chromium carbides that precipitate at grain boundaries. The highest magnification image (Figure 12) shows the extensive cracking paths across parent metal grains. The generally transgranular nature of the cracking is characteristic of chloride-induced SCC in non-sensitized austenitic stainless steel.

Similar SCC occurred in a second series 4a test coupon, 304L–20 from container 4a-2, which was exposed for 335 days or about twice the exposure of container 4a-3. Figure 13 shows the prominent stress corrosion cracks at the weld metal/parent metal interfaces of the coupon. A third series 4a container, container 4a-1, held 316L stainless teardrop coupons in both the solid contact and headspace positions for 506 days. Although teardrop coupon 316L–40 experienced extensive pitting and localized general corrosion, visual inspection revealed no cracking. Type 316L stainless steel contains molybdenum to impart resistance to chloride attack. This resistance takes the form of a greater induction time for SCC rather than immunity to SCC.

Figure 13. Stress corrosion cracking along the autogenous weld in coupon 304L-20 from container 4a-2

As stated above, SCC has not been observed in 304L teardrop coupons that were exposed in any containers other than 4a-2 and 4a-3. Notably, cracking was absent from coupons exposed in the 4b test containers, whose PuO_2/Cl^- salt mixtures contained $CaCl_2$ at a concentration of 0.92 wt percent compared with 0.2 wt percent $CaCl_2$ in the 4a containers. Clearly a corrosive electrolyte did form in container 4b-1, and considerable corrosion is evident in the stressed region of its teardrop coupon. The reason for the absence of cracking in this instance is not known, but further testing at elevated temperature (of the order of 70°C) must be conducted to draw conclusions about the corrosivity of the 0.92 wt percent $CaCl_2$ mixture. The results at room temperature show that oxide/salt mixtures containing $MgCl_2$ rather than $CaCl_2$ (the series 3 tests and the series 5 tests, with their higher radiation level) did not initiate SCC.

Stress Analysis of Teardrop Coupon

A finite-element analysis was used to estimate the initial stress in the 304L tear drop specimens in which cracking occurred.[8] The ABAQUS program was used to perform the finite element analysis.[9] Only one-half of the 304L strip and one-half of the mandrel are needed in the finite element calculation because of geometric symmetry. The stress analysis was based on the fabrication of the teardrop coupon by the bending of a starting 10-cm-long strip around a 2.5-cm-diameter mandrel. The 0.2 percent offset yield stress for the 304L stainless steel is 351 MPa (50.93 ksi), the ultimate tensile strength (UTS) is 662 MPa (96.05 ksi), and the elongation (at fracture) with a 50.8 mm (2 in.) gage length is 45.85 percent. The full stress-strain curve necessary for the finite element analysis was not provided. A preliminary assessment of the stress state of the teardrop specimen was made without material-specific testing. A stress-strain curve with similar values of yield stress (455 MPa or 66 ksi) and ultimate tensile strength (689 MPa or 100 ksi) was used for the present analysis. The tensile properties of the small volume of autogenous weld metal were assumed to be the same as those of the base metal (304L).

It was determined that the maximum stress level is about 731 MPa (106 ksi). The highest bending stress in the teardrop specimen is not located at the apex as expected. The finite element analysis showed that the apex stress is relieved and continuously redistributed as the 304L strip is being bent around the mandrel, and the location of the highest stress is shifted from the apex to

Figure 14. The location of maximum stress in the teardrop specimen. The stress distribution is symmetrical with respect to the plane containing the apex (center of curvature) and the welded ends of the coupon.

the specimen shoulders. This is caused by the increasing contact surface between the 304L strip and the mandrel in the course of forming the specimen, which effectively changes the bending moment of the system. The analysis showed that for this specimen geometry, the stress at the apex location of the autogenous weld is about 483 MPa (70 ksi, see the apex stress in Figure 14).

That the cracking seen in the 4a teardrop coupons was associated with the autogenous welds and not with predicted highest-stress region may well be associated with microstructural and compositional effects brought about by the weld process, such as the phenomenon of sensitization mentioned above. As reported in the previous issue of this journal, there is sufficient tensile stress throughout the curved region of the teardrop coupon to induce SCC.[10]

Analysis of Water Content

Table 3 shows the analysis of the water content of materials removed from the thirteen opened test containers. This net water loading assumes water content prior to exposure to humid atmosphere was negligible. As a cross-check of the initial water content of each sample that was determined by weight gain, the post-exposure water content was measured by TGA-MS analysis and then corrected for water loss via radiolytic or chemical hydrogen production on the basis of headspace gas analysis results. This correction is based on the assumptions that (1) water is the only significant source of hydrogen and (2) one mole of water yields one mole of hydrogen. This correction does not account for water that may have been consumed by chemical reactions to produce, for example, hydroxyl groups on the surface of PuO_2 or oxychloride compounds. The post-exposure moisture content by TGA-MS and the amount of water consumed by hydrogen production were summed to yield a calculated initial water content for each test container, which is the value listed in Table 3. The final column in Table 3 lists the theoretical water content needed to fully hydrate the $MgCl_2$ or $CaCl_2$ present in each container. These values are included for comparison to the measured water contents as an indication of the extent to which (1) the alkaline earth salts were hydrated and (2) a corrosive aqueous electrolyte was formed. The data suggest that the initial water content of the 4a series tests was sufficient to create such an electrolyte, while the higher calcium chloride salt content of the 4b tests bound the available water.

Calculated initial water contents based on post-exposure water analyses were generally equal to or higher than values for initial water added based on weight gain. This is probably because most of the samples contained some amount of moisture prior to exposure to humidified helium. The calculated initial water contents are considered to be more accurate because of the difficulties associated with handling and weighing the samples in the helium glove bag, the high RH required to load up to 0.5 wt percent water, and the possibility that some samples had measurable water content prior to moisture uptake.

Table 3. Water concentration of PuO_2/salt materials (weight percent)

Sample ID	Calculated Initial Water Content	Water Content Fully Hydrated[a]
1a-1	0.38	No salts to hydrate
1b-1	1.00	1.64
1b-2	0.94	1.64
3c-1	0.35	0.23
4a-1	0.58	0.19
4a-2	0.63	0.19
4a-3	0.50	0.19
4b-1	0.66	0.90
4b-2	0.61	0.90
4b-3	0.61	0.90
5a-1	0.49	0.57
5a-2	1.24	0.57
5a-3	0.45	0.57

[a] *Fully hydrated is assumed to mean six moles of water for each mole of $MgCl_2$ or $CaCl_2$.*

Conclusions

Laboratory corrosion tests on room temperature 304L stainless steel coupons exposed to moist (nominally 0.6 wt percent water) PuO_2/$CaCl_2$-bearing salt mixtures show that this alloy is susceptible to pitting and SCC under specific conditions of mixture water loading, total chloride salt concentration *and* composition, and physical contact with the solid mixture. Cracking was associated with the heat-affected zone of an autogenous weld in the test coupons. SCC was produced by a mixture containing 98 wt percent PuO_2, 0.9 wt percent NaCl, 0.9 wt percent KCl, and 0.2 wt percent $CaCl_2$ (total salt concentration of 2 wt percent). Type 316L stainless steel undergoes pitting but not SCC when exposed to this same mixture with similar water loading as in the 304L tests. Type 304L stainless steel showed pitting but did not exhibit cracking under exposure to a mixture with an identical 2 wt percent total salt concentration but with a higher $CaCl_2$ concentration of 0.92 wt percent. A mixture with a very high total salt concentration of 28 wt percent did not induce pitting or cracking. Cracking was not observed in any coupon that was contacted by headspace gas, but pitting was observed on areas of some coupons that were in headspace gas contact. Pitting measurements on coupons that have been examined microscopically to date showed depths up to 100 μm.

The corrosion tests were conducted in small stainless steel containers that were sealed under a helium atmosphere. At com-

pletion of the test, the headspace gas composition was determined, and the water loading of the PuO_2/Cl^- salt mixture was evaluated. Actual water loading of the PuO_2/Cl^- salt mixtures ranged from 0.35 to 1.24 wt percent. These values represent gravimetric data corrected with the results of the headspace gas analysis, in particular analysis of hydrogen gas generation from water radiolysis.

The corrosion results and water analyses point to the significance of the relative humidity of the test environment to the susceptibility of austenitic stainless steels to corrosion. The relative humidity in the test environment is controlled by the water loading and the concentration of the hydrating salts such as $CaCl_2$. For each salt or salt mixture there is a threshold relative humidity below which the necessary liquid electrolyte cannot exist, and therefore below which the SCC risk is very low. This threshold is a thermodynamic quantity known as the deliquescence relative humidity that is dependent on the identity of the salt but is independent of the quantity of salt. Below the deliquescence RH there should be low corrosion risk, and above it the corrosion risk increases rapidly as a liquid phase, which is initially saturated with salt, grows and becomes more widespread in the container. At extremely high relative humidity the risk of corrosion decreases again due to the formation of less corrosive, dilute salt solutions. Additionally, if the hydrating salt content is high, all the moisture in the container may be consumed by the formation of the hydrate and the risk of corrosion will decrease because deliquescence cannot occur. The test results demonstrate that the risk of corrosion is function of the moisture and salt contents and other exposure variables that control the tendency for deliquescence and the formation of a corrosion supporting electrolyte on the metal surface.

Acknowledgements

Funding for this work was provided by the Surveillance and Monitoring Program, U.S. Department of Energy Office of Environmental Management. This work was conducted at Los Alamos National Laboratory operated by Los Alamos National Security, LLC under contract DE-AC52-06NA25396 and at the Savannah River National Laboratory operated by Savannah River Nuclear Solutions for U.S. Department of Energy under contract DE-AC09-08SR22470.

Philip E. Zapp is a fellow engineer at Savannah River National Laboratory. He has a Ph. D. in metallurgical engineering from the University of Illinois at Urbana-Champaign and a B.A. in physics from Cornell University.

Jonathan M. Duffey is a principal scientist at Savannah River National Laboratory. He has a Ph.D. and M.S. in inorganic chemistry from the University of Tennessee and a B.S. in chemistry from Union University.

Poh Sang Lam is a senior fellow engineer at Savannah River National Laboratory. He has a Ph.D. in theoretical and applied mechanics from the University of Illinois at Urbana-Champaign, an M.S. in engineering and applied science from Yale University, and a B.S. in naval architecture and marine engineering from National Cheng Kung University Taiwan.

Kerry A. Dunn is an advisory engineer at the Savannah River National Laboratory. She has an M.S. in Materials Science and Engineering and a B.S. in Metallurgy from Pennsylvania State University.

D. Kirk Veirs is a staff scientist at Los Alamos National Laboratory. He has a Ph.D. in physical chemistry from Pennsylvania State University and a B.S. in chemistry and environmental science from Northern Arizona University.

Laura A. Worl is a project manager at Los Alamos National Laboratory. She has a Ph.D. in chemistry from the University of North Carolina and a B.S. in chemistry, Magna Cum Laude, from the University of Delaware.

John M. Berg is a staff scientist at Los Alamos National Laboratory. He has a Ph.D. in chemistry from Princeton University and a B.A. in chemistry from St. John's University.

References

1. Sedriks, A. J. 1996. *Corrosion of Stainless Steels,* 2nd edition, Wiley, New York.
2. Dunn, K. A., G. T. Chandler, C. W. Gardner, M.R. Louthan, J. W. McClard, and L. A. Worl. 2010. Supporting Safe Storage of Plutonium-Bearing Materials Through Science, Engineering and Surveillance, *Journal of Nuclear Materials Management* Vol. 38, No. 2.
3. Veirs, D. K., L. A. Worl, D. M. Harradine, M. A. Martinez, R. S. Lillard, D. S. Schwartz, C. V. Puglisi, D. D. Padilla, A. Carrillo, R. E. McInroy, and A. R. Montoya. Gas Generation and Corrosion in Salt-Containing Impure Plutonium Oxide Materials: Initial Results for ARF-102-85-223, LA-UR-04-1788, Los Alamos National Laboratory, Los Alamos, N.M., USA.
4. Zapp, P. E., and R. R. Livingston. 2005. Corrosion Tests of 304L and 316L Stainless Steels for the 3013 Container, WSRC-TR-2005-00191, Savannah River National Laboratory, Aiken, S.C., USA, September 2005.
5. Shoji, S., and N. Ohnaka. 1989. *Boshoku Gijutsu* 38 (2) (1989) 92.
6. Lillard, R. S., D. G. Kolman, M. A. Hill, M. B. Prime, D. K. Veirs, L. A. Worl, and P. E. Zapp, *Corrosion* 65 (3) (2009) 175.

7. Zapp, P. E., J. M. Duffey, K. A. Dunn, R. R. Livingston, and D. Z. Nelson. 2009. Localized Corrosion of Austenitic Stainless Steel Exposed to Mixtures of Plutonium Oxide and Chloride Salts, presented at CORROSION/2009, paper no. 09409.
8. Lam, P. S., P. E. Zapp, J. M. Duffey, and K. A. Dunn. *Proceedings of PVP2009, 2009 ASME Pressure Vessels and Piping Division Conference,* Prague, Czech Republic, paper 77432.
9. 2008. ABAQUS Implicit Version 6.6.3, Dassault Systèmes Simulia Corporation (formerly ABAQUS Inc.), Providence, Rhode Island.
10. Mickalonis, J. I., and K. A. Dunn. 2010. Residual Stresses in 3013 Containers, *Journal of Nuclear Materials Management* Vol. 38, No. 2.

Thermal Gradients and the Potential to Form Liquids in 3013 Containers

John M. Berg, Joshua E. Narlesky, F. Coyne Prenger, and D. Kirk Veirs
Los Alamos National Laboratory, Los Alamos, New Mexico USA

Narendra K. Gupta
Savannah River National Laboratory, Aiken, South Carolina USA

Binh V. Nguyen and Lance E. Traver
Savannah River Nuclear Solutions, Aiken, South Carolina USA

Abstract

The potential for internal corrosion of hermetically sealed stainless steel containers of plutonium oxide is assumed to increase dramatically when an aqueous electrolyte phase of high chloride ion concentration forms in contact with an internal container surface. This potential for liquid formation will not be uniformly distributed over the inner surface, but rather will be influenced by contact with solid phase contained material, by total moisture content, by temperature, and by the hydration and solution thermochemical properties of the various phases in the heterogeneous material. With knowledge of the amount of contained moisture, the contained quantities of certain material phases with highest affinity for moisture, and the thermal profile of the container and contents, it is possible in principle to determine whether a liquid phase can form and if so, where in the container it will occur. This paper discusses the likely moisture distribution and liquid phase formation in existing packages based on temperature measurements, thermal models, thermodynamics of known phases, and measured water partial pressures.

Introduction

Corrosion of 304L and 316L stainless steel has been observed in laboratory studies[1-3] and field surveillances[4] of sealed containers with plutonium bearing material that meet the requirements of the U.S. Department of Energy's (DOE) 3013 Standard.[5] The corrosion observed in these studies, either pitting or stress corrosion cracking, is mainly attributed to the presence of concentrated chloride solutions. The chloride solutions arise from deliquescence of chloride salts present, i.e., the absorption of water vapor from the atmosphere by the salt to form a saturated solution. The packaging glovebox relative humidity (RH) at ambient temperature was controlled per procedure to 3.5 percent or less at Rocky Flats Environmental Technology Site (RFETS) and below 25 percent at Savannah River Site (SRS), was controlled by normal facility operations to below 1 percent at Los Alamos National Laboratory (LANL) and Lawrence Livermore National Laboratory (LLNL), and was uncontrolled at Hanford although the highest observed was 53 percent during packaging. The NaCl and KCl pure phases do not form hydrates at ambient temperature or above, and the deliquescent RH (RH_{DEL}) for these salts are above any packaging glovebox RH, therefore these salts are not of concern for corrosion. Characterization of chloride salts that were prepared in mole ratios similar to those found in pyrochemical processes has identified a number of crystalline chloride phases formed with magnesium and calcium that could lead to water absorption from the glovebox atmosphere after calcination.[6] The magnesium and calcium based chloride salt phases can form hydrates at very low water vapor pressures. For instance, magnesium chloride forms the hexahydrate at 3.2 percent/6.9 percent RH at 25°C/70°C and calcium chloride forms the dihydrate at 4.3 percent/6.5 percent at 25°C/70°C.

It is well known that water migrates to cold spots and that thermal gradients exist within the material and container in the 3013 package due to internal heat generation from radioactive decay (wattage). The question we address in this paper is: does the potential exist for material initially with no liquid phase but with hydrated alkaline earth chlorides to form a solution phase at the cold spots within the container? We assume a constant water vapor pressure within the inner container/convenience container/material system. The information needed to address this question includes the thermal profile within the 3013 package, the RH_{DEL} of the salts that might be present, and the RH at which various hydrated salt phases are formed.

3013 Thermal Environment

The 3013 container, consisting of the outer container, the inner container, and the convenience container with its material payload, has been the subject of increasingly sophisticated finite element (FE) thermal models.[7-9] The latest revision includes algebraic equations that allow computation of the temperature at three loca-

tions (top, middle, bottom) on each of the three container walls for two configurations—a bare 3013 container standing upright and a 3013 container in a 9975 transportation package.[8] The 9975 configuration is how the majority of 3013 containers are stored at SRS. Input parameters to the algebraic equations are the material density, the total heat output of the material due to radioactive decay, and the ambient temperature. The algebraic equations allow the temperature to be estimated for a wide range of conditions without conducting a full FE calculation for each case; however, because they are derived from a small subset of the possible material configurations, the output from the algebraic equations will not be as accurate as the more complete FE model results.

To the best of our knowledge the FE thermal models have not been verified with temperature measurements of actual 3013 containers. We have conducted a verification measurement on a 3013 container in the 9975 configuration. A 3013 container was removed from its 9975 shipping container and instrumented with six self-adhesive K-type thermocouples (Omega SA1-K-72-SC) on its outer wall. Thermocouple positions were (Figure 1):

1. Center of bottom
2. Center of side wall
3. Top of side wall
4. Center of lid
5. Bottom of side wall
6. Midpoint between center and bottom of side wall

The 3013 container was then placed back into the 9975 package, the thermocouple wires were routed to the outside of the package, and the lids of the primary containment vessel (PCV), secondary containment vessel (SCV) and 9975 were set in place but not threaded down in order to allow egress of the thermocouple wires. Polyvinyl chloride tape was placed over the thermocouple wires where they exited the PCV and SCV to protect them from damage from the respective lids. All components of the 9975, including the Celotex cap were put in place as completely as possible. This configuration was left undisturbed for 48 hours. Temperature readings were taken from the six thermocouples at 43 and 48 hours in order to verify a steady-state condition. The temperature readings ranged from 33°C to 39°C. The readings were unchanged during the five hour period between measurements indicating that the system reached steady-state. The midpoint of the 9975 outer wall and center of the 9975 lid were also measured at 43 and 48 hours and both were 20°C.

The self-adhesive thermocouple dimensions are 2.5 x 2.0 cm. Thermocouples placed on the 3013 side wall were oriented horizontally as shown in Figure 1. For the thermocouple located at the top of the 3013 side wall, the top edge of the patch was aligned with the top edge of the sidewall with the thermocouple junction 1.0 cm below the edge. For the thermocouple located at the bottom of the side wall, the bottom edge of the adhesive patch was aligned with the bottom edge of the side wall with the thermocouple junction 1.0 cm above the bottom edge.

Figure 1. Thermocouple placement on the outer 3013 container used to verify the 3013 finite element thermal model. Stick-on thermocouples were placed on a 3013 container as shown and the container was placed into a 9975 transportation container. Positions 3, 2, and 5 correspond to temperatures that can be computed using the algebraic equations from the thermal model.

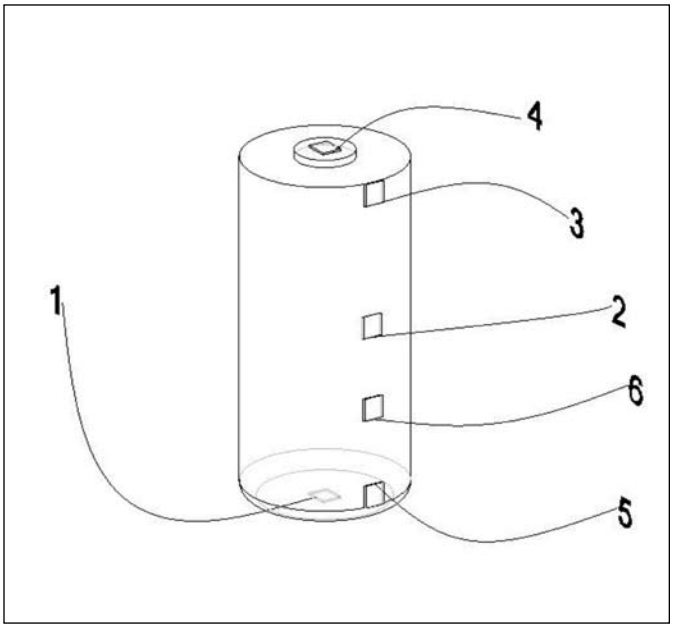

Table 1. Material properties of the 3013 container contents used to verify the thermal model

Mass	2.4 kg
Total thermal output	5.0 W
Material specific wattage	2.7 W kg^{-1}
Pu content	76 percent
PuO_2 content	86 percent
Salt content	14 percent
Density (estimated)	3 g cm^{-3}

Table 2. Temperature in degree centigrade observed on a 3013 container and computed using algebraic equations derived from a finite element thermal model

Position	43 hours	48 hours	Thermal Model
Center top	33	33	
Center bottom	38	39	
Side wall top	34	34	38
Side wall midpoint	36	36	40
Side wall bottom	36	36	38
Side wall between midpoint and bottom	37	37	
9975 outside wall	20	20	
9975 outside lid	20	20	

Figure 2. Two-dimensional axi-symmetric thermal profiles of material within a 3013 convenience container showing five volume regions with equally spaced average temperature. The 3013 assembly is H003119. Left profile shows material temperatures when the convenience container is in an isolated configuration. Right profile shows material temperatures when the convenience container is packaged into 3013 inner and outer containers and placed into a 9975 transportation package.

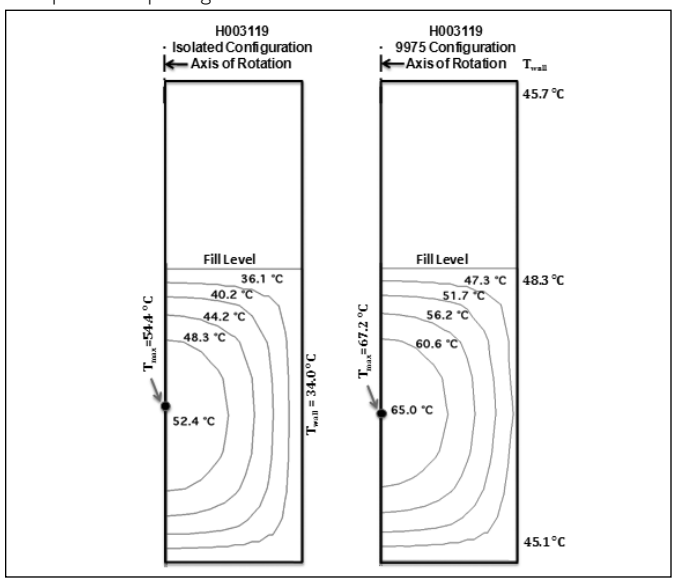

Figure 3. Two-dimensional axi-symmetric thermal profiles of material within a 3013 convenience container showing five volume regions with equally spaced average temperature. The 3013 assembly is R610806. Left profile shows material temperatures when the convenience container is in an isolated configuration. Right profile shows material temperatures when the convenience container is packaged into 3013 inner and outer containers and placed into a 9975 transportation package.

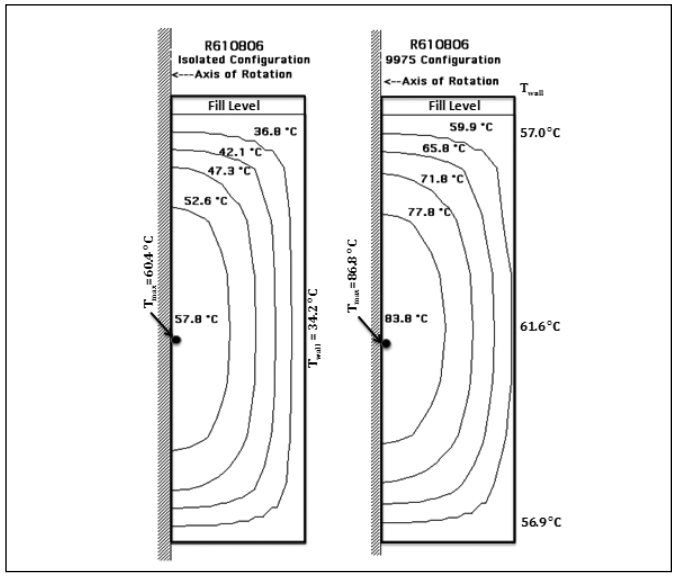

The material properties of the contents of the 3013 container are given in Table 1. The ambient temperature was 20°C. The temperature at thermocouple positions 3, 2, and 5 were calculated using the algebraic equations for the outer container in the 9975 configuration.[8] The measured temperatures and the thermal model temperatures are compared in Table 2. The thermal model overestimates the wall temperature of the 3013 container by four degrees centigrade. This may arise from uncertainties in the Celotex thermal conductivity,[8] uncertainties in the Celotex packing configuration, or from the lack of tight closure on the PCV, SCV, and the 9975. The temperature increase from the top to the center of the sidewall, which is of importance to estimating the thermal gradients, was correct at 2°C. The measured temperature at the bottom of the si dewall stayed the same rather than decreasing as seen in the thermal model. This may arise from incomplete thermal contact at the bottom of the container. Details from Gupta's report[8,9] indicate that the axial temperature of the material at the bottom of the convenience container and the wall temperature at the bottom of the outer container are within 0.8°C of each other. However, the measured 3°C difference between the center bottom of the container and the sidewall bottom of the container is likely influenced by the thermal contact of the bottom of the container with the packing materials on the bottom of the PCV. We conclude that the algebraic equations can be used to determine the temperature gradients of the container walls with an accuracy of 2°C.

Table 3. Container temperatures for materials H003119 and R610806 computed for the 9975 configuration with an ambient temperature of 23.9°C. Temperature labels correspond to positions in Figure 1.

		H003119	R610806
Wattage, total (W)		5.54	8.18
Density, bulk (g cm^{-3})		2.40	2.51
Mass, (kg)		2.43	4.26
Inner container wall Temperature (°C)	3	44.6	55.4
	2	47.2	59.7
	5	45.4	57.4
Convenience container wall temperature (°C)	3	45.7	57.0
	2	48.3	61.6
	5	45.1	56.9

Temperatures within the radioactive material were computed using the material thermal conductivity model of Bielenberg.[10, 11] An axi-symmetric two-dimensional FE model was used to calculate five volume fractions of material contained between six isotherms spread uniformly across the maximum temperature range defined by the maximum centerline temperature and the minimum sidewall temperature. Two materials were examined for which the material thermal conductivity had been evaluated

Table 4. Volume fractions of five equally spaced temperature regions for the isolated convenience container and in the 9975 configuration as shown in Figure 2 for H003119

	Isolated		9975	
	Isothermal Region Vol/V_{tot}	T_{avg} (°C)	Isothermal Region Vol/V_{tot}	T_{avg} (°C)
Maximum temperature	-	54.4	-	67.2
Region 1	0.077	52.4	0.083	65.0
Region 2	0.134	48.3	0.154	60.6
Region 3	0.194	44.2	0.219	56.2
Region 4	0.244	40.2	0.266	51.7
Region 5	0.351	36.1	0.279	47.3
Wall temperature	-	34.0	-	46.8

Table 5. Volume fractions of five equally spaced temperature regions for the isolated convenience container and in the 9975 configuration as shown in Figure 3 for R610806

	Isolated		9975	
	Isothermal Region Vol/V_{tot}	T_{avg} (°C)	Isothermal Region Vol/V_{tot}	T_{avg} (°C)
Maximum temperature	-	60.4	-	86.8
Region 1	0.083	57.8	0.092	83.8
Region 2	0.138	52.6	0.156	77.8
Region 3	0.190	47.3	0.213	71.8
Region 4	0.249	42.1	0.267	65.8
Region 5	0.341	36.8.	0.272	59.9
Wall temperature	-	34.2	-	59.3

from temperature measurements obtained during SRS destructive examination (DE), H003119 and R610806.[11] Table 3 lists the calculated sidewall temperatures of the inner container and the convenience container when the 3013 container is within a 9975 transportation container assuming an ambient temperature of 23.9°C along with the total wattage, material density and material mass. The sidewall temperatures for the isolated convenience container when the outer and inner containers are removed are 34°C and 34.2°C respectively.[2] The average temperature of each volume element, the maximum material temperature, and the sidewall temperatures for H003119 in the 9975 configuration and for the isolated convenience container are shown in Figure 2 and for R610806 in Figure 3. The temperatures were calculated using the wall temperatures in Table 2 for the 9975 configuration and 34°C and 34.2°C respectively for the wall temperatures in the bare configuration. These results are summarized in Tables 4 and 5 which also list the fraction of the total material that each volume element occupies. Comparing the two configurations, the principal effect is an increase in temperature upon enclosure within the 9975. The magnitude of the temperature increase depends upon the total wattage of the material. The maximum and wall temperatures of material H003119 (5.54 W) increase by 12.8°C and the temperatures of material R610836 (8.18W) increase 26.4°C and 25.1°C respectively. The volume of the temperature regions 1 through 4 increase by about 10 percent and the volume of region 5 decreases by about 20 percent for both materials. As shown below, the nearly uniform temperature increase of the material will be used to determine the increase of the water vapor pressure when an isolated convenience container is placed into the 9975 configuration.

Material Hydration and Deliquescence Behavior

The known chloride salt phases from the pyrochemical processes that are typically used across the DOE complex have been discussed by Joyce.[6] The sodium chloride and potassium chloride pure phases do not form hydrates at expected packaging temperatures and do not deliquesce at the water vapor pressures found in glovebox atmospheres during processing and packaging in 3013 containers, therefore these chloride salts are not of concern in regards to forming solutions capable of corrosion. The calcium and magnesium salts are of concern due to their potential to form hydrates and aqueous solutions at low values of RH, the latter process occurring when the RH exceeds RH_{DEL}.[2] The relevant reactions for the binary salts, for example, are:

$$MCl_2(s) + nH_2O(g) \longrightarrow MCl_2 \cdot nH_2O(s) \quad (1)$$

$$MCl_2 \cdot nH_2O(s) \xrightarrow{P_{H_2O(g)} > RH_{DEL}} M^{2+}(aq) + 2Cl^-(aq) \quad (2)$$

Extensive thermodynamic data exist for both $CaCl_2$ and $MgCl_2$ and their hydrates which allow the temperature and water vapor conditions for the formation of the hydrates to be determined.[12-15] The available information for $KMgCl_3$ and $KCaCl_3$ are limited. Hydrates of $KCaCl_3$ are not known and hydrates of $KMgCl_3$ appear to be bounded by the hydrates of $MgCl_2$, e.g. the reported RH at which $KMgCl_3 \cdot 6H_2O$ is formed is either equal or less than the RH at which $MgCl_2 \cdot 6H_2O$ is formed. The reported deliquescence behavior of $KCaCl_3$ is very similar to the deliquescence behavior of $CaCl_2$ as will be shown below. Since we are concerned with the highest RH of the hydrates and the lowest RH of deliquescence, the hydration behavior of $MgCl_2$ and $CaCl_2$ will be considered as bounding for all materials of interest. In regards to deliquescence, the calcium salts clearly deliquesce at a lower relative humidity than the magnesium salts.

Figure 4. The water vapor pressure required for the formation of the magnesium chloride hydrates with P_{H2O} of the glovebox atmospheres at the various packaging sites indicated.

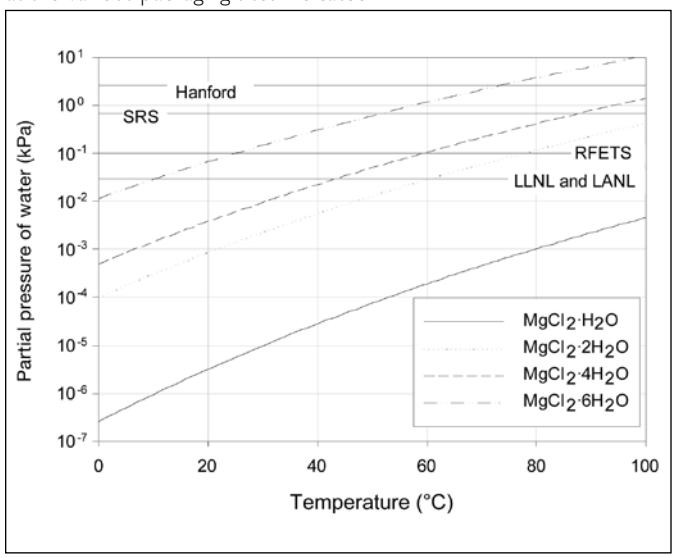

Figure 5. The water vapor pressure required for the formation of the calcium chloride hydrates with P_{H2O} of the glovebox atmospheres at the various packaging sites indicated.

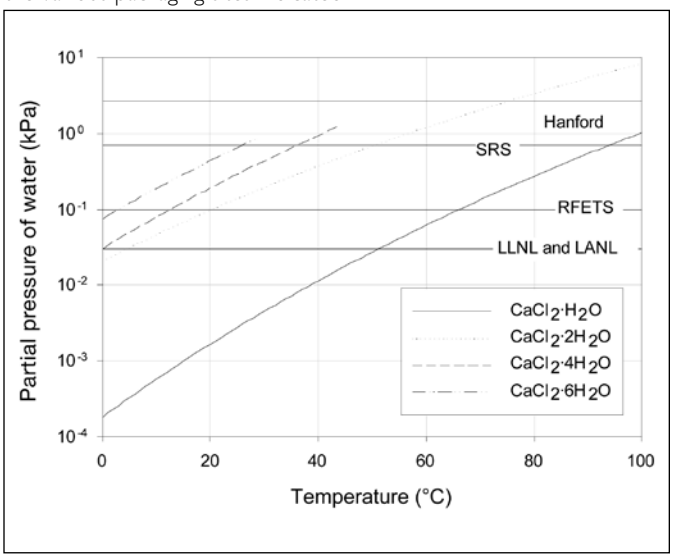

Hydration and deliquescent behavior can be reported as RH versus temperature or as water partial pressure (P_{H2O}) versus temperature. We will use P_{H2O} versus temperature because P_{H2O} will be the same at all locations within a 3013 container at steady-state conditions and will be the same throughout the material during handling operations as long as gas diffusion is fast relative to the hydration and deliquescence reactions. The RH is a less convenient parameter for these cases because it will vary due to variations in the temperature. The P_{H2O} for formation of the hydrates of $MgCl_2$ and $CaCl_2$ are given in Figures 4 and 5 respectively. The curves are labeled with the reaction product, i.e $MgCl_2 \cdot 6H_2O$ refers to the water partial pressure required to form $MgCl_2 \cdot 6H_2O$ from $MgCl_2 \cdot 4H_2O$. The calculations leading to Figure 4 and 5 are given in Appendix A. Examination of Figures 4 and 5 reveal that $\log(P_{H2O})$ is a nearly linear function of temperature over small changes of temperature. The temperatures of interest lie between 34°C and 86°C, the minimum and maximum material temperatures. The maximum slope for all of the hydrated species occurs at the lowest temperature. The partial pressure of water can be estimated conservatively at higher temperatures if the water vapor pressure, the maximum slope over the temperature interval, and the change in temperature are known,

$$\log(P_2) = \log(P_1) + \Delta T \cdot m$$
$$P_2 = P_1 \cdot 10^{\Delta T \cdot m} \qquad (3)$$

where P is the water partial pressure in kPa, ΔT is the change in temperature in °C, and m is slope for the hydrated species of interest. The maximum slopes, which were determined at 34°C for all of the hydration reactions in Figures 4 and 5, are given in Table 6.

Table 6. The rate of change with temperature in the log of water partial pressure at 34°C is given for the hydration reactions of magnesium and calcium chloride. The higher hydrates of calcium chlorides do not exist over the temperature range of interest.

Hydration Reaction	Slope (K^{-1})
$CaCl_2 + H_2O \rightarrow CaCl_2 \cdot H_2O$	0.0406
$CaCl_2 \cdot H_2O + H_2O \rightarrow CaCl_2 \cdot 2H_2O$	0.0282
$CaCl_2 \cdot 2H_2O + 2H_2O \rightarrow CaCl_2 \cdot 4H_2O$	--
$CaCl_2 \cdot 4H_2O + 2H_2O \rightarrow CaCl_2 \cdot 6H_2O$	--
$MgCl_2 + H_2O \rightarrow MgCl_2 \cdot H_2O$	0.0460
$MgCl_2 \cdot H_2O + H_2O \rightarrow MgCl_2 \cdot 2H_2O$	0.0392
$MgCl_2 \cdot 2H_2O + 2H_2O \rightarrow MgCl_2 \cdot 4H_2O$	0.0374
$MgCl_2 \cdot 4H_2O + 2H_2O \rightarrow MgCl_2 \cdot 6H_2O$	0.0321

In addition to P_{H2O} at which the hydrates are formed, P_{H2O} of the glovebox atmospheres at the various packaging sites are indicated. The maximum P_{H2O} during packaging are estimated to be 2.62 kPa at Hanford (55 percent RH at 32°C) and 0.70 kPa at SRS (25 percent RH at 23°C). RFETS had an upper limit of 0.1 kPa (1000 ppm) and LLNL and LANL have limits estimated to be 0.030 kPa (dew point of -32°C) or lower. The potential for forming the various hydrates during packaging can be evaluated from Figures 4 and 5. Material containing anhydrous $MgCl_2$ will begin to form $MgCl_2 \cdot H_2O$ while cooling after calcination before the temperature falls to 100°C under even the driest conditions maintained at any of the packaging sites. On the other hand, formation of $MgCl_2 \cdot 6H_2O$ could not occur under the maximum P_{H2O} encountered in LLNL, LANL, or RFETS packaging operations even if the material temperature fell all the way to ambi-

Figure 6. The water vapor pressures at which calcium salts deliquesce are shown. The values for $CaCl_2 \cdot 2H_2O$ are from Pitzer and Oakes[14]. The values for $CaCl_2 \cdot 4H_2O$ and $CaCl_2 \cdot 6H_2O$ are from the International Critical Tables online.[19] The values for $KCaCl_3$ are from Joyce.[6] The calcium chloride salts will not deliquesce at the conditions at RFETS, LLNL, and LANL. In order to avoid deliquescence, the temperature of material should remain above 40° C at SRS.

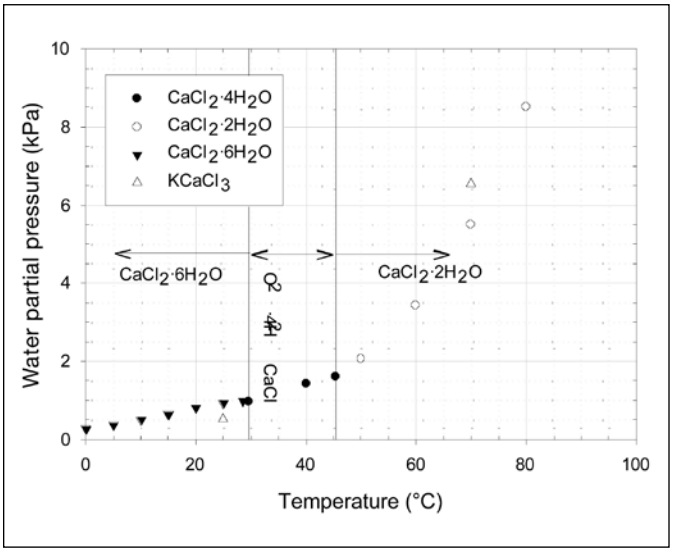

ent. In order to avoid the formation of $MgCl_2 \cdot 6H_2O$ the material would have to remain above ~50°C at SRS and ~73°C at Hanford.

For material containing anhydrous calcium chloride after calcination, $CaCl_2 \cdot 2H_2O$ will not form at LLNL, LANL, and RFETS whereas the material would have to remain above ~50°C at SRS and ~75°C at Hanford to avoid formation. The hydrates $CaCl_2 \cdot 4H_2O$ and $CaCl_2 \cdot 6H_2O$ melt above 45°C and 30°C, respectively. Both of these hydrates could form at Hanford and $CaCl_2 \cdot 4H_2O$ could form at SRS.

The deliquescent P_{H2O} for the calcium salts are shown in Figure 6. The RH_{DEL} for $CaCl_2 \cdot 2H_2O$ is nearly constant at 17 percent and the rapid rise in P_{H2O} is due to the increase in the saturated water vapor pressure over the temperature range of 45°C to 80°C. The shallow rise in P_{H2O} for $CaCl_2 \cdot 6H_2O$ occurs because RH_{DEL} decreases from over 40 percent to ~20 percent from 0°C to 30°C.

Potential for Formation of Liquids

Materials with $MgCl_2$ and $CaCl_2$ salts have the potential to form deliquesced liquids that facilitate corrosion of the container walls. Of particular interest is the possibility that even minor liquid formation could be problematic because it might be localized at the walls due to shifts in alkaline earth chloride salt hydration and dehydration reactions driven by thermal gradients within the containers. Consider, for example, the case of a material containing both $CaCl_2$ and $MgCl_2$, along with sufficient H_2O to fully hydrate both of them at the time of packaging. The two reactions relevant to liquid formation in this case at 34°C are:

Table 7. Water vapor pressure above $MgCl_2 \cdot 6H_2O$ and required for deliquescence of $CaCl_2$ determined from the temperatures of the material and container wall in the 9975 configuration

	R610806			H003119		
	T_{avg} (°C)	P_{H2O} (kPa)	P_{DEL} (kPa)	T_{avg} (°C)	P_{H2O} (kPa)	P_{DEL} (kPa)
Maximum temperature	86.8	5.53	-	67.2	1.83	-
Region 1	83.8	4.70	-	65.0	1.60	-
Region 5	59.9	-	3.4	47.3	-	1.8
Wall temperature	59.3	-	3.3	46.8	-	1.8

$$\begin{aligned} MgCl_2 \cdot 6H_2O(s) &\longrightarrow MgCl_2 \cdot 4H_2O(s) + 2H_2O(g) \\ CaCl_2 \cdot 4H_2O(s) + H_2O(g) &\longrightarrow CaCl_2(aq) \end{aligned} \quad (4)$$

The $MgCl_2$ dehydration reaction can occur near the center of the container where the material is warmer. This releases additional water into the vapor phase which, if P_{H2O} becomes great enough, can then drive the $CaCl_2$ deliquescence reaction to form pockets of liquid in the cooler regions near the walls.

If the combination of the masses of $MgCl_2$ plus $CaCl_2$ are such that the total amount of water when $MgCl_2 \cdot 4H_2O$ and $CaCl_2 \cdot 2H_2O$ are formed exceeds 0.5 wt percent, then deliquescence is not a concern. A temperature greater than 90°C (which is not exceeded under typical storage conditions) is needed for $MgCl_2 \cdot 4H_2O$ to begin to decompose to $MgCl_2 \cdot 2H_2O$ at a water partial pressure of 1 kPa. However, a water partial pressure of 1 kPa is not sufficient to deliquesce calcium chloride salts at temperatures above 30°C. All inner and convenience container temperatures are above 30°C, therefore material with $MgCl_2 \cdot 4H_2O$ will not cause deliquescence of the calcium chloride component. Packaging conditions at RFETS, LLNL, and LANL are too dry to form $MgCl_2 \cdot 6H_2O$, therefore containers from these sites have very low potential to form corrosive liquids due to temperature gradients within the container.

The temperature profiles calculated from measured temperatures during destructive evaluation at SRS can be evaluated for the potential to form liquids for materials packaged at Hanford. We assume that $MgCl_2$ salts have picked up sufficient moisture to form $MgCl_2 \cdot 6H_2O$ but have not deliquesced and that $CaCl_2$ salts have picked up sufficient moisture to form $CaCl_2 \cdot 2H_2O$ but have not deliquesced. We also assume that the material has no liquids present when introduced into the container. The formation of $MgCl_2 \cdot 6H_2O$ will determine the water partial pressure within the container. If the water partial pressure required to form

Table 8. The 3013 containers for which RH and T have been measured during DE. The water partial pressure is calculated from the RH and T. The appropriate magnesium chloride phase determined by the water partial pressure and temperature range within the container is given. The slope and the water vapor partial pressure predicted if the container was placed in the 9975 configuration is calculated from the temperature rise using Eq. 3. The temperature rise is 13°C for the Hanford containers and 26°C for the RFETS containers.

Container	RH (percent)	T (°C)	P_{H2O} Isolated (kPa)	Phase	Slope ($°C^{-1}$)	P_{H2O} 9975 (kPa)
H004111	11.3	27.2	0.41	$MgCl_2 \cdot 6H_2O$	0.0321	1.1
H002554	5.5	27.2	0.20	$MgCl_2 \cdot 6H_2O$	0.0321	0.52
H002509	5.1	29.4	0.22	$MgCl_2 \cdot 6H_2O$	0.0321	0.55
H002565	1.8	31.1	0.081	$MgCl_2 \cdot 4H_2O$	0.0374	0.25
H002657	7.4	27.2	0.27	$MgCl_2 \cdot 6H_2O$	0.0321	0.70
R611398	4.7	30.0	0.20	$MgCl_2 \cdot 6H_2O$	0.0321	1.4
H002200	1.4	33.3	0.072	$MgCl_2 \cdot 4H_2O$	0.0374	0.22
H002667	1.1	27.2	0.040	$MgCl_2 \cdot 4H_2O$	0.0374	0.12
H002715	3	27.8	0.11	$MgCl_2 \cdot 4H_2O$	0.0374	0.34
R610806	0.3	30.0	0.013	$MgCl_2 \cdot 4H_2O$	0.0374	0.12
R610573	0.6	27.8	0.022	$MgCl_2 \cdot 4H_2O$	0.0374	0.21
H003119	2.8	29.4	0.11	$MgCl_2 \cdot 4H_2O$	0.0374	0.35
H002496	12.1	24.4	0.37	$MgCl_2 \cdot 6H_2O$	0.0321	0.97
H003710	5.3	29.4	0.22	$MgCl_2 \cdot 6H_2O$	0.0321	0.57
H004251	3.7	28.9	0.15	$MgCl_2 \cdot 4H_2O$	0.0374	0.45

$MgCl_2 \cdot 6H_2O$ in the hottest volume of the container exceeds the $CaCl_2$ deliquescent water partial pressure (P_{DEL}), then water will be transferred from the hottest part of the container to the coldest region to form a solution. If the $MgCl_2 \cdot 6H_2O$ component P_{H2O} of the next hottest volume also exceeds P_{DEL} of the coldest region, then there will be sufficient water available for a significant amount of liquid to form.

The comparison of P_{H2O} and P_{DEL} for the 9975 configuration are given in Table 7. The absolute temperature of the 9975 configuration results in sufficiently high P_{H2O} for P_{DEL} to be exceeded at the wall for containers that are full of material such as R610806 and are barely sufficient in the case of half-full containers such as H003119. However, if only a small amount of the available $MgCl_2$ was not hydrated to $MgC_2 \cdot 6H_2O$, then P_{H2O} will be determined by the next hottest volume and no deliquescence will occur within the half-full container.

Comparison to Measured Water Partial Pressure During Destructive Evaluation

The relative humidity and temperature has been measured for some of the field surveillance destructive examinations of 3013 containers that have been carried out at SRS.[16] These measurements can be used to estimate the water vapor pressure of a container in the 9975 configuration. After gas samples have been obtained[17] and the convenience container removed, the convenience container lid is replaced with a modified lid with a humidity sensor and Viton gasket. The humidity sensor, a Vaisala HMI41 indicator with HMP45 probe, provides humidity and temperature readings which are recorded once every hour for twelve hours. Water vapor is lost during gas sampling, handling during removal of the convenience container, and when the lid is replaced, but these should be minor perturbations on the moisture content because the amount of water in the vapor phase is only a small fraction of the total amount of water in the container. For instance, the fraction of water in the vapor phase at 20 percent RH and average gas temperature of 34°C for a convenience container with 2.5 kg of material with 0.2 wt percent water is about 0.001 of the total water. The P_{H2O} equilibrates with the material in less than an hour. However, thermal stabilization of the convenience container once it is removed from the inner and outer containers takes many hours.

The water vapor pressure within the convenience container is obtained from the final relative humidity and temperature. With the heat generated by weapons grade material, the temperature rise for a half-full 3013 container, typical of many Hanford containers, is 13°C and for a full 3013 container, typical of many RFETS containers, the temperature rise is 26°C. The water partial pressure is determined by the formation of a particular salt hydrate. For instance, if a packaged material has a temperature range of 35°C to 60°C and a water vapor pressure of 0.1 kPa, the formation of $MgCl_2 \cdot 4H_2O$ would determine the water vapor

Table 9. The enthalpies of formation, entropies, and heat capacity functions used to describe the hydration formation of the alkaline earth chlorides. The values for magnesium chlorides are from Pabalan and Pitzer[13], the enthalpies and heat capacities for the calcium chlorides are from Kelly and Wexler[12], the entropies for the calcium chlorides and the heat capacity for $CaCl_2$ are from Pitzer and Shi[15] and Pitzer and Oakes[14], and the values for water are from the CRC Handbook[18]. The tabulated heat capacities for water from the CRC Handbook were fit to the form $C_p/R = a + bT + c/T$.

Substance	ΔH_{298}° (kJ mol^{-1})	S_{298}° (J mol^{-1} K^{-1})	a	b	c
$CaCl_2$	-795.39	105.4	8.645	0.0015[3]	-3x10^4
$CaCl_2 \cdot H_2O$	-1110.83	134.7	13.645	0	0
$CaCl_2 \cdot 2H_2O$	-1403.97	206.2	18.73	0	0
$CaCl_2 \cdot 4H_2O$	-2009.60	271.9	28.729	0	0
$CaCl_2 \cdot 6H_2O$	-2609.94	341.8	38.729	0	0
$MgCl_2$	-641.33	89.6	9.511	0.7146x10^{-3}	-1.037x10^5
$MgCl_2 \cdot H_2O$	-966.65	137.2	10.95	9.788x10^{-3}	0
$MgCl_2 \cdot 2H_2O$	-1279.7	179.9	15.05	13.74x10^{-3}	0
$MgCl_2 \cdot 4H_2O$	-1899.0	264.0	22.56	21.65x10^{-3}	0
$MgCl_2 \cdot 6H_2O$	-2499.07	366.1	29.08	29.56x10^{-3}	0
H_2O	-241.826	188.834	3.447	1.46x10^{-3}	1.375x10^4

pressure because it is the only phase being formed under these conditions. As the temperature increases, the water partial pressure increases along the $MgCl_2 \cdot 4H_2O$ line shown in Figure 4. Thus, one can determine the hydrated phase present based on the measured relative humidity and temperature inside the convenience container, and then the slope for that phase (Table 6) along with the temperature rise can be used to calculate the water vapor pressure in the 9975 configuration using Equation 3. The observations and results of analysis for the destructive examination (DE) containers are given in Table 8.

The lowest water vapor partial pressure required to deliquesce the calcium chloride component, if it is present, for a half-full container is 1.8 kPa and for a full container is 3.3 kPa. All of the calculated water vapor pressures for the 9975 configuration in Table 8 are below 1.8 kPa indicating that the sampled containers at the time of DE would not have a sufficient water vapor pressure for deliquescence to occur within the material when the container was stored in 9975 packaging.

Discussion

Analysis of (1) the material phases, (2) the RH at which hydrates form, and (3) the RH_{DEL} of all known salt phases show that the combination of $MgCl_2 \cdot 6H_2O$ at the hottest region of material and $CaCl_2 \cdot 2H_2O$ at the coolest region of material is of most concern. The temperature drop from the hottest material to the coolest material within a 3013 container stored in a 9975 package is sufficiently large to cause $CaCl_2 \cdot 2H_2O$ to deliquesce if $MgCl_2 \cdot 6H_2O$ is present for both a full container (R610806) or a half-full container (H003119) as shown in Table 7. For a full container, the water partial pressure when $MgCl_2 \cdot 6H_2O$ is present is over 65 percent larger than necessary to deliquesce $CaCl_2 \cdot 2H_2O$. However, for the half-full container the water partial pressure when $MgCl_2 \cdot 6H_2O$ is present is nearly equal to that necessary to deliquesce $CaCl_2 \cdot 2H_2O$. The large differences in behavior of the full container and the half-full container are due to several factors: 1) the differences in temperature drops (20.4°C for the half-full container and 27.3°C for the full container); 2) the increase with increasing temperature of the relative humidity above $MgCl_2 \cdot 6H_2O$ (6.4 percent at 67°C in the half-full container to 8.9 percent at 87°C in the full container) while RH_{DEL} of calcium chloride remains nearly constant; and 3) the total wattage, which increases the temperature within a 9975 package and the temperature drop across the material. In addition, the temperature drop across the material decreases as the amount of impurities increase. Therefore, the potential to form liquid solutions at the container walls will be highest for full containers with high wattage and relatively low impurities containing less than 0.5 wt percent of magnesium and calcium chloride salts.

Conclusion

The potential for salts commonly found in materials packaged in 3013 containers to form a concentrated chloride liquid at the container walls has been studied. The materials most likely to develop such a liquid are those with less than 0.5 wt percent of magnesium and calcium chloride. The presence of $MgCl_2 \cdot 6H_2O$ and $CaCl_2 \cdot 2H_2O$ at the time of packaging could result in movement of water from $MgCl_2 \cdot 6H_2O$ at the hottest regions of the material to deliquesce the $CaCl_2 \cdot 2H_2O$ at the coolest regions of the material near the container walls. The potential to form liquid solutions at the container walls will be highest for full containers with high wattage and relatively low impurities containing less than 0.5 wt percent of magnesium and calcium chloride salts.

John M. Berg is a staff scientist at Los Alamos National Laboratory. He has a Ph.D. in chemistry from Princeton University and a B.A. in chemistry from St. John's University.

Binh V. Nguyen is a process engineer, Registered PE, at Savannah River Nuclear Solutions. He has an M.S. in chemical engineering from University of South Carolina and a B.S. in chemical engineering from Clemson University.

Narendra K. Gupta is a principal engineer at Savannah River National Laboratory. He holds an M.S. in aerospace engineering and another in mechanical engineering.

Joshua E. Narlesky is a research and development scientist at Los Alamos National Laboratory. He received his B.S. from New Mexico Institute of Mining and Technology and his M.S. from Colorado State University, both in chemical engineering.

F. Coyne Prenger is a retired Registered Professional Engineer. He has a Ph.D. in mechanical engineering from Colorado State University.

Lance E. Traver is a lead engineer for surveillance operations at Savannah River Nuclear Solutions. He has an M.S. in environmental engineering from the University of Maryland and a B.S. in civil engineering from Rice University.

D. Kirk Veirs is a staff scientist at Los Alamos National Laboratory. He has a Ph.D. in physical chemistry from Pennsylvania State University and a B.S. in chemistry and environmental science from Northern Arizona University.

Acknowledgements

Funding for this work was provided by the Surveillance and Monitoring Program, U.S. Department of Energy Office of Environmental Management. This work was conducted at Los Alamos National Laboratory operated by Los Alamos National Security, LLC under contract DE-AC52-06NA25396 and Savannah River National Laboratory operated by Savannah River Nuclear Solutions for U.S. Department of Energy under contract DE-AC09-08SR22470.

Apppendix A.

Calculation of the Partial Pressure of Water Required for Formation of Calcium and Magnesium Chloride Hydrates

The reaction of a solid alkaline earth chloride with water vapor can be generalized as

$$MCl_2 \cdot x\,H_2O(s) + y\,H_2O(g) \rightarrow MCl_2 \cdot (x+y)H_2O(s) \quad (1)$$

where M is Ca or Mg. For a solid reacting with a gas, the equilibrium constant K is expressed in terms of the fugacity of the gas,

$$K = f_{H_2O}^{y} \quad (2)$$

where the fugacity is expressed in bar. At equilibrium,

$$K = \exp\left(\frac{\Delta G_T^{\circ}}{RT}\right). \quad (3)$$

Standard thermodynamics gives the equation

$$\begin{aligned}\Delta G_T^{\circ} = {} & \Delta H_T^{\circ}(MCl_2 \cdot (x+y)H_2O(s)) - \Delta H_T^{\circ}(MCl_2 \cdot x\,H_2O(s)) - y\,\Delta H_T^{\circ}(H_2O(g)) \\ & - T\left(S_T^{\circ}(MCl_2 \cdot (x+y)H_2O(s)) - S_T^{\circ}(MCl_2 \cdot x\,H_2O(s)) - yS_T^{\circ}(H_2O(g))\right)\end{aligned} \quad (4)$$

where

$$\Delta H_T^{\circ} = \Delta H_{298}^{\circ} + \int_{298}^{T} C_p\,dT$$

$$S_T^{\circ} = S_{298}^{\circ} + \int_{298}^{T} \frac{C_p}{T}\,dT \quad (5)$$

and C_p is expressed as

$$\frac{C_p}{R} = a + bT + \frac{c}{T^2} \quad . \quad (6)$$

The values of the thermodynamic quantities required to complete the calculations are given in Table 9.

References

1. Lillard, R. S., D. G. Kolman, M. A. Hill, M. B. Prime, D. K. Veirs, L. A. Worl, and P. E. Zapp. 2009. Assessment of Corrosion-Based Failure in Stainless Steel Containers Used for the Long-term Storage of Plutonium-Based Salts. *Corrosion* 65, 175 - 186.
2. Veirs, D. K., L. A. Worl, J. M. Berg, P. E. Zapp, J. M. Duffey, P. S. Lam, and K.A. Dunn. 2010. Relative Humidity and the Susceptibility of Austenitic Stainless Steel to Stress-corro-

sion Cracking in an Impure Plutonium Oxide Environment, *Journal of Nuclear Materials Management* Vol. 38, No 3.
3. Zapp, P. E., and J. M. Duffey. 2008. Status report for SRNL 3013 corrosion tests; WSRC-STI-2008-00046. Savannah River National Laboratory: Aiken, S.C., August 2008.
4. Nelson, D. Z., G. T. Chandler, K. A. Dunn, T. M. Stefek, and M. E. Summer. 2010. Stainless Steel Interactions with Salt Containing Plutonium Oxides, *Journal of Nuclear Materials Management* Vol. 38, No. 3.
5. *Stabilization, Packaging, and Storage of Plutonium-bearing Materials.* 2004. DOE-STD-3013-2004. U.S. Department of Energy: Washington, D.C.
6. Joyce, S. A., J. E. Narlesky, D. K. Veirs, E. Garcia, O. W. Gillispie, J. M. Jackson, B. Scott, and L. A. Worl. 2010. Salt Phases in Calcined Materials and Their Hydration Properties, *Journal of Nuclear Materials Management* Vol. 38, No. 2.
7. Hensel, S. 1998. Thermal Analysis of the 9975 Package as a Plutonium Storage Container; WSRC-TR-98-00203. Savannah River National Laboratory: Aiken, S.C.
8. Gupta, N. K. 2007. Thermal Models for the 3013 Containers in KAMS; M-CLC-K-00720, Rev. 2. Savannah River National Laboratory. Aiken, S.C.
9. Gupta, N. K. 2010. Thermal Analysis of the 3013/9975 Configuration, *Journal of Nuclear Materials Management* Vol. 38., No. 2.
10. Bielenberg, P. A., F. C. Prenger, D. K. Veirs, and G. F. Jones. 2006. Effects of Pressure on Thermal Transport in Plutonium Oxide Powder, *International Journal of Heat and Mass Transfer* 49, 3229-3239.
11. Veirs, D. K., and F. C. Prenger. 2010. Thermal Conductivity of High-purity and Impure Plutonium Oxide Materials, *Journal of Nuclear Materials Management* Vol. 38, No. 2.
12. Kelly, J. T., and A. S. Wexler. 2005. Thermodynamics of Carbonates and Hydrates Related to Heterogeneous Reactions Involving Mineral Aerosol, *Journal of Geophysical Research* 110, D11201.
13. Pabalan, R. T., and K. S. Pitzer. 1987. Thermodynamics of Concentrated Electrolyte Mixtures and the Prediction of Mineral Solubilities to High Temperatures for Mixtures in the System Na-K-Mg-Cl-SO_4-OH-H_2O, *Geochimica et Cosmochimica Acta* 51, 2429-2443.
14. Pitzer, K. S., and C. S. Oakes. 1994. Thermodynamics of Calcium Chloride in Concentrated Aqueous Solutions and Crystals, *Journal of Chemical and Engineering Data* 39, 553-559.
15. Pitzer, K. S., and Y. Shi. 1993. Thermodynamics of Calcium Chloride in High Concentrated Aqueous Solution and in Hydrated Crystals, *Journal of Solution Chemistry* 22, 99-105.
16. Dunn, K. A., J. W. McClard, G. T. Chandler, C. W. Gardner, L. A. Worl, and G. D. Roberson. 2010. Supporting Safe Storage of Plutonium-bearing Materials through Science, Engineering, and Surveillance, *Journal of Nuclear Materials Management* Vol. 38, No. 2.
17. Almond, P., R. R. Livingston, L. E. Traver, M. J. Arnold, N. Bridges, G. F. Kessinger, and J. M. Duffey. 2010. Gas Analysis from Headspace of Plutonium-bearing Materials Packages, *Journal of Nuclear Materials Management* Vol. 38, No. 2.
18. Lide, D. R., ed. 2003. *CRC Handbook of Chemistry and Physics,* 84th ed: CRC Press.
19. Washburn, E. W., ed. 1926 - 1930;2003. *International Critical Tables of Numerical Data, Physics, Chemistry and Technology (1st Electronic Edition).* Online version available at: http://knovel.com/web/portal/browse/display?_EXT_KNOVEL_DISPLAY_bookid=735&VerticalID=0 ed: Knovel.

Evidence of Corrosive Gas Formed by Radiolysis of Chloride Salts in Plutonium-bearing Materials

D. Kirk Veirs, John M. Berg, Laura A. Worl, and Joshua E. Narlesky
Los Alamos National Laboratory, Los Alamos, New Mexico USA

Kerry A. Dunn and McIntyre R. Louthan, Jr.
Savannah River National Laboratory, Aiken, South Carolina USA

Abstract
Corrosion and pitting have been observed in headspace regions of stainless steel containers enclosing plutonium oxide/salt mixtures. These observations are consistent with the formation of a corrosive gas, probably HCl, and transport of that gas to the headspace regions of sealed containers. The NH_4Cl films found on the walls of the sealed containers is also indicative of the presence of HCl gas. Radiolysis of hydrated alkaline earth salts is the probable source of HCl.

Introduction
The U.S. Department of Energy (DOE) 3013 Standard[1] provides criteria for stabilization of plutonium-bearing materials to forms that can be packaged and placed in storage in hermetically sealed, stainless steel (SS) containers with minimal surveillance for up to fifty years. Because these materials originate from a variety of plutonium processing and disposition programs, the range of materials is extensive, ranging from nearly pure PuO_2 to impure Pu-bearing salts and compounds (PuO_2 mixed with NaCl, KCl, $MgCl_2$, $CaCl_2$ and other metal oxides). The 3013 Standard requires that, prior to packaging and storage, the materials are treated in an oxidizing atmosphere to reduce the volatile components of the stored material and to reduce the absorbed moisture to less than 0.5 weight percent. The DOE-sponsored Surveillance and Monitoring Program incorporates both field and shelf-life surveillance evaluations to monitor the condition of the storage inventory and ensure long-term safe storage of 3013 containers.[2] The field surveillance activities include non-destructive examination (NDE) and destructive examination (DE) projects currently underway at Savannah River Site (SRS). Shelf-life surveillance and material characterization are currently underway at Los Alamos National Laboratory (LANL) and Savannah River National Laboratory (SRNL) as part of the Materials Identification and Surveillance (MIS) project.

Since the inception of the Surveillance and Monitoring Program in 2003, corrosion of 300 Series stainless steels (SS), which are used as materials of construction for the 3013 containers, has been observed in both laboratory studies and in DE of 3013 containers. The corrosion is correlated with the presence of both chloride salt impurities and a relatively high humidity in the container. Corrosion has been found in both the headspace region where there is no contact between the SS and the bulk material and in the contact region where the SS is in direct contact with the bulk material. This paper specifically discusses the headspace corrosion observations and associated evidence that suggest radiolytically-produced gas-phase species may play an important role in the corrosion processes.

Materials and Methods
The results presented here involve MIS represented materials,[2] materials prepared for MIS stress corrosion cracking studies conducted at SRS,[3] and observations and characterizations carried out during DE of 3013 containers at SRS.[4] The MIS represented materials reported here are named ARF-102-85-223, PMAXBS, and PEOF1. They have been characterized for elemental compositions, actinide content, density, and specific surface area.[5] The results of gas generation studies on these materials are reported elsewhere in this issue.[6] These materials were studied in either a full-scale test container or a small-scale (1:500) test container. The full-scale test container is a modified inner 3013 container made of 316L SS. The container is four inches in diameter and approximately nine inches tall with internal volume of 2.3 liters. The lid is also made of 316L SS. The small-scale container is a 316L stainless steel container approximately 0.5 inches in diameter and 2.5 inches tall with internal volume of 5 mL. The container body is welded to a mini-Conflat flange and the lid is a modified mini-Conflat lid. An inner liner bucket made of 304L SS holds the plutonium-bearing material and fits snugly into the body of the small-scale test container. The details of the stress corrosion cracking studies[3] and the DE activities[4] are described elsewhere in this issue. The stress corrosion cracking observations included in this paper are from Series 4 tests[3] and the techniques used during DE include photography, scanning electron microscopy (SEM), elemental analysis of thin films and corrosion products using energy dispersive X-ray (EDX), and crystalline phase identification using X-ray diffraction (XRD).

Results

Observations from MIS Shelf-life Studies

As part of its mission to provide technical information to support safe storage of plutonium-bearing materials, the MIS project has conducted numerous laboratory investigations of gas generation and corrosion in sealed stainless steel test containers loaded with pure and impure plutonium oxide materials. Specimen and container exposure times ranged from months to years. Most studies have included deliberate addition of moisture up to the allowed limit of 0.5 wt. percent by exposing the material to a humid atmosphere prior to sealing. Corrosion has been observed on 300 Series stainless steel (SS) container walls and test coupons when impure plutonium oxide materials containing chlorides with added moisture are sealed into the containers. These observations of corrosion include interesting differences between the headspace region where there is no contact between the SS and the bulk material and the contact region where the SS is in direct contact with the bulk material. The observed differences include a clear demarcation between headspace region and contact region (Figure 1a[7] and f[3]). The corrosion in the headspace region can be extensive, especially around the heat affected zone (HAZ) of welds (Figure 1b, c and e[3]), and the headspace region can also have broad discoloration as well as corrosion (Figure 1a[7], b and d). Details of the observations and analyses may be found in the referenced reports.

Surveillance Program Destructive Examination Observations

The Surveillance and Monitoring Program's DE of 3013 containers from the storage inventory has been described and a compendium of results presented in this issue.[2,4,8] One of these DEs (3013 container H004111) produced several interesting observations in the headspace region that are relevant to the question of whether gas-phase corrosive species could exist in some containers. The relevant information concerning the chemical composition of the contained material and the gas composition at the time of the evaluation is given in Table 1. The observations of the conditions of the convenience container and the inner container are:

Convenience container

1. A coating was observed on the wall of the convenience container in the headspace region but not in the region where the container wall was in contact with the plutonium bearing materials, Figure 2a;
2. The convenience container coating contained Cl but not Na, K, Mg,Ca, or Pu, Figure 2b;
3. X-ray diffraction analysis of convenience container coating detected only NH_4Cl.[4]
4. No pitting corrosion was observed under the convenience container coating.[4]
5. Pitting was observed on the convenience container lid, Figure 2c, and the corrosion products associated with the pit contained Cl but not Na, K, Mg, or Ca, Figure 2d.

Inner container

1. Corrosion was observed in an annular pattern on the inner surface of the inner container lid, Figure 3a.
2. Corrosion on the inner container lid includes pitting, Figure 3b, c, and d.
3. Corrosion products associated with the pits contain Cl and the major elements found in stainless steel, but not Na, K, Mg, Ca, or Pu, Figure 3e.

Discussion

Pitting corrosion of stainless steel container surfaces in direct contact with salt-bearing plutonium oxide material has been observed in some cases and is thought to be due to deliquesced chlorides of magnesium and calcium, which are a minor constituent (<1 percent) of processing salts.[3] The relative humidity in gloveboxes during packaging of 3013 containers is too low for deliquescence of NaCl or KCl to occur.[9] Deliquescence of the alkaline earth chlorides could conceivably play a role in corrosion in the headspace regions through a dusting of small particles that will inevitably occur when handling these fine powders. However, the observations of even discoloration (Figure 1a), corrosion within crevices (Figure 1c), corrosion covering large areas (Figure 1b, e, and f), and extensive headspace corrosion when moisture loading is extreme (Figure 1d) collectively suggest the participation of gas phase species may be important in the corrosion processes in the headspace regions.

The surveillance DE provides more specific evidence that HCl is the crucial species involved in the corrosion process. The detection of Cl but not the bulk salt cations Na, K, Mg, or Ca in the convenience container wall deposits, and in the corrosion pits on the convenience and inner container lids suggest that significant Cl reached the headspace surfaces in a form other than as one of the chloride salts found in the bulk material. Gas-phase HCl could plausibly be formed within the material for reasons detailed below and, because HCl is volatile, it could transport Cl to the corrosion sites in the headspace and increase the corrosion potential at these locations.

The identification of NH_4Cl deposited on the convenience container surface in the headspace region is direct evidence that both NH_3 and HCl were present in the gas phase within the container. The argument for the existence of these gaseous species is thermodynamic. Solid ammonium chloride does not sublime to molecular NH_4Cl to any significant extent, but rather sublimes dissociatively to gas-phase NH_3 and HCl through the reversible decomposition reaction

$$NH_4Cl(s) \leftrightarrows NH_3(g) + HCl(g). \qquad (1)$$

The sublimation equilibrium constant, equal to the product of the pressures of the two gases ($K_P=P_{NH3}\cdot P_{HCl}$), ranges from 6 to 730 ppb^2 between 15 and 35°C[10] (typical headspace tempera-

Figure 1. Examples of differences between headspace region corrosion and contact region corrosion: (a) 304L inner bucket from a small-scale test container where headspace region (left of the vertical line) is characterized by discoloration and large number of small pits and contact region (right of the vertical line) is characterized by large pits on a shiny surface, material – ARF-102-85-223 (b) headspace region of fill-scale test containers showing 316L lid with HAZ and large patches of corrosion and pitting, the contact region is shiny with no corrosion, material – PMAXBS (c) lid section of a Lawrence Livermore National Laboratory inner container of 316L SS that was suspended in head-space region of a full-scale test container showing extensive corrosion in the crevice (lid section is opened for observation) between lid and wall, material – PMAXBS (d) headspace region of small-scale test container body made of 316L SS showing massive corrosion, material – PEOF1 with 5 wt percent $CaCl_2$, (e) teardrop coupon of 304L that was positioned in headspace region of the corrosion tests showing extensive corrosion in heat affected zone around weld, material – Series 4 and (f) flat coupon of 304L SS from a corrosion test where the top half is in headspace region and bottom half is in contact region illustrating the boundary between them, material – Series 4.

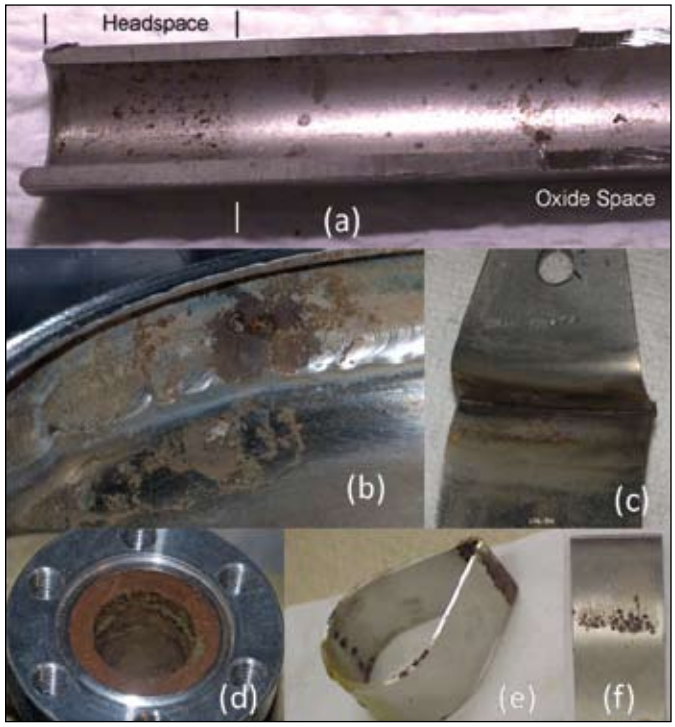

tures are below 60°C). If NH_4Cl exists in a closed system with no sources or sinks for NH_3 or HCl then each gas will have a partial pressure equal to the square root of the equilibrium constant, or 2.4 to 27 ppb over this temperature range. If either NH_3 or HCl gas are involved in other reactions within the system, their individual pressures may become unequal, but their product must still satisfy the equilibrium equation if NH_4Cl is present. Consequently, the presence of NH_4Cl guarantees that both NH_3 and HCl existed in the headspace of this container before it was opened.

The specific location of NH_4Cl as a coating on the container surface in the headspace region strongly suggests that it formed

Figure 2. Observations of the conditions on the inside surfaces of the convenience container from destructive examination of 3013 container H004111: (a) a composite of photographs of the wall, (b) EDX spectrum of the thick film, (c) SEM of a corroded region on the lid, and (d) EDX spectrum of the corrosion products associated with a pit on the lid.

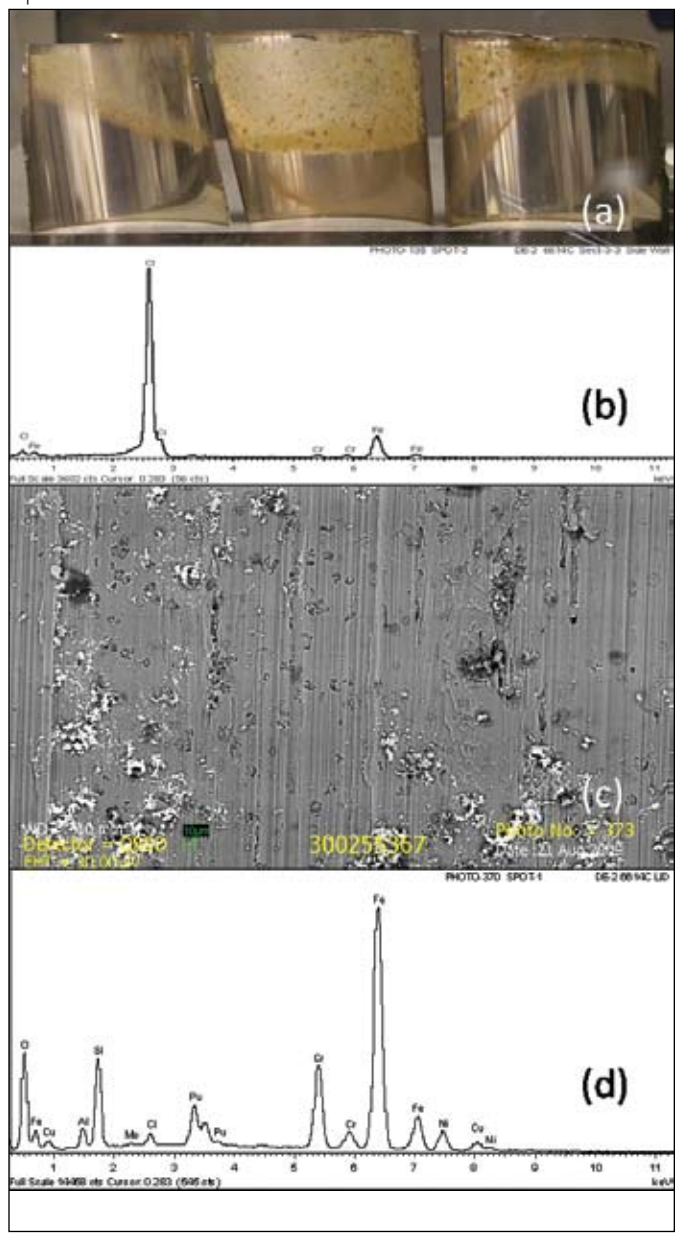

within the container from gas-phase reactants, with HCl and NH_3 being the obvious candidates. It is highly doubtful that the primary source of either gas could have been NH_4Cl that existed in the material at the time of packaging because NH_4Cl would not have survived high temperature calcination. However, there are plausible mechanisms for formation of NH_3 and HCl gases through radiolysis reactions of known constituents of the contained material.

Figure 3. Observations of the conditions on the inside surfaces of the inner container from destructive examination of 3013 container H004111: (a) photograph of the inner surface of the lid showing an annular pattern of corrosion, (b) SEM of the annular corroded region showing pitting pattern associated with the machining grooves, (c) SEM showing a pit with corrosion product, (d) SEM of the annular corroded region showing clustering of pits along the machining groove, and (e) EDX of corrosion product shown in (c).

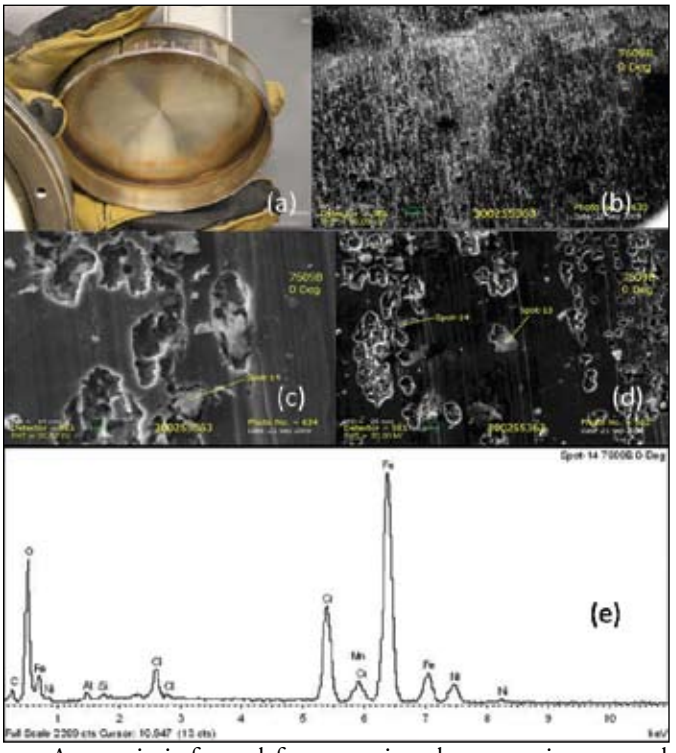

Ammonia is formed from reactions between nitrogen and hydrogen in the gas phase.

$$N_2(g) + 3H_2(g) \rightarrow 2NH_3(g) \qquad (2)$$

The reaction when used industrially to produce ammonia typically includes a catalyst and is carried out at temperatures above 400°C and pressures above 100 atmospheres. Radiation induced ammonia formation has been observed in tritium systems,[11] in laboratory experiments with gamma radiation[12] and during alpha radiation with G_{NH3} of 1 (1 molecule of NH_3 formed for every 100 eV of adsorbed radiation)[13] so the formation of NH_3 could occur in the 3013 containers when N_2 and H_2 gases are present. The gases N_2 and H_2 comprise over 60 percent by volume of the gases observed in this container at the time of opening, Table 1. It is therefore reasonable to assume that ammonia is formed by radiolysis from the gases within the container over time.

The most likely source of HCl is the hydrolysis of alkaline earth chloride salts in the stored material. The behavior of $MgCl_2 \cdot 6H_2O$ upon heating at ambient pressure has been extensively studied.[14-17] Two final products are possible.

Table 1. Data from container H004111 (FY09 DE#2)

Date inner container welded	12/3/2003
Date opened	9/30/2008
Elemental contents in weight percent	
Actinides	72
Cl	5.8
Na	1.9
K	3.0
Mg	0.7
Ca	0.06
Gas composition, vol percent	
He	34
H_2	22
N_2	44
O_2	0

$$MgCl_2 \cdot 6H_2O(s) \xrightarrow{\text{heat}} MgO(s) + 2HCl(g) + 5H_2O(g) \qquad (3)$$

$$MgCl_2 \cdot 6H_2O(s) \xrightarrow{\text{heat}} MgCl_2(s) + 6H_2O(g) \qquad (4)$$

The intermediate products MgOHCl and $Mg(OH)_2$ proceed to MgO upon further heating and are considered as part of reaction (3) for our purposes. The chemistry is complex and the branching ratio between reaction 3 and 4 varies considerably with conditions, although reaction 3 tends to dominate. It is difficult to make anhydrous $MgCl_2$ thermally without a substantial overpressure of HCl(g).

The thermal behavior of $CaCl_2 \cdot xH_2O(s)$ (where x is 2 or 4) at ambient pressure is simpler than the thermal behavior of $MgCl_2 \cdot 6H_2O$. Hydrated calcium chloride loses all waters of hydration to form anhydrous $CaCl_2$ before the temperature is sufficiently high for detectable hydrolysis to occur. However, at elevated temperatures when water vapor is available calcium chloride solid undergoes hydrolysis to form HCl and calcium oxide.[18]

$$CaCl_2 \cdot xH_2O(s) \xrightarrow{\text{heat}} CaCl_2(s) + xH_2O(g) \qquad (5)$$

$$CaCl_2(s) + H_2O(g) \xrightarrow{T>500°C} CaO(s) + 2HCl(g) \qquad (6)$$

The observation of HCl during thermograve; metric analysis/Fourier transform infrared specrtoscopy(TGA/FTIR) determination of water in samples from material post calcination is attributed to reaction (3) and/or (6).[19-20]

The radiolysis products from gamma (γ) and alpha (α) irradiation of $CaCl_2 \cdot 2H_2O(s)$, $CaCl_2 \cdot 6H_2O(s)$, $MgCl_2 \cdot 2H_2O(s)$ and $MgCl_2 \cdot 6H_2O(s)$ have been studied.[21-22] Hydrogen is found in the gas phase. Neither study had the experimental capability to observe either $Cl_2(g)$ or HCl(g), however, in the γ radiolysis of

$CaCl_2$ with low water loadings some Cl_2 was observed trapped in the solid.

The chemistry of the alkaline earth chlorides supports the possibility of formation of HCl during α radiolysis, but in studies of the radiolysis of these salts no attempt to observe HCl has been conducted because it is extremely reactive and difficult to detect. In shelf-life studies, pH paper was used to assess the possibility of an acidic atmosphere above plutonium oxide materials that contained hydrated alkaline earth chlorides. The pH paper showed an acidic environment and registered pH values between 1 and 4.

The NH_4Cl deposit on the convenience container wall of H004111 appears to be significantly thicker immediately above the material than higher in the headspace. This indicates that at the time the deposition occurred the concentration of NH_3, HCl, or both gases was higher near the material surface than at the top of the headspace region. This is consistent with the formation of one or both gases within or very close to the material bed and subsequent diffusion to other regions where only depletion reactions can occur. The ammonia, if formed by α radiolysis of the N_2 and H_2 gases present, will be formed within and up to 1 to 2 cm from the top of the material. The hydrochloric acid, if formed by α radiolysis of the alkaline earth chlorides present, will be formed within the material.

In this hypothesis HCl and NH_3 are produced by independent reactions from different reactants so one gas will almost certainly be in excess after NH_4Cl condensation proceeds to equilibrium. The gas in excess would be free to diffuse higher up in the headspace of the convenience container and diffuse through the filter and into the inner container, where it could then interact with the inner container lid. The existence of pitting and associated chloride corrosion products on the inner container lid suggests that HCl is the gas produced in excess in this particular container.

Water vapor and the relative humidity inside the sealed container also play important roles in gas generation/corrosion process.[3] The relative humidity within this container at the time of opening has been determined to be 11 percent.[9] At this relative humidity, the water and HCl vapor present within the container may condense sufficiently in the colder portions of the container to react and form the pits that are observed on the inner container lid. These pitted regions are the areas that are most accessible to vapors coming through the filter and that region should be colder than the side wall of the container.[3] The annular corroded region seen in Figure 3a should also be cooler than the rest of the lid.

Pitting is observed within this container on the lids of the convenience and inner containers and not on the walls. It is possible that material surface properties of the walls are different than material surface properties of the lids. The bodies of the inner and convenience container are flow-formed and the lids are plate machined to size.[23] The machining operations, which include cutting to remove metal, significantly work hardens a volume of metal immediately beneath the machined surface by cold work. The depth of this work-hardened layer depends on machining variables including tool sharpness, depth of cut, cutting rate and nature of surface lubrication. Microhardness measurements on cross-sections from machined surfaces of 300 series austenitic stainless steels have shown that the work hardened layer beneath the surface may extend 0.25 mm into the metal.[24] Types 304 and 304L stainless steels are very prone to surface hardening because these steels partially transform to martensitic phases during room temperature plastic deformation. Alpha prime (body centered cubic) and epsilon (hexagonal close packed) martensite phases are generally both formed.[25] This highly deformed surface layer is very susceptible to pitting and can serve as an initiation site for stress corrosion cracking.[26] The characteristics of this cold worked surface layer will play a role in any surface initiated corrosion processes and will influence the observations made during the surveillance and monitoring programs. Therefore, determination of the significance of corrosion observations must include considerations of the cold worked layer on container lids and side walls.

Conclusion

The DOE 3013 Standard identifies two potential mechanisms for container degradation: internal pressurization and corrosion.[1] However, if the plutonium oxide-salt bearing material has been properly processed and stored following the DOE-STD-3013 storage standard, there are no pressurization concerns.[6] The remaining concern is the formation of localized corrosion events within the hermetically sealed containers. The conditions for corrosion are controlled by the salt phase, moisture and corresponding relative humidity inside the storage container. Ionizing radiation (alpha particles) may result in acidic gas production such as HCl in these plutonium salt environments and HCl could be a significant factor in headspace corrosion. The generation of NH_3 when N_2 and H_2 are present would lead to the generation of the weak base NH_4Cl, which has a low vapor pressure and a high deliquescence relative humidity. The ammonium chloride deposits are evidence that HCl can be present in the headspace of a container in storage. The HCl is a potential mode for gas-phase chloride transport from the convenience container to the observed corrosion sites on the inner surfaces of the inner container. Transport via HCl is consistent with the absence at the corrosion sites of salt cations originally associated with the chloride in the packaged material. However, despite the formation of an apparent corrosive gas and the potential for corrosion in regions outside the contained material, these conditions have not led to formation of large through wall corrosion pits or stress corrosion cracking. The headspace corrosive conditions result in only small shallow pitting events that should not produce a through-wall corrosion event within a fifty year storage life.[7,27] This, in combination with an extremely robust container design will assure the

ongoing safe storage of these materials within 3013 containers. These conclusions are expected to be confirmed through continuing surveillance of the 3013 storage inventory.

D. Kirk Veirs is a staff scientist at Los Alamos National Laboratory. He has a Ph.D. in physical chemistry from Pennsylvania State University and a B.S. in chemistry and environmental science from Northern Arizona University.

John M. Berg is a staff scientist at Los Alamos National Laboratory. He has a Ph.D. in chemistry from Princeton University and a B.A. in chemistry from St. John's University.

Kerry A. Dunn is an advisory engineer at the Savannah River National Laboratory. She has an M.S. in Materials Science and Engineering and a B.S. in Metallurgy from Pennsylvania State University.

M. R. Louthan, Jr. is a retired consulting scientist at Savannah River National Laboratory. He has a Ph.D. in Materials Science and Engineering from University of Notre Dame.

Laura A. Worl is a project manager at Los Alamos National Laboratory. She has a Ph.D. in chemistry from the University of North Carolina and a B.S. in chemistry, Magna Cum Laude, from the University of Delaware.

Joshua E. Narlesky is a research and development scientist at Los Alamos National Laboratory. He received his B.S. from New Mexico Institute of Mining and Technology and his M.S. from Colorado State University, both in chemical engineering.

Acknowledgements

Funding for this work was provided by the Surveillance and Monitoring Program, U.S. Department of Energy Office of Environmental Management. This work was conducted at Los Alamos National Laboratory operated by Los Alamos National Security, LLC under contract DE-AC52-06NA25396 and at the Savannah River Site and Savannah River National Laboratory operated by Savannah River Nuclear Solutions for U.S. Department of Energy under contract DE-AC09-08SR22470.

References

1. *Stabilization, Packaging, and Storage of Plutonium-bearing Materials.* 2004. DOE-STD-3013-2004. U.S. Department of Energy: Washington, D.C.
2. Dunn, K. A., J. W. McClard, G. T. Chandler, C. W. Gardner, L. A. Worl, and G. D. Roberson. 2010. Supporting Safe Storage of Plutonium-bearing Materials through Science, Engineering, and Surveillance, *Journal of Nuclear Materials Management* Vol. 38, No. 2.
3. Veirs, D. K., L. A. Worl, J. M. Berg, P. E. Zapp, J. M. Duffey, P. S. Lam, and K. A. Dunn. 2010. Relative Humidity and the Susceptibility of Austenitic Stainless Steel to Stress-corrosion Cracking in an Impure Plutonium Oxide Environment, *Journal of Nuclear Materials Management* Vol. 38, No. 3.
4. Nelson, D. Z., G.T. Chandler, K.A. Dunn, T. M. Stefek, and M. E. Summer. 2010. Stainless Steel Interactions with Salt Containing Plutonium Oxides, *Journal of Nuclear Materials Management* Vol. 38, No. 3.
5. Permalinks to the material datasheets are
ARF-102-85-223: http://permalink.lanl.gov/object/view?what=info:lanl-repo/lareport/LA-UR-09-07116
PMAXBS: http://permalink.lanl.gov/object/view?what=info:lanl-repo/lareport/LA-UR-09-07129
PEOF1: http://permalink.lanl.gov/object/view?what=info:lanl-repo/lareport/LA-UR-09-07130
6. Duffey, J. M., D. K. Veirs, R. R. Livingston, and J. M. Berg. 2010. Pressure Development in Sealed Packages Containing Plutonium-bearing Materials, *Journal of Nuclear Materials Management* Vol. 38, No. 3.
7. Veirs, D. K., L. A. Worl, D. M. Harradine, M. A. Martinez, R. S. Lillard, D. S. Schwartz, C. V. Puglisi, D. D. Padilla, A. Carrillo, R. E. McInroy, and A.R. Montoya. 2004. Gas Generation and Corrosion in Salt-containing Impure Plutonium Oxide Materials: Initial Results for ARF-102-85-223, *LA-UR-04-1788,* Los Alamos National Laboratory: Los Alamos, N.M., USA.
8. Almond, P., R. R. Livingston, L. E. Traver, M. J. Arnold, N. Bridges, G. F. Kessinger, and J. M. Duffey. 2010. Gas Analysis from Headspace of Plutonium-bearing Materials Packages, *Journal of Nuclear Materials Management* Vol. 38, No. 3.
9. Berg, J. M., N. K. Gupta, B. Nguyen, J. E. Narlesky, F. C. Prenger, L. E. Traver, and D. K. Veirs. 2010. Thermal Gradients and the Potential to Form Liquids in 3013 Containers, *Journal of Nuclear Materials Management* Vol. 38, No. 3.
10. Pio, C. A. and R. M. Harrison. 1987. The Equilibrium of Ammonium Chloride Aerosol with Gaseous Hydrochloric Acid and Ammonia under Tropospheric Conditions, *Atmospheric Environment,* 21, 1243.
11. Heung, L.K. 1994. Tritiated Ammonia Formation, *WSRC-TR-0132,* Savannah River Technology Center, Aiken, S.C., USA.
12. Cheek, C. H., and V. J. Linnenbom. 1958. The Radiation-induced Formation of Ammonia, *Journal of Physical Chemistry* 62, 1475.

13. Bryan, S. A., and L. R. Pederson. 1995. Thermal and Combined Thermal and Radiolytic Reactions Involving Nitrous Oxide, Hydrogen, and Nitrogen in the Gas Phase: Comparison of Gas Generation Rates in Supernate and Solid Fractions of Tank 241-SY-101 simulated waste, *PNL-10490,* Pacific Northwest Laboratory: Richland, WA.
14. Shoval, S., and S. Yariv. 1985. The Effect of Alkali-chloride on the Thermal Hydrolysis of Hydrated Magnesium-chloride, *Thermochimica Acta* 92, 819-822.
15. Kirsh, Y., S. Yariv, and S. Shoval. 1987. Kinetic analysis of thermal dehydration and hydrolysis of $MgCl_2 \cdot 6H_2O$ by DTA and TG, *Journal of Thermal Analysis* 32, 393-408.
16. Galwey, A. K., and G. M. Laverty. 1989. The Thermal Decomposition of Magnesium Chloride Dihydrate, *Thermochimica Acta* 138, 115-127.
17. Kashani-Nejad, S., K.-W. Ng, and R. Harris. 2005. MgOHCl Thermal Decompostion Kinetics, *Metallurgical and Materials Transactions* B 36B, 153-157.
18. Kondo, H., Z. Asaki, and Y. Kondo. 1978. Hydrolysis of Fused Calcium Chloride at High Temperature. *Metallurgical Transactions B* 9, 477-483.
19. Berg, J. M. 2005. Re-analysis of RFETS PuSPS TGA-FTIR Moisture Measurement Data, *LA-UR-05-7395;* Los Alamos National Laboratory: Los Alamos, N.M., USA.
20. Baca, G., J. Berg, M. Martinez, L. Peppers, D.K. Veirs, C. Williams, and L. Worl. 2009. Acid Gas Evidence in Stabilized Material, in *3013 Surveillance and Monitoring Program Review* pages 2 - 7, *LA-UR-09-01498;* Los Alamos National Laboratory: Los Alamos, N.M.
21. LaVerne, J. A., and L. Tandon. 2005. H_2 and Cl_2 Production in the Radiolysis of Calcium and Magnesium Chlorides and Hydroxides, *Journal of Physical Chemistry* 109, 2861-2865.
22. Kelm, M. and E. Bohnert. 1996. Radiolytic Compounds Formed by Dissolution of Irradiated NaCl and $MgCl_2 \bullet 6H_2O$ in Water, *Radiochimica Acta* 74, 155-158.
23. Dunn, K.A., M. R. Louthan, Jr., G. B. Rawls, R. L. Sindelar, P. E. Zapp, J. W. McClard. 2010. Container Materials, Fabrication, and Robustness, *Journal of Nuclear Materials Management* Vol. 38, No. 3.
24 Outokumpu International Steel Company. 2008. Machinability and Work Hardening, http://www.outokumpu.com/pages/Page 5763.aspx.
25. ASM Specialty Handbook: Stainless Steels. 1994. ASM International, Materials Park, Ohio, p. 186.
26. M. Koshiishi, H. Fujimori, M. Okada and A. Hirano. 2008. Hitachi's Activities for Suppression of Stress Corrosion Cracking, http://www.hitachi.com/ICSFiles/afieldfile/2009/04/28/r2009_02_108.pdf, p. 90.
27. Lillard, R. S., D. G. Kolman, M. A. Hill, M. B. Prime, D. K. Veirs, L. A. Worl, and P.E. Zapp. 2009. Assessment of Corrosion-Based Failure in Stainless Steel Containers Used for the Long-Term Storage of Plutonium-Based Salts, *Corrosion* 65, 175–186.

Pressure Development in Sealed Containers with Plutonium-bearing Materials

Jonathan M. Duffey
Savannah River National Laboratory, Aiken, South Carolina USA

D. Kirk Veirs and John M. Berg
Los Alamos National Laboratory, Los Alamos, New Mexico USA

Ronald R. Livingston
Savannah River Nuclear Solutions, Aiken, South Carolina USA

Abstract

Gas generation by plutonium-bearing materials in sealed containers has been studied. The gas composition and pressure are determined over periods from months to years. The Pu bearing materials studied represent those produced by all of the major processes used by the U.S. Department of Energy (DOE) in the processing of plutonium and include the maximum amount of water (0.5 percent by weight) allowed by DOE's 3013 Standard. Hydrogen generation is of high interest and the Pu bearing materials can be classed according to how much hydrogen is generated. Hydrogen generation by high purity plutonium oxides packaged under conditions typical for actual 3013 materials is minimal, with very low generation rates and low equilibrium pressures. Materials with chloride salt impurities have much higher hydrogen gas generation rates and result in the highest observed equilibrium hydrogen pressures. Other materials such as those with high metal oxide impurities generate hydrogen at rates in between these extremes. The fraction of water that is converted to hydrogen gas as equilibrium is approached ranges from 0 percent to 25 percent under conditions typical of materials packaged to the 3013 Standard. Generation of both hydrogen and oxygen occurs when liquid water is present. The material and moisture conditions that result in hydrogen and oxygen generation for high-purity plutonium oxide and chloride salt-bearing plutonium oxide materials have been characterized. Other gases that are observed include nitrous oxide, carbon dioxide, carbon monoxide, and methane.

Introduction

Since the end of the Cold War, the disposition of surplus plutonium-bearing materials that are no longer needed for nuclear weapons production has become an increasing mission for the U.S. Department of Energy (DOE). The safe packaging, transportation, and storage of surplus plutonium materials are required until disposition processes are implemented. Since disposition of weapons grade plutonium involves complex international agreements, storage times for material awaiting disposition may be many decades.

Nuclear materials are typically packaged in sealed containers for transportation and storage to prevent the spread of radioactive contamination. The sealing of the storage containers also provides a potential for pressurization that might lead to loss of containment of the contents. Thus, pressure development during storage has been an important consideration. Pressure buildup in sealed containers of plutonium-bearing materials may result from several causes including: (1) temperature increase of the container and contents after sealing (minor effect), (2) helium production from alpha decay of the packaged material (minor effect), and (3) gases evolved due to desorption from the contained materials, radiolysis of water or other decomposable compounds, or chemical reactions that may produce one or more gaseous species (potentially major effect).

The DOE-STD-3013 contains requirements for the stabilization, packaging and safe storage of plutonium-bearing metals and oxides containing 30 wt percent or more of plutonium plus uranium.[1] This standard requires stabilized plutonium-bearing materials to be packaged in two individually welded, nested containers where the minimum design pressure of the outer container is 4920 kPa. According to DOE-STD-3013, "The only evolved gas of significance anticipated during extended storage is hydrogen from decomposition of adsorbed water." The standard assumes that oxygen is not produced in any significant quantity by radiolysis or chemical reaction, and that oxygen present at the time of packaging is consumed by recombination with hydrogen or reaction with the packaged contents. Because DOE-STD-3013 conservatively assumes that all the adsorbed water associated with the packaged material is either desorbed or converted to hydrogen gas, the water content of materials packaged in the 3013 storage container is limited to 0.5 wt percent or less to ensure the container does not exceed an internal pressure of 4920 kPa.

Existing literature appears to suggest that gas generation from high-purity plutonium oxide packaged in accordance with

the 3013 Standard could range from minimal hydrogen steady-state pressures[2-5] to explosive high-pressure mixtures of hydrogen and oxygen.[6] Although there is minimal literature information concerning gas generation for plutonium oxide materials with chloride salt impurities, hydrogen production is observed in the gamma and helium ion radiolysis of magnesium and calcium chlorides[7] and in the gamma irradiation of NaCl and $MgCl_2 \cdot 6H_2O$.[8] In order to clarify the gas generation behavior of materials packaged according to the 3013 Standard, the standard recommends establishment of an experimental program tasked with determining the gas generation behavior of representative materials.[9] This paper presents the results of the gas generation studies on a range of materials specifically chosen to be representative of the full range of materials actually stored in 3013 containers to date. Additional studies using prepared materials are included when needed to clarify important observations such as the conditions required to generate both hydrogen and oxygen.

Experimental

Savannah River National Laboratory (SRNL) and Los Alamos National Laboratory (LANL) have been collaborating in studies of gas generation by samples of plutonium oxide material representative of material to be stored in 3013 containers, or known to be intended for storage. Each laboratory has prepared samples of pure and impure PuO_2, added moisture to them, sealed the material into test containers, and monitored gases for periods of months to years. Because these studies are conducted differently at the two sites, they are described separately below.

MIS Shelf-Life Studies

In the Materials Identification and Surveillance (MIS) Shelf-Life Studies conducted at LANL, gas pressures and compositions are monitored over periods of months to years for Pu-bearing materials stored in full-scale (i.e., 3013 size) and small-scale (1:500 scale) test containers. The full-scale test container is a 316L stainless steel cylinder four inches in diameter and approximately nine inches tall with internal volume of 2.3 liters. This container reproduces size, shape, and materials of construction of a typical production 3013 inner container. The container is instrumented with thermocouples, a pressure transducer, a Raman chamber, and a gas manifold. The gas manifold is used to extract 5-mL gas samples for gas chromatography (GC) analysis with a thermal conductivity detector (Agilent 6890). The Raman chamber allows measurement of all gases except He without extracting a gas sample. The sensitivity for both methods was approximately 0.1 kPa. The GC was calibrated for He, H_2, N_2, O_2, CO_2, CO, and N_2O.

The MIS small-scale test container is a 316L stainless steel container approximately 0.5 inches in diameter and 2.5 inches tall with internal volume of 5 mL. The small-scale container is approximately a 1:500 scale version of the inner 3013 container. Fifty-microliter gas samples are extracted through a gas manifold and analyzed using a GC (Agilent 5890) calibrated for the same gases evaluated in the large-scale sample studies. Each container is instrumented with a pressure transducer. Nine small-scale containers are placed in a heated aluminum block and five aluminum blocks are held in an insulated tray to form the small-scale array with a total capacity of forty-five simultaneous experiments. Each aluminum block is temperature regulated at 55°C.

The small-scale containers are loaded with samples having a range of impurity compositions and processing histories representative of the full diversity of oxide material stored in 3013 containers. The distinguishing emphasis is on understanding the material-dependent aspects of gas generation, so other parameters such as moisture content, temperature, and free gas volume, are varied as little as possible. Each experiment is designed to have an equal total moisture content of 0.5 wt percent when the test begins. The initial moisture content of each material is measured by mass loss of a sample heated to 200°C and adding 0.07 wt percent for residual water not lost at 200°C. Then the moisture content of the material is adjusted up to 0.5 wt percent by exposing the material to humid air and monitoring the weight gain until it reaches the target value. The uncertainty in the moisture content is estimated to be 0.05 wt percent.

Small-scale Corrosion Studies with Gas Analysis

Laboratory-scale studies conducted at SRNL were designed to investigate the corrosivity of moist plutonium oxide/chloride salt (PuO_2/Cl^-) mixtures on 304L and 316L stainless steel coupons.[10,11] They are relevant to this paper because internal test container pressures and final gas compositions were measured as part of these tests. These experiments were conducted with PuO_2 obtained by anion exchange and oxalate precipitation of Pu from nitric acid solutions followed by calcination in air to 950°C for two hours to convert to the oxide. PuO_2 prepared in this way was of two different isotopic compositions – a "weapons grade" composition with a specific decay heat of 2.3 W/kg Pu and a "high-alpha" composition, consisting of "fuel grade" material doped with ^{238}Pu and ^{241}Am, with a specific decay heat of 5.1 W/kg Pu (Table 1).

Table 1. Isotopic composition of PuO_2 Used in SRNL corrosion tests

Material	Isotope (wt percent)						Decay Power
	Pu-238	Pu-239	Pu-240	Pu-241	Pu-242	Am-241	(W/kg Pu)
Weapons Grade	0.013	93.6	6.2	0.15	0.02	–	2.3
Increased α-dose	0.38	83.3	15.2	0.80	0.02	0.32	5.1

Table 2. MIS represented material with report references. NA – reports not available.

MIS Sample Item	Pu/U (percent)	Cl	Source Site	Characterization Report	Pressure and Composition Report
SCP711-56	17/69		LANL	LA-UR-09-07099	LA-UR-09-07149
TS707013	69.7/0	Y	RFETS	LA-UR-09-07100	LA-UR-09-07167
63-88-06-121	35/0		HANFORD	LA-UR-09-07101	NA
64-85-12-1858	32.7/0		HANFORD	LA-UR-09-07102	LA-UR-09-07171
011589A	77.7/0	Y	RFETS	LA-UR-09-07103	LA-UR-09-07151[a] LA-UR-09-07152[a]
053038	62.6/0	Y	RFETS	LA-UR-09-07104	LA-UR-09-07153[a]
669194	13.8/69		RFETS	LA-UR-09-07105	LA-UR-09-07138
1000089	84.6/0		RFETS	LA-UR-09-07106	LA-UR-09-07150[a]
5501407	65.7/11		RFETS	LA-UR-09-07107	LA-UR-09-07141
5501579	88.1/0		RFETS	LA-UR-09-07108	LA-UR-09-07136
07032282A	69.4/0	Y	RFETS	LA-UR-09-07109	LA-UR-09-07169
07161856	84/0		RFETS	LA-UR-09-07110	LA-UR-09-07134
07242141A	69.7/0		RFETS	LA-UR-09-07111	LA-UR-09-07156[a]
07242165A	34/0		RFETS	LA-UR-09-07112	LA-UR-09-07155
07242201A	63.5/0		RFETS	LA-UR-09-07113	LA-UR-09-07140
520610020	33.7/0	Y	RFETS	LA-UR-09-07114	LA-UR-09-07154[a]
ARF-102-85-114-1	86.3/0		HANFORD	LA-UR-09-07115	LA-UR-09-07173
ARF-102-85-223	67/0	Y	HANFORD	LA-UR-09-07116	LA-UR-09-07144
ARF-102-85-295	28-40/0	Y	HANFORD	LA-UR-09-07117	LA-UR-09-07174 LA-UR-09-07175
ARF-102-85-355	69.5/0		HANFORD	LA-UR-09-07118	LA-UR-09-07158
BLO-39-11-14-004	87.5/0		HANFORD	LA-UR-09-07119	LA-UR-09-07146
ARF-102-85-365	65.9/0	Y	HANFORD	LA-UR-09-07120	LA-UR-09-07159
C00024A	73.4/0	Y	RFETS	LA-UR-09-07121	LA-UR-09-07163
C00695	73.9/0	Y	RFETS	LA-UR-09-07122	LA-UR-09-07166
CAN92	82.6/2.8		RFETS	LA-UR-09-07123	LA-UR-09-07162
C06032A	74/0	Y	RFETS	LA-UR-09-07124	LA-UR-09-07143
CLLANL025	77.7/0	Y	RFETS	LA-UR-09-07125	LA-UR-09-07139
MISSTD-1A	85/0		LANL	LA-UR-09-07126	LA-UR-09-07180
MT-1490	78/0		RFETS	LA-UR-09-07127	LA-UR-09-07137
PBO-47-09-012-023	88/0		HANFORD	LA-UR-09-07128	LA-UR-09-07157
PMAXBS	68/0	Y	LANL	LA-UR-09-07129	LA-UR-09-07177
PEOF1	86/0		LANL	LA-UR-09-07130	LA-UR-09-07178
PSU-84-06-05	14.4/65.1		HANFORD	LA-UR-09-07131	LA-UR-09-07147
TS707001	87/0		RFETS	LA-UR-09-07132	LA-UR-09-07135
PuF4-1	72/0		LANL	LA-UR-09-07133	LA-UR-09-07176
R441	67/0		HANFORD	NA	LA-UR-09-07148
R438	28.1/0		HANFORD	NA	LA-UR-09-07161[a]
41-85-08-1379B	41/0		HANFORD	NA	LA-UR-09-07170

[a] These samples experienced a temperature excursion from December 3, 2007, to December 10, 2007, to between 146°C and 154°C.

Mixtures of NaCl, KCl, $MgCl_2$, and $CaCl_2$ were prepared by combining the desired amounts of each salt in a dry argon glovebox. The dry salt mixtures were heated in a static air atmosphere to between 820°C and 850°C for two hours, then ground and pre-weighed into screw-cap glass vials in the dry argon glovebox. The salt mixtures were combined with pre-weighed amounts of PuO_2, heated in a static air atmosphere at 850°C for two hours, and stored in screw-lid glass jars inside sealed plastic bags until ready for use.

PuO_2/salt mixtures and corrosion test coupons were loaded into test containers in a He-purged glove bag deployed inside a radiological glovebox. The glove bag was purged with dry He until the relative humidity was below 10 percent. PuO_2/salt mixtures (20 to 30 g) were then weighed into glass inserts containing the corrosion test coupons and placed in small stainless steel pans for ease of handling during moisture uptake. The relative humidity in the glove bag was gradually increased by bubbling He through distilled water. Sample sets were weighed periodically until the weight gain corresponded to a water uptake of approximately 0.3 wt percent for the sample of pure PuO_2 and from 0.5 to 0.6 wt percent for salt-containing materials. The maximum relative humidity required for samples to reach the target moisture loading in an eight-hour period ranged from 50 percent to 94 percent. Test materials were packaged in He at ambient pressure in stainless steel test containers equipped with a pressure transducer and a micro-valve for gas sampling. Each container with the oxide/salt mixtures and coupons in place had a free volume of 100 ± 5 mL.

The sealed containers were stored at ambient temperature for extended times while their pressures were monitored. At the end of each test, the container headspace was diluted with He, sampled, and analyzed by GC (Varian CP 4900) or by mass spectrometry (MS) using a residual gas analyzer (Pfeiffer Prisma QME 200). After exposure, the test coupons were removed for visual and metallographic examination, and thermogravimetric analysis with mass spectrometric detection (TGA-MS) was performed on each PuO_2/salt mixture to determine the post-exposure H_2O content.[10,11]

Results

MIS Shelf-Life Studies

Reports documenting material characterization and gas pressure and composition data for the MIS represented materials are available on the Internet. The MIS material designation, source site, actinide content, presence of chloride, and references to the relevant reports are given in Table 2.[12]

MIS Shelf-Life Studies: High-purity oxides

The MIS representative materials with plutonium content greater than 85 percent are considered high-purity oxides for this discussion. The batch designations of the high-purity plutonium oxides included in this study are listed in Table 3 along with the source and process, the calcination and loading dates, the wattage, and the specific surface area. The gas generation from TS707001 illustrates the gas composition behavior typical of high-purity oxides packaged with 0.5 wt percent water observed in the MIS Shelf-life Studies, Figure 1. The gas generation is dominated by N_2 and CO_2 with H_2 being a minor component. The hydrogen generation for all of the high-purity oxides identified in Table 3 shows a maximum hydrogen pressure of 6 kPa, Figure 2.

One high-purity oxide, PEOF1, has been studied using the full-scale container. After exposure to humid gas, the oxide mass had increased by 0.9 g, corresponding to adding approximately 0.72 monolayers of water. No hydrogen gas was observed.[13]

Table 3. MIS represented materials with plutonium content greater than 85 percent studied in the MIS Small-scale Tests

Sample	Pu	Source	Process	Calcine Date	Load Date	Remove Date	Wattage W/kg	SSA m^2/gm
TS707001	87 percent	RFETS	Metal oxidation	1/21/1998	12/16/2003	---	2.20	2.35
5501579	88 percent	RFETS	Hydride oxidation	7/17/1997	12/17/2003	---	2.21	0.58
PBO-47-09-012-023	88 percent	HANFORD	Oxalate precipitation and calcination	8/20/1997	4/7/2004	6/18/2007	3.20	1.2
ARF-102-85-114-1	86 percent	HANFORD	Peroxide precipitation and calcination	6/30/2004	2/2/2005	11/6/2007	2.18	1.02
PEOF1 at 0.08 percent H_2O	86 percent	LANL	Oxalate precipitation and calcination	10/17/2001	8/22/2005	---	2.10	1
BLO-39-11-14-004	88 percent	HANFORD	Oxalate precipitation and calcination	6/19/1997	1/8/2004	---	14.70	3.48
MISSTD1	85 percent	LANL	Oxalate precipitation and calcination	1/1/1997	8/22/2005	---	2.09	31

Figure 1. The gas pressure and composition observed for MIS represented material TS707001. The major gases are shown in the top graph and the minor gases in the lower graph.

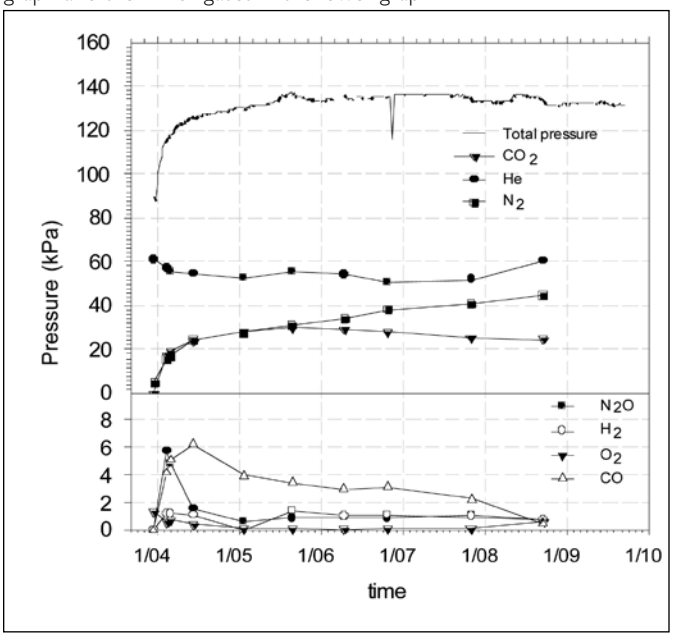

Figure 2. Hydrogen partial pressure gas generation for all high-purity oxide MIS represented materials in the MIS Small-dcale Studies. The maximum hydrogen gas pressure observed is 6 kPa. All materials are loaded with 0.5 wt percent water except PEOF1 which contains 0.08 wt percent water. The hydrogen partial pressures for BLO-39-11-14-004 and MISSTD-1A may be close to the maximum these materials produce because the hydrogen generation for high-purity plutonium oxides level off after the first three months and the pressure curves for these materials also level off after three months.

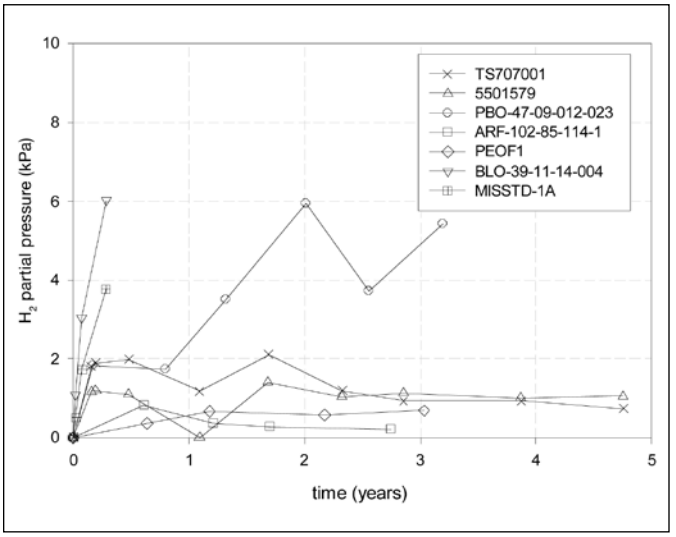

MIS Shelf-Life Studies: Chloride Containing Materials

The MIS representative materials with greater than 1 percent chloride are listed in Table 4. The pressure and composition of gases from the material that has generated the most hydrogen,

Figure 3. Gas pressure and composition for MIS represented material C06032A

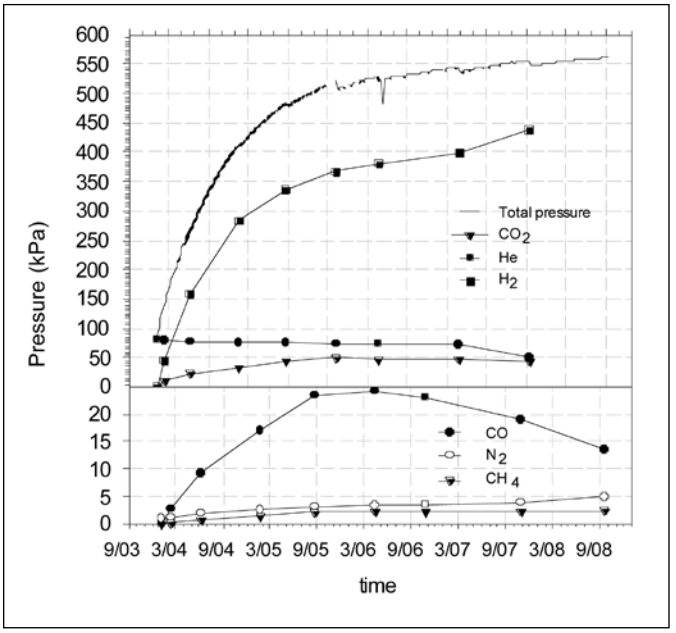

C06032A, is given in Figure 3. The hydrogen partial pressure for this material has reached 425 kPa in about 4.5 years. All chloride containing materials exhibit qualitatively similar behavior: the hydrogen pressure asymptotically approaching a maximum after an initial increase. Other gases such as CO_2 and N_2 are also seen. When CO_2 is present with high partial pressures of hydrogen, such as with chloride containing materials, CO and CH_4 are also seen at maximum pressures of less than 25 kPa with CO always exceeding CH_4. The observed increases in hydrogen pressure are reasonably fit to single exponential functions of time.[14] These functions extrapolate to sample-specific steady-state H_2 pressures that are all less than 25 percent of the amount of hydrogen expected if alpha radiolysis converts all of the water to hydrogen gas, Table 5.

One MIS chloride-bearing material, 011589A, generated oxygen in nearly stoichiometric ratio to hydrogen. The three conditions common to previously observed cases of generation of both hydrogen and oxygen by chloride-containing materials are:[15] (1) an alkaline earth chloride such as $MgCl_2$ or $CaCl_2$ is present, (2) the molar ratio of water to alkaline earth chloride is at least 4, and (3) the absolute water content exceeds 0.3 wt percent. Calcium chloride deliquesces and forms a liquid with slightly more than four waters of hydration while magnesium chloride requires about nine waters to form a liquid.[16]

MIS Shelf-Life Studies: Other materials

The results for all other materials, those with <85 percent Pu and <1 percent chloride, show much less hydrogen gas generation than observed in chloride-containing materials. For example, materials formed from magnesium hydroxide precipitation that con-

Table 4. MIS represented materials with chloride

Sample	Pu	Source	Process	Wattage W/kg
CLLANL025	78 percent	RFETS	Pyrochemical	1.96
C06032A	74 percent	RFETS	Screenings from pyrochemical	1.85
ARF-102-85-223	67 percent	HANFORD	Scrap from pyrochemical	1.67
11589	78 percent	RFETS	Metal oxidation	1.99
53038	63 percent	RFETS	Hydroxide precipitation	2.28
520610020	34 percent	RFETS	Pyrochemical	0.95
ARF-102-85-365	66 percent	HANFORD	Scrap from pyrochemical	1.6
C00024A	73 percent	RFETS	Pyrochemical	1.89
C00695	74 percent	RFETS	Pyrochemical	1.86
TS707013	70 percent	RFETS	Metal oxidation	1.71
ARF-102-85-295	40 percent	HANFORD	Scrap from pyrochemical	0.98
PMAXBS	68 percent	LANL	ER salt	1.69
07032282A	69 percent	RFETS	Foundry scrap oxide	1.73

Table 5. The results of fitting the hydrogen partial pressure to a single exponential formation. The fitting parameters are expressed as the maximum pressure and time to reach half of the maximum pressure. The fitting parameters can be used to calculate how complete the reaction will be at five years. The 3σ error in P_{max} is estimated as between 5 percent and 10 percent of the value and in $t_{1/2}$ is estimated as between 15 percent and 30 percent of the value.

Material	Pmax (kPa)	$t_{1/2}$ (yr)	Fraction Complete at 5 Years	PH_2 from 3013 Pressure Equation (kPa)	Ratio of Hydrogen Partial Pressures
CLLANL025	171	0.65	99.5 percent	1490	11 percent
C06032A	425	0.70	99.3 percent	1780	24 percent
ARF-102-85-223	137	0.51	99.9 percent	1870	7 percent
011589A	103	-	-	2070	5 percent
53038	112	0.32	100.0 percent	2200	5 percent
520610020	101	0.80	98.7 percent	970	10 percent
ARF-102-85-365	144	0.86	98.2 percent	1680	9 percent
C00024A	7	0.09	100.0 percent	1820	0 percent
TS707013	32	0.55	99.8 percent	1910	2 percent
ARF-102-85-295	379	1.03	96.5 percent	1660	23 percent
ARF-102-85-295 HT	178	0.59	99.7 percent	2200	8 percent
PMAXBS	87	0.38	100.0 percent	1350	6 percent

tain significant amounts of magnesium oxide, R441 and R438, generate hydrogen with a maximum observed partial pressure of 50 kPa. Additionally, many materials generate CO_2 and N_2, although not as much as the high-purity oxides.

Small-scale Corrosion Studies with Gas Analysis

Temperature corrected pressure traces for selected small-scale corrosion test samples are shown in Figure 4. Chemical compositions of the small-scale corrosion test materials are given in Table 6. Pressure and temperature signals were not recorded for the first sixty to eighty days after the test containers were sealed. The total headspace gas pressure and partial pressures of hydrogen, oxygen, and nitrogen just prior to opening each container are shown in Table 7. The presence of nitrogen is assumed to be due to residual air remaining at the time the container was sealed. Only trace amounts of gases other than He, H_2, N_2, and O_2 were detected.

The rates of hydrogen and oxygen generation (in excess of the amount of oxygen from trace air remaining at the time the con-

Figure 4. Pressure vs. time curves for selected corrosion test compositions with initial water contents (wt percent) as follows: 5a-2 (1.2 percent); 5a-3 (0.45 percent); 4a-1 (0.58 percent); 4b-3 (0.61 percent); 1b-1 (1.0 percent); and 1a-1 (0.38 percent). All pressures are corrected to 25°C. Pressures for 5a-2 and 5a-3 were corrected for pressure changes due to dilution with He and sampling prior to opening the container.

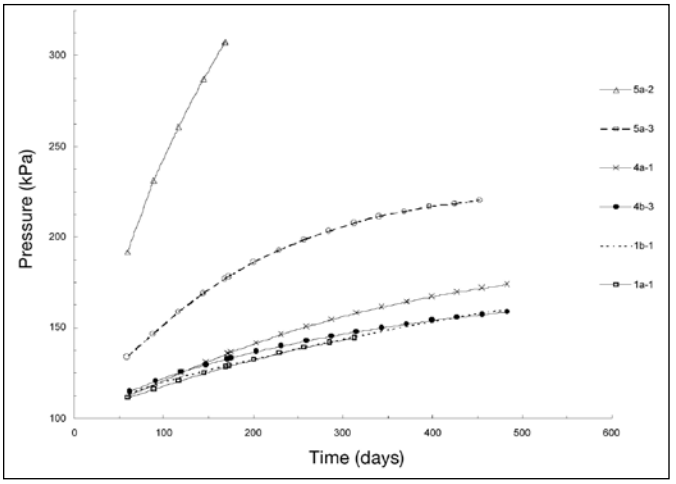

Table 6. Chemical compositions of corrosion test mixtures

Test Mixture ID	Chemical Composition (wt percent)				
	PuO_2	NaCl	KCl	$MgCl_2$	$CaCl_2$
1a	100	-	-	-	-
1b	72	11.7	14.8	1.1	0.4
4a	98	0.90	0.90	-	0.20
4b	98	0.54	0.54	-	0.92
5a	95	2.25	2.25	0.5	-

tainer was sealed in helium) are presented as radiolytic *G*-values (i.e., G_{H2} and G_{O2}), where *G* is equal to the number of molecules of gas produced per 100 eV of absorbed radiation dose either by the material plus water or by the water. The *G*-values were calculated from the initial rates of hydrogen or oxygen production during the first 60 days using the total alpha radiation dose and the fraction of alpha decay energy absorbed by the electrons from water contained in the sample. The fraction of alpha decay energy absorbed was corrected for the decreasing dose to water over time due to consumption of water by radiolysis (Table 8). The amount of water consumed by radiolysis was determined from the initial *G*-value. Because gas compositions were only measured at the end of each test, the ratio of hydrogen to oxygen generation at sixty days was assumed to be equal to the ratio of hydrogen and oxygen generated over the entire test period.

Table 7. Headspace gas composition at end of exposure

Sample ID	Days Until Sampled	Pressure (kPa)					
		P_{final}	P_{H2}	P_{O2}	P_{N2}	P_{H2corr}	P_{O2corr}
1a-1	324	147	31.5	0.8	2.4	45.6	0.21
1b-1	486	162	61.3	0.5	1.9	61.1	-0.04
1b-2	149	134	32.3	0.0	1.4	33.8	-0.36
4a-1	496	175	61.8	9.6	1.0	64.2	9.7
4a-2	334	165	52.5	11.3	0.0	52.6	11.4
4b-1	192	142	26.5	7.0	0.3	32.8	8.6
4b-2	340	147	38.3	12.4	-0.1	34.4	11.2
4b-3	487	161	50.9	6.5	0.5	53.0	6.7
5a-1[a]	352	221[b]	73.2	27.3	0.0	95.4	35.6
5a-2[a]	168	506[b]	63.0	30.5	0.0	143	69.3
5a-3[a]	459	217[b]	56.8	19.3	0.2	88.9	30.2

[a] Containers 5a-1, 5a-2, and 5a-3 were diluted with helium and sampled prior to opening due to higher than expected rate of pressure increase for 5a-2 and preliminary gas analysis indicating a nearly stoichiometric ratio of H_2 and O_2 generated.

[b] Total pressure increases from gas generation were 131 kPa for 5a-1, 212 kPa for 5a-2, and 119 kPa for 5a-3.

Discussion

The hydrogen gas generation by high-purity oxides in the MIS Shelf-Life studies differs markedly from that in the Small-scale Corrosion Studies as well as from that in results reported by Duffey and Livingston[4,5] and Vladimirova and Kuilikov.[6] The differences probably stem from large differences in the number of monolayers of water on the plutonium oxide surfaces. The differences in surface water coverage are due to differences in test container designs and thermal gradients rather than differences in plutonium oxide material properties. The adsorption of 0.5 wt percent water onto the surfaces of typical PuO_2 of moderate surface area (i.e., 1 to 2 m^2/g) corresponds to an average surface coverage of approximately 10 to 20 monolayers of water. Such high coverage can only be achieved and maintained under conditions of extremely high RH (>80 percent).[13] Multilayer water coverage will be maintained during storage only as long as the relative humidity of the gas in contact with the material within the container remains high. Any reduction in relative humidity to more moderate levels will cause rapid evaporation of this liquid layer and reduction in surface coverage to approximately one monolayer. In the Small-scale Corrosion Studies and experiments by Duffey and Livingston and Vladimirova and Kuilikov, the experimental apparatus is isothermal, meaning that the multiple layers of adsorbed water will remain in place on the surface until depleted by radiolysis during the experiments. In the LANL MIS Shelf-Life experimental apparatus the test container and the material within are held at 55°C, but the gas sampling manifold, which extends some distance away from the heated block, is as cool as 35°C. These cooler locations pro-

Table 8. H_2 and O_2 yields and H_2O consumption during Small-scale Corrosion Studies

Exp ID	Initial H_2O Content[a]	Yield Per Total Absorbed Dose (molecules/100 eV)		Yield Per Dose Absorbed by H_2O (molecules/100 eV)		H_2O Consumed During Exposure (percent)	
	wt percent	G_{H2}	GO_2	G_{H2}	GO_2	Measured	Predicted
1a-1	0.38	0.019	0.00009	3.8	0.02	41	42
1b-1	1.00	0.021	-0.00001	1.7	0.00	14	21
1b-2	0.94	0.027	-0.00028	2.2	-0.02	8.3	9.4
4a-1	0.58	0.022	0.0034	3.0	0.44	38	47
4a-2	0.63	0.023	0.0049	2.8	0.60	30	31
4b-1	0.66	0.022	0.0057	2.5	0.66	17	18
4b-2	0.61	0.020	0.0065	2.5	0.81	21	30
5a-1	0.49	0.023	0.0085	3.7	1.4	63	71
5a-2	1.24	0.057	0.028	3.7	1.8	43	45
5a-3	0.45	0.018	0.0061	3.2	1.1	58	75

[a] *The initial moisture content of each sample was calculated from the measured post-exposure H_2O content plus the amount of H_2O converted to H_2 during test period.*

vide a sink for water to condense as it evaporates from the warmer material. The dew point of water at 35°C corresponds to about 35 percent relative humidity at 55°C. Since multiple layers of water on PuO_2 surfaces are not stable at 35 percent RH, water will evaporate from the surface of the material as soon as the container is placed in the heated block, condensing in the cooler tubing until the dew point of the gas in the container is reduced to ≤35°C. The surface coverage at 35 percent RH is approximately one monolayer.[17] Therefore, the LANL MIS shelf-life results should be interpreted as showing that the single monolayer of water expected on high-purity PuO_2 material under storage conditions is not converted to hydrogen or oxygen gas at a significant rate. In contrast, the Small-scale Corrosion Studies and the results of Duffey and Livingston[4,5] and Vladimirova and Kuilikov[6] show that if multiple layers of water are forced onto the oxide surface at high RH and conditions are maintained so that those layers persist, hydrogen and oxygen are generated in significant quantity.

These results can be applied to the 3013 storage inventory in order to understand the hydrogen and oxygen gas generation behavior of packaged high-purity oxides because the relative humidity conditions during packaging are known. The RH was/is controlled per procedure to 3.5 percent or less at Rocky Flats Environmental Technology Site (RFETS) and 25 percent or less at SRS. At LANL and Lawrence Livermore National Laboratory (LLNL), facility operations control the relative humidity to less than 1 percent. At Hanford, the relative humidity of the dry packaging line (SPE line) was controlled to below 1 percent by facility operations, and the relative humidity of the wet packaging line (C line) was controlled per procedure to less than 60 percent.

Figure 5. Measured and extrapolated pressure vs. time curves for selected corrosion test compositions. Extrapolated pressure curves were calculated from G-values for initial H_2 and O_2 generation rates and initial sample water contents, correcting for water consumed by radiolysis. Percentages are fractions of initial water consumed at test end; values in parentheses are calculated values for the same time period.

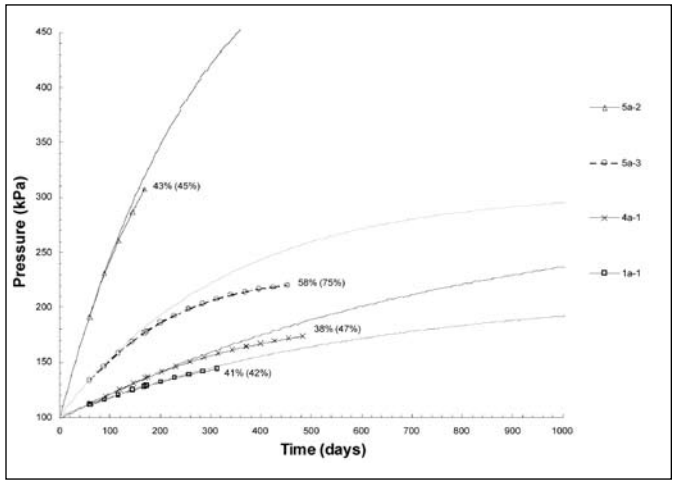

Thus, the >80 percent RH required to form multiple layers of water from adsorption of water vapor onto PuO_2 surfaces did not occur during packaging of the existing inventory. In addition, the thermal gradients within a 3013 container stored in a 9975 transportation package result in the material being approximately five degrees Centigrade higher in temperature than the coolest part of the inner container,[18] so the condensation on the container surface would limit the RH at the material in similar manner

to the condensation in the tubing of the MIS Shelf-Life experimental conditions discussed above. Therefore, the production of hydrogen and oxygen by high-purity oxides in the existing 3013 inventory is extremely unlikely.

The situation is different when alkaline earth chloride salts are present as impurities. Alkaline earth salts deliquesce to form aqueous solution when exposed to much lower RH than is required to condense multiple layers of water on oxide surfaces. Liquids almost certainly formed in the Small-scale Corrosion Studies series 4a, 4b, and 5a and probably formed in the MIS Shelf-life Studies on sample 011589A. The gas generation results are consistent with the hypothesis that the generation of oxygen is strongly correlated with the existence of liquid water within the material bed, whether on high-purity oxides that exist at very high RH or through the deliquescence of chloride salts, which can occur down to 16 percent RH.[19] The possibility of having a persistent aqueous phase inside a container packaged in accordance with the 3013 Standard depends on additional factors including thermal gradients within the containers, and is still being addressed.[18]

For the small-scale corrosion tests at SRNL, the solid lines in Figure 5 show extrapolated H_2, or H_2 plus O_2, partial pressures calculated from the initial G-values given in Table 8 and assuming that the reactions producing H_2 and O_2 are pseudo first-order in total remaining H_2O in the system, and that the gases produced undergo no other reactions. These model curves approach asymptotic pressure values dictated by the total initial water, the container's free volume and the temperature. While the measured and extrapolated pressures are in good agreement up to a point that varies somewhat between materials, the measured pressures consistently fall below the extrapolations, indicating that the kinetics are actually more complicated and that the ultimate pressures are limited by factors in addition to the initial water content. The deviations from the first-order model are quantified in Figure 5 by listing the consumed fraction of the initial H_2O required to produce the observed and the predicted (parentheses) pressures at the time of the last experimental data point available for each sample.

The fraction of water converted to H_2 in the small-scale corrosion tests in less than two years ranged from 8 to 63 percent (Table 8). The larger values are significantly higher than the fraction of water consumed in the MIS shelf-life studies, which range from 0 to 24 percent of the total water content after five years. The corrosion test results are consistent, however, with literature reporting complete conversion of water to hydrogen at steady state for PuO_2 samples with varying amounts of added water.[6]

One possible explanation for these discrepancies is that the H_2 gas may undergo additional reactions that deplete it from the headspace, and the ultimate H_2 pressure is reached when the consumption rate equals the generation rate. The Small-scale Corrosion Studies have significantly greater free volume relative to the mass of contained material than do either the MIS shelf-life experiments or actual 3013 containers. Therefore, under this hypothesis the corrosion studies would not reach the equilibrium-condition H_2 pressure until much more of the initial water had been converted to H_2. Although there is not sufficient information in Reference 6 to determine the volume-to-mass ratios, this line of reasoning would lead one to speculate that the free gas volumes were relatively large.

The MIS Shelf-Life Studies were undertaken to obtain gas generation information from a diverse set of samples representing the full range of stored materials, and containing the maximum fraction of moisture allowed by the 3013 Standard. The results of the MIS Shelf-life Studies are compared qualitatively in Table 9 with the headspace gases found inside containers selected from the storage inventory for destructive evaluation (DE) as reported by Almond et al.[20] The major trends observed in the MIS Shelf-life Studies are also observed in the 3013 DE observations. The most significant difference is the observation of a flammable mixture of hydrogen and oxygen within the 0.5 wt percent water limit in the MIS Shelf-Life Studies for one chloride bearing material whereas no oxygen is observed when hydrogen is present in the 3013 DE observations.

Table 9. Qualitative comparison of the MIS Shelf-life results to the destructive evaluation gas analysis

	MIS Shelf-Life	3013 DE Gas Analysis
Gases observed	He, H_2, O_2, N_2, CO_2, CO, CH_4, N_2O	He, H_2, O_2, N_2, CO_2, CO, CH_4, N_2O
High-purity oxide		
Hydrogen	Little to none	None
Oxygen	None	None
Chloride impurities		
Hydrogen	Yes, 0 percent to 24 percent of avail. H_2O	Yes, 0 percent to ~10 percent of avail. H_2O
Oxygen	No, unless liquid water present	None

Conclusions

Both small and full-scale experiments with sealed containers of pure and impure PuO_2 containing moisture demonstrate that maximum steady state pressures are well below the minimum design pressure for the 3013 containers in which stabilized Pu-bearing materials are stored. Contrary to assumptions in the 3013 Standard, both hydrogen and oxygen generation are observed for materials with 0.5 wt percent water when liquid water is present. Test results from containers with different free volume-to-sample mass ratios suggest that the small volume-to-mass ratios in the 3013 container configuration contribute to the relatively small amounts of moisture (typically less than 10 percent) converted to H_2 gas after up to five years of storage because hydrogen consumption reactions, with rates governed by the hydrogen partial pressure, reach equilibrium with regard to hydrogen generation

sooner. These results along with data from actual 3013 containers examined after approximately five years of storage provide confidence that the maximum pressure within the 3013 storage inventory will remain nearly an order of magnitude below the allowed container pressure of 4920 kPa. The achievement of steady-state hydrogen partial pressures long before all moisture is consumed suggests that a balance is achieved between hydrogen production and consumption reactions. The factors leading to this balance, particularly the mechanisms of consumption, remain an area for future study.

Jonathan M. Duffey is a principal scientist at Savannah River National Laboratory. He has a Ph.D. and an M.S. in chemistry from the University of Tennessee and a B.S. in chemistry from Union University.

D. Kirk Veirs is a staff scientist at Los Alamos National Laboratory. He has a Ph.D. in physical chemistry from Pennsylvania State University and a B.S. in chemistry and environmental science from Northern Arizona University.

John M. Berg is a staff scientist at Los Alamos National Laboratory. He has a Ph.D. in chemistry from Princeton University and a B.A. in chemistry from St. John's University,

Ronald R. Livingston is a continuous improvement expert at Savannah River Nuclear Solutions. He has a B.S. in chemistry from Augusta College.

Acknowledgments

Funding for this work was provided by the Surveillance and Monitoring Program, U.S. Department of Energy Office of Environmental Management. This work was conducted at Savannah River National Laboratory operated by Savannah River Nuclear Solutions for the U.S. Department of Energy under contract DE-AC09-08SR22470 and Los Alamos National Laboratory operated by Los Alamos National Security, LLC under contract DE-AC52-06NA25396.

References

1. *Stabilization, Packaging, and Storage of Plutonium-bearing Materials.* 2004. DOE-STD-3013-2004. U.S. Department of Energy: Washington, D.C.
2. Eller, P. G., R. E. Mason, D. R. Horrell, S. D. McKee, N. A. Rink, and C. S. Leasure. 1999. *Gas Pressurization from Calcined Plutonium Oxides,* LA-UR-99-3804, Los Alamos National Laboratory.
3. Bailey, G., E. Bluhm, J. Lyman, R. Mason, M. Paffett, G. Polansky, G. D. Roberson, M. Sherman, D. K. Veirs, and L. Worl. 2000. *Gas Generation from Actinide Oxide Materials,* LA-13781-MS, Los Alamos National Laboratory.
4. Livingston, R. R., and J. M. Duffey. 2001. *Effects of Plutonium Dioxide Moisture Content and Calcination Temperature on the Headspace Gas Composition of Sealed Containers,* WSRC-TR-2001-00420, Westinghouse Savannah River Company.
5. Duffey, J. M., and R. R. Livingston. 2002. *Gas Generation Testing of Plutonium Dioxide,* WSRC-MS-2002-00705, Westinghouse Savannah River Company.
6. Vladimirova, M. V., and I. A. Kulikov. 2002. Formation of H_2 and O_2 in Radiolysis of Water Sorbed on PuO_2, *Radiochemistry,* Vol. 44, No. 1, 86-90.
7. Laverne, J. A,. and L. Tandon. 2005. H_2 and Cl_2 Production in the Radiolysis of Calcium and Magnesium Chlorides and Hydroxides, *J. Phys. Chem.* A, Vol. 109, 2861-2865.
8. Kelm, M., and E. Bonhert. 1996. Radiolytic Compounds Formed by Dissolution of Irradiated NaCl and $MgCl_2 \cdot 6H_2O$ in Water, *Radiochimica Acta,* Vol. 74, 155-158.
9. Dunn, K. A., McClard, J. W., Chandler, G. T., Gardner, C. W., Worl, L. A., and G. D. Roberson. Supporting Safe Storage of Plutonium-Bearing Materials through Science, Engineering and Surveillance. *Journal of Nuclear Materials Management* Vol. 38, No. 2.
10. Zapp, P. E., and R. R. Livingston. 2005. *Corrosion Tests of 304L and 316L Stainless Steels for the 3013 Container,* WSRC-TR-2005-00191, Savannah River National Laboratory.
11. Zapp, P. E. and J. M. Duffey. 2008. *Status Report for the SRNL 3013 Corrosion Tests (U),* SRNS-STI-2008-00093, Savannah River National Laboratory.
12. The references in Table 1 are accessed using http://permalink.lanl.gov/object/view?what=info:lanl-repo/lareport/LA-UR-09-xxxxx where xxxxx are replaced by the last five digits of the report reference given in Table 1. For instance, to access the material characterization data for MIS material SCP711-56 use the permalink http://permalink.lanl.gov/object/view?what=info:lanl-repo/lareport/LA-UR-09-07099 and to access the gas pressure and composition data use the permalinkhttp://permalink.lanl.gov/object/view?what=info:lanl-repo/lareport/LA-UR-09-07149. These links include bibliographic information as well as the actual report. Data collection on these items is continuing. Updated reports will be available at the same permalink.
13. Veirs, D. K. 2005. Gas Generation From Water Adsorbed onto Pure Plutonium Dioxide Powder," *pp. 343-348 in Actinides 2005 - Basic Science, Applications and Technology,* Vol. 893. Edited by J.L. Sarrao, et al. Materials Research Society, Boston.
14. Veirs, D. K., and J. M. Berg. Maximum Hydrogen Pressure Predicted in MIS Salt-bearing Materials, LA-UR-08-06289.

15. Berg, J. M., E. Garcia, G. Long, M. Martinez, J. Narlesky, D. K. Veirs, C. Williams, and L. Worl. 2008. *The Effect of Moisture Content on Oxygen Generation for 011589A Substitute Materials,* LA-UR-08-1487, Los Alamos National Laboratory.
16. Seidell, A. 1940. *Solubilities of Inorganic and Metal Organic Compounds: A Compilation of Quantitative Solubility.* Vol. 1. New York: D. Van Nostrand.
17. Paffett, M. T., D. Kelly; S. A. Joyce, J. Morris, and D. K. Veirs. 2003. A Critical Examination of the Thermodynamics of Water Adsorption on Actinide Oxide Surfaces. *Journal of Nuclear Materials,* Vol. 322, 45-56.
18. Veirs, D. K., J. M. Berg, and F. C. Prenger. 2010. Thermal Gradients, Relative Humidity Gradients, and Moisture Gradients in 3013 Containers, *Journal of Nuclear Materials Management* Vol. 38, No. 3.
19. Joyce, S.A., J. E. Narlesky, D. K. Veirs, E. Garcia, O. W. Gillespie, B. L. Scott, and L. A. Worl. 2010. Salt Phases in Calcined Materials and Their Hygroscopic Properties, *Journal of Nuclear Materials Management,* Vol. 38, No. 2.
20. Almond, P. M., R. R. Livingston, L. E. Traver, M. J. Arnold, N. J. Bridges, G. F. Kessinger, and J. M. Duffey. 2010. Gas Analysis from Headspace of Plutonium-Bearing Materials Containers. *Journal of Nuclear Materials Management,* Vol. 38, No. 3.

Pressure Integrity of 3013 Container Under Postulated Accident Conditions

George B. Rawls Jr.
Savannah River National Laboratory, Aiken, South Carolina USA

F. Coyne Prenger
Los Alamos National Laboratory, Los Alamos, New Mexico USA

Joe E. Shepherd
California Institute of Technology, Pasadena, California USA

Zhe Liang
Atomic Energy of Canada Limited, Chalk River Laboratories, Chalk River, Ontario, Canada

Abstract

A series of tests was carried out to determine the threshold for deflagration-to-detonation transition (DDT), structural loading, and structural response of the U.S. Department of Energy 3013 storage systems for the case of an accidental explosion of evolved gas within the storage containers. Three experimental fixtures were used to examine the various issues and three mixtures consisting of either stoichiometric hydrogen-oxygen, stoichiometric hydrogen-oxygen with added nitrogen, or stoichiometric hydrogen-oxygen with an added nitrogen-helium mixture were tested. Tests were carried out as a function of initial pressure from 1 to 3.5 bar and initial temperature from room temperature to 150°C. The elevated temperature tests resulted in a slight increase in the threshold pressure for DDT. The elevated temperature tests were performed to ensure the test results were bounding. Because the change was not significant, the elevated temperature data are not presented in the paper. The explosions were initiated with either a small spark or a hot surface. Based on the results of these tests under the conditions investigated, it can be concluded that DDT of a stoichiometric hydrogen-oxygen mixture (and mixtures diluted with nitrogen and helium) within the 3013 containment system does not pose a threat to the structural integrity of the outer container.

Introduction

A system composed of triple-nested stainless steel 3013 storage canisters used to store plutonium-bearing powders was evaluated to determine the probability of plutonium bearing material release in the event of a hydrogen-oxygen explosion. Generation of hydrogen and oxygen within the storage containers by radiolysis of water, hydrated salts or corrosion raises the possibility of internal combustion in the highly unlikely event of an ignition source being present. The 3013 Containment System contains no identifiable ignition source. However, because hydrogen has a very low ignition energy, a concern was raised that friction-generating events caused by a physical interaction between the nested containers may have the potential to provide sufficient energy to ignite a combustible hydrogen-oxygen mixture.

The California Institute of Technology, Explosion Dynamics Laboratory[1] was contracted to perform a series of tests designed to evaluate the potential for detonation and the resulting structural response of the 3013 container system. This containment system is used throughout the U.S. Department of Energy (DOE) complex to package plutonium metal and oxides under the DOE 3013 Packaging Standard. An illustration of the 3013 containers is shown in Figure 1. The convenience and inner containers used at each DOE facility differ but the 3013 outer containers are the same for all configurations throughout the DOE complex.

Figure 1. Nested 3013 containers. The outer container is on the left, the inner container in the middle, and the convenience container on the right.

The test program used deliberate ignition of explosive mixtures of hydrogen and oxygen to determine the type of explosion, (i.e., a deflagration having a subsonic burn front or a detonation having a supersonic burn front), structural loading (pressure history), and structural response (strain history) in both simulated test fixtures and actual 3013 outer containers.

Testing Methodology

The initial gas pressures, temperatures and gas compositions in the storage containers were based on the surveillance data for the storage material containers of interest. The test fixtures and explosive mixtures were designed to address all the identifiable modes of explosions possible in the 3013 storage system. The 3013 outer container was treated as the final containment barrier and, for added conservatism, the final evaluation neglected any structural benefit derived from the inner containers.

Three phases of testing determined the threshold for deflagration-to-detonation transition (DDT), the container structural loading, and the structural response of the nested storage canisters. Three experimental fixtures were used to examine the variables that might influence the test results. The first series of tests was performed to understand the influence on DDT of the small gaps between the inner and outer containers. Because the ratio of gap thickness between the outer and inner containers to container diameter was small, a planar fixture was used to simulate the combustion behavior. Because of the planar configuration, only the pressure-time history was measured in these tests. A second series of tests was performed in a thick-walled cylindrical container fitted with a cylindrical insert to simulate the outer container-inner container configuration. In this cylindrical geometry, strain gauges were used to measure the structural response of the thick-walled outer container. In addition, the eccentricity in the annular gap between outer and inner cylinders was also investigated. The final test fixture was an actual 3013 outer container modified with penetrations for pressure transducers, gas handling, and ignition sources.

Three gas mixtures, chosen to bound the anticipated container gas compositions were tested:

1) a stoichiometric hydrogen-oxygen mixture (Mixture A),
2) a stoichiometric hydrogen-oxygen mixture added to 60 kPa of nitrogen (Mixture B); and
3) a stoichiometric hydrogen-oxygen mixture added to 60 kPa of nitrogen and 16 kPa of helium (Mixture C).

Tests were carried out as a function of initial pressure (which was varied from 1 to 3.5 bar(KPA = 1 bar)) and initial temperature (room temperature to 150°C). The explosions were initiated with either a small spark or a glow plug (hot surface).

Planar Gap Tests

The planar gap test fixture was designed to determine the threshold for DDT in the storage system annular gaps. When the containers are nested, annular spaces are created between the various container walls and gaps are also formed between the container lids, as shown in Figure 2. The tests were carried out in a planar geometry simulating the annular gaps between the outer and inner containers of the 3013 storage system. The test fixture consisted of a pair of rigid flat plates with the gap between them an adjustable, representing the annular space between the nested storage system containers. Figure 3 is a drawing of the planar test fixture showing the location of the pressure transducers. The gap was filled with a representative explosive gas mixture, ignited, and the subsequent explosion development was monitored using pressure transducers. For each mixture composition, the threshold for DDT was determined by varying initial pressures. Because the inner and outer containers could be eccentric, the gap size was treated as a parameter, and values of 0.01", 0.02", 0.05", 0.1", 0.44" (0.254, 0.508, 1.27, 2.54, 11.18 mm) were investigated. The annular gap between the containers comprising the storage system could vary from 0 to 0.185" (0-4.7 mm) depending on the eccentricity of the containers. The largest gap represented the headspace gap of approximately 0.5" (12.7 mm).

Figure 2. A close-up drawing of an inner container nested within an outer container showing the headspace gap

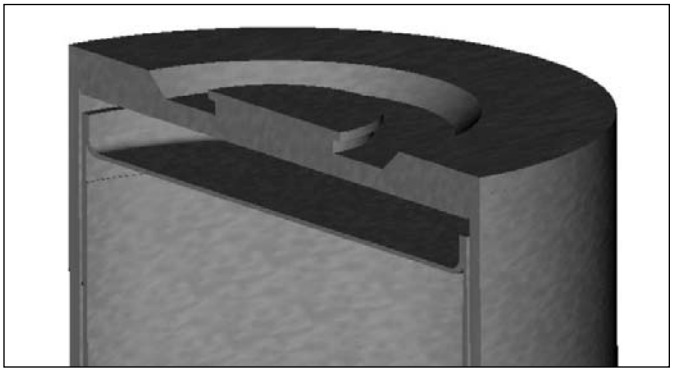

Figure 3. Planar fixture assembly; 1-bottom plate, 2-top plate, 3-pressure transducer holes, 4-spacer, SP-spark plug, GP-glow plug

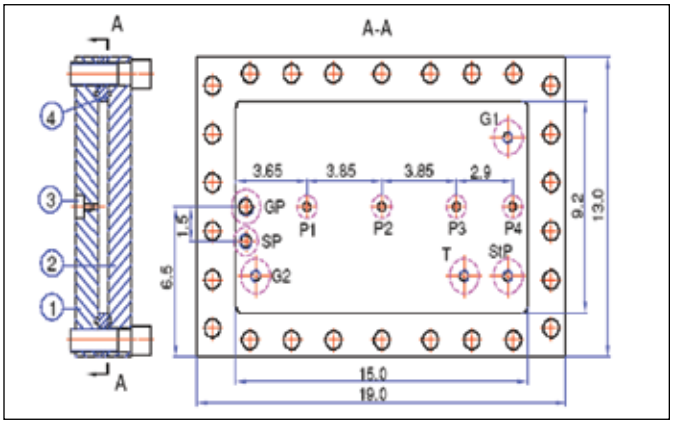

Figure 4. Peak pressures for gap size 0.44-inch and 0.10-inch for planer tests. The shaded region is the estimated threshold for the onset of DDT.

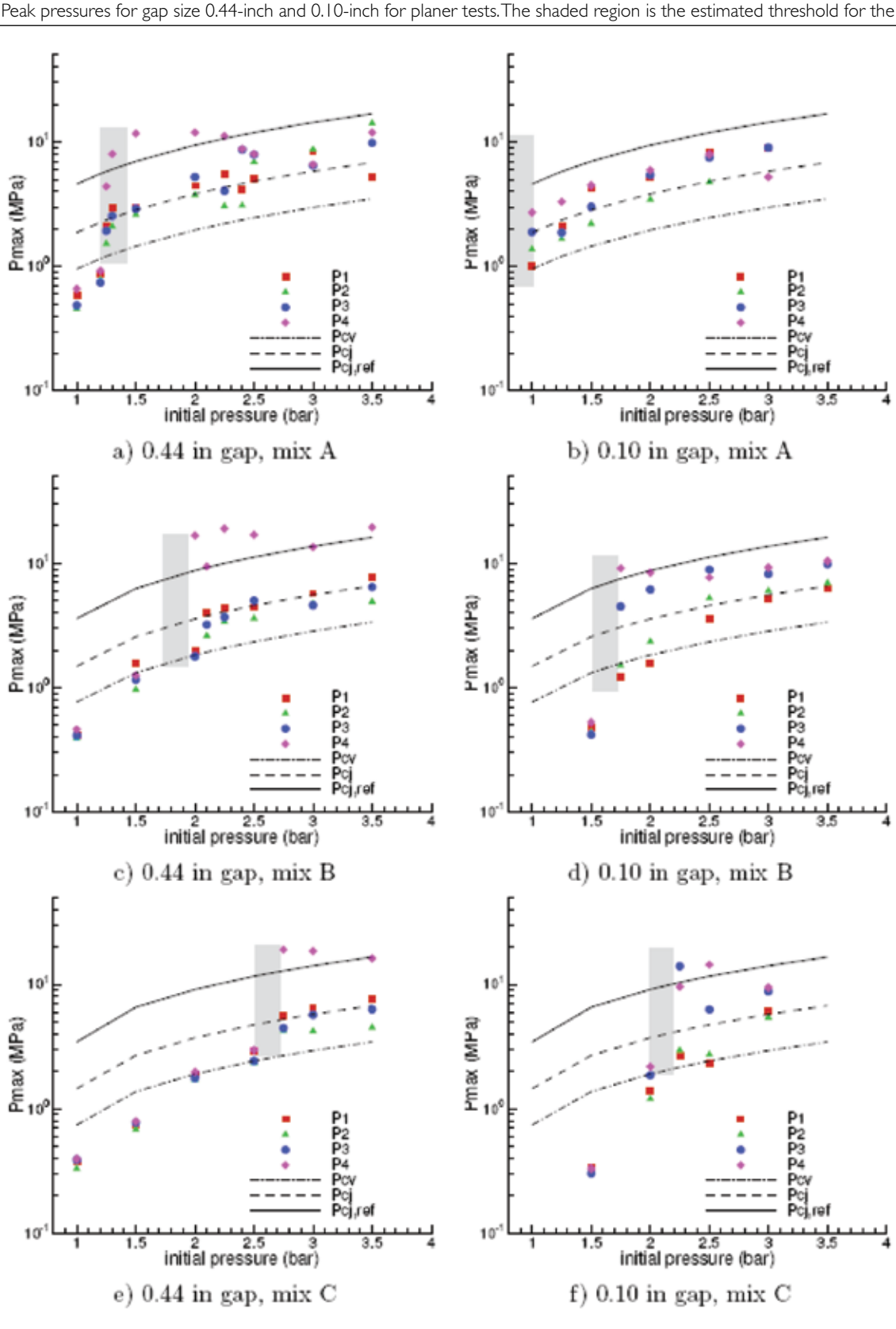

Figure 5. Thick-walled fixture assembly. 1-thick tube, 2-flange, 3-spark plug, 4-solid bar, 5-gas fill, 6-pressure transducer, 7-flange, 8-strain gauges

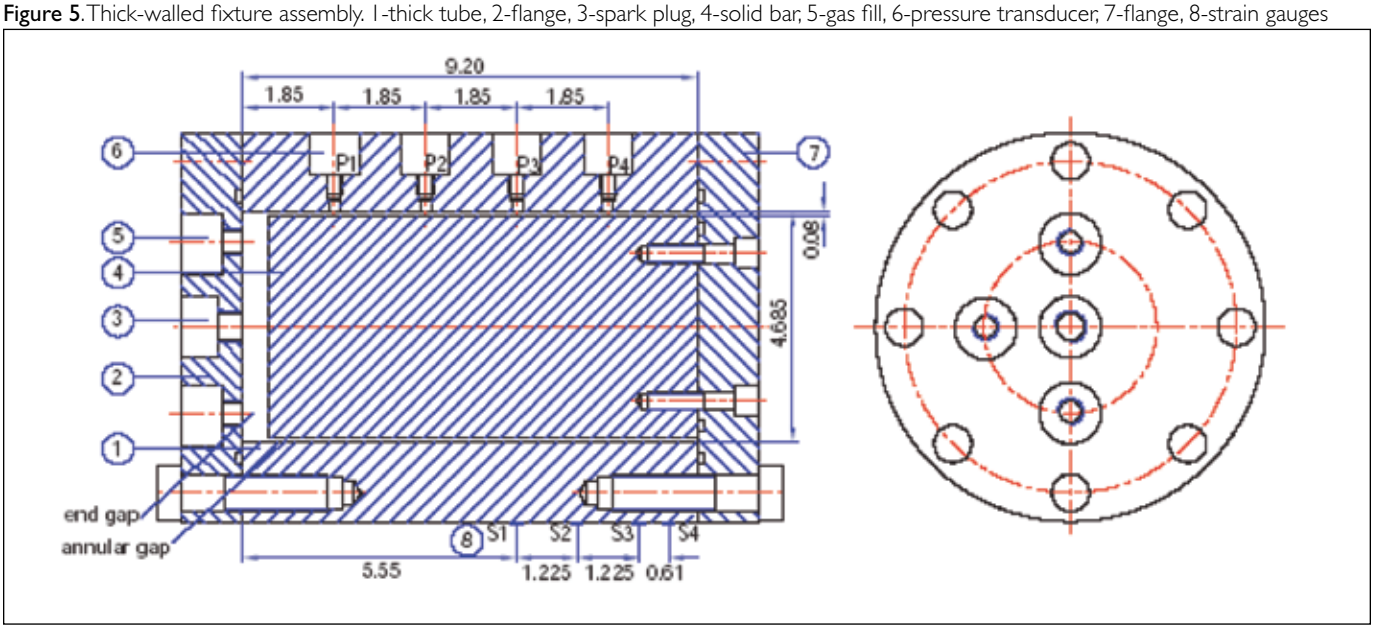

The planar tests showed that all three mixtures would undergo DDT with threshold initial pressures between 1 and 3 bar. Typical test results representing gap sizes between 0.1" and 0.44" and the three mixtures tested at room temperature are shown in Figure 4. The nomenclature used in Figure 4 for the pressure traces is as follows: the data points are the maximum measured pressures at P1, P2, P3, and P4 respectively, P_{CV} is the calculated constant volume explosion pressure, P_{CJ} is the calculated Chapman-Jouguet (CJ) pressure, and P_{CJref} is the calculated reflected CJ pressure, all using the chemical equilibrium program in reference 2, with realistic thermochemical properties.

The results, illustrated in Figure 4, show that mixture A is the most sensitive to initial pressure and gap width, providing the lowest DDT threshold pressure, mixture B is intermediate, and mixture C is the least sensitive, providing the highest DDT threshold pressure. The smaller the gap size, the lower the threshold pressure for DDT. Again, as seen in Figure 4 for mixture A, DDT was observed at an initial pressure of 1.25 bar for a gap of 0.44" (11.18 mm) and 0.9-1.0 bar initial pressure for a gap of 0.1" (2.54 mm).

Thick-walled Cylinder Tests

The thick-walled tube was fitted with a solid cylindrical insert to simulate the annular gap between the outer and inner containers. Figure 5 provides a drawing of the thick-walled test fixture showing the location of the pressure transducers and strain gauges. The positions of the strain gauges do not correspond to the positions of the pressure transducers. Three types of tube configurations were used: (1) empty tube (no insert), (2) tube with a concentrically located cylindrical insert, and (3) tube with an eccentrically located cylindrical insert. The gap configurations (2) and (3), together with the empty tube configuration (1), were chosen to cover the entire range of anticipated configurations in the 3013 storage system geometries. The test fixture was filled with one of the three representative explosive gas mixtures (A, B, or C), ignited with a low energy spark, and the subsequent explosion development monitored with pressure transducers and strain gages. For each mixture composition and tube configuration, the threshold for DDT and corresponding structural response was determined for various initial pressures. Use of the thick-walled test fixture allowed all tests to be conducted with a single, fully instrumented test fixture because the deformations in each test remained in the elastic range.

Thick-walled Cylinder Tests; Configuration 1 (Empty Tube)

As demonstrated in the planar tests, the DDT threshold shifted to higher initial pressures for larger gap sizes. Tests with an open cylinder (Configuration 1) had no gap present and the highest DDT threshold pressures for all the gas mixtures were observed. Figure 6 shows the peak pressures and strains for mixture A. The DDT threshold was observed at an initial pressure of 2.5-2.6 bar for mixture A, and is twice as large as the DDT threshold initial pressure of 1.2-1.25 bar for the largest gap size of 0.44" in the planar fixture (Figure 4a). All the transitions occurred near the tube end. The maximum strain was on the order of 170 microstrain. For mixtures B and C, no DDT transition was observed in the empty tube for initial pressures up to 3.5 bar. In the 0.44" planar fixture, DDT was observed at an initial pressure of 2.1 bar for mixture B and 2.75 bar for mixture C (Figures 4c and e).

Figure 6. Peak pressures and strains for mixture A for thick-walled cylinder tests in configuration 1. The gray vertical shaded region indicates the DDT threshold.

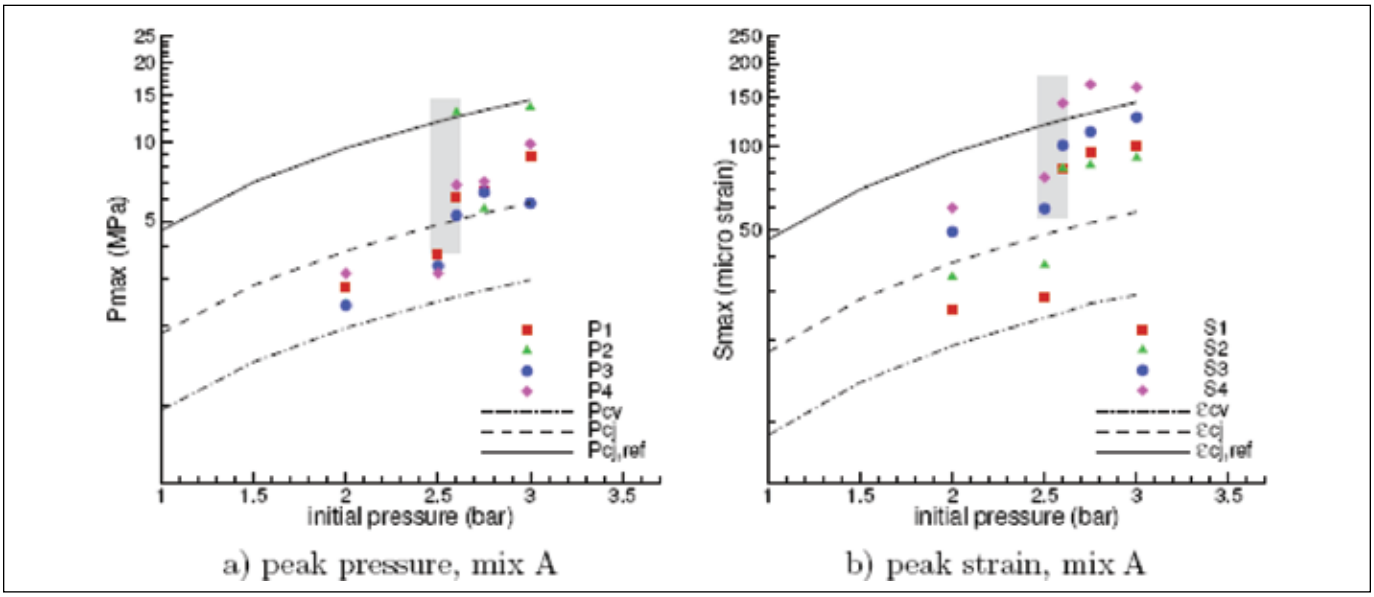

Figure 7. Peak pressures and strains for mixture A of thick-walled cylinder tests in Configuration 2.The gray vertical shaded region indicates the DDT threshold.

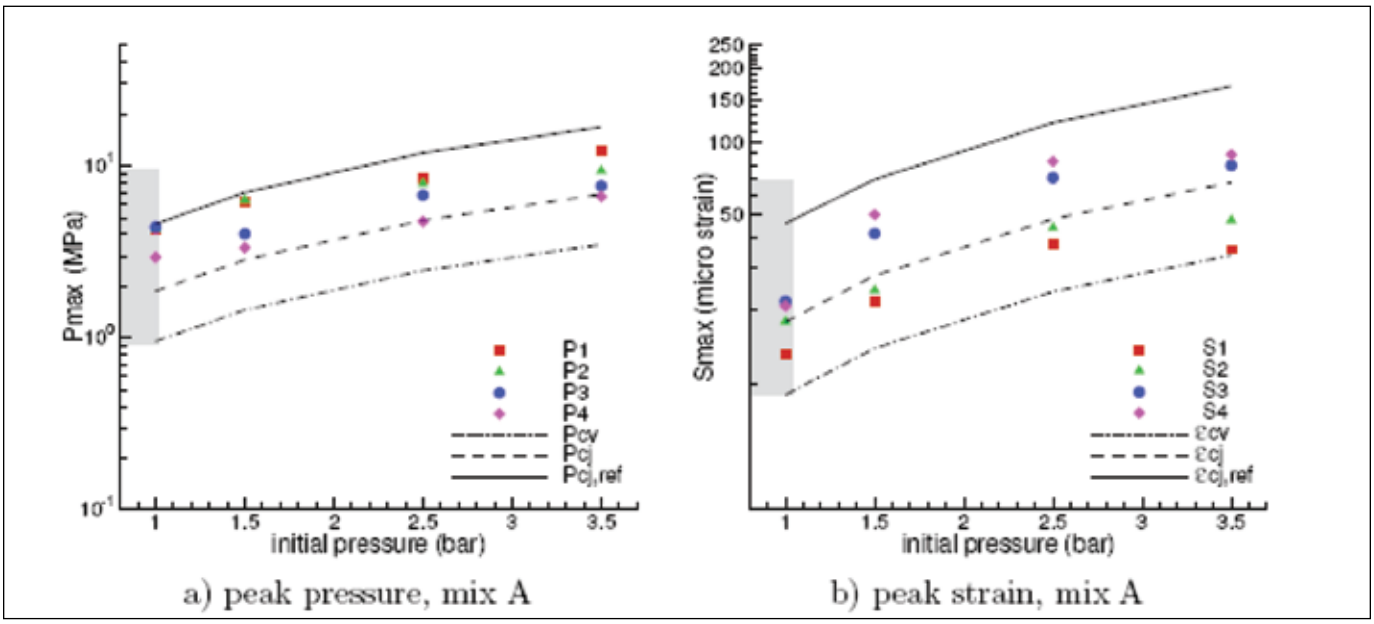

Thick-Walled Cylinder Tests; Configuration 2 (Concentric Insert)

The annular gap between inner and outer containers of the 3013 storage system varies between 0" and 0.16" (0–4.06 mm) depending on the eccentricity of the containers. The gap between the lids of the containers varies from 0.375" to 0.6" (9.5–15 mm) depending on the inner container cut-off length. For the thick-walled cylinder with concentric insert tests an average annular gap of 0.08" with an average end gap of 0.5" was used. A solid circular bar was inserted concentrically into the outer tube to create this geometry.

As shown in Figure 7, the DDT transition occurred at an initial pressure of 1 bar for mixture A. For mixtures B and C (not shown) only the cases with an initial pressure of 3.5 bar, close to the DDT threshold, were tested. The peak strains were always observed on the strain gauge furthest from the ignition source. The maximum value was on the order of 100 microstrain at an initial pressure of 3.5 bar.

Figure 8. Diagram of the two eccentric configuration thick-walled fixture assemblies

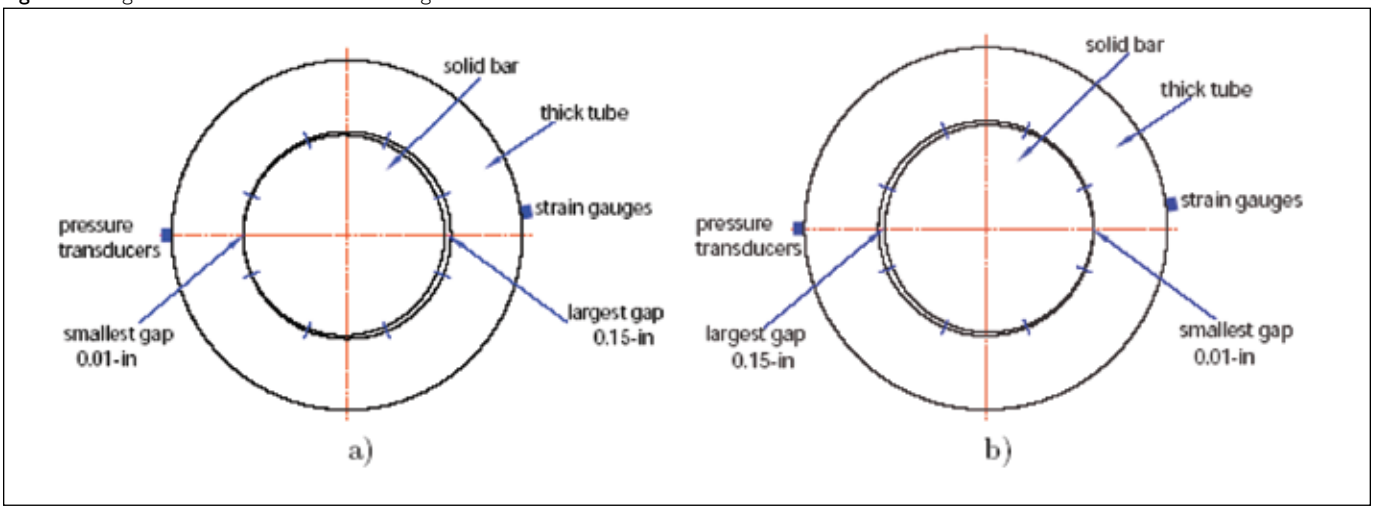

Figure 9. Peak pressures and strains for mixture A of thick-walled cylinder tests in configuration 3a. The gray vertical shaded region indicates the DDT threshold.

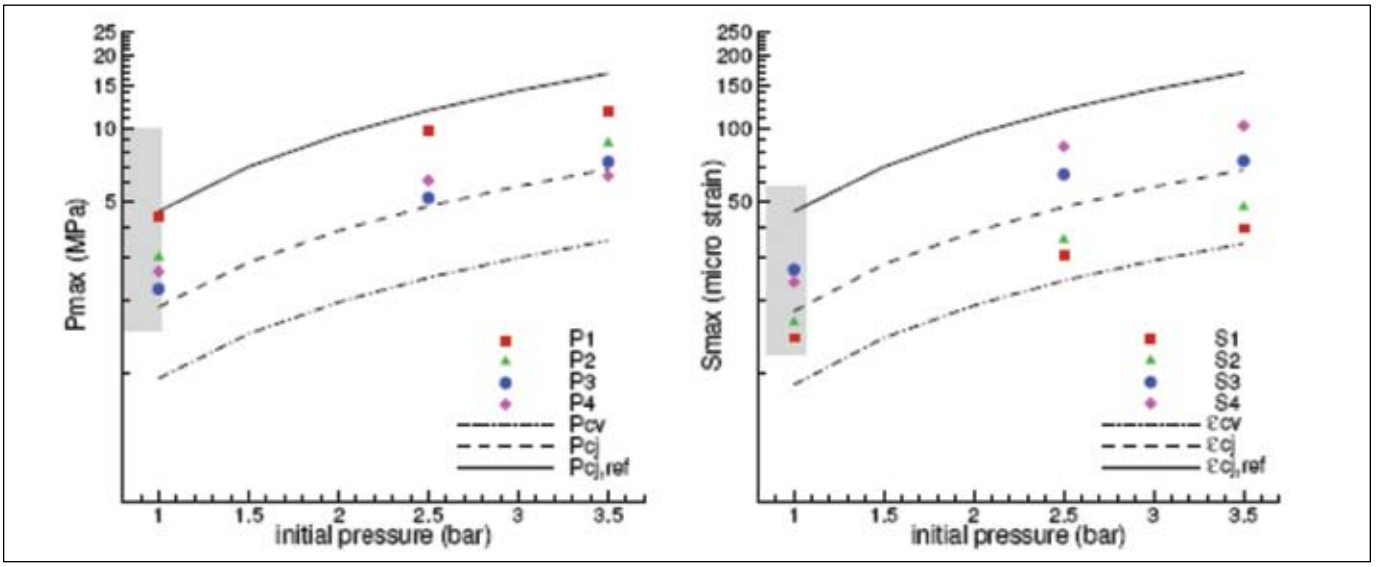

Thick-Walled Cylinder Tests; Configuration 3 (Eccentric Insert)

In configuration 3, the more realistic case of inner container eccentricity was examined. In this test series, the solid cylinder inside the test cylinder was mounted eccentrically. The nominal minimum gap was 0.01" and maximum gap was 0.15". By rotating the solid insert, data were obtained with the minimum gap of 0.01" aligned with and 180 degrees opposed to the pressure transducers with the strain gauges being opposite the pressure transducers in each case. A diagram of the two configurations is shown in Figure 8.

In contrast to configuration 2, the annular gap size for configuration 3a (Figure 8a) was reduced on the pressure transducer side; therefore, one would expect faster DDT transition on this side. As shown in Figure 9, DDT indeed occurred right away at an initial pressure of 1 bar for mixture A, but the maximum strain was on the same order as the values recorded in configuration 2.

In configuration 3b (Figure 8b), the solid bar was rotated 180 degrees, therefore, the largest gap, 0.15 in, appeared on the pressure transducer side, and the smallest gap was on the strain gauge side. For mixture A with an initial pressure of 1 bar, DDT appeared near the last transducer, P4 with configuration 3b but it was near the first transducer P1 with configuration 3a. This means that DDT occurred earlier on the smaller gap side and later on the larger gap side. This is consistent with the previous findings about the effect of the gap size on DDT thresholds in the planar fixture. As shown in Figure 10, there are no significant differences in the peak pressures and strains for the two configurations.

Figure 10. Peak pressures and strains for mixture A of thick-walled cylinder tests in configuration 3b. The gray vertical shaded region indicates the DDT threshold.

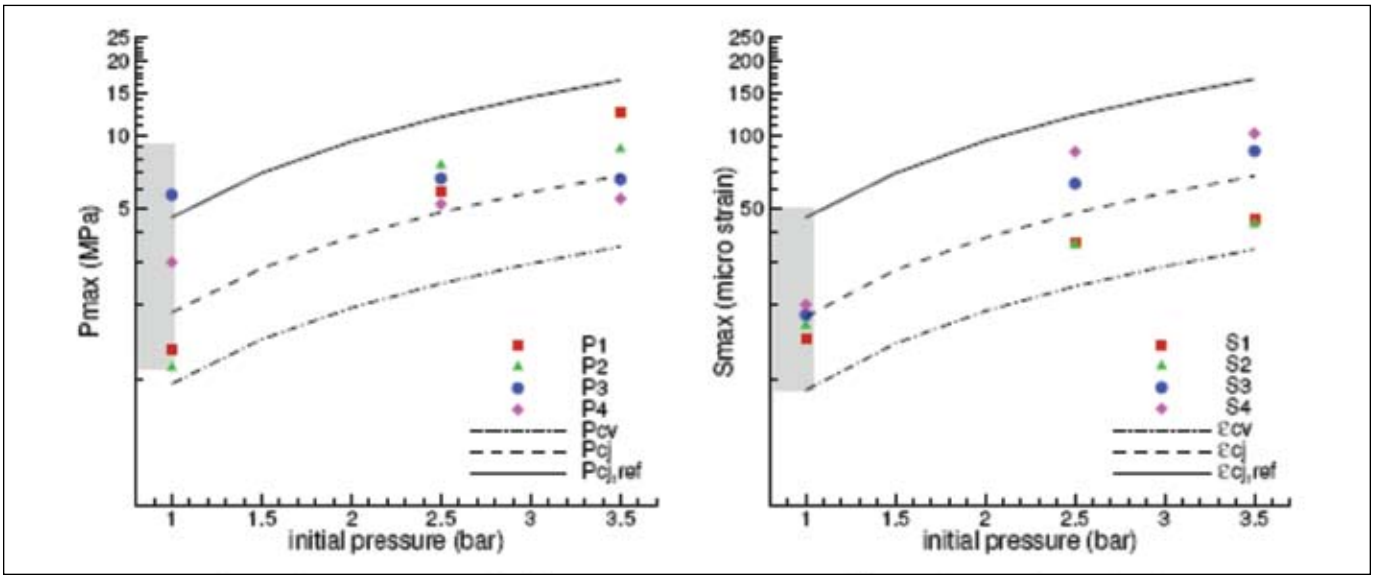

Calculated Pressures and Strain

The values for CJ pressure (P_{CJ}), reflected CJ pressure (P_{CJref}) and (P_{CV}) for each test were calculated using the chemical equilibrium program in Reference 2 with realistic thermochemical properties.

The static strains, ε_{CJ}, $\varepsilon_{CJ\ ref}$, ε_{CV}, corresponding to the CJ, reflected CJ and constant volume explosion pressures, were inferred from the approximate stress-strain relation for a uniformly, statically loaded tube

$$\varepsilon = \frac{(P - P_a)R}{Eh} \qquad (1)$$

where ε, E, R, h and P_a are strain, Young's modulus, average radius (R=(ID+h)/2), thickness of the tube, and atmospheric pressure, respectively.

Dynamic Load Factor

One of the most frequently used methods [3,4] to evaluate structural response to transient loads is the use of a dynamic load factor (DLF). This method uses the measured or calculated peak pressure of the transient load corrected by the DLF to compute a static response, which has an equivalent deflection to the peak transient response. This method is useful if the dynamic load factor and peak pressure can be readily computed for the cases of interest.

The peak value of the strain signals can be analyzed by finding the DLF (Φ), which is defined as the ratio of the measured peak strain to the peak strain expected in the case of quasi-static loading

$$\Phi = \frac{\varepsilon_{\max}}{\frac{\Delta P R}{Eh}} \qquad (2).$$

The pressure term (ΔP) in Equation 2 can be based on either the measured peak value or one of the computed pressure values. Using the experimental pressure allows an evaluation of what type of loading (impulsive, sudden or mixed) is taking place. For an ideal single-degree of freedom structure and a simple pressure-time history with a single step function followed by a monotonic decay [3,4] values of DLF close to two are associated with the limit of "sudden loading" in which the pressure jumps to a high value and does not significantly decay on the time scale of the tube radial oscillation (breathing) period. In this regime, the peak elastic deformation is proportional to the peak pressure. As the decay time of the pressure after the step change becomes shorter, the dynamic load factor becomes less than two, decreasing as the decay time decreases. In the limit of very short pressure pulses, the loading is in the impulsive regime and the peak elastic deformation is proportional to the impulse. Between these two extremes, in the mixed regime, the peak elastic deformation will depend on both the impulse and peak pressure.

Evaluation of the experimentally determined pressures from the empty thick-walled tube provides DLFs between 1.2 and 2.6 for mixture A. The evaluation of the thick-walled tube with concentric annular gap provides DLFs between 0.7 and 1.8 for experimentally determined pressure values. The dynamic load factors of the annulus configuration are less than the DLFs for the empty tube. One reason is that the gas volume for the annular gap is only 7.5 percent of the empty tube so that the total energy released in the combustion event is much smaller in the annulus

Figure 11. (a) Modified 3013 outer can. **(b)** Drawing showing modified 3013 outer can with instrumentation locations. 1-3013 outer can, 2-welded flange, 3-spark/glow plug, 4-pressure transducer adapters, 5-strain gauges, 6-thermocouple, 7-static pressure gauge, 8 and 9-gas fill/circulation lines.

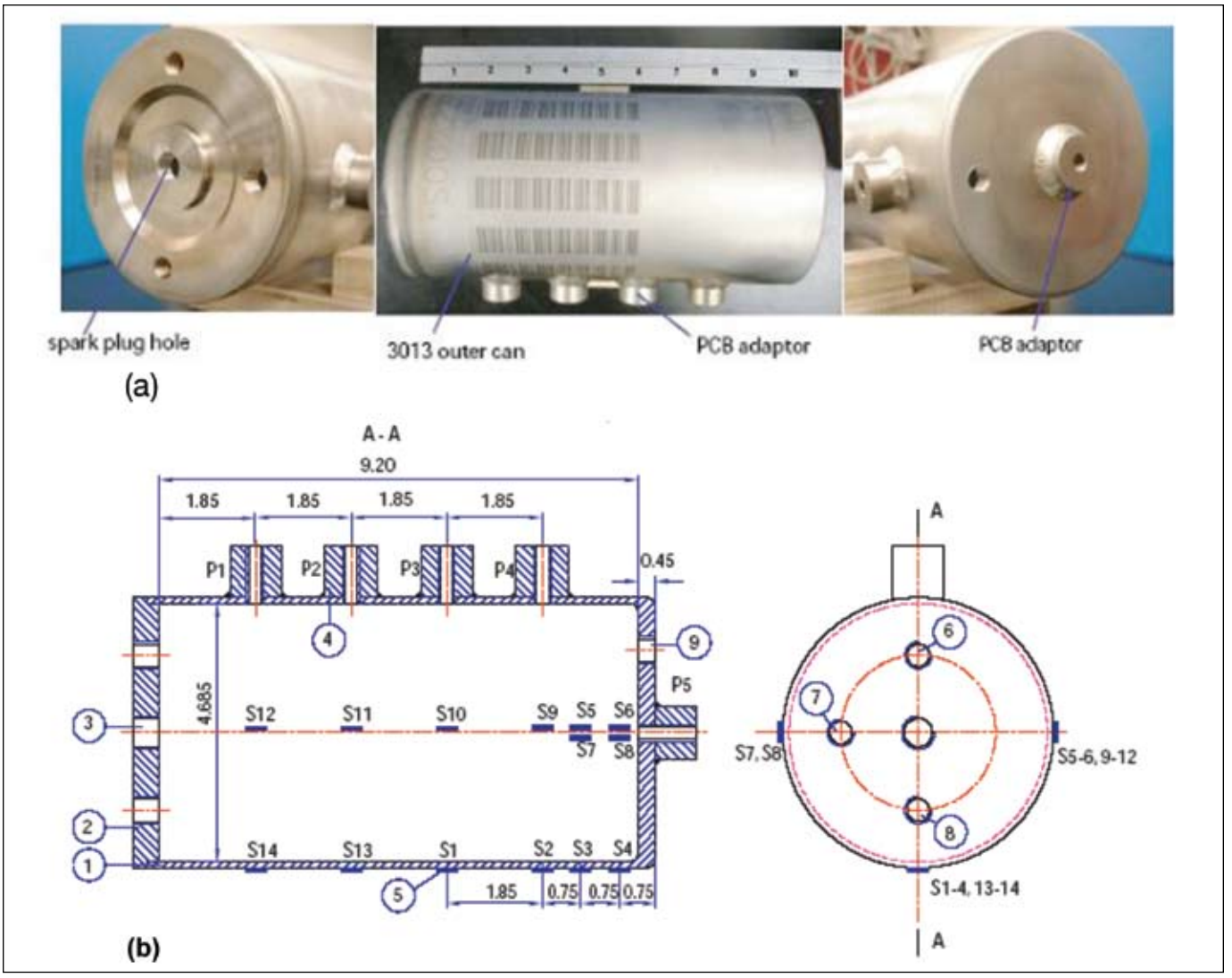

than in the empty tube. Another reason is that DDT was initiated promptly for the annulus configuration, so the detonation was approximately an ideal CJ wave when it propagated to the tube end, while for the empty tube, the detonation wave was highly overdriven due to the DDT event.

3013 Container Testing

As a confirmation of the applicability of the test results, actual 3013 containers were instrumented with strain gauges and fitted with pressure ports to measure structural loading and response to deliberate ignition of the explosive mixtures. Figure 11 provides a photo of the modified 3013 container and a drawing of the test setup. Filling the 3013 container, which is the outermost container and has the largest volume, with the various explosive mixtures was considered to provide the worst case structural loading for the storage system because it maximizes the energy content within the system. The presence of the inner containers, not included in this test, not only reduces the gas volume but also acts as energy absorbing media, thus reducing the energy absorbed by the outer container. These observations demonstrate that the assumption of filling the empty 3013 container with the explosive mixture as the worst case condition for evaluating loss-of-containment for the system is justified.

Figure 12 shows the recorded peak pressures on pressure transducers P1-P5, and peak strains on S1-S9 for all the shots and mixtures. The static strains, ε_{CJ}, $\varepsilon_{CJ\ ref}$, ε_{CV}, corresponding to the CJ, reflected CJ and constant volume explosion pressures,

Figure 12. Peak pressures and strains for the three mixtures in the 3013 empty can tests. Gray vertical shaded region indicates the DDT threshold. DDT was not observed for mix B or C.

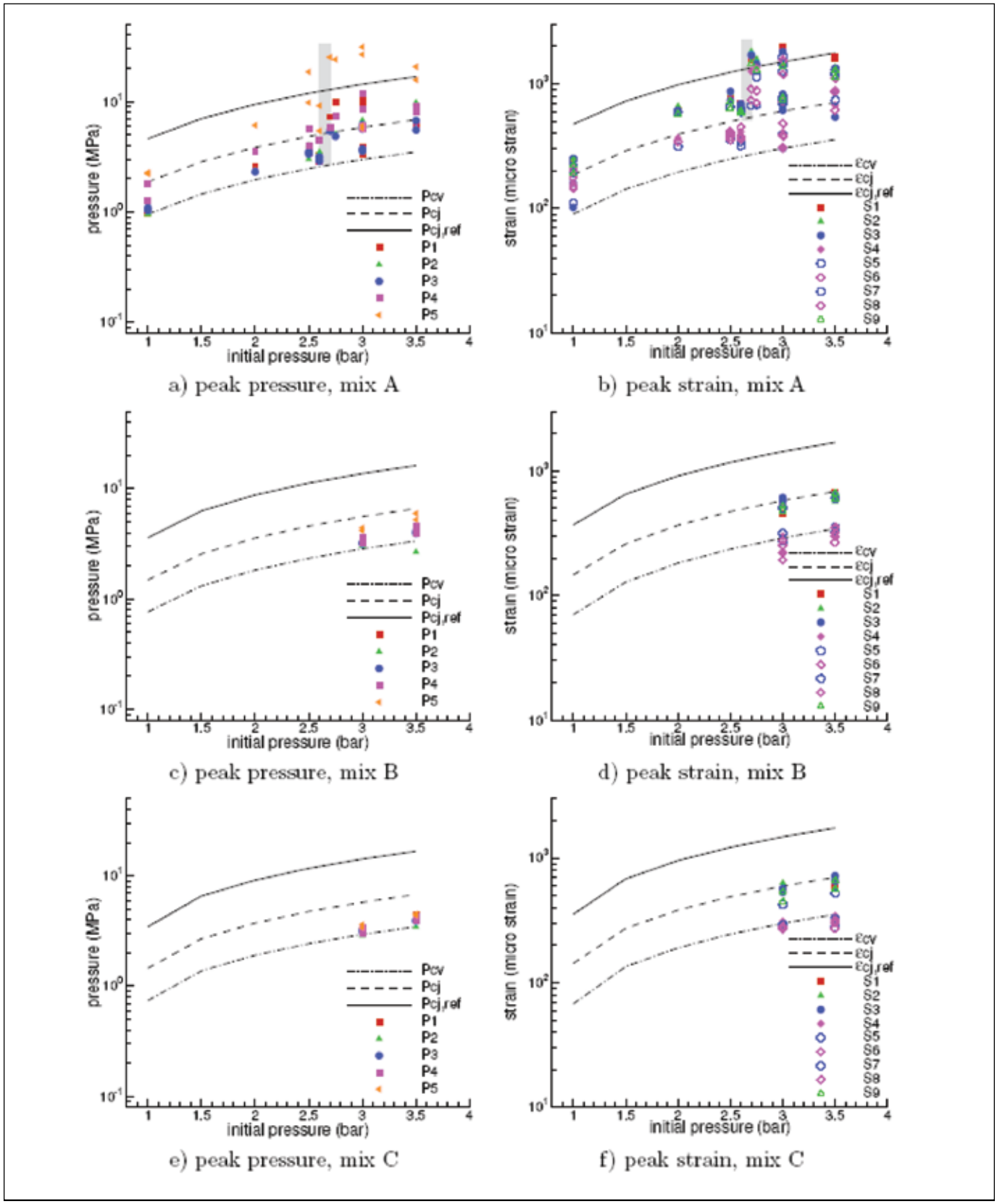

Figure 13. Comparison between the measured strains and the estimated strains (ε_{CJ}) based on P_{CJ} and Φ = 1, 2, and 5 for mixture A of the 3013 empty can tests

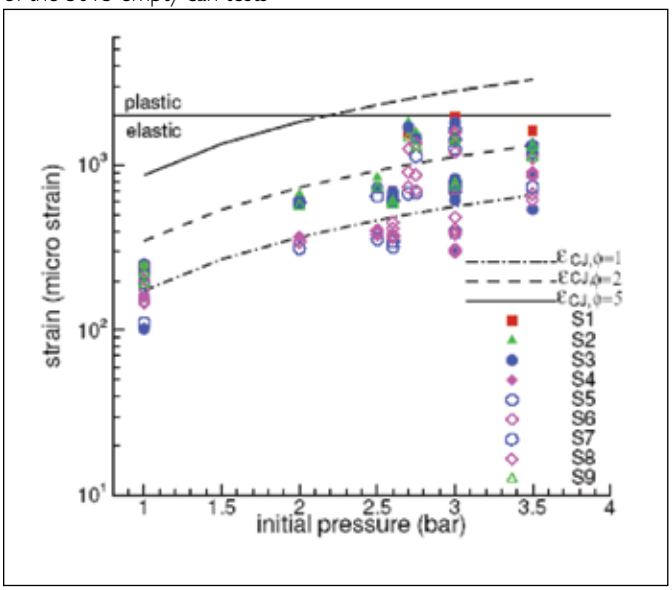

were calculated using equation (1) for the 3013 outer can, where E = 193 GPa, R = 2.40 in, and h = 0.118 in.

For the empty 3013 outer can configuration, the DDT transition was observed at an initial pressure of 2.6-2.7 bar for mixture A. This is essentially the same threshold initial pressure (2.5-2.6 bar) as observed for the empty thick-walled fixture (Figure 6a). The maximum peak strain was usually observed near the middle of the 3013 can on either S1 or S2 instead of close to the reflecting end as observed for the thick-walled fixture (Figure 6b). Peak strain increases with increasing initial pressure, and the overall trend is linear with sharp increases in the vicinity of the DDT threshold. Below the threshold at initial pressure of 2.6 bar, the peak strain was on the order of 700 μstrain, which is 1.33 times larger than the calculated ε_{CJ} value. Above the threshold at an initial pressure of 2.7 bar, the peak strain was on the order of 1800 μstrain, which is 1.34 times larger than the calculated ε_{CJref} value and very close to the convention for the onset of plastic behavior (2000 μstrain). For mixtures B and C, no DDT transition was observed for initial pressures up to 3.5 bar, which is consistent with the findings with the thick-walled tube.

The DLF for the tests performed on the 3013 containers ranged between 0.4 and 1.2. Values between 1.2 and 2.6 were measured for the empty thick-walled tube configuration. The values obtained indicate mixed mode loading between the impulsive and sudden regimes. The calculated values of Φ_{CJ} for the 3013 container varied between 1.2 and 3.2. Values of Φ_{CJ} between 1.7 and 3.5 were calculated for the thick-walled tube. The slightly higher values measured for the thick-walled tube configuration are most likely due to differences in the structural response associated with the detonation loads.

In Figure 13, the measured strains are compared with estimated strains based on P_{CJ} with dynamic load factors of 1 (static loading), 2 (sudden loading) and 5 (sudden loading with reflected detonation). For the empty 3013 container within the DDT range (initial pressure > 2.6 bar), the maximum measured strains are all larger than $\varepsilon_{CJ,\Phi=2}$, which is consistent with the results from the thick-walled tube. This is because DDT occurred close to the tube end, producing much higher strains than the case where detonation was initiated promptly.

Discussion

For the 3013 storage containment system, DDT transition is possible within the annulus between the containers for all gas mixtures as demonstrated by the results of testing the planar fixture and the thick-walled cylinder with annular gaps. DDT was also observed in the empty thick-walled cylinder tests and the actual 3013 container tests (without an inner container) at sufficiently high initial pressure with stoichiometric hydrogen-oxygen mixtures.

For the three mixtures tested, the peak hoop strains measured in the outer 3013 container are slightly less than the 0.2 percent strain conventionally used to determine the onset of plastic deformation. No structural failure or measurable deformation was found in the 3013 outer containers that were tested. Based on the results of these tests, it can be concluded that DDT of a stoichiometric hydrogen-oxygen mixture (and mixtures diluted with nitrogen and helium) within the 3013 nested containment system does not pose a threat to structural integrity of the outer container at initial pressures up to 3.5 bar and temperatures up to 150°C.

The inner or convenience containers were not tested. Based on these test results and analytical studies[1] the DDT threshold initial pressures are expected to be lower for small diameter containers and containers filled with granular material. Because peak pressures are proportional to initial pressures, the peak DDT pressures measured in the 3013 outer containers will bound the peak DDT pressures that will occur in the inner and convenience containers. If an explosion were to occur in the inner or convenience containers the peak strains and deformations will be higher for the inner and convenience containers than for the outer container because the outer container is more robust structurally than the inner and convenience containers.

Conclusion

The 3013 outer container is the credited safety pressure boundary for the nested 3013 storage canister system. The test results demonstrate that the 3013 container system will maintain its structural integrity following the postulated explosion accident.

George B. Rawls Jr. is a senior fellow engineer at Savannah River National Laboratory. He has an M.E. in mechanical engineering from the University of South Carolina and a B.S. in mechanical engineering from Clemson University.

F. Coyne Prenger is a retired Registered Professional Engineer. He has a Ph.D. in mechanical engineering from Colorado State University.

Joseph E. Shepherd is a professor of aeronautics and professor of mechanical engineering at California Institute of Technology. He has a Ph.D. in applied physics from the California Institute of Technology and a B.S. in physics from the University of South Florida.

Zhe Liang is a combustion scientist at Atomic Energy of Canada Limited – Chalk River Laboratories. Liangh has a Ph.D. in mechanical engineering from the University of Calgary, Canada, an M.S.in mechanical engineering from Sichuan University, China, and a B.S. in mechanical engineering from Chengdu University of Science and Technology, China.

Acknowledgements

Funding for this work was provided by the Surveillance and Monitoring Program, U.S. Department of Energy Office of Environmental Management. This work was conducted at California Technology Institute Los Alamos National Laboratory operated by Los Alamos National Security, LLC under contract DE-AC52-06NA25396 and at the Savannah River National Laboratory operated by Savannah River Nuclear Solutions for the U.S. Department of Energy under contract DE-AC09-08SR22470.

References

1. Liang, Z., and J. E. Shepherd. 2007. *Explosion Testing of Nested Can Containment System, in three parts,* Report No. FM2007. 001-.003, Explosion Dynamics Laboratory, California Institute of Technology.
2. Reynolds, W. C. 1986. *The Element Potential Method for Chemical Equilibrium Analysis: Implementation in the Interactive Program STANJAN,* Technical Report, Mechanical Engineering Department, Stanford University.
3. Biggs, J. 1964. *Introduction to Structural Dynamics.* McGraw-Hill Inc.
4. Paz, M., and W. Leigh. 2004. *Structural Dynamics.* Fifth Edition. Springer Publishing.

Gas Analyses from Headspace of Plutonium-bearing Materials Containers

Philip M. Almond, Nick J. Bridges, Glen F. Kessinger, and Jonathan M. Duffey
Savannah River National Laboratory, Aiken, South Carolina USA

Ronald R. Livingston, Lance E. Traver, and Matthew J. Arnold
Savannah River Nuclear Solutions, Aiken, South Carolina USA

Abstract

The Savannah River National Laboratory (SRNL) 3013 destructive examination program performs surveillance on 3013 containers originating from multiple sites across the U.S. Department of Energy (DOE) complex. The bases for the packaging, storage, and surveillance activities are derived from the DOE's 3013 Standard (DOE-STD-3013-2004). During destructive examination, headspace gas samples are obtained from the 3013 inner container and the annulus between the outer and inner containers. To characterize gas species, the samples are analyzed by gas chromatography (GC), direct-inlet mass spectrometry (DIMS), and Fourier-transform infrared spectroscopy (FTIR). The GC results, as well as other parameters, are utilized as input into the gas evaluation software tool (GEST) program for computation of pre-puncture gas compositions and pressures.

More than thirty containers from the Hanford Site and the Rocky Flats Environmental Technology Site (RFETS) have been examined in the first three years of the surveillance program. Several containers were shown to have appreciable hydrogen content (some greater than thirty mol percent), yet little or no oxygen was detected in any of the containers, including those exhibiting high hydrogen concentrations. Characteristics including moisture content, surface area, and material composition, along with the headspace gas composition, are utilized in an attempt to explain the chemical behavior of the packaged materials.

Introduction

The 3013 Destructive Examination Program—Headspace Gas Analysis

Plutonium-bearing materials packaged at the Savannah River Site (SRS) and other sites across the U.S. Department of Energy (DOE) complex, including Rocky Flats Environmental Technology Site (RFETS), Hanford, Los Alamos National Laboratory (LANL), and Lawrence Livermore National Laboratory (LLNL), are presently being stored at SRS in 3013 containers. The Department of Energy (DOE) 3013 Standard (DOE-STD-3013-2004) requires periodic surveillance of 3013 containers to verify container integrity during storage over their design life of fifty years.[1] As part of the surveillance requirements, a portion of the stored inventory is destructively examined under the 3013 surveillance program. Container selection is based upon random statistical sampling and engineering judgment provided by the Materials Identification and Surveillance (MIS) working group, a counsel of inter-laboratory experts in the field of packaging, corrosion, and radiolysis. More than thirty containers from Hanford and RFETS have been destructively examined at SRS during the first three years of the program.

Sampling and analysis of headspace gas from within 3013 containers is performed as part of the destructive examination of selected samples within the surveillance program. The potential presence of high container pressure in combination with the presence of hydrogen and oxygen within the container system is a primary concern because of the potential for container over-pressurization. A secondary concern is combustion upon opening the container.[2] During surveillance, headspace gas is extracted from the sealed 3013 container by using a specially designed can puncture device (CPD). Analysis of the gas is subsequently performed by gas chromatography (GC), Fourier-transform infrared spectroscopy (FTIR), and direct-inlet mass spectrometry (DIMS). Gas chromatography results and other input parameters are entered into the Gas Evaluation Software Tool (GEST), a program to calculate pre-puncture gas composition and pressure conditions of the inner container.[3] This suite of data provides valuable information regarding the behavior of 3013 containers during storage and is summarized in the paper.

Gas Generation in Hanford and RFETS Containers Packaged to the 3013 Standard

DOE-STD-3013-2004 requires containers of plutonium-bearing oxide to be welded and leak tight with a moisture content of less than 0.5 wt percent. Based on the standard requirements, it is possible that up to 25 g of water could be present, distributed throughout the container based on a maximum allowed material content of 5 kg. Although this is a small amount of water compared to the total amount of packaged material, radiolytic decomposition of any adsorbed moisture and waters of hydration, could have a significant effect on the hydrogen and oxygen

Figure 1. Can puncture device

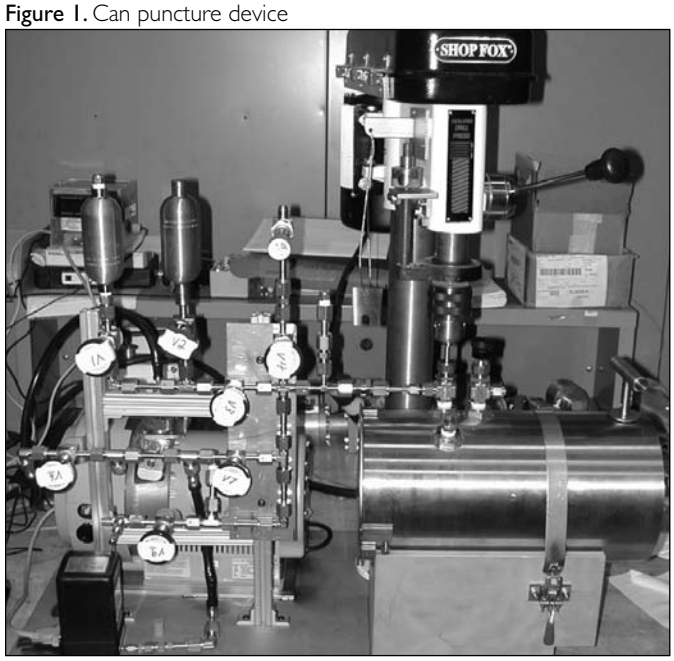

Figure 1. 150-cc Swagelok gas sample cylinders

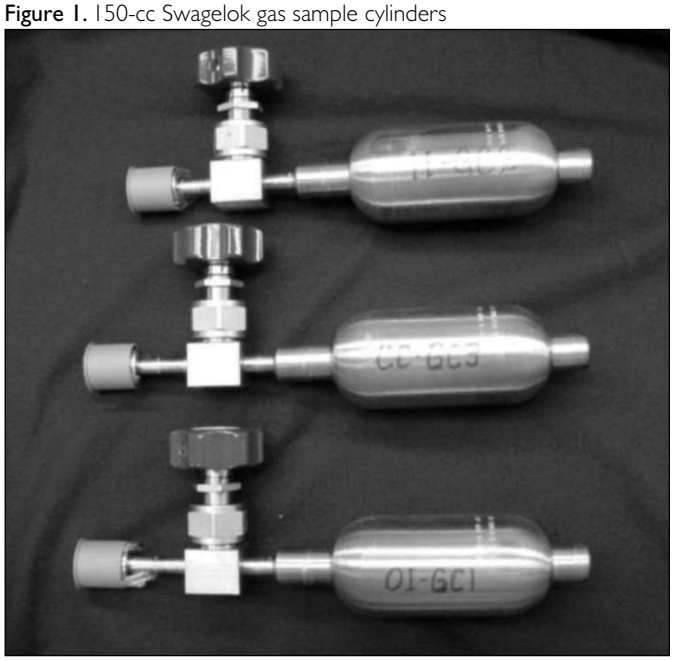

generation rates and the pressure of hydrogen and oxygen ultimately developed in the sealed container.[4-7]

The decomposition of water by radiolysis may produce hydrogen and oxygen, and ideally should produce them in stoichiometric quantities;[1] however, stoichiometric hydrogen and oxygen production was rarely observed in sealed container studies when the moisture content of the packaged material was less than 0.5 wt percent.[8] Rather, oxygen, if seen at all, was observed in substoichiometric amounts. This observation may be explained by the formation of a superstoichiometric plutonium oxide or corrosion reactions that produce metal oxides or hydroxides and release hydrogen.[1] The decomposition of water can occur by solid-state chemical reaction on the plutonium oxide surface to produce hydrogen, yet retain oxygen as PuO_{2+x}.[1,9] However, oxygen and hydrogen can also be removed from the headspace through recombination to form water. Recombination can be catalyzed by PuO_2,[10] other impurity oxides,[1,11] or even the stainless steel container itself.[11] Radiolytic recombination from alpha and gamma radiation has also been reported.[12]

Studies were performed by the MIS program on representative materials previously stabilized at Hanford and RFETS and packaged in small containers designed to mimic the behavior of packaged 3013 containers. Because of the material origin and the fact that no additional water was intentionally added by exposure to high humidity environments before packaging, these experiments are considered to be most closely related to material currently stored under the 3013 Standard.[8] The material water content in these small-scale MIS packages was estimated to be less than 0.2 wt percent. The experiments demonstrated that over a few years, oxygen present in test containers sealed in air was consumed, and little hydrogen was produced. These trends have also been observed for aged Hanford containers that were sealed for up to eighteen years.[13,14]

In a separate set of experiments, thirty-nine MIS small-scale containers of plutonium-bearing oxide material representative of the inventory of materials at RFETS, Hanford, and LANL were targeted at 0.5 wt percent moisture to create a bounding study for the effects of moisture. Nearly all of the MIS containers that produced hydrogen (as high as ~73 mol percent) did not produce much oxygen, or, if initially produced, the oxygen was later consumed, and therefore the gas content seldom reached the flammability region.[8] Two containers from this study were observed to reach flammable mixtures of hydrogen and oxygen. Sample 011589A had a hydrogen content of 46.0 mol percent at a maximum of 14.0 mol percent oxygen and 1000089 had a hydrogen content of 12.0 mol percent at a maximum of 7.5 mol percent oxygen. Sample 011589A reached approximately a four times greater maximum pressure increase and maximum partial pressure of oxygen and hydrogen than sample 1000089.[8]

Following this study, a database survey was performed for the items in the 3013 storage inventory that had the highest probability of being similar to the composition of sample 011589A. The evaluation, based on variables such as binning classification, prompt gamma analyses, moisture content, and process knowledge, was performed on the Integrated Safety Program (ISP) database and identified fifteen items originating from Hanford, RFETS, and SRS that are of specific interest.[15] Item R602498 has been analyzed and the results are communicated in this article.

SRNL has examined the headspace gas recovered from more than thirty Hanford and RFETS containers that had been sealed

for between four and six years. Physical properties, such as moisture content, as measured by thermogravimetric analysis—mass spectrometry (TGA-MS), surface area as measured by the Brunauer-Emmett-Teller (BET) method, and chemical composition are compared for hydrogen generating materials and non-hydrogen generating materials in an effort to deduce how hydrogen and oxygen are generated during storage.

Experimental

Can Puncture Device

The ability to drill into a 3013 container, measure pressure, and collect a pure gas sample at the Savannah River Site (SRS) was achieved through the development and implementation of the can puncture device (CPD). The CPD consists of three main parts: the pressure vessel, the drill press, and the piping system. The pressure vessel component of the CPD has a design pressure of 700 psig and is capable of holding the gases released up to the 699 psig design pressure of a 3013 outer container.[1] A quarter inch titanium drill bit is used for penetrating each wall of the 3013 container. Differential pressures are used as the motive force to move gases out of the 3013 container and into the gas sample cylinder. A picture of the CPD is shown in Figure 1.

The CPD is completely enclosed within a radiological glovebox that contains an air atmosphere. The air must be removed from the CPD prior to drilling to prevent contamination of the gas samples. The entire CPD system is evacuated to a pressure of less than 1.0 psia and then backfilled with N_2 to a pressure of 14.5 psia; this evacuation and backfill process is repeated two additional times. After this operation, the oxygen content in the system should be less than 0.008 mol percent. After a fourth evacuation, N_2 is then added to a pressure between 2.25 psia and 6.25 psia and a blank sample is collected in a 150-cc Swagelok stainless steel gas sample cylinder (Figure 2). The blank sample provides a positive means for demonstrating air has been removed from the CPD and that the system diagnostics are performing as expected prior to puncturing the 3013 container.[16,17]

Next, a sample of the gas between the outer and inner container is collected. A new Swagelok gas sample cylinder is connected to the piping system and the evacuation and back-fill process described above is repeated. A final pressure of 0.5 psia or less is established in the CPD, and a ten-minute leak check is also performed to ensure that in-leakage can be quantitatively addressed when analyzing the sample results. Once an acceptable leak rate of 0.004 psia/min has been established, the wall of the outer 3013 container is punctured. Gases expand from the 3013 annulus into the evacuated CPD pressure vessel and piping manifold, and the gas is subsequently drawn into a Swagelok gas sample cylinder. The evacuation, backfilling, and drilling procedure is repeated for penetration of the inner container and collection of the associated gas sample. The inner container (IC), annulus (OI), and blank (BL) samples are sent to Savannah River National Laboratory (SRNL) for analysis.[16,17]

Gas Evaluation Software Tool

The Gas Evaluation Software Tool (GEST - Version 2.0) was developed to calculate the pre-puncture gas conditions within the 3013 inner container. GEST calculates nitrogen, oxygen, hydrogen, helium, methane, and carbon dioxide percentages and inner container pressure. GEST input includes gas composition results from GC analysis and pressure data acquired from the CPD. The GEST accounts for pre-puncture glovebox in-leakage and post-puncture mixing of gases within the CPD. The actual transport or mixing of gases in the CPD following puncture of the inner 3013 container is extremely complex. The transport process is complicated by the tortuous path that the gases must follow to get to the sample cylinder (i.e., passing through the drill bit assembly, metal sintered filter, and quarter inch piping). Immediately after the container is punctured, the pressure will rapidly equilibrate and individual gas species will be quickly mixed with the residual gases left in the CPD. The gas composition becomes homogeneous through diffusion. A statistically designed test was developed to evaluate the transport of gases in the CPD. The test used various combinations of inner can pressures, CPD pressures and inner can free gas volumes. Results from the testing indicated that the "uniform mixing model," in which the gaseous composition of all volumes is identical after puncture of the inner container, best models the behavior of the gases inside the CPD system.[3]

Headspace Gas Analysis

The primary method of characterizing headspace gas from within 3013 containers is by GC. GC measurements are performed using a Varian CP-4900 micro-gas chromatograph that contains two columns, a 10-meter PoraPLOT Q column heated to 45°C using helium as the carrier gas and a twenty-five-meter Molsieve 5Å column heated to 60°C using argon as the carrier gas. Gas samples are analyzed quantitatively to determine helium, hydrogen, oxygen, nitrogen, methane, carbon dioxide, carbon monoxide, and nitrous oxide concentrations. The GC is installed in a radiological glovebox and controlled by an external computer. It is connected to a gas manifold utilized for evacuation, purging, and sample introduction. The GC is configured to measure gas sample pressures between 2 and 34.7 psia.

A Swagelok gas sample cylinder containing gas sampled by the CPD is connected to the gas manifold to be initially analyzed by GC. The manifold is flushed with argon and evacuated below 1 x 10^{-5} torr. Initially, analysis of argon passed through the manifold is performed to verify a blank background. After evacuation of the manifold, the sample gas is expanded into the system; if necessary, argon gas is added immediately before sampling to provide a constant inlet pressure of approximately 20 psia. A plugged flow configuration precludes the dilution of the gas sampled by the GC. The GC samples a 1-µL aliquot of the gas with a one second injection time. Sample gases are identified by comparing retention times to previously analyzed NIST-traceable gas standards. Peak areas are integrated to calculate mole

percentages of each gas. Qualitative measurements from DIMS and Fourier-transform infrared spectroscopy (FTIR) analyses are used to compliment the GC analysis. These measurements are performed using a MIDAC series 1 model I1301 FTIR with a 10 m beam path and a Pfeifer Omnistar 301 Quadrupole DIMS each connected to the gas manifold.

Results and Discussion

A selection of thirty-one 3013 material containers has been destructively examined at SRS after being stored for approximately four to six years, as of this writing. When attempting to understand gas behavior in a sealed container, the original gas composition and pressure at packaging is important; unfortunately, it was not possible to characterize the initial headspace gas compositions and pressures. There is, however, some knowledge of the packaging conditions.

The 3013 containers discussed herein were prepared at two different facilities. The average glovebox pressure at Hanford was near 742 torr, whereas the RFETS glovebox pressures averaged approximately 620 torr.[13] Variation in packaging conditions is clearly evident in the helium to nitrogen ratios observed between facilities. Containers packaged at both the Hanford Radioactive Material Center (RMC) line and RFETS were purged with helium in an air glovebox atmosphere before sealing, in an attempt to substitute inert gas (He) for air, and to reduce the oxygen content of the headspace gas to below 5 percent. The GC analyses of the inner can gas samples showed that most Hanford containers contained a He:N_2 ratio of approximately 1:1 upon opening, whereas most RFETS containers had a He:N_2 ratio of about 5:1. Other gases measured by GC included hydrogen, oxygen, methane, carbon dioxide, carbon monoxide, and nitrous oxide. A summary of GC results for the blank, annulus, and inner container, and final GEST reported gas compositions and pressures for the inner container are presented in Tables 1, 2, and 3.

The headspace gas composition during storage of plutonium oxide is important because the radiolytic production of gas can result in can pressurization and/or flammability. Pressures measured by the CPD and calculated by GEST for RFETS containers ranged from 11.7 to 13.7 psia and Hanford containers ranged from 11.1 to 20.6 psia. From an over-pressurization standpoint, helium production from alpha decay is expected to be small (less than 1 psia in five years).[1] Postulating RFETS and Hanford RMC containers were sealed having helium equal to that measured at opening less helium produced, the remainder of container contents at packaging would be air at packaging pressure. An analysis of pre-puncture container pressures calculated by the GEST software showed that GEST-calculated pressures for containers with hydrogen were less than predicted based on these assumptions (Table 4), even after accounting for oxygen depletion during storage. A mechanism for nitrogen gas removal by reaction of nitrogen and hydrogen gas to form ammonia and subsequently ammonium chloride solid is hypothesized as a possible explanation for the lower than predicted pressures. Crystalline ammonium chloride has been detected in the corrosion product of H004111 on the inside walls of its convenience container in the headspace region.[18]

The GC results for the 3013 containers packaged at Hanford measured a hydrogen content as high as 36.3 mol percent. Seven containers that produced hydrogen over 0.1 percent are compiled in Table 4. Oxygen contents for each of these containers were below 0.1 mol percent, precluding any in-container flammability concerns. The material contents of the seven containers were very similar with respect to moisture content, surface area, and chloride content. Moisture analysis was performed by TGA-MS on samples of material taken from each container immediately after opening.[19] Moisture levels ranged from 0.19 to 0.33 wt percent. Based on measured hydrogen concentration and moisture content at opening, up to approximately 0.02 wt percent, or up to ~7 percent of the calculated original moisture content was decomposed to hydrogen during storage (Table 4). BET surface area measurements from a representative sampling of each container ranged from 0.99 to 1.30 m^2/g.[19] Approximately 5.7-7.4 wt percent chloride, originating from pyrochemical operations, was measured by ion chromatography (IC) of solutions from representative material leached with nanopure deionized water for three hours at 90°C. Because of the presence of hygroscopic alkaline earth chlorides remaining after calcination in these materials, such as magnesium and calcium chlorides that form hydrates, most of the moisture is likely associated with the chloride salt.

Twenty-four remaining containers that were examined did not produce hydrogen greater than 0.01 mol percent (Tables 1, 2, and 3). Of these containers, only four, H002088, H003157, R610735, and R602498, contained moisture at levels greater than or equal to 0.1 wt percent after opening. Therefore, only these four containers had moisture contents in the range anticipated for hydrogen producing containers. (The moisture contents for each of these materials, as measured by TGA-MS, were 0.18, 0.10, 0.19, and 0.13 wt percent, respectively). Chloride contents measured from leached solutions by IC were at or below detection limits for H002088 and H003157. R610735 and R602498 measured 20 wt percent and 0.7 wt percent chloride, respectively. BET surface area measurements for these materials were 2.02, 1.98, 0.58, and 0.93 m^2/g, respectively.[19] R610735 was most similar to the hydrogen-generating containers in total chloride content and reported moisture. However, the material from R610735 was observed to have increased hygroscopic properties, and possibly adsorbed moisture between opening of the 3013 container and TGA-MS analysis of the initial moisture sample, giving an overestimation of moisture. H003157 measured 1.7 mol percent oxygen, the highest oxygen concentration observed.

One container, R602498, was identified through a study of the ISP database as a possible candidate for hydrogen and oxygen generation similar to 011589A (from the MIS investigation).

Table 1. FY07 Gas analysis results from gas chromatography and GEST Report

Sample Information	N_2 (%)	O_2 (%)	H_2 (%)	CO_2 (%)	CH_4 (%)	He (%)	CO (%)	He:N_2	GEST Pressure (psia)
FY07-01 (R600885)									
BL-0009	98.30	2.31	Trace	Trace	ND	ND	ND		
OI-0009	28.20	0.53	0.12	0.19	ND	70.20	ND		
IC-0009	10.30	0.11	Trace	Trace	ND	89.40	ND		
GEST (IC)	**9.2**	**0.0**	**0.0**	**0.0**	**0.0**	**90.8**	**NC**	**9.9**	**12.8**
FY07-02 (R601722)									
BL-0016	93.70	2.62	0.03	Trace	ND	ND	ND		
OI-0016	37.80	4.20	0.10	0.14	ND	54.70	ND		
IC-0015	15.90	0.05	Trace	ND	ND	82.20	ND		
GEST (IC)	**12.7**	**<0.1**	**0.0**	**0.0**	**0.0**	**87.2**	**NC**	**6.9**	**12.5**
FY07-03 (R601957)									
BL-0014	93.50	0.12	0.08	Trace	Trace	Trace	ND		
OI-0014	17.90	ND	0.12	0.22	ND	77.90	ND		
IC-0014	11.90	ND	Trace	Trace	ND	86.20	ND		
GEST (IC)	**10.4**	**0.0**	**0.0**	**0.0**	**0.0**	**89.6**	**NC**	**8.6**	**12.8**
FY07-04 (R600719)									
BL-0005	80.00	0.02	Trace	Trace	ND	Trace	ND		
OI-0005	NM	NM	NM	NM	NM	NM	NM		
IC-0005	18.30	ND	Trace	Trace	ND	80.00	ND		
GEST (IC)	**16.2**	**0.0**	**0.0**	**0.0**	**0.0**	**83.8**	**NC**	**5.2**	**12.9**
FY07-05 (R610735)									
BL-0002	96.80	0.04	Trace	Trace	ND	Trace	ND		
OI-0002	23.50	ND	0.10	0.10	Trace	72.80	Trace		
IC-0001	19.20	ND	Trace	0.14	ND	75.80	ND		
GEST (IC)	**17.5**	**0.0**	**0.0**	**0.2**	**0.0**	**82.3**	**NC**	**4.7**	**12.4**
FY07-06 (R610697)									
BL-0017	97.00	ND	0.05	Trace	Trace	0.05	ND		
OI-0017	24.70	0.70	0.05	0.10	Trace	73.40	Trace		
IC-0017	18.60	ND	0.01	Trace	Trace	80.80	ND		
GEST (IC)	**18.0**	**0.0**	**0.0**	**0.0**	**0.0**	**82.0**	**NC**	**4.6**	**12.5**
FY07-07 (R601285)									
BL-0013	67.80	0.03	0.03	Trace	ND	0.03	ND		
OI-0013	21.80	ND	0.13	0.11	Trace	76.90	0.02		
IC-0013	24.40	ND	Trace	Trace	0.02	75.40	ND		
GEST (IC)	**22.5**	**0.0**	**0.0**	**0.0**	**<0.1**	**77.4**	**NC**	**3.4**	**13.4**

RFETS site origin contains the letter R or H<1000, Hanford site origin contains H>1000, BL = blank, OI = annulus, IC = inner container, ND = not detected, NC = not calculated, NM = not measured, trace = <0.01 mol %

Oxygen was measured at <0.1 mol percent and hydrogen was not detected. Analysis of material from R602498, by ICP-ES, gave 0.7 percent Ca and 0.5 percent Mg, while Na and K were below detection limits.[20] While R602498 was determined to be similar to 011589A based on Query 1,[15] the moisture content of 0.13 wt percent was well below 0.3 wt percent suggested to permit oxygen generation from MIS 011589A experiments.[21]

Table 2a. FY08 gas analysis results from gas chromatography and GEST Report

Sample Information	N_2 (%)	O_2 (%)	H_2 (%)	CO_2 (%)	CH_4 (%)	He (%)	CO (%)	He:N_2	GEST Pressure (psia)
FY08-01 (R602731)									
BL-0001	100.10	ND	ND	Trace	ND	ND	ND		
OI-0007	31.20	0.90	0.02	0.12	Trace	67.20	ND		
IC-0006	18.70	0.07	Trace	Trace	Trace	81.30	ND		
GEST (IC)	**16.1**	**<0.1**	**Trace**	**Trace**	**Trace**	**83.9**	**NC**	**5.2**	**12.3**
FY08-02 (R601318)									
BL-0004	100.20	ND	ND	Trace	ND	ND	ND		
OI-0008	24.20	0.46	0.08	0.06	Trace	74.70	ND		
IC-0007	11.20	ND	Trace	Trace	ND	87.50	ND		
GEST (IC)	**8.5**	**0.0**	**Trace**	**Trace**	**0.0**	**91.5**	**NC**	**10.8**	**12.6**
FY08-03 (H000898)									
BL-0011	101.90	ND	Trace	Trace	ND	ND	ND		
OI-0010	31.80	ND	0.15	0.09	Trace	69.30	ND		
IC-0008	23.00	0.05	Trace	0.25	ND	76.30	ND		
GEST (IC)	**19.3**	**<0.1**	**Trace**	**0.3**	**0.0**	**80.3**	**NC**	**4.2**	**12.3**
FY08-04 (R610327)									
BL-0012	100.30	ND	0.02	Trace	ND	ND	ND		
OI-0011	23.50	0.17	0.04	0.09	Trace	74.00	ND		
IC-0018	19.70	ND	Trace	0.41	ND	78.20	ND		
GEST (IC)	**16.7**	**0.0**	**Trace**	**0.4**	**0.0**	**82.8**	**NC**	**5.0**	**12.4**
FY08-05 (R610298)									
BL-0007	97.90	1.02	ND	Trace	ND	ND	ND		
OI-0001	25.10	ND	0.18	0.11	Trace	72.70	ND		
IC-0019	17.80	ND	Trace	Trace	ND	79.40	ND		
GEST (IC)	**16.0**	**0.0**	**Trace**	**Trace**	**0.0**	**84.0**	**NC**	**5.3**	**13.0**
FY08-06 (R610324)									
BL-0018	102.30	ND	ND	Trace	ND	ND	ND		
OI-0018	29.10	0.03	0.11	0.07	Trace	72.00	ND		
IC-0020	21.00	ND	Trace	ND	ND	78.70	ND		
GEST (IC)	**17.7**	**0.0**	**Trace**	**0.0**	**0.0**	**82.3**	**NC**	**4.6**	**13.1**
FY08-07 (H001992)									
BL-0019	99.40	ND	ND	Trace	ND	ND	ND		
OI-0019	17.80	0.04	0.25	0.02	Trace	79.50	ND		
IC-0021	43.30	ND	Trace	ND	ND	54.40	ND		
GEST (IC)	**42.2**	**0.0**	**Trace**	**0.0**	**0.0**	**57.8**	**NC**	**1.4**	**13.3**
FY08-08 (H003157)									
BL-0021	101.40	0.01	Trace	Trace	ND	Trace	ND		
OI-0021	15.70	Trace	0.38	Trace	Trace	83.60	ND		
IC-0023	45.60	1.57	Trace	Trace	ND	52.10	ND		
GEST (IC)	**44.0**	**1.7**	**Trace**	**Trace**	**0.0**	**54.3**	**NC**	**1.2**	**12.4**

RFETS site origin contains the letter R or H<1000, Hanford site origin contains H>1000, BL = blank, OI = annulus, IC = inner container, ND = not detected, NC = not calculated, NM = not measured, trace = <0.01 mol %

Table 2b. FY08 gas analysis results from gas chromatography and GEST Report

Sample Information	N_2 (%)	O_2 (%)	H_2 (%)	CO_2 (%)	CH_4 (%)	He (%)	CO (%)	He:N_2	GEST Pressure (psia)
FY08-09 (R610584)									
BL-0020	94.10	6.34	Trace	<0.1	ND	ND	Trace		
OI-0020	26.20	ND	0.13	0.20	Trace	73.00	0.04		
IC-0022	18.00	ND	Trace	0.64	ND	80.90	ND		
GEST (IC)	**14.8**	**0.0**	**Trace**	**0.7**	**0.0**	**84.6**	**NC**	**5.7**	**13.7**
FY08-10 (R610578)									
BL-0022	97.10	3.40	Trace	0.01	ND	Trace	ND		
OI-0022	22.90	Trace	0.11	0.06	Trace	76.40	ND		
IC-0025	21.00	ND	Trace	0.02	ND	77.80	ND		
GEST (IC)	**17.8**	**0.0**	**Trace**	**<0.1**	**0.0**	**82.1**	**NC**	**4.6**	**12.5**
FY08-11 (H001916)									
BL-0023	101.40	0.37	Trace	Trace	ND	ND	ND		
OI-0023	19.00	Trace	0.20	0.03	Trace	80.60	ND		
IC-0024	48.90	ND	Trace	Trace	ND	52.40	ND		
GEST (IC)	**45.6**	**0.0**	**Trace**	**Trace**	**0.0**	**54.5**	**NC**	**1.2**	**13.3**
FY08-12 (H002088)									
BL-0024	101.80	ND	Trace	Trace	ND	ND	ND		
OI-0024	16.40	ND	0.62	Trace	Trace	83.80	ND		
IC-0026	44.40	ND	Trace	Trace	ND	56.80	ND		
GEST (IC)	**41.6**	**0.0**	**Trace**	**Trace**	**0.0**	**58.4**	**NC**	**1.4**	**12.4**
FY08-13 (H003409)									
BL-0025	100.30	ND	Trace	ND	ND	ND	ND		
OI-0025	17.50	ND	0.28	Trace	Trace	81.10	ND		
IC-0027	38.10	ND	18.10	Trace	Trace	45.60	ND		
GEST (IC)	**34.2**	**0.0**	**18.7**	**Trace**	**Trace**	**47.1**	**NC**	**1.4**	**13.4**
FY08-14 (H002573)									
BL-0026	103.10	ND	Trace	Trace	ND	ND	ND		
OI-0026	18.40	Trace	0.22	0.01	Trace	80.90	ND		
IC-0028	35.10	ND	28.80	0.31	Trace	41.20	ND		
GEST (IC)	**33.9**	**0.0**	**27.9**	**0.3**	**Trace**	**37.9**	**NC**	**1.1**	**17.6**
FY08-15 (H002534)									
BL-0027	101.50	ND	Trace	Trace	ND	ND	ND		
OI-0027	NM	NM	NM	NM	NM	NM	NM		
IC-0029	29.30	ND	30.10	2.62	0.39	40.40	0.75		
GEST (IC)	**24.0**	**0.0**	**30.8**	**2.7**	**0.4**	**41.4**	**0.8**	**1.7**	**13.7**
FY08-16 (R610679)									
BL-0028	100.30	ND	ND	Trace	ND	ND	ND		
OI-0028	14.10	ND	0.27	0.17	Trace	83.80	ND		
IC-0030	30.50	ND	Trace	2.76	ND	65.60	0.07		
GEST (IC)	**26.7**	**0.0**	**Trace**	**3.0**	**0.0**	**70.3**	**NC**	**2.6**	**11.7**
FY08-17 (H002750)									
BL-0029	101.00	ND	ND	Trace	ND	ND	ND		
OI-0029	19.50	Trace	0.21	0.01	Trace	79.70	ND		
IC-0031	40.50	0.34	Trace	Trace	ND	58.50	ND		
GEST (IC)	**36.8**	**0.1**	**Trace**	**Trace**	**0.0**	**63.1**	**NC**	**1.7**	**13.1**

RFETS site origin contains the letter R or H<1000, Hanford site origin contains H>1000, BL = blank, OI = annulus, IC = inner container, ND = not detected, NC = not calculated, NM = not measured, trace = <0.01 mol %

Table 3. FY09 gas analysis results from gas chromatography and GEST Report

Sample Information	N_2 (%)	O_2 (%)	H_2 (%)	CO_2 (%)	CH_4 (%)	He (%)	CO (%)	He:N_2	GEST Pressure (psia)
FY09-01 (H004099)									
BL-0030	100.00	1.11	ND	ND	ND	Trace	Trace		
OI-0030	19.94	<0.1	0.59	<0.1	ND	78.28	ND		
IC-0032	55.10	0.19	Trace	0.34	ND	41.11	Trace		
GEST (IC)	**53.0**	**0.2**	**Trace**	**0.4**	**0.0**	**45.0**	**NC**	**0.8**	**11.7**
FY09-02 (H004111)									
BL-0031	102.00	ND	ND	<0.1	ND	ND	ND		
OI-0031	26.54	Trace	0.28	<0.1	ND	72.64	ND		
IC-0033	47.82	<0.1	20.43	Trace	ND	32.30	ND		
GEST (IC)	**44.4**	**<0.1**	**21.5**	**Trace**	**0.0**	**34.1**	**NC**	**0.8**	**14.4**
FY09-03 (H002554)									
BL-0032	100.00	ND	ND	<0.1	ND	Trace	ND		
OI-0032	33.26	Trace	19.31	Trace	Trace	49.44	ND		
IC-0034	NM	NM	NM	NM	NM	NM	NM		
GEST (IC)	**32.6**	**Trace**	**22.1**	**Trace**	**Trace**	**45.3**	**NC**	**1.4**	**12.4**
FY09-04 (H001941)									
BL-0033	101.55	ND	ND	Trace	ND	ND	ND		
OI-0033	4.66	<0.1	0.31	Trace	Trace	95.97	ND		
IC-0035	49.72	ND	Trace	Trace	ND	49.16	ND		
GEST (IC)	**49.8**	**0.0**	**Trace**	**Trace**	**0.0**	**50.2**	**NC**	**1.0**	**13.2**
FY09-05 (R602498)									
BL-0034	102.60	Trace	ND	Trace	ND	ND	ND		
OI-0034	18.34	0.24	<0.1	0.15	Trace	83.04	ND		
IC-0036	13.65	<0.1	ND	Trace	ND	88.78	ND		
GEST (IC)	**12.5**	**<0.1**	**0.0**	**0.0**	**0.0**	**87.5**	**NC**	**7.0**	**12.3**
FY09-06 (H002509)									
BL-0035	103.10	0.31	ND	Trace	ND	Trace	ND		
OI-0035	3.61	0.19	0.29	<0.1	Trace	98.70	ND		
IC-0037	31.18	<0.1	34.00	0.41	<0.1	31.95	ND		
GEST (IC)	**29.2**	**<0.1**	**36.3**	**0.4**	**0.0**	**34.1**	**NC**	**1.2**	**20.6**
FY09-07 (H002565)									
BL-0036	103.36	<0.1	ND	Trace	ND	ND	ND		
OI-0036	3.69	0.11	0.23	<0.1	Trace	98.29	ND		
IC-0038	41.37	<0.1	4.45	<0.1	Trace	56.27	ND		
GEST (IC)	**39.8**	**<0.1**	**4.4**	**<0.1**	**Trace**	**55.8**	**NC**	**1.4**	**11.1**

RFETS site origin contains the letter R or H<1000, Hanford site origin contains H>1000, BL = blank, OI = annulus, IC = inner container, ND = not detected, NC = not calculated, NM = not measured, trace = <0.01 mol %

Conclusions

Gas composition and container pressure results obtained from the destructive surveillance of 3013 containers packaged at Hanford and RFETS provide important data on the gas generation characteristics of plutonium-bearing material from actual 3013 storage inventory. Containers having greater than trace hydrogen had less than 0.1 mol percent oxygen, averting flammability concerns for similar containers in storage. Their material moisture levels were at least 0.19 wt percent upon opening. All observed pressures are well below the 699 psig design pressure for a 3013

Table 4. Results for hydrogen containers

Sample Information	N_2 (%)	O_2 (%)	H_2 (%)	CO_2 (%)	CH_4 (%)	He (%)	CO (%)	He:N_2	GEST Pressure (psia)	Predicted Pressure (psia)	Measured Moisture (wt %)	Calculated Moisture at Packaging (wt %)	Packaging Moisture Consumed (%)	Leached Chloride (wt %)
FY08-13 (H003409)														
GEST (IC)	34.2	ND	18.7	Trace	Trace	47.1	NC	1.4	13.4	15.4	0.29	0.30	2.2	6.4
FY08-14 (H002573)														
GEST (IC)	33.9	ND	27.9	0.3	Trace	37.9	NC	1.1	17.6	18.1	0.33	0.34	3.9	6.3
FY08-15 (H002534)														
GEST (IC)	24.0	ND	30.8	2.7	0.4	41.4	0.8	1.7	13.7	17.7	0.19	0.20	5.7	6.3
FY09-02 (H004111)														
GEST (IC)	44.4	<0.1	21.5	Trace	0.0	34.1	NC	0.8	14.4	15.9	0.26	0.27	3.2	5.8
FY09-03 (H002554)														
GEST (IC)	32.6	Trace	22.1	Trace	Trace	45.3	NC	1.4	12.4	15.7	0.22	0.23	3.2	6.7
FY09-06 (H002509)														
GEST (IC)	29.2	<0.1	36.3	0.4	ND	34.1	NC	1.2	20.6	20.8	0.26	0.28	7.3	5.7
FY09-07 (H002565)														
GEST (IC)	39.8	<0.1	4.4	<0.1	Trace	55.8	NC	1.4	11.1	13.6	0.25	0.25	0.5	7.4

RFETS site origin contains the letter R or H<1000, Hanford site origin contains H>1000, BL = blank, OI = annulus, IC = inner container, ND = not detected, NC = not calculated, NM = not measured, trace = <0.01 mol %

outer container. The ISP database was utilized to identify 3013 containers in storage with a potential to have a composition similar to test material in MIS item 011589A, which generated both hydrogen and oxygen when loaded with 0.5 wt percent moisture. R602498, identified by the MIS program as possibly being similar to that of 011589A, did not contain a flammable gas mixture in the headspace. R602498, with a moisture content of 0.13 wt percent, had no detectable hydrogen and an oxygen content <0.1 mol percent, supporting the conclusion of MIS 011589A experiments, that greater than 0.3 wt percent moisture is needed for oxygen to be generated for 011589A-like materials.[21]

Monitoring gas composition and pressure of containers with plutonium-bearing oxide materials during storage provides a key piece of information to evaluate potential container behavior. Headspace gas results from the surveillance program to date support the ability of 3013 containers to store these materials safely over their expected life of fifty years. However, more data from the continued destructive examination of 3013 containers as well as further experimental work are needed to meet the established statistical evaluation basis[22] and to satisfactorily explain differences between observed and predicted pressures for hydrogen-generating materials. Additional work is also needed to understand why observed hydrogen pressures are much lower than might be predicted based on moisture content and experimentally determined rates of hydrogen generation. Finally, multiple small-scale studies in which simultaneous hydrogen and oxygen generation were observed for materials with moisture contents allowed by the 3013 standard point to the importance of continued surveillance of the 3013 inventory to ensure these materials can continue to be safely stored.

Philip M. Almond is a senior scientist a at Savannah River National Laboratory. He has a B.S. and a Ph.D. in chemistry from Auburn University.

Ronald R. Livingston is a continuous improvement expert at Savannah River Nuclear Solutions. He has a B.S. in chemistry from Augusta College.

Lance Traver is a lead engineer for surveillance operations in K-Area at Savannah River Nuclear Solutions. He has an M.S. in environmental engineering from University of Maryland and a B.S. in civil engineering from Rice University.

Matthew J. Arnold is a destructive examination system engineer at Savannah River Nuclear Solutions. He has a B.S. in chemical engineering from Auburn University.

Nick J. Bridges is a senior scientist at Savannah River National Laboratory. He has a Ph.D. in chemistry from the University of Alabama and a B.S. in chemistry from Tennessee Technological University.

Glen F. Kessinger is a Fellow Scientist at Savannah River National Laboratory. He has a Ph.D. in physical chemistry from the University of Kansas and a B.A. in chemistry from the University of Northern Colorado.

Jonathan M. Duffey is a principal scientist at Savannah River National Laboratory. He has a Ph.D. and an M.S. in chemistry from the University of Tennessee and a B.S. in Chemistry from Union University.

Acknowledgements

This work was performed at the Savannah River Site and Savannah River National Laboratory. Savannah River National Laboratory is operated by Savannah River Nuclear Solutions for the U.S. Department of Energy under contract DE-AC09-08SR22470.

References

1. *Stabilization, Packaging, and Storage of Plutonium-bearing Materials.* 2004. DOE-STD-3013-2004. U.S. Department of Energy: Washington, D.C.
2. Bailey, G., E. Bluhm, J. Lyman, R. Mason, M. Paffet, G. Polansky, G. D. Roberson, M. Sherman, D. K. Veirs, and L. Worl. 2000. Gas Generation from Actinide Oxide Materials, LA-13781-MS.
3. Hardy, B. J. 2009. Gas Evaluation Software Tool (GEST), G-TRT-A-00005.
4. LaVerne, J. A., and L. Tandon. 2002. H_2 Production in the Radiolysis of Water Sorbed on CeO_2 and ZrO_2, *Journal of Physical Chemistry B* 106, 380-386.
5. Livingston, R., and J. Duffey. 2001. Effects of Plutonium Dioxide Moisture Content and Calcination Temperature on the Headspace Gas Composition of Sealed Containers, WSRC-TR-2001-00420.
6. Veirs, K. D. 2006. Gas Generation from Water Adsorbed onto Pure Plutonium Dioxide Powder, *Materials Research Society Symposium Proceedings,* 893, 3.1-3.6.
7. Vladimirova, M. V., I. A. Kulikov. 2002. Formation of H_2 and O_2 in Radiolysis of Water Sorbed on PuO_2, *Radiochemistry* 44, 86-90.
8. Berg, J., K. Veirs, and L. Worl. 2006. Maximum Pressure for Structural Response Calculation of 3013 Containers, LA-UR-06-4051.
9. Haschke, J. M., T. H. Allen, and L. A. Morales. 2000. Reaction of Plutonium Dioxide with Water: Formation and Properties of PuO_{2+x}, *Science* 287(5451), 285-287.
10. Morales, L. 1998. Preliminary Report on the Recombination Rates of Hydrogen and Oxygen over Pure and Impure Plutonium Oxides, LA-UR-98-5200.
11. Quigley, G. 1998. Hydrogen/Oxygen Recombination Rates in 3013-Type Environments: A Report on the Loss of Hydrogen and Oxygen from Cells Containing Non-Radiolytic Samples, LA-UR-98-4557.
12. Lloyd, J., L. Hyder, and P. G. Eller. 1998. Literature Search on Hydrogen/Oxygen Recombination and Generation in Plutonium Storage Environments, LA-UR-98-4557.
13. Mason, R., T. Allen, L. Morales, N. Rink, R. Hagan, D. Fry, L. Foster, B. Beneder, E. Wilson, C. Martinez, P. Martinez, M. Valdez, F. Hampel, O. Peterson, J. Rubin, and K. Hollis. 1999. Materials Identification and Surveillance: June 1999 Characterization Status Report, LA-UR-99-3053.
14. Eller, P. G., R. E. Mason, D. R. Horrell, S. D. McKee, N. A. Rink, and C. S. Leasure. 1999. Gas Pressurization from Calcined Plutonium Oxides, LA-UR-99-3804.
15. Friday, G. P., and L. G. Peppers. 2006. Investigation of MIS Item 011589A and 3013 Containers Having Similar Characteristics, WSRD-TR-2006-00236.
16. Traver, L. E. 2006. Safety Assessment of the Can Puncture Device, WSRC-TR-2006-00415.
17. Traver, L. E. 2009. KIS Can Puncture Device Process Flow Sheet, U-TRT-K-00001.
18. Veirs, D. K., J. M. Berg, K. A. Dunn, M. R. Louthan, Jr., L. A. Worl, and J. E. Narlesky. 2010. Evidence of Corrosive Gas Formed by Radiolysis of Chloride Salts in Plutonium-Bearing Materials, *Journal of Nuclear Materials Management* Vol. 38, No. 3.
19. Crowder, M. L., J. M. Duffey, R. R. Livingston, J. H. Scogin, G. F. Kessinger, and P. M. Almond. 2009. Moisture and Surface Area Measurements of Plutonium-Bearing Oxides, *Journal of Alloys and Compounds,* 488, 565-568.
20. Kessinger, G. F., P. M. Almond, M. G. Bronikowski, M. L. Crowder, J. M. Duffey, A. R. Jurgensen, D. M. Missimer. J. H. Scogin, and M. E. Summer. 2010. Material Properties of Plutonium-Bearing Oxides Stored in Stainless Steel Containers, *Journal of Nuclear Materials Management,* Vol. 38, No. 3.
21. Berg, J. M., E. Garcia, G. Long, M. Martinez, J. Narlesky, D. K. Veirs, C. Villiams. and L. Worl. The Effect of Moisture Content on Oxygen Generation for 011589A Substitute Materials, LA-UR-08-2546.
22. Peppers, L., E. Kelly, J. McClard, G. Friday, T. Venetz, and J. Stakebake. Selection of 3013 Containers for Field Surveillance, LA-14310.

Nondestructive Examination of Containers with Plutonium-bearing Materials

Lester Yerger, James McClard, Lance Traver, and Tom Grim
Savannah River Site, Aiken, South Carolina USA

Theodore Venetz
CH2MHill Plateau Remediation, Richland, Washington USA

Elizabeth Kelly
Los Alamos National Laboratory, Los Alamos, New Mexico USA

David Riley
Lawrence Livermore National Laboratory, Livermore, California USA

Abstract

The first nondestructive examination (NDE) of 3013-type containers as part of the U.S. Department of Energy's (DOE's) Integrated Surveillance Program (ISP)[1] was performed in February 2005. Since that date 280 NDE surveillances on 255 containers have been conducted. These containers were packaged with plutonium-bearing materials at multiple DOE sites. The NDE surveillances were conducted at Hanford, Lawrence Livermore National Laboratory (LLNL), and Savannah River Site (SRS). These NDEs consisted of visual inspection, mass verification, radiological surveys, prompt gamma analysis, and radiography.

The primary purpose of performing NDE surveillances is to determine if there has been a significant pressure buildup inside the inner 3013 container. This is done by measuring the lid deflection of the inner 3013 container using radiographic images. These lid deflection measurements are converted to pressure measurements to determine if a container has a pressure of 100 psig or greater. Making this determination is required by Surveillance and Monitoring Plan (S&MP).[2] All 3013 containers are designed to withstand at least 699 psig as specified by DOE-STD-3013.[3] To date, all containers evaluated have pressures under 50 psig. In addition, the radiographs are useful in evaluating the contents of the 3013 container as well as determining the condition of the walls of the inner 3013 container and the convenience containers. The radiography has shown no signs of degradation of any container, but has revealed two packaging anomalies.

Quantitative pressure measurements based on lid deflections, which give more information than the "less than or greater than 100 psig" (pass/fail) data are also available for many containers. Statistical analyses of the pass/fail data combined with analysis of the quantitative data show that it is extremely unlikely that any container in the population of 3013 containers considered in this study (e.g., containers packaged according to the DOE-STD-3013 by 2006) would exceed a pressure of 100 psig. At this time, Los Alamos National Laboratory (LANL) and LLNL continue to package containers. Future NDE surveillances will address containers packaged after 2006 for both sites as well as containers requested by the Materials Identification Surveillance (MIS) working group based on knowledge gained from shelf-life study and surveillance results.

Introduction

The first Integrated Surveillance Program (ISP) nondestructive examination (NDE) was performed February 27, 2005, in the F-Area Material Storage Facility at the Savannah River Site (SRS). Since this time, 255 3013-type containers have undergone NDE at Hanford, Lawrence Livermore National Laboratory (LLNL), and SRS. These containers were packaged at multiple DOE sites, including Hanford, LLNL, Rocky Flats Environmental Technology Site (RFETS), and SRS.

The Surveillance and Monitoring Plan (S&MP) sampling specification includes binning the population of containers into three bins based on a container's contents and assumed potential for experiencing selected degradation mechanisms.[4,5] Potential degradation mechanisms include corrosion and pressurization. The three bins have been designated: Pressure and Corrosion (pressurization and corrosion mechanisms possible), Pressure Only (pressurization only, corrosion unlikely), and Innocuous (pressurization and corrosion unlikely). A random sample of 3013 containers is selected from each bin with containers proportionally selected from each packaging site. The random sample is augmented with containers selected based on the engineering judgment of the MIS working group. In addition, the program allows the packaging sites to perform non-destructive examina-

tion (NDE) on 3013s to address facility-specific concerns. Table 1 shows the allocation of the 255 NDE containers to the three bins (Pressure and Corrosion, Pressure Only, and Innocuous) and identifies the sample selection criterion (random, judgmental, and additional).

Table 1. NDE on containers broken out by site, bin and type

Site	Innocuous Bin	Pressure Only Bin	Pressure and Corrosion Bin	Total
Hanford **total**	4 (R) **4**	63 (R) 5 (J) 9 (A) **77**	22 (R) 10 (J) 29 (A) **61**	**142**
LLNL	-	1(R)	2 (R)	**3**
RFETS **total**	4 (R) **4**	58 (R) 3 (A) **61**	21 (R) 13 (J) 1 (A) **35**	**100**
SRS	2 (R)	8 (R)	-	**10**
Sub Totals	10 (R)	130 (R) 5 (J) 12 (A)	45 (R) 23 (J) 30 (A)	
Total	**10**	**147**	**98**	**255**

R = Random, J = Judgmental, and A = Additional

Nondestructive Examinations (NDEs)

The surveillances performed to verify the integrity of the 3013 containers includes the following: contamination survey, visual inspection, mass verification, and full container radiography of the 3013 container and its contents.

A radiological survey is required for radiological protection purposes prior to handling the 3013 container. The survey also provides verification that at least one of the containers in the 3013 container set is intact. The DOE-STD-3013 requires that the outside of the inner 3013 container is free of radioactive contamination at the time of packaging, thus, any indication of radiological contamination on the external surface of the outer 3013 container could be an indication of penetration of both the inner and outer 3013 container walls. Of the 3013 containers that have undergone NDE to date no contamination on the external surface of the outer 3013 has been detected.

A visual inspection of the external 3013 container surface is performed to identify both breaches in the outer container and conditions that could lead to a breach in the outer container. None of the 3013 containers that have undergone NDE surveillance have had a breach in the outer container or any evidence of pitting corrosion, large dents, scratches, or other conditions adverse to quality on the outer 3013 container surface.

The 3013 container mass determinations monitor for changes in the mass of the 3013 container/package system. The purpose of the mass monitoring include verifying the as-packaged system mass and determining if any changes in the mass could indicate a failure in the 3013 container integrity. For example, over time plutonium metal will be converted to plutonium oxide if exposed to air and the calcined plutonium oxide may adsorb moisture from the air. These effects would result in a weight gain of the 3013 container. No 3013 container evaluated by the surveillance program has failed the mass verification. At the Savannah River Site, this means the mass of all 3013 containers at the time of surveillance was within one gram of the buoyancy corrected baseline mass measurement. A buoyancy correction is needed to correct for the difference between the air density between packaging site (RFETS) and SRS due to the difference in elevation. For example, the buoyancy corrected baseline mass is typically approximately 0.4 grams less than the RFETS measured baseline mass. In fact, the majority of the 3013 containers measured have been within 0.2 grams of the buoyancy corrected baseline mass.

Full container radiography is used as part of NDE at the SRS and LLNL to examine the contents of the 3013 container. At LLNL, the surveillance is performed using film. At the SRS, digital radiography is used to obtain full-container (composite) images at 0 degrees and 90 degrees. Full-container radiography is useful as part of an NDE program, as it allows some conclusions about the condition of the inner 3013 and any convenience cans present. This is done by examining the air gap between the outer and inner 3013 container and between the convenience container and inner 3013 container for the presence of nuclear material. If no material is observed in these air gaps, the container walls are most likely intact. The full can radiography performed to date has not revealed any 3013 containers with nuclear material in the gaps between the various nested containers. It should be noted that the majority of the packaging sites did not perform full-container radiographs, but only radiographed the lid of the inner container to document the initial lid location to use for future pressure measurements. LLNL is the only packaging facility that performed full-container radiography.

Full-container radiography has identified two 3013 containers with content anomalies. In both of these cases, the subject 3013 container subsequently underwent destructive examination (DE). In the first case, a metal scoop used for sampling the oxide at the packaging site (Figure 1) was found in the oxide material. The full-container radiographic image (Figure 2) clearly shows the presence of a piece of high-density material (metal) protruding above the surface of the bulk oxide material.

During a later NDE surveillance of another 3013 container, the field surveillance engineer observed an unusual object and made notifications to the surveillance program. Further review was performed, including taking images at additional angles. The 3013 container was also shaken and rotated by the operator followed by additional images to observe any changes. The full-container radiograph clearly shows darker material (Pu ox-

Figure 1. Spatula pitcure
Figure 2. Full can radiography image showing spatula

Figure 3. Full can radiography image showing glove

ide) above the surface of the bulk oxide suspended in some low density material (indicated by the light wispy areas of the image) (Figure 3). DE of this 3013 revealed that a plastic glove (Figure 4) had been inadvertently left in the 3013 during packaging operations. It should be noted that in both of these cases, the tramp material extended above the surface of the bulk oxide. If it had been completely submerged within the bulk oxide, full container radiography may not have been able to distinguish the material. Based on this, full container radiography can indicate the presence of tramp material if it extends above the oxide surface, but the failure to see an anomaly in an image of a container does not conclusively prove that tramp material is not present. Review of the original packaging data for these containers revealed that both containers had small weight discrepancies. As a result, the MIS Working Group identified eighteen Hanford containers that have potential weight discrepancies and requested that SRS perform DE on two containers and NDE on the remaining sixteen containers. To date, SRS has completed DE on both of the identified containers and NDE on ten of the identified containers. No foreign material was found in the DEs, but two of the NDEs have indicated that a scoop is present.

Figure 4. Glove tramp material

Pressurization Measurements

Historically, container pressurization in plutonium bearing materials in convenience cans was measured through the use of mechanical lid deflection measurements. However, in the 3013

container configuration, the deflecting component is the inner 3013 container lid, which is inaccessible without the destruction of the outer 3013. Therefore, radiography was selected to determine the amount of lid deflection in a 3013 inner container. DOE-STD-3013 requires a baseline measurement be performed within thirty days after welding of the container. The standard also requires that the container and radiographic system be capable of detecting a pressure increase of 100 psig or greater. Therefore, all packaging sites are required to be able to perform radiography on 3013 containers. Each packaging site has some degree of flexibility on the configuration of the inner 3013, as well as on how radiography is performed. The Savannah River National Laboratory developed a method to correlate the amount of lid deflection with the amount of pressure in the 3013 container[6,7,8] and the associated uncertainties. The ADRIS (Automated Digital Radiography Inspection System) was developed at SRS. It is based around an industrial 440 KV X-ray unit. It uses digital radiography to measure the amount of lid deflection, compares it to the measured baseline deflection and correlates this difference to the change in pressure in the 3013 container.[6,7,8]

RFETS and LLNL used inner 3013 containers with a relatively thin lid. The thin lid deflects easily, allowing changes in the lid deflection to be readily observed. RFETS used a digital radiographic system to establish the baseline radiographs, while LLNL used film radiographs. The scanned LLNL radiography images do not support quantitative pressure assessments using ADRIS, however, studies show that LLNL lids exhibit "snap through" between 20 psig and 30 psig.[6] Thus the LLNL data are "pass/fail" data with a trigger point well below 100 psig.

The Hanford Plutonium Finishing Plant and SRS FB-Line used a thicker lid on the inner container. Digital radiography for lid deflection measurements was performed at Hanford using the ADRIS. Baseline measurements were taken within thirty days of container closure and at thirty-, sixty-, and ninety-day intervals for many containers. More than 2,000 radiographs were taken. These initial efforts uncovered problems with accurately determining the lid deflection for containers with severely tilted inner lids. The *shadow* from the edge of the tilted lid would obscure the true center lid deflection point. Called the "dead zone," a joint SRS/Hanford resolution of this issue resulted in several findings:[9]

- The standard four-view inspection program (view at every 90 degrees) was adequate for most cans.
- An optimal viewing angle exists, unique to each container, where the field of view for lid deflection measurement is minimally affected by lid edge shadow. Special inspection programs for these cans were developed.
- For cans with baseline measurement in this dead zone, the digital micrometer measurement could serve as the baseline measurement and equivalency methods for comparing micrometer measurements to digital radiographs were developed.
- Equivalency in measurement for all three digital radiographic systems in use (one at Hanford, two at SRS) was demonstrated.

Figure 5. FBL 3013 can configuration with button on inner 3013 lid I

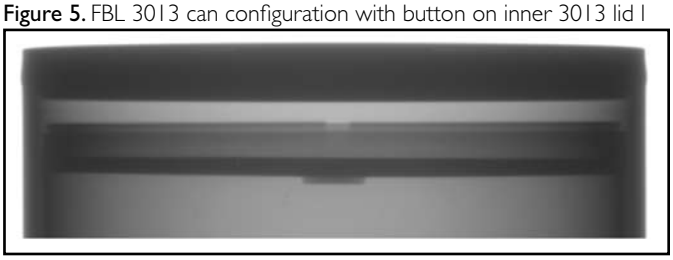

FB-Line addressed the dead zone issue by revising the design of the inner 3013 lid to include a button on the center portion of the inner 3013 lid bottom. The *button* was shaped to preclude the creation of a dead zone (Figure 5).

NDE at the SRS addresses the dead zone issue for Hanford 3013s by using the optimal viewing angle. This angle is calculated based upon the radiograph images at the four standard viewing angles. A radiograph is taken at both the optimal viewing angle and 180 degrees away from the optimal viewing angle. This image is compared to the closest Hanford standard view baseline and correlated to a pressure. However, there are clearly larger pressure measurement uncertainties associated with Hanford containers with dead zone problems than with other containers.[10]

One 3013 at Hanford was discovered to have been packaged in excess of the standard specification of 0.5 wt percent water during a thorough QA review of all containers. Radiography was performed on this container and the results showed a slight positive detection of lid deflection, attributed to be from 35-50 psig. The NDE findings on this item were instrumental in demonstrating the ability of NDE to detect pressurization and in assuring that the container could continue in safe storage until the development of the technical basis to allow shipment offsite was completed. This item is currently scheduled for destructive analysis and further evaluation by LANL in 2010.

Statistical Analysis of Pressurization Data

The data used in this analysis include 252 containers with lid deflection pressurization (LDF psig) measurements (note that there are 252 rather than 255 because the three LLNL containers have only pass/fail data, thus they are not included). In the case of multiple measurements on a single container, the most recent measurement was selected from the larger database, as this is considered the best measurement to accurately reflect pressurization. In addition to the LDF psig measurements, there are 110 containers evaluated at SRS that have calibration-based standard deviations for the measurements (sigmas). The containers undergoing DEs also have gas measurements taken at the time of the DE using the Gas Evaluation Software Tool (GEST).[11] There are forty-three containers with GEST data.

The ISP sampling design (described in References 4 and 5) requires 130 randomly selected containers from the Pressure Only bin. These 130 are spread proportionately across the sites

Figure 6. Box plots of the LDF psig measurements for each bin

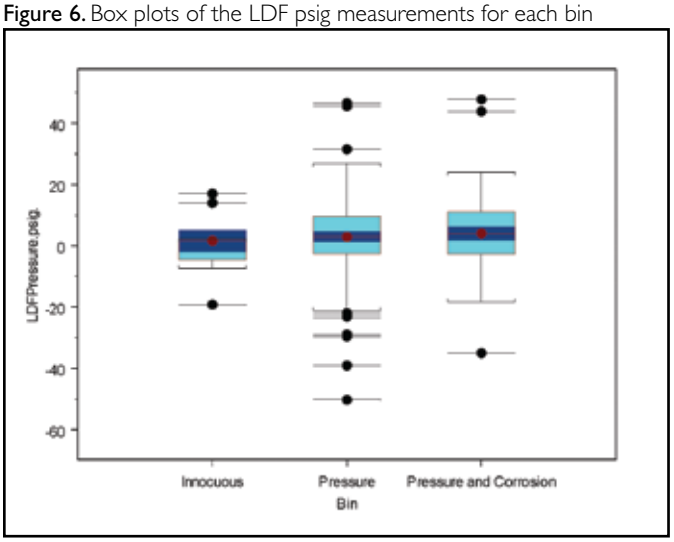

Figure 7. Box plots of the LDF psig measurements for the various sampling selection criteria

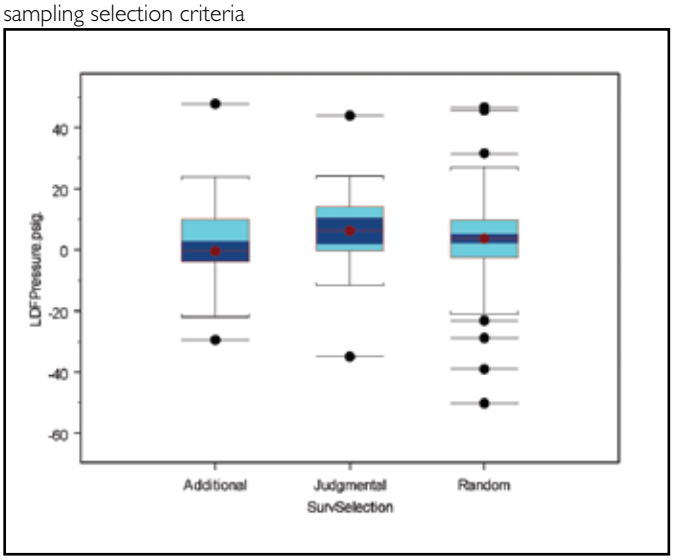

Figure 8. Box plots of the LDF psig measurements for the three packaging sites, Hanford, RFETS, and SRS

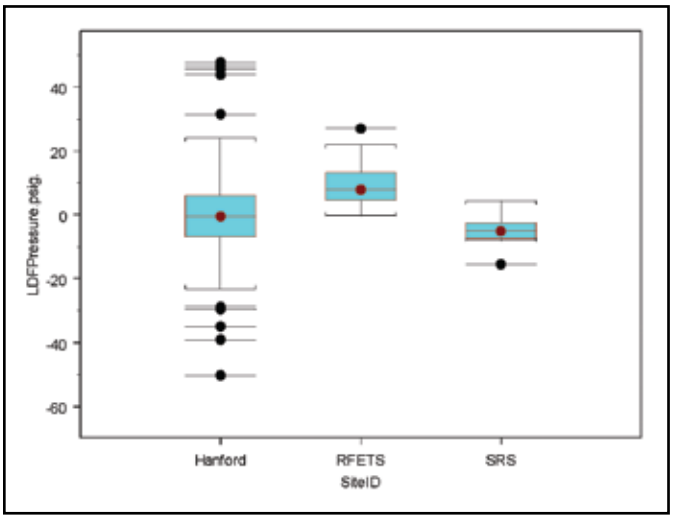

Figure 9. Q-Q plots of all LDF psig measurements compare the distribution of these measurements to a normal distribution

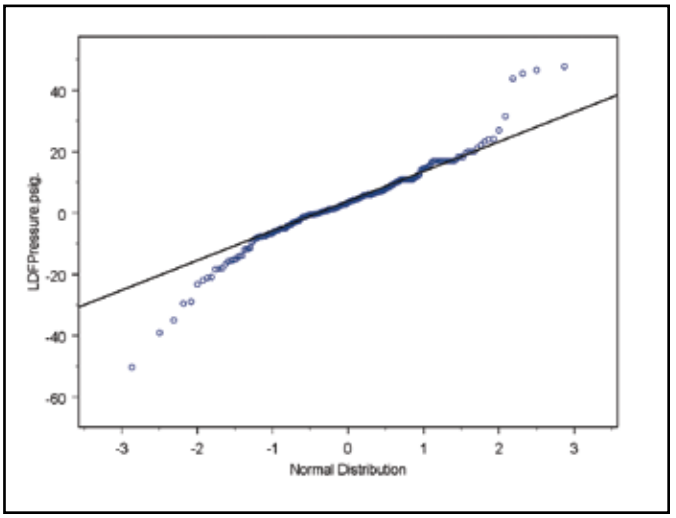

that have generated containers by 2006—Hanford, LLNL, RFETS and SRS. The specification of 130 containers is based on the criterion that if pass/fail data (less than 100 psig/greater than 100 psig) are available, then, if no containers in the 130 observations are greater than 100 psig, the conclusion is that there is 99.9 percent confidence that not more than 5 percent of the entire Pressure Only Bin population could have a pressurization greater than 100 psig. The sampling criterion is met and the conclusion follows for the Pressure Only Bin.

In addition to the pass/fail data, quantitative pressure measurements (LDF psig) exist for all containers except those from LLNL. Figure 6 compares these data across bins (box plots[i] are used for the comparison) and Figure 7 compares these data across the sample selection criterion (random, judgmental, and additional). These figures show that LDF psig measurements do not differ significantly between the various groupings, therefore, these data can be combined across bins and sample selection criterion to obtain more reliable results.

Figure 8 compares the LDF psig data across packaging sites. This figure shows that the Hanford data have more outliers than the other sites. Note that the highest LDF psig measurements are identified as potential outliers in the Hanford data. These outliers are likely due to measurement errors resulting from dead zone measurement problems.[10] However, even these high measurements are under 50 psig.

A comparison of the distribution the LDF psig measurements to a normal distribution using a Q-Q plot[ii] shows that the outliers in the Hanford data result in tails (the largest and small-

est data values) that deviate significantly from those of a normal distribution (Figure 9). When the Hanford data (except for the Innocuous bin measurements) are removed, the comparison to a normal distribution is much better (Figure 10). In this case, the lower tail falls below the normal line, however, it is only the upper bound on the population that is of interest. Using the normal distribution for the upper tail is a reasonable assumption for these data. Applying normal distribution theory to this reduced data set, one finds that there is 99.5 percent confidence that 99.99 percent of the population is less than 42 psig (the 99.5 percent/99.99 percent upper tolerance limit [UTL]).[12] This result indicates that it is unlikely that a LDF psig measurement from RFETS or SRS would exceed 42 psig. Consequentially, it is exceedingly unlikely that a measurement would exceed 100 psig. Although the Hanford data outliers do not permit using normal theory to get tolerance limits, it is useful to note that it would take almost seven standard deviations from the mean of the Hanford data to get to 100 psig (Table 2 contains the mean and standard deviation).

Table 2. Means, standard deviations (SD), number of containers (N), and 95% confidence intervals (CI)

Site	Mean	SD	N	CI
Hanford*	-0.27	14.4	138	(-2.7, 2.2)
RFETS*	9.2	6.0	96	(8.0, 10.4)
SRS*	-5.1	5.7	8	(-9.9, -0.3)
RFETS & SRS (with Innocuous)	7.4	7.7	114	(6.0, 8.9)

** Containers from the Innocuous bin are not included.*

Many of the container lid deflection pressure measurements have an associated sigma (standard deviation) based on the calibration results.[6,7,8] These sigmas vary from 3 psig to almost 9 psig. The sigmas are based on experimental conditions in the laboratory and it is highly probable that they underestimate the actual measurement uncertainty occurring in the field (particularly for Hanford containers with dead zone issues). Table 2 shows the means, standard deviations, number of containers and 95 percent confidence intervals for the means calculated from the field data for each packaging site. RFETS and SRS standard deviations are within the range of calibration measurement errors, indicating that the main source of variability is from measurement error with negligible variability between containers. Hanford has a larger standard deviation than seen in the calibration measurement sigmas, but it is the outliers causing this variability and these outliers are likely a result of dead zone measurement problems.

Containers undergoing destructive examinations (DE) have actual gas measurements (GEST) collected at the time of the DE.[11] There are forty-three containers with GEST measurements, twenty from Hanford and twenty-three from RFETS. These GEST measurements provide the best possible assessment

Figure 10. Q-Q plot of LDF psig data with Hanford data removed

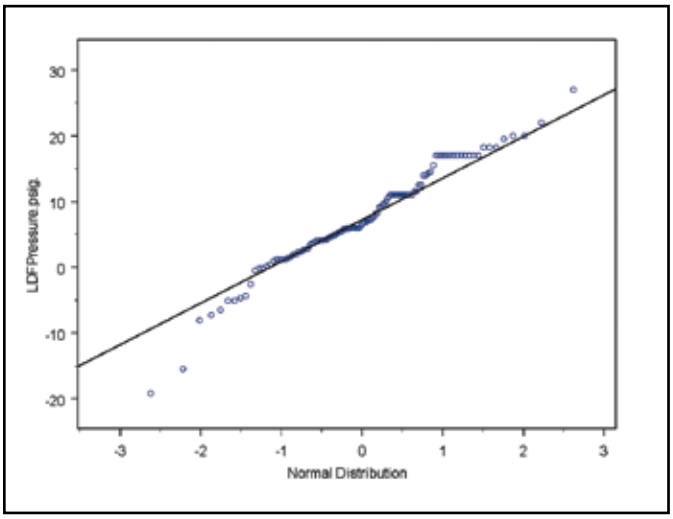

of pressurization. For the containers with GEST measurements the LDF psig can be compared to the GEST (adjusted for atmospheric pressure at the packaging site (e.g., GEST-11.8 for RFETS and GEST-14.4 for Hanford). These differences provide an estimate of the bias of the field LDF psig measurements. The RFETS bias is positive (5.2 psig) with 95 percent confidence bounds, (3.8, 6.7) psig. This positive bias shows that the LDF psig measurements for the RFETS data are conservative, e.g., overestimate the actual pressure by a small amount. The Hanford bias is -1.6 psig with 95 percent confidence bounds (-9.3, 6.1) psig. Although the bias confidence bounds bracket zero, there is so much scatter in the data it is impossible to draw conclusions other than that the Hanford biases are quite variable and can be both negative and positive.

The sampling specification for the Innocuous Bin was to evaluate the assumption of no pressurization and essentially no variability between containers.[4,5] However, because the main source of variability is measurement variability, it is not possible to definitively evaluate this assumption. Nevertheless, as shown in Figure 6, the Innocuous Bin items do not look significantly different from the other bins. In this analysis the Innocuous Bin containers are included in the calculation of the 99.5 percent/99.99 percent UTL of 42 psig.

Conclusions

Nondestructive examination surveillances of 255 3013 containers have not identified any conditions challenging the 3013 container integrity. Pressure measurements based on lid deflection measurements from digital radiography images (LDF psig measurement) have not indicated any appreciable pressurization in any of these 255 containers. Comparison of LDF psig measurements to actual gas measurements made during destructive examinations of RFETS containers indicates that the LDF psig measurements

are conservative (e.g., slightly overestimate pressure changes) for the RFETS containers.

The 3013 Standard requires containers be designed to withstand 699 psig of internal pressure, but the S&MP set a normal acceptance criterion of 100 psig during surveillance. Using the "greater than 100 psig" criterion as a trigger for pass/fail decisions, the conclusion from the 130 randomly selected Pressure Only bin samples is that there is 99.9 percent confidence that a container having a pressure above 100 psig would not occur in more than 5 percent of the population of containers from Hanford, LLNL, RFETS, and SRS packaged by 2006. In addition to the pass/fail data, there are 252 pressure LDF psig measurements. All of these measurements are under 50 psig.

Comparison of field LDF psig measurement variability based on the NDE surveillance data to LDF psig variability estimated from laboratory-controlled-calibration experiments indicates that the main source of variability in the field LDF psig measurements for RFETS and SRS is from the measurement process. The Hanford data have many potential outliers (likely from dead zone measurement problems) that result in variability greater than the laboratory calibration results. However, it is unlikely that any containers exceed 100 psig.

The RFETS and SRS data can be used to develop an upper tolerance limit for the general population of 3013 containers packaged by 2006 and following the specifications of DOE STD 3013.[ii] (The large measurement errors seen in the Hanford data require removing these data from the analysis data set used to develop the upper tolerance limit.) The upper 99.5 percent/99.99 percent tolerance limit based on the remaining data is 42 psig (this means that there is 99.5 percent confidence that 99.99 percent of the population is below 42 psig). This finding makes it extremely unlikely that RFETS or SRS containers would exceed 100 psig. Even though the Hanford data have increased variability due to dead zone measurement issues, it requires approximately seven standard deviations from the mean to reach 100 psig for these data.

Based on these results it appears that there is little or no pressurization occurring in the 3013 containers and that variability in the data is a result of inherent measurement variability rather than container-to-container variability.

Future NDE surveillance will be guided by these NDE findings. For example the discovery of anomalies in Hanford packaging has focused NDE surveillance on Hanford containers with weight discrepancies. Future NDE surveillances will also evaluate containers generated after 2006 from LANL and LLNL.

NOTES

i. A box plot provides an excellent visual summary of many important aspects of a distribution and allows quick comparison between data sets. The box stretches from the 25th percentile to the 75th percentile (middle half of the data). The median is shown as a line across the box. The "inter-quartile range" is the difference between the top and bottom of the box. The whiskers come out from the top and bottom of the box (lines with tops) to the first data points that are not beyond 1.5 times the inter-quartile range. These are either the max and min of the data, or, if points lie beyond these, the max and min of the data will be the top and bottom filled circles. The points outside the whiskers are considered potential outliers.

ii. Quantile-Quantile (Q-Q) plots (in this analysis) compare the quantiles of the data with the quantiles of the normal distribution. If the data are normal they will lie approximately along the line (the normal line).

iii. Tolerance limits specify a region that covers a certain portion of the population (e.g., 99.99 percent) with a certain level of confidence (e.g., 99.5 percent). Tolerance limits can also be viewed as confidence limits on population percentiles.

Lester Yerger is a fellow engineer at Savannah River Nuclear Solutions. He has a B.S. in chemical engineering from Rose-Hulman Institute of Technology.

James W. McClard is a fellow technical advisor at Savannah River Nuclear Solutions. He has a B.S. in Chemical Engineering from Clemson University.

Lance E. Traver is a lead engineer for surveillance operations at Savannah River Nuclear Solutions. He has an M.S. in environmental engineering from the University of Maryland and a B.S. in civil engineering from Rice University.

Tom Grim is an Engineer for Surveillance Operations in K-Area at Savannah River Nuclear Solutions. He has a B.S. in environmental management from Southern Illinois University at Carbondale.

Elizabeth J. Kelly is a scientist at Los Alamos National Laboratory. She has a Ph.D. in biostatistics from the University of California at Los Angeles, and an M.A. and a B.S. in mathematics from University of Southern California.

Ted Venetz is a technical advisor at CH2M Hill Plateau Remediation Company. He has an M.S. in engineering and technology management from Washington State University and a B.S. in chemical engineering from Montana State University.

David Riley is a deinventory project lead engineer at Lawrence Livermore National Laboratory. He has an M.S. and a B.S. in chemical engineering from San Jose State University.

Acknowledgements

Funding for this work was provided by the Surveillance and Monitoring Program, U.S. Department of Energy Office of Environmental Management. This work was conducted at Los Alamos National Laboratory operated by Los Alamos National Security, LLC under contract DE-AC52-06NA25396 and at the Savannah River Site operated by Savannah River Nuclear Solutions for the U.S. Department of Energy under contract DE-AC09-08SR22470.

References

1. Los Alamos National Laboratory. 2001. Integrated Surveillance Program in Support of Long-Term Storage of Plutonium-Bearing Materials. *Los Alamos National Laboratory Report LA-UR-00-3246, Rev. 1.*
2. Savannah River Site. 2003. Surveillance and Monitoring Plan for DOE-STD-3013 Materials. *Savannah River Site SR-NMPD-03-001, Rev. 1.*
3. *Stabilization, Packaging, and Storage of Plutonium-bearing Materials.* 2004. DOE-STD-3013-2004. U.S. Department of Energy: Washington, D.C.
4. Peppers, L., E. Kelly, J. McClard, G. Friday, T. Venetz, and J. Stakebake. 2009. Selection of 3013 Containers for Field Surveillance: LA-14310, Revision. *Los Alamos National Laboratory Report, LA-14395.*
5, Kelly, E., L. Peppers, L. Worl, and J. McClard. 2010. Sampling Approach to Validate the Safe Storage of Plutonium-Bearing Materials. *Journal of Nuclear Materials Management, Vol. 38, No.2.*
6. Gibbs, K. M. 2004. Pressure Test Results of Digital Radiography of BNFL Type Inner 3013 Cans. *WSRC-TR-2004-00309.*
7. Gibbs, K. M. 2005. Pressure Test Results of Digital Radiography of Hanford Type Inner 3013 Cans. *WSRC-TR-2005-00089.*
8. Gibbs, K. M. 2005. Pressure Test Results of Digital Radiography of Tall SRS Type Inner 3013 Cans with DR Buttons. *WSRC-TR-2005-00252.*
9. Gibbs, K. M., et.al. 2003. Resolution of Issues Associated with Digital Radiography of 3013 Containers. NMS-19056, Rev. 0.
10. Kelly, E., and T. Venetz. 2007. Analysis Approaches for Lid Deflection Data—Illustrated with Hanford Data from 2005 and 2006. *Los Alamos National Laboratory Report, LAUR 07-8040.*
11. Hardy, B. J. 2007. Version 2.0 of 3013 Gas Evaluation Software Tool (GEST). *WSRC-TR-2007-00218, Rev.0.*
12. Odeh, R. E., D. B. Owen. 1980. *Tables for Normal Tolerance Limits, Sampling Plans and Screening.* New York: Marcel Dekker, Inc.

Stainless Steel Interactions with Salt-Containing Plutonium Oxides

D. Zane Nelson, Gregory T. Chandler, Kerry A. Dunn, Tina M. Stefek, and Michael E. Summer
Savannah River National Laboratory, Aiken, South Carolina USA

Abstract

Salt-containing plutonium oxide materials are treated, packaged and stored within nested, stainless steel containers based on requirements established in the U.S. Department of Energy (DOE) 3013 Standard. The moisture limit for the stored materials is less than 0.5 weight percent. Surveillance activities that are conducted to assess the condition of the containers and assure continuing 3013 container integrity include the destructive examination of a select number of containers to determine whether corrosion attack has occurred as a result of stainless steel interactions with salt containing plutonium oxides. To date, some corrosion has been observed on the innermost containers, however, no corrosion has been noted on the outer containers and the integrity of the 3013 container systems is not expected to be compromised over a fifty-year storage lifetime.

Introduction

The 3013 container system was designed to contain plutonium bearing materials that are >30 wt. percent plutonium plus uranium and are stabilized to achieve a moisture content <0.5 wt. percent. The requirements and assumptions documented in the DOE-STD-3013[1] were defined to support a fifty-year storage lifetime that may be required prior to the final disposition of the plutonium bearing materials. To ensure that the 3013 container system maintains integrity during storage the DOE-STD-3013 specifies that a surveillance program be performed at the storage site. The current surveillance program includes both destructive and non-destructive surveillances. This paper focuses on the destructive surveillances of a statistical sampling of packaged 3013 containers stored at SRS[2,3,4] and a number of engineering judgment samples that were chosen for destructive examination[5] because of their package contents and data obtained from laboratory testing and the ongoing storage surveillance program.

The 3013 container system consists of nested welded 300 series stainless steel containers with the outer container credited to stay leak tight throughout a fifty-year storage period. To date containers packaged at Rocky Flats Environmental Test Site (RFETS) and Hanford have been examined destructively, Figure 1. Future examinations will include containers from Lawrence Livermore National Laboratory (LLNL), Savannah River Site (SRS), and Los Alamos National Laboratory (LANL). During de-

Figure 1. 3013 container configurations (a) RFETS 3013 container. Note silver coated threads on convenience container body (circled). Note: the inner container in Figure 1a is shown prior to cutting to height. (b) Hanford 3013 container. Difference between the two include convenience container design and lid material. Additionally, the inner container body design varied toward bottom of container.

structive examination, the containers are punctured to collect gas samples,[6] sectioned to collect Pu oxide samples[7] and the empty containers are metallurgically examined to determine the condition of the various containers, including the welds, lids and other regions in the container system. The results of these metallurgical examinations are provided in this paper.

Destructive Examination Observations

During the destructive examinations (DE), the outer, inner, and convenience containers are visually examined with an emphasis on the condition of the welds, other regions of high residual stress, and the Pu-bearing material/container metal interface. These regions are of particular interest because of the possibility of stress-corrosion cracking (SCC),[8,9] in these areas. Other areas of significance include the headspace of the containers because environments generated above the Pu-bearing materials have been known to create pits in stainless steel[10] and such pitting may be a precursor to SCC if sufficient chloride containing electrolyte is available at the metal surface.

Figure 2. Typical outer container examination

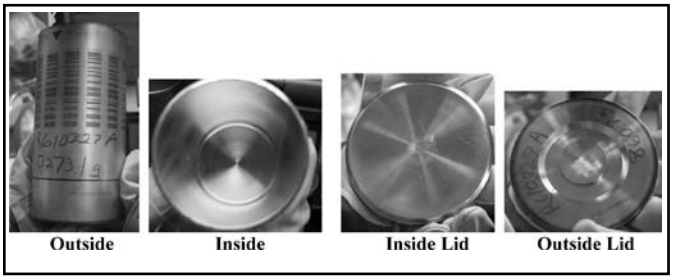

The outer container is a standard design and is used at all the packaging sites. It is the barrier credited to contain the plutonium-bearing materials while in a storage configuration. One or two other stainless steel containers in the nested system provide separation between the plutonium-bearing materials and the outer container that is neither in contact with the plutonium-bearing materials nor the headspace gas. Because of this lack of contact with the plutonium-bearing materials, little to no degradation of the outer container was expected[11] and a typical outer container visually examined as part of the DE showed no indication of degradation, Figure 2. Additionally, the metallurgical examination of the outer containers corroborates the visual observations and showed little or no storage induced degradation of the container welds, lids or walls.

Conversely, the inner and convenience containers are exposed directly to the Pu-bearing materials and/or the headspace gas over the Pu-bearing materials and are therefore more susceptible to corrosion induced degradation. A number of destructively examined 3013 containers have been evaluated via optical metallography, scanning electron microscopy (SEM), and/or energy dispersive X-ray (EDX) analysis. Table 1 provides a list of containers examined to date and indicates the extent of the analyses performed. In general, extensive analyses were only conducted on a small number of 3013 containers that were packaged with high chlorides because these were the only containers that showed evidence of significant corrosion.

Convenience Container Examinations

Analyses of several convenience containers from the stored 3013 packages showed evidence of corrosion but nothing significant

Table 1. Summary of additional container analyses performed during destructive examination of 3013 containers

Material Type and Sury. Reason**	Description	Moisture (At Packaging/DE)	Percent Actinide	Inner Container Analyzed	Convenience Container Analyzed
P / R	No chlorides	0.11 / 0.05	86.6	N/A	N/A
P / R	No chlorides	0.18 / 0.04	84.4	N/A	N/A
P&C / R		0.03 / 0.04	87.6	N/A	N/A
P&C / R		0.10 / 0.19	86.4	N/A	N/A
P&C / EJ	Chloride bearing, Like C06032A	0.36 (FTIR) / 0.19	53.5	N/A	Threads, outside lid
P&C / EJ	Chloride bearing, Like ARF-223	0.28 (FTIR) / 0.06	69.9	N/A	Threads
P&C / R		0.15 / 0.10	86.0	N/A	N/A
P&C / R		0.07 / 0.03	97.4	N/A	N/A
P / R	>3 yrs old	0.17 / 0.02	83.6	N/A	N/A
P&C / R		0.14 / 0.04	77.7	N/A	N/A
P&C / R		0.39 / 0.04	80.8	N/A	N/A
P&C / R		0.16 / 0.14	64.8	N/A	N/A

***P=Pressure, P&C=Pressure & Corrosion, R=Random, J=Engineering Judgment*

Table 1. (cont.) Summary of additional container analyses performed during destructive examination of 3013 containers

Material Type and Sury. Reason**	Description	Moisture (At Packaging/DE)	Percent Actinide	Inner Container Analyzed	Convenience Container Analyzed
P&C / R		0.07 / 0.10	71.6	N/A	N/A
P&C / R		0.37 / 0.03	52.3	N/A	N/A
P&C / R		0.19 / 0.10	85.0	N/A	N/A
P&C / R		0.14 / 0.07	71.4	N/A	N/A
P&C / R		0.04 / 0.07	64.7	Radius below weld, inside lid	N/A
P / R	No chlorides	0.06 / 0.06	34.3	N/A	N/A
P / R	No chlorides	0.22 / 0.23	86.7	N/A	N/A
P&C / R		0.29 / 0.29	74.0	N/A	Filter housing
P&C / J	Like ARF-223, high TGA	0.37 / 0.33	74.3	Closure weld, container bottom	Filter housing, container bottom
P&C / J	ARF with weight gain	0.35 / 0.19	70.5	Closure weld, container body inside	Filter housing, lid, container body
P&C / R		0.26 / 0.03	70.4	N/A	N/A
P&C / R		0.07 / 0.07	69.8	N/A	N/A
P&C / J		0.23 / 0.03	78.9		
P&C / J	Visually able to see oxide/gas interface	0.40 / 0.26	71.8	Inside container wall and inside lid adjacent to weld	Inside lid, inside wall sections
P&C / J		0.32 / 0.22	70.6	N/A	N/A
P&C / R		0.06 / 0.02	60.1	N/A	N/A
P&C / J		0.26 / 0.13	81.6	N/A	N/A
P&C / J	Coating on CC – wiped clean	0.39 / 0.26	70.7	N/A	N/A
P&C / J	Coating on CC and IC – wiped clean	0.39 / 0.25	70.1	N/A	N/A
P&C / J	Coating on CC – wiped clean	0.23 / 0.22	77.4	N/A	N/A
P&C / J		0.29 / 0.02	70.8	N/A	N/A
P&C / R		0.24 / 0.03	71.1	N/A	N/A
P&C / R	Coating on CC & IC – wiped clean	0.23 / 0.19	72.4	N/A	N/A
P&C / R	Coating on CC – collected on SEM stub for analysis	0.38 / 0.28	70.3	N/A	Coating analyzed by SEM and corresponding sections cut for SEM
P&C / R		0.23 / 0.03	65.4	N/A	N/A
P&C / R		0.06 / 0.05	62.6	N/A	N/A
P&C / R		0.25 / 0.22	63.5	N/A	N/A
P&C / R		0.04 / 0.01	87.9	N/A	N/A
P&C / R		0.28 / 0.27	76.7	N/A	N/A
P&C / R	No corrosion seen	0.18 / 0.09	70.8	N/A	Section cut for SEM to compare to DE[12]
P&C / R		0.11 / 0.01	84.1	N/A	N/A

***P=Pressure, P&C=Pressure & Corrosion, R=Random, J=Engineering Judgment*

enough to affect the integrity of the container. For example, two RFETS convenience containers showed signs of pitting corrosion on the silver coated threads of the convenience container body, as shown in Figure 3. The silver coated threads, specific to the RFETS convenience containers, were used to ensure galling did not occur during packaging and unpackaging operations. Although discreet particulates of the chloride containing plutonium oxide appear to be associated with the pitting, initial observations of the threaded region did not provide evidence for the pitting. Subsequent evaluation suggests that the pitting happened after

Figure 3. Examination of silver coated threads from RFETS convenience container body. Superficial corrosion pitting observed at threads.

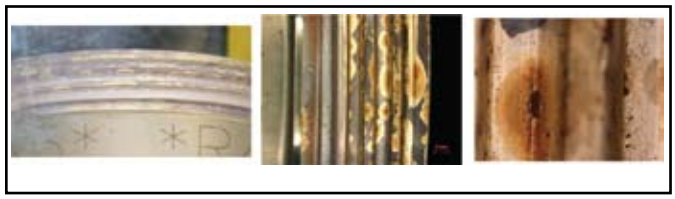

Figure 4. Typical examination of filter area from Hanford convenience container lid. Discoloration (circled) caused by oxidation from weld process. No degradation observed.

Figure 5. Typical examination of particulate and coating on interior of convenience container.

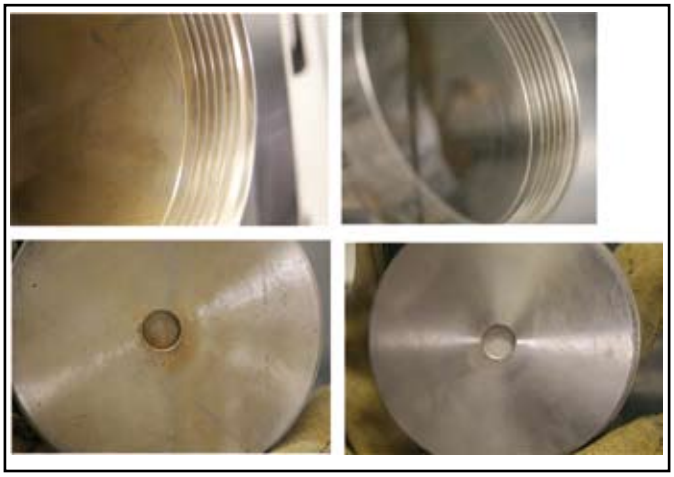

Figure 6. Visual examination photographs from the inside walls of the convenience container. Coated looking surface of convenience container is the headspace region. Sections cut for SEM and EDX examination were taken from region in the box. Portion of coating flaked off during cutting of sample for SEM, as seen in box on left.

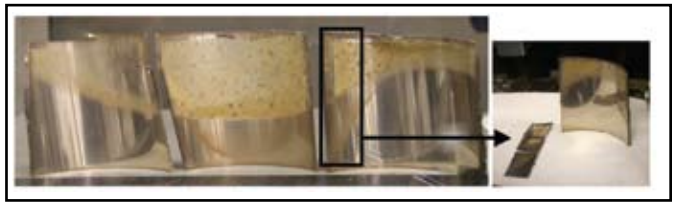

the container was opened for surveillance because seasonal high temperatures and humidities were experienced during the surveillance process. These conditions coupled with the high chloride content of the container were the primary contributory factors for this pitting.

One feature specific to the Hanford convenience containers is a metal filter welded into the center of the lid. This filter prevents the possibility of gas buildup in the convenience container because any gases generated are free to flow through the filter to the inner container. However, the filter is designed to prevent the transfer of oxide particulate. Three filter sections were examined to evaluate unanticipated features observed during the visual examination. Ultimately, it was decided that the observed features were inherent to the welding process used to install the filter into the convenience can lid and did not represent storage-induced degradation. Figure 4 shows a typical weld interface for a filter housing and because this feature was shown to be typical of the welding process, no anomalous conditions are attributed to this visual observation.

The most common observation evaluated as part of the DE metallurgical examination was the presence of particulates and coatings on the inside surface of the convenience container walls and lid. In several cases the particulates and coating were easily removed by gentle wiping with a clean cloth and no degradation of the stainless steel was observed. This is illustrated in Figure 5, which shows the steel surface after coating removal. The fact that the coating was so easily removed is consistent with a conclusion that the particles simply deposited on the surface and that there were no interactions with the underlying metal. However, one convenience container had evidence of minimal corrosion beneath the coating.

Visual examination photographs from the inside walls of the convenience container that showed evidence of corrosion are shown in Figure 6. The coated surface was in the headspace region of the container and the coating easily flaked off the wall when the can was sectioned for further analysis. This is seen in Figure 6 as the clear edge around the perimeter of the cut sections. This particular 3013 container was an engineering judgment sample chosen for DE because it had one of the highest moisture and chlorides content in the packaged materials. The analyses performed on this container included SEM and EDX of the container surface, Figure 7. The regions of the sample surface where the coating flaked off during sectioning are readily observed in the SEM and, in general, the coating is chloride rich with no evidence of the alkaline salts being present. X-ray diffraction and Fourier Transform Infrared Resonance analysis of the coating identified it as ammonium chloride (NH_4Cl). This coating formed during storage and condensed onto the cool surface of the container above the oxide material.[12] Beneath the NH_4Cl coating the surface of the container is nearly void of machining grooves and irregularly oriented fissures are seen across the surface, Figure 8. These features are artifacts from

Figure 7. SEM examination and EDX spectrum from convenience container section seen in Figure 6, (a) shows coating flaked off of sample around perimeter (b) shows higher magnification of coating still adhered to surface. (c) EDX spectrum shows chlorine rich peak typical of coating on surface.

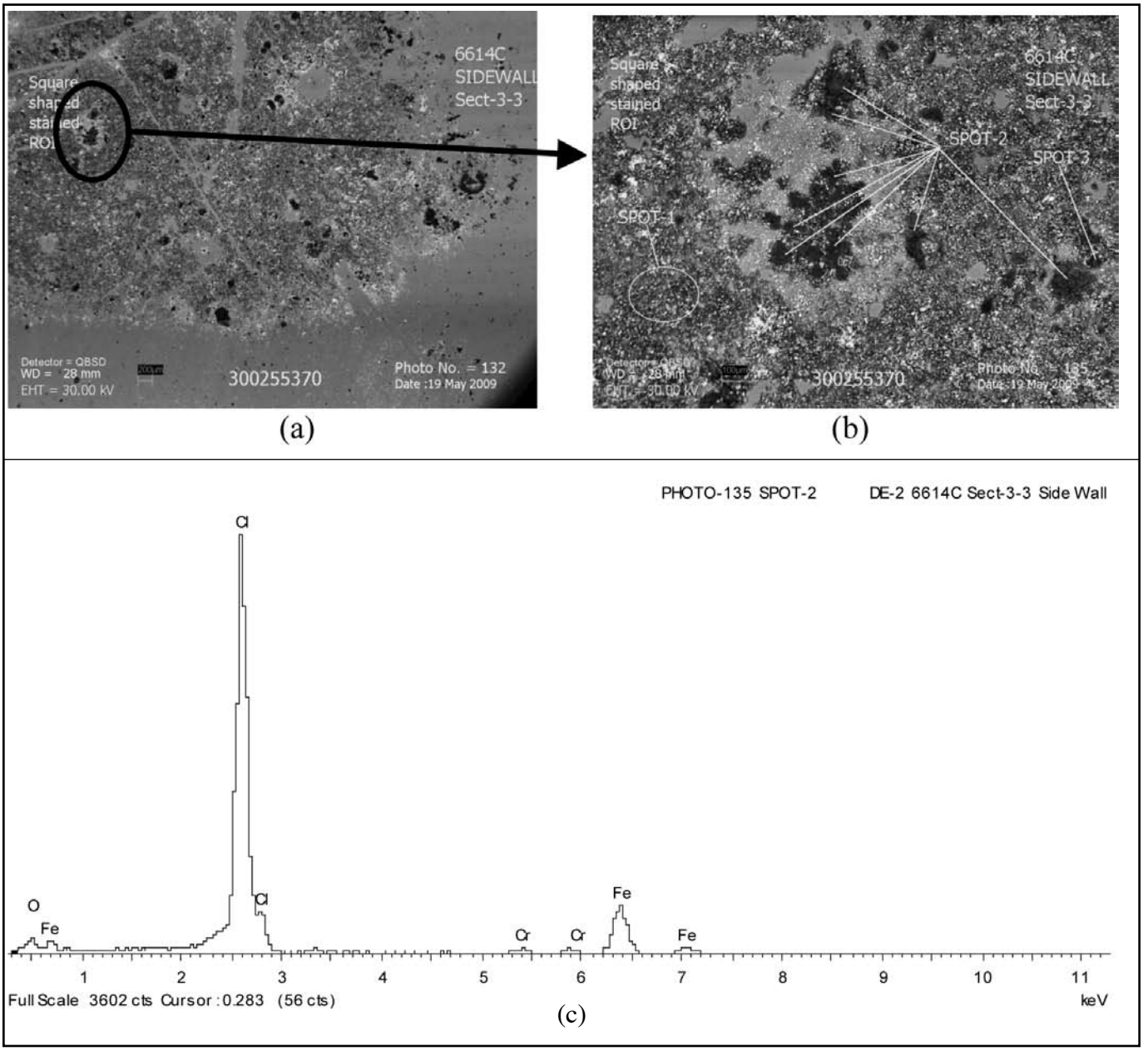

the flow forming process used to manufacture the container. The bottom of this same convenience container was also sectioned for SEM/EDX examination of the inside surface, as shown in Figure 9. A network of regularly shaped pits across the bottom inside surface of the container was observed. The depth of pitting is superficial at approximately 5 µm and is not severe enough to affect the integrity of the convenience container.

The inside lid from another convenience container showed particulate matter adhering to the surface. Samples of the particulate were collected for SEM/EDX analysis and pits were noted on the underlying surface. No evidence of alkaline earth salts was seen and the particulate was identified by EDX to contain chlorine, Figure 10. Further evaluation of this convenience container is in progress with emphasis on determining the extent of the degradation resulting from chloride rich particulates.

The convenience can observations demonstrate that, under certain conditions, a chloride rich deposit (probably ammonium chloride) can be generated. This deposit provides evidence for

Figure 8. Shows irregularly oriented fissures at location where coating flaked off as seen on SEM

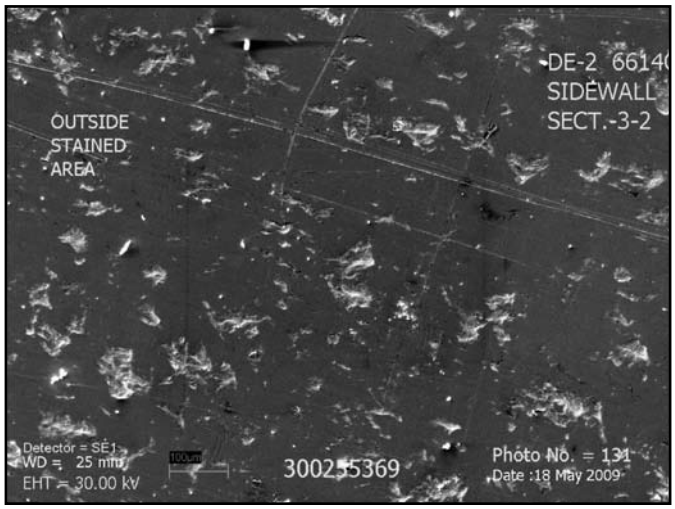

chloride transport from the convenience can to the inner can.[12] Additionally, the development of chloride rich particles on surfaces exposed to the headspace region of the containers may induce pitting on the container surfaces, particularly the lids.[12]

Inner Container Examinations

One RFETS inner container showed the presence of soot from the closure welding operation, Figure 11. This observation was consistent with RFETS reports that there were times when excessive soot developed during welding of the inner containers. No corrosion and/or corrosion product was observed in the sooted region. This observation was therefore considered a pre-storage condition and no evidence of container degradation was attributed to the soot.

Detailed analyses were conducted on several Hanford inner containers that showed evidence for corrosion and/or corrosion products during the DE visual examination. In the majority of examinations, SEM/EDX identified a heavy coating on the container walls and/or chloride rich particulates adhering to the inside lid surface, as shown in Figure 12. The SEM examination of these lids showed no significant depth to the observed corrosion.

Additionally, several of the inner containers examined by DE had a thin powdery coating adhering to the surface. This observation of coating development was similar to what was seen in the convenience containers, but the coating developed to a lesser extent. The coating and particulates were easily removed by wiping the surface and no pitting or surface corrosion was seen. Figure 13 shows the container surface beneath a layer of particulates that was removed during the DE inspections.

One inner container was analyzed because of the unusual features observed on the inner surfaces of the convenience container, Figure 6. These features suggested the presence of

Figure 9. Bottom of convenience container (a) shows regular network of small pits (b) shows EDX spectrum of cracked looking debris rich in chlorine

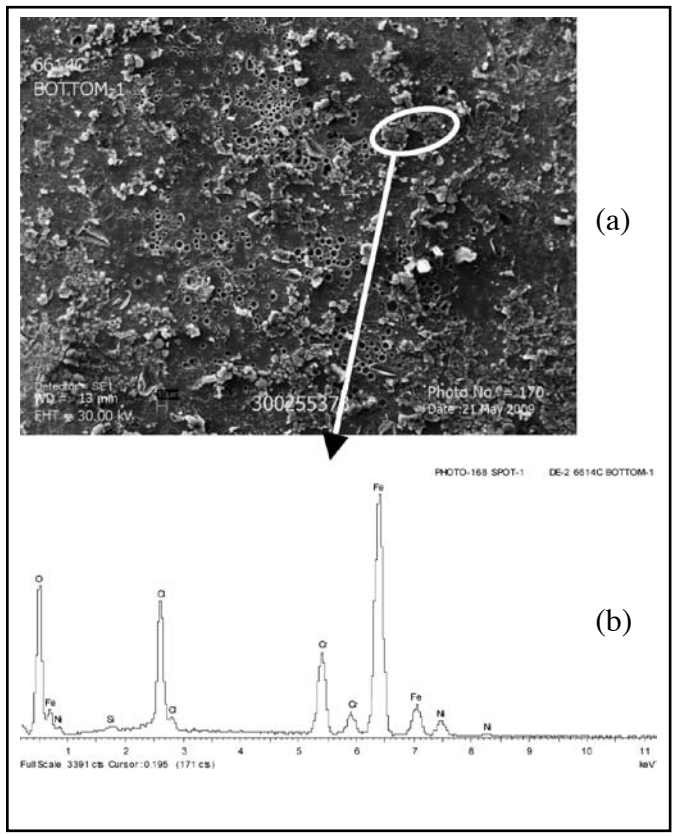

chloride on the inner container surfaces. To evaluate the possibility of chloride transport to the inner container, sections were obtained from the closure weld region, as shown in Figure 14, where a gap exists between the can sidewall and the lid, Figure 15. This gap and associated weld region are of interest because these areas are more susceptible to corrosion, including SCC, than other regions of the container.[8,9] In order to better examine this region of the inner container, each section was cut to remove the weld ligament thereby creating two samples, one of the lid and one of the sidewall. The examination emphasized the gap and weld region but no evidence of corrosion or surface coatings was seen except on the lid region adjacent to the gap. However, examination of the surface of the inner container lid including the lid region adjacent to the gap showed the presence of small, closely spaced, and coalesced pits which formed along the machining grooves, Figure 16. The maximum pit depth observed was approximately 23 µm which is more conservative than the depth predicted by laboratory studies of pit growth in stainless steel exposed to the headspace gas of plutonium bearing oxides.[10] Sidewall sections of the inner container, particularly near the gap region, also showed the presence of particulate matter, some of which is expected to be associated with the Pu-

Figure 10. Chlorine rich particulate analyzed from inside lid of convenience can. (a) inside convenience can lid; (b) area where particulate was obtained for analysis (circled); (c) particulate analyzed; (d) EDX spectrum of particulate

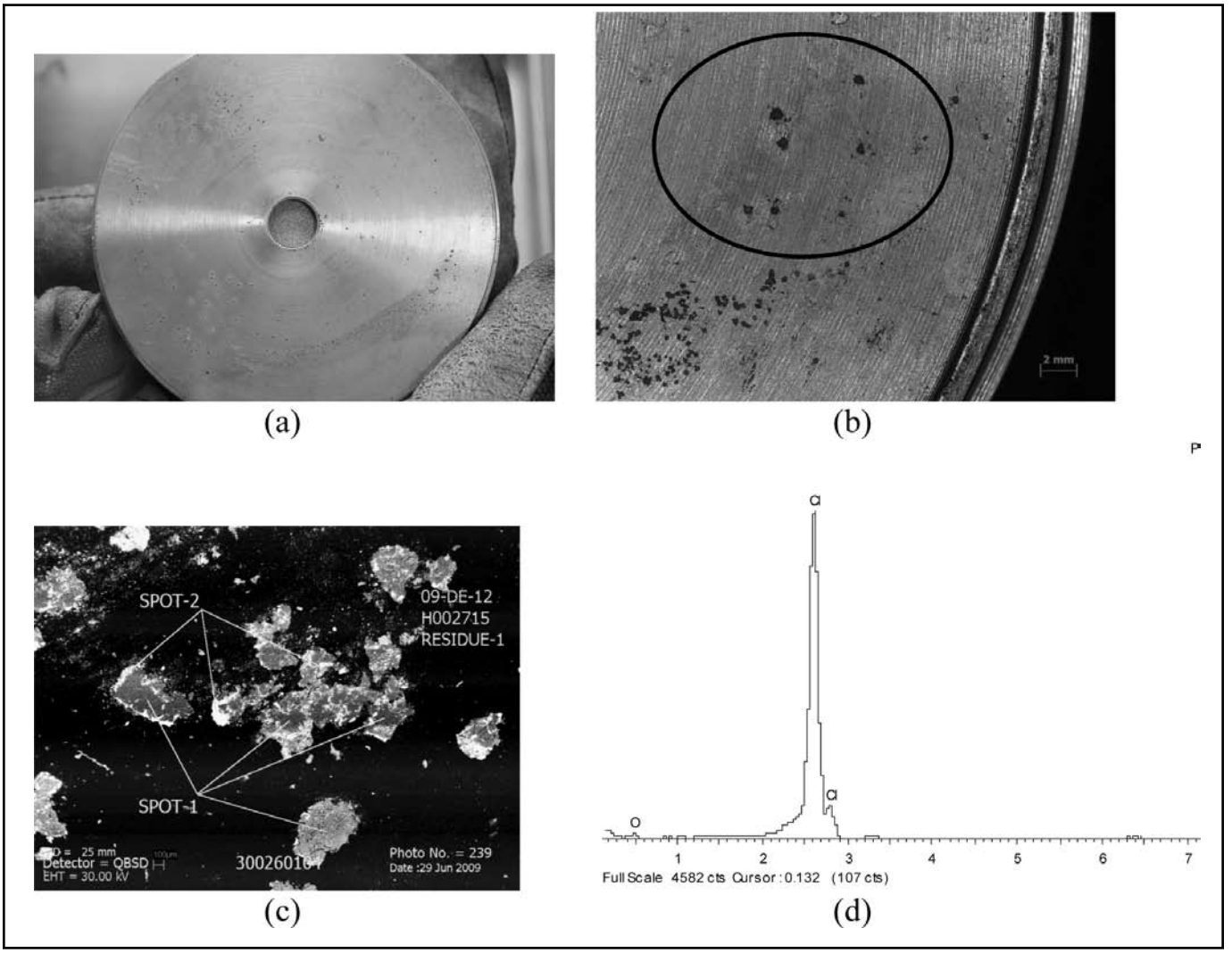

bearing materials and some of which is considered miscellaneous debris. The inner container evaluation showed that, even under conditions where chloride transport to the inner container has occurred, its integrity was not compromised.

Discussion and Conclusions

The presence of pitting corrosion in the headspace region of certain 3013 containers has been observed during destructive examination. The postulated headspace pitting mechanism requires the presence of a radiation source, alpha from the plutonium material, to dissociate and ionize the gases present and form a more volatile vapor or gas containing chlorine. The chloride rich vapor or gas provided a mechanism to transport chloride to stainless steel surfaces exposed only to the headspace region and make that region susceptible to corrosion.[12]

Figure 11. Examination of RFETS inner container. The presence of soot from the welding operation was observed. No contact with salt containing Pu oxide.

Figure 12. Additional sections from inner container for further analysis during DE. (a) appearance of corrosion particulates and "coating" adhering to surface of lid and side wall. No corrosion depth was seen by SEM. (b) coating product on sidewall likely an iron oxide product with the oxide peak shown in the EDX spectrum at top right. Bottom photo and corresponding spectrum at bottom right shows a chloride peak from corrosion product within incipient pit.

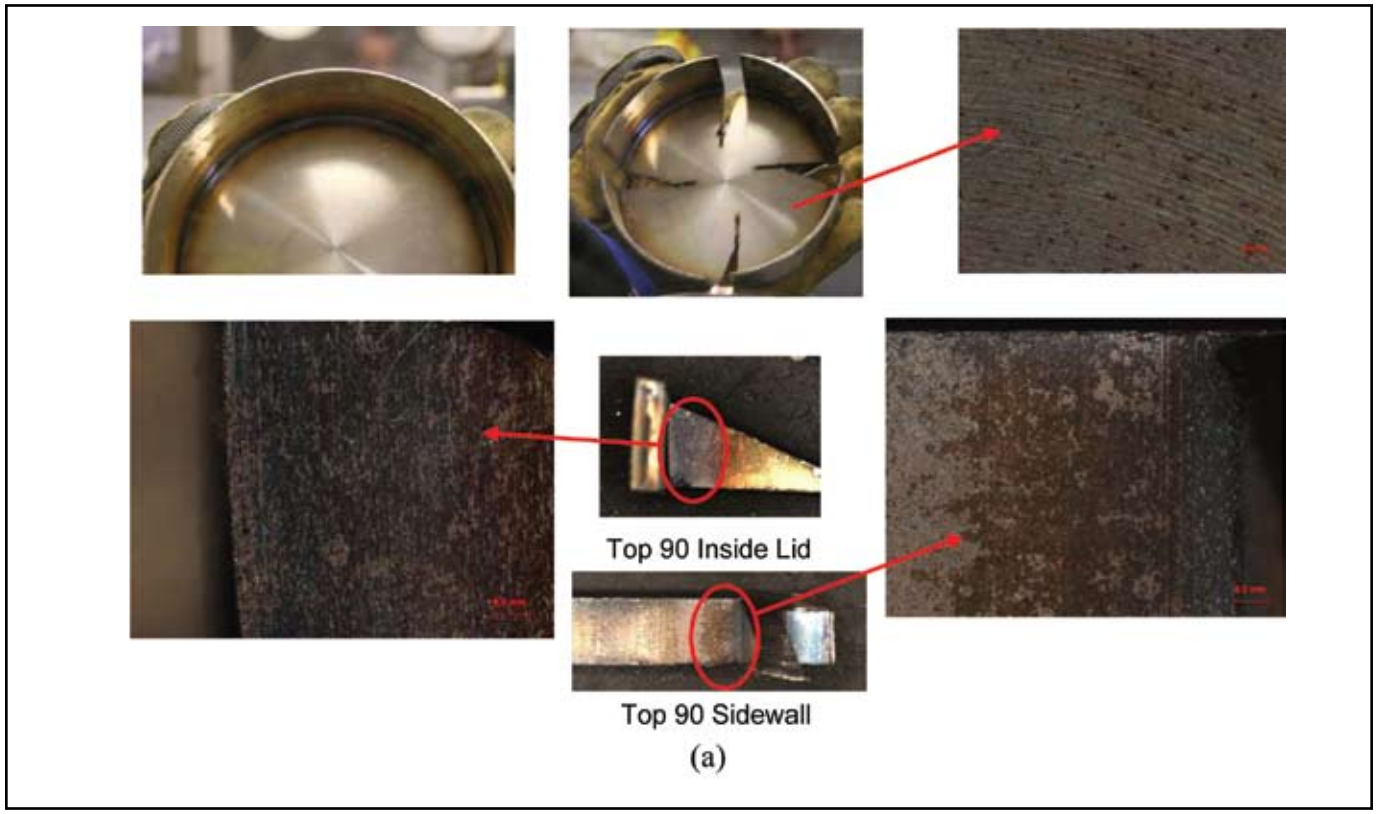

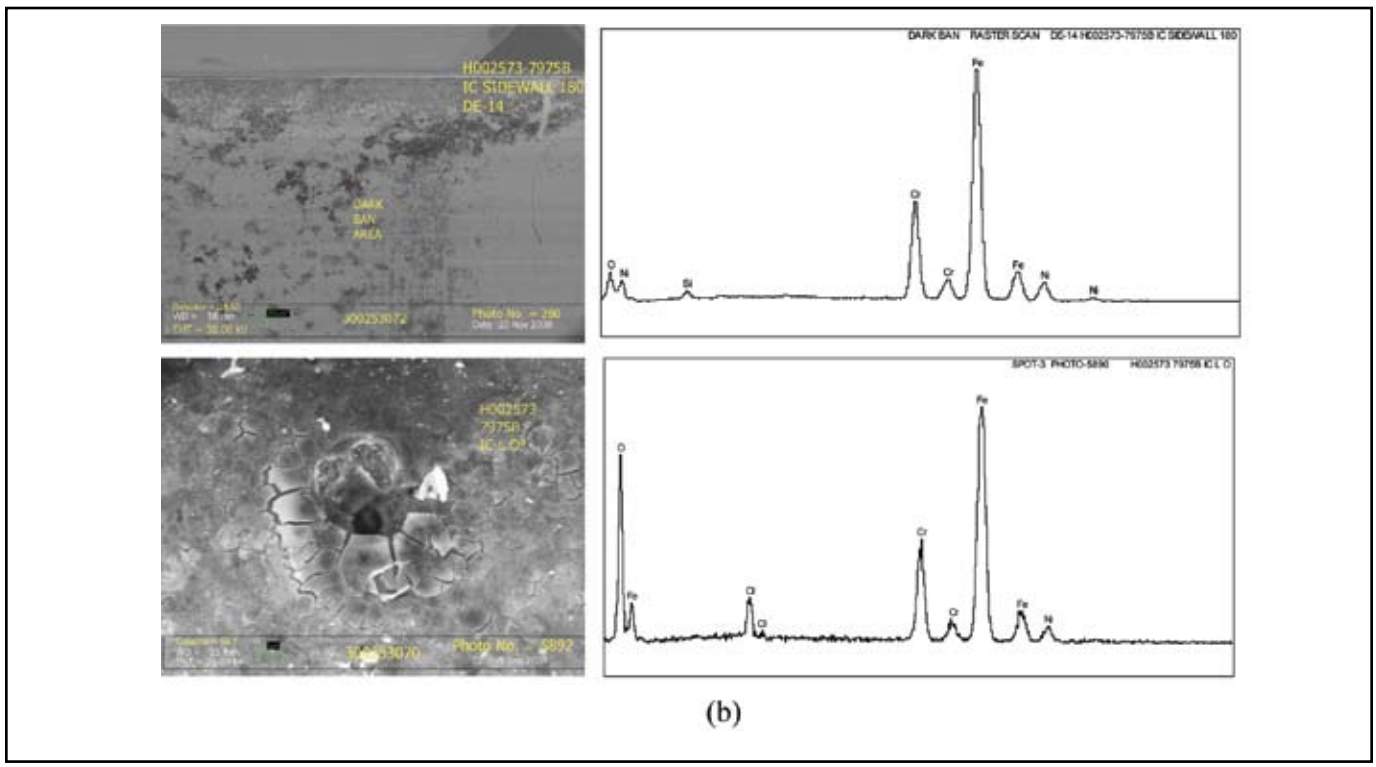

Figure 13. (a) Presence of adherent layer on inside inner container surface and (b) layer removed through light wiping with clean cloth

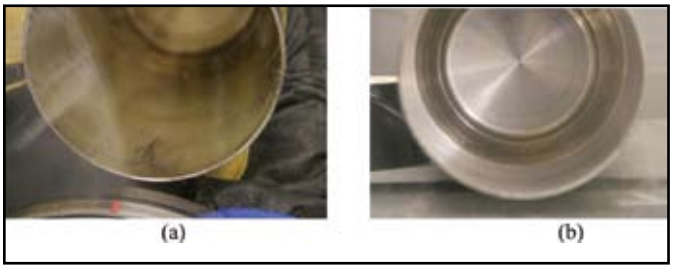

Figure 14. Sections cut from inner container for SEM and EDX analysis

The degradation, if any, observed during DE of convenience and inner containers could be correlated with the chemistry of the plutonium bearing materials stored in the convenience containers. The surveillance observations showed that none of the containers from the pressure bin displayed any evidence of corrosion on any of the surfaces. The majority of indications of incipient corrosion occurred in the headspace gas region of containers that stored plutonium bearing materials with high chloride and moisture contents. Little to no damage was observed in the plutonium oxide contact region of the convenience container. All of these observations are consistent with observations in laboratory testing of small containers.[10] Additionally, no evidence of stress-corrosion cracking has been observed in any of the containers examined to date.

Perhaps the most significant observation was that a chloride rich gas was created under certain conditions and provided a mechanism for chloride transport and deposition to regions of the container system that were only exposed to headspace gases. This observation emphasizes the importance of continued surveillances of the stored containers. The surveillance program will continue to evaluate containers to gain sufficient data to validate the fifty-year container integrity criteria, as specified in the DOE-STD-3013. Gaseous transport of chloride and the potential for SCC will still be a strong focus of the evaluations as will particle induced pitting corrosion. The integrity of the containers has not been compromised at this time and there is no evidence that the potential for a fifty-year storage lifetime will be compromised. However, the observation of incipient, storage-induced corrosion in some containers demonstrates the necessity for continuing surveillance evaluations during storage of plutonium-bearing materials in 3013 container systems.

Figure 15. Inner container weld cross-section (a) Schematic (b) metallographically prepared section.

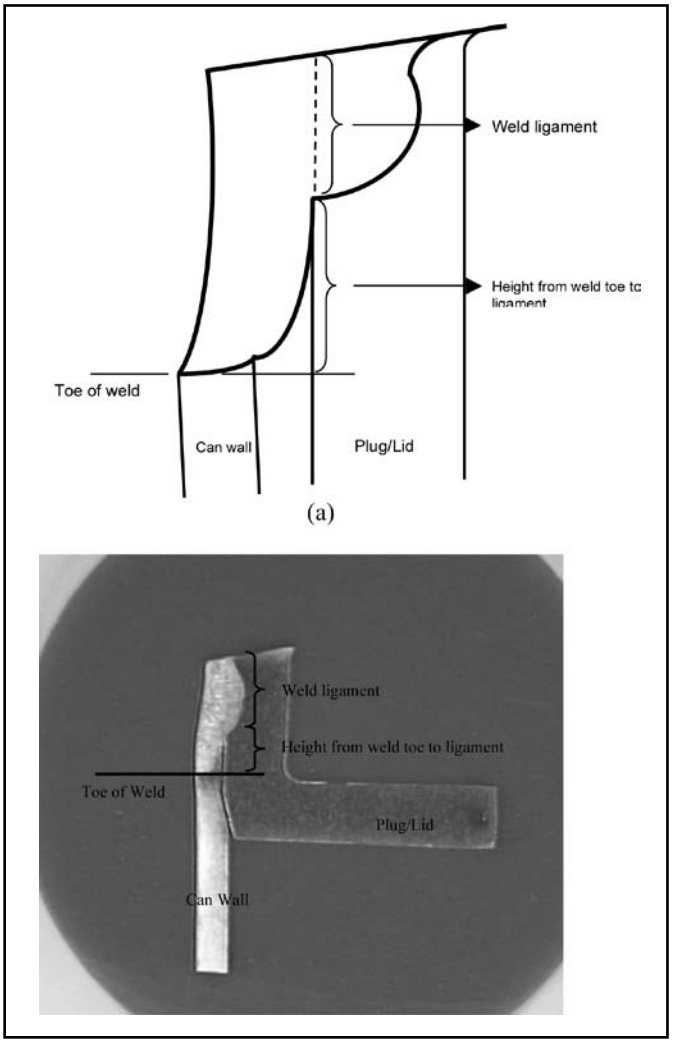

D. Zane Nelson is a lead technical specialist at Savannah River National Laboratory.

Gregory T. Chandler is a manager at the Savannah River National Laboratory. He has an M.S. in materials science and engineering from the University of Florida and a B.S. in chemical engineering from Clemson University.

Kerry A. Dunn is an advisory engineer at the Savannah River National Laboratory. She has an M.S. in materials science and engineering and a B.S. in metallurgy from Pennsylvania State University.

Tina M. Stefek is a principal engineering and technical support

Figure 16. Small coalesced pits on the machining grooves of the inner container lid

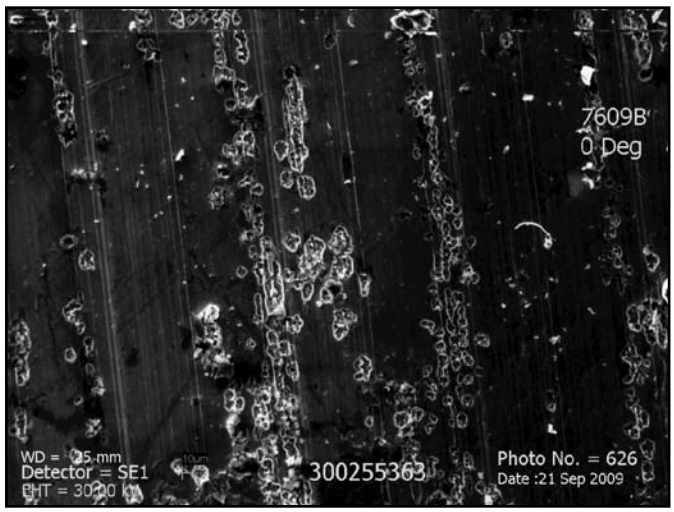

specialist at Savannah River National Laboratory. She has a B.S. in business management from Augusta State University.

Michael E. Summer is a principal scientist at Savannah River National Laboratory. He has a B.S. in biology from University of South Carolina.

Acknowledgements

This work was performed at the Savannah River National Laboratory which is operated by Savannah River Nuclear Solutions for the U.S. Department of Energy under contract DE-AC09-08SR22470.

References

1. *Stabilization, Packaging, and Storage of Plutonium-bearing Materials.* 2004. DOE-STD-3013-2004. U.S. Department of Energy: Washington, D.C.
2. LANL. 2001. Integrated Surveillance Program in Support of Long-Term Storage of Plutonium-bearing Materials. *LA-UR-00-3246, Revision 1.* Los Alamos National Laboratory, Los Alamos, N.M.
3. DOE. 2003. Surveillance and Monitoring Plan for DOE-STD-3013 Materials. *SR-NMPD-03-001, Revision 0.* U.S. Department of Energy.
4. WSRC. 2008. The Savannah River Site Surveillance Program for the Storage of 9975/3013 Plutonium Packages in KAC. *WSRC-TR-2001-00286, Rev. 4.* Westinghouse Savannah River Company.
5. Peppers, L., E. Kelly, J. W. McClard, G. P. Friday, T.J. Venetz, and J. Stakebake. 2009. Selection of 3013 Containers for Field Surveillance: LA-14310, Revision 1. *LA-14395.* Los Alamos National Laboratory, Los Alamos, N.M.
6. Almond, P., R. L. Livingston, L. E. Traver, M. J. Arnold, N. Bridges, and G. F. Kessinger. 2010. Gas Analysis from Headspace of Plutonium-Bearing Materials Containers,. *Journal of Nuclear Materials Management* Vol. 38, No. 3.
7. Kessinger, G. F., P. M. Almond, M. G. Bronikowski, M. L. Crowder, J. M. Duffey, A. R. Jurgensen, D. M. Missimer, and J. H. Scogin, M.E. Summer. 2010. Material Properties of Plutonium-Bearing Oxides Stored in Stainless Steel Containers, *Journal of Nuclear Materials Management* Vol. 38, No. 3.
8. Zapp, P. E., L. A. Worl, D. K. Veirs, J. M. Duffey, J. I. Mickalonis, K. A. Dunn, and P. S. Lam. 2010. Relative Humidity and the Susceptibility of Austenitic Stainless Steel to Stress Corrosion Cracking in an Impure Plutonium Oxide Environment, *Journal of Nuclear Materials Management* Vol. 38, No. 3.
9. Mickalonis, J. I., and K. A. Dunn. 2010. Residual Stresses in 3013 Containers, *Journal of Nuclear Materials Management* Vol. 38, No. 2.
10. Lillard, R. S., D. G. Kolman, M. A. Hill, M. B. Prime, D. K. Veirs, L.A. Worl, and P.E. Zapp. 2009. Assessment of Corrosion-based Failure in Stainless Steel Containers Used for the Long-term Storage of Plutonium-based Salts, *Corrosion* Vol. 65, No. 3.
11. Dunn, K. A., M. R. Louthan, G. B. Rawls, R. L. Sindelar, P. E. Zapp, and J. W. McClard. 2010. Container Materials, Fabrication and Robustness, *Journal of Nuclear Materials Management* Vol. 38, No. 2.
12. Veirs, D.K., J.M. Berg, K.A. Dunn, M.R., Louthan, Jr., L.A. Worl, and J.E. Narlesky. 2010. Evidence of Corrosive Gas Formed by Radiolysis of Chloride Salts in Plutonium-Bearing Materials, *Journal of Nuclear Materials Management* Vol. 38, No. 3.

Material Properties of Plutonium-bearing Oxides Stored in Stainless Steel Containers

Glen F. Kessinger, Philip M. Almond, Nick J. Bridges, Mike G. Bronikowski, Mark L. Crowder, Jonathan M. Duffey, Dave M. Missimer, John H. Scogin, and Michael E. Summer
Savannah River National Laboratory, Aiken, South Carolina USA

Ronald R. Livingston, and Morgan M. McElwee
Savannah River Nuclear Solutions, Aiken, South Carolina USA

Art R. Jurgensen
Retired, Savannah River National Laboratory, Aiken, South Carolina USA

Abstract

The destructive examination of 3013 containers after storage is part of the Surveillance and Monitoring Program based on the U.S. Department of Energy's standard for long-term storage of Pu (DOE-STD-3013). The stored, Pu-bearing materials may contain alkali halide contamination that varies from trace amounts of salt to about 50 weight percent, with smaller fractions of other compounds and oxides. These materials were characterized prior to packaging, and surveillance characterizations are conducted to determine the behavior of the materials during long-term storage.

The surveillance characterization results are generally in agreement with the pre-surveillance data. The predominant phases identified by X-ray diffraction are in agreement with the expected phase assemblages of the as-received materials. The measured densities are in reasonable agreement with the expected densities of materials containing the fraction of salts and actinide oxide specified by the pre-surveillance data. The radiochemical results are generally in good agreement with the pre-surveillance data for mixtures containing "weapons grade" Pu (nominally 94 percent ^{239}Pu and 6 percent ^{240}Pu); however, the inductively coupled plasma-mass spectroscopy results from the present investigation generally produce lower concentrations of Pu than the pre-surveillance analyses. For mixtures containing "fuel grade" Pu (nominally 81-93 percent ^{239}Pu and 7-19 percent ^{240}Pu), the ICP-MS results from the present investigation appear to be in better agreement with the pre-surveillance data than the radiochemistry results.

Introduction

The destructive examination (DE) of the Pu-bearing materials from 3013 containers is part of the Surveillance and Monitoring Program based on the U.S. Department of Energy's requirements for long-term storage of Pu (DOE-STD-3013).[1] The materials studied in this investigation include plutonium oxide materials only; no metal items were investigated. Nevertheless, these oxide-based materials exhibited a wide range of chemical characteristics. At one compositional extreme was nearly pure plutonium oxide. At the other compositional extreme is a variety of impure materials from processing and experimental programs that had been stored in vaults for decades awaiting Pu recovery. In some cases, the only information available on the scrap material was the quantity of nuclear material present and the site of origin. In other cases, there are varying levels of "process knowledge" that describe how the material was generated and what possible impurities might be present. Alkali metal-halide salts, which are a result of the molten salt processing associated with weapons production, are the primary contaminant in these materials. This halide salt contamination varies from trace quantities to about 50 weight percent. Other non-actinide metals, halide salts, and compounds may also be present, but generally at much lower concentrations than the alkali metal-halide salt contamination.

The materials being investigated have been in storage in 3013 containers for four to seven years. A variety of characterization techniques have been utilized to deduce the chemical and phase composition of these materials. The characterization techniques include:

- density determination,
- dissolution/leaching studies,
- inductively coupled plasma-mass spectrometry (ICP-MS), inductively coupled plasma-emission spectroscopy (ICP-ES), and radiochemical analyses of dissolution products,
- ion chromatography (IC) and ICP-ES analyses of aqueous leachates,
- moisture content determination,
- surface area determination, and
- phase and elemental characterization by X-ray powder diffraction (XRD) and scanning electron microscopy (SEM) with energy dispersive spectrometry (EDS), respectively.

Samples of contents from twenty-eight 3013 containers that originated at the Hanford or Rocky Flats sites are included in this investigation. All handling of the initial samples, including removal of material from the 3013 containers, was performed in gloveboxes under air atmosphere. This paper describes the material characterization methodologies, presents the results of the characterizations and compares the results with pre-storage characterization results.

Experimental

Sampling

The 3013 containers were opened in a once through air glovebox at the Savannah River Site's K Area Material Storage Facility. An initial sample of the Pu-bearing material was taken immediately after opening each convenience can (the inner-most container in the 3013 container). This sample, referred to as the initial moisture (IM) sample was placed in an air-tight stainless steel ampoule (B-vial) and was analyzed by thermogravimetric analyzer mass spectrometry (TGA-MS) to determine the moisture content of the material (which is assumed to be a representation of the condition of the solid just prior to opening the 3013 container).

Figure 1. Sample H002509 after removal from the 3013 inner can. This material contains approximately 70 percent actinides by weight.

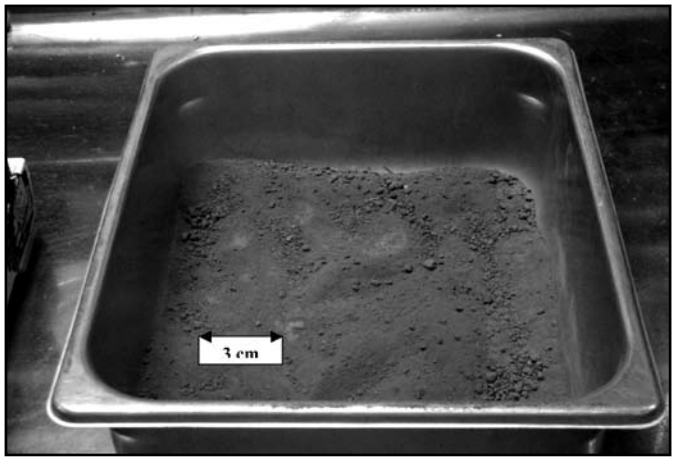

The solid was then poured from the convenience can into a rectangular tray and spread out to cover the entire surface of the tray (Figure 1). A sample was taken from each of four quadrants of the tray and the four samples were combined to make a single sample for analysis. It was from this sample that a sub-sample (hereafter referenced as the representative (RP) sample) was selected, loaded into a uniquely-numbered B-vial and transferred to Savannah River National Laboratory (SRNL) for analysis. While the material was in the tray, it was visually inspected. Unique items, such as pieces of oddly colored or shaped material referred to as 'if required' (IR) samples, were collected and loaded into a uniquely numbered B-vial and sent to SRNL for analysis. The decision to take such a sample is based solely on engineering judgment. The surveillance engineer looks for foreign material that is different in appearance than the bulk of the oxide (Figure 2). If such material is present an IR sample is taken. In addition to the IM, RP and IR samples, a final moisture (FM) sample was collected just prior to repackaging the solids, and sent to SRNL for determination of the moisture content of the repackaged material.

Figure 2. Sample H001992 after removal from the 3013 inner can. The small [blue and] whitish flecks are indicative of material that might be sampled and designated as 'if required' samples. This material contains approximately 52 percent actinides by weight.

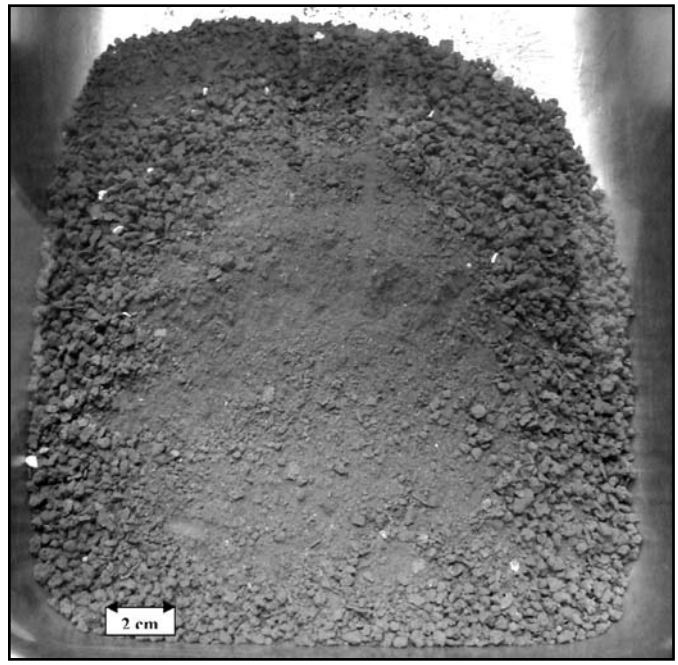

Characterization of As-Received Samples

Density Determination, Visual Inspection, and Sub-sampling

The density of each RP sample was determined by He gas pycnometry (Micromeritics AccuPyc model 1330 He Gas Pycnometer); the bulk density of each sample was measured using a calibrated graduated cylinder. Generally 50 percent or more of the sample was subjected to density determination by pycnometry while the entire sample was used for the bulk density determination. The bulk determination was performed first. The RP sample was transferred into a weighed and calibrated 10-mL graduated cylinder resting on a flat, level surface, and the volume of the material in the cylinder was recorded. The graduated cylinder was weighed and the mass of the RP solid in the cylinder was determined. The average level of solid in the cylinder was computed from the high and low level measurements and these measurements were used to compute the average volume of material. The bulk density was computed by dividing the mass of the

solid by the average volume. Upon completion of the bulk density determination, the pycnometry density determination was performed. The pycnometer determines the volume and density of the material three times, and then computes the average volume and density.

Upon successful completion of the density determination, the material was poured into a clean glass Petri dish, visually inspected, and photographed. If the particle size distribution of the material did not appear to be uniform, the material was ground with an alumina mortar and pestle, and the pycnometry and bulk and tapped density measurements were repeated. Upon completion of the inspection and size reduction (when required), the material was sub-sampled for additional analyses. Portions of the solid were taken for dissolution, aqueous leaching, surface area determination, SEM/EDS, and XRD.

Dissolutions

The dissolution studies were performed to produce aqueous solutions for characterization of the elemental content of the material. Because the chemical compositions, phase compositions, and solubilities of the materials were not known, two dissolution regimens were utilized. Both were based on the use of nitric acid-hydrofluoric acid media, but one of the dissolutions also included the addition of a complexant, boric acid, to the dissolver solution in an attempt to identify complex halides present in the solution (which would, in turn, reduce the likelihood of PuF_4 precipitation).

Two aliquots of 0.25-grams each were removed from each sample lot for dissolution studies. Each sample to be dissolved was transferred to a flat-bottomed, screw lid 60 mL polypropylene reaction tube. Each tube was placed in a thermostated hot block heater capable of holding six reaction tubes. During each run, the hot block contained the two reaction tubes, a blank, and a *dummy* tube containing water into which a thermocouple was inserted (as an independent temperature measurement to which the thermostated hot block controller could be compared). During some runs a second dummy tube (containing silica sand) into which a second thermocouple was inserted was also used (in an attempt to determine the temperature of the material in the reaction tubes).

To each sample-containing tube and each blank tube, a 30-mL aliquot of 12 M HNO_3-0.2 M HF (nominal concentration) was added. A small polypropylene "watch glass" was placed over the lid of each tube, and the temperature was ramped up to approzimately 95°C over a period of sixty to ninety minutes; each watch glass was filled with water to facilitate condensation of vapor emanating from the solution. After temperature stabilization, the temperature was held constant for three hours. Just prior to de-energizing the hot-block, 2.5 mL of 0.9 M H_3BO_3 was added to the complexed dissolution tube, and then the temperature of the hot block was allowed to cool to ambient temperature. After the tubes had returned to ambient temperature, the volume of each dissolution tube was checked and the solution volumes were adjusted, as necessary, to 30 mL using deionized water. For samples believed to be high in chloride, a condenser containing permanganate-coated media was utilized to capture acidic vapors.

The solid-solution mixtures were filtered through a 0.45-µm acid-resistant filter in 10 mL increments. The resulting solids were dried to a constant mass at 120°C, in a Mettler-Toledo model HR83 Moisture Analyzer. A portion of the recovered solids were subjected to XRD analysis. The resulting filtered solutions were subjected to ICP-ES, ICP-MS, and radiochemical (α and γ spectrometry) analyses to determine the cation concentrations in the solutions.

In addition to two dissolution samples, two aliquots of 1-gram each were leached in 30 mL of de-ionized water. A small watch glass was placed over the lid of the tube, and the temperature was ramped up to approximetely 90°C, generally over a period of sixty to ninety minutes. A lower temperature was utilized, as compared to the dissolutions, to retard the evaporation of chlorine-containing vapor species. After temperature stabilization, the temperature was held constant for three hours. After the hot block had returned to ambient temperature, the volume of each leaching tube was checked and the solution volumes were adjusted, as necessary, to 30 mL using deionized water. The resulting solutions were subjected to IC and ICP-ES analyses to determine the concentrations of the cations and anions of interest.

Results and Discussion

In an attempt to determine the chemical composition of the initial solids, the resulting solution and any recoverable insoluble solids were analyzed. The results of the analyses performed to characterize the initial solids are presented in the attached tables; however, it is outside the scope of this discussion to discuss all of the analytical results related to the interrogation of these samples, so only those results germane to the discussion of the characterization of the chemical and phase compositions will be presented and discussed.

As-Received Samples

Characterization of the as-received samples by XRD (see Table 1) suggests that these materials are, as expected, PuO_2 (and sometimes uranium oxide phases as well) accompanied by a variety of contaminants. Based on the pre-surveillance data reports, the 3013 materials can be conveniently classified as high purity oxide materials, containing 75 wt. percent Pu, and low-purity materials containing less Pu. In general, all of the samples contain varying quantities of simple oxide phases such as $NiCr_2O_4$, NiO, SiO_2, and Cr_2O_3. Some of the samples also contain other more complex oxide phases such as aluminosilicate and tungstate phases.

The presence of the Ni, Cr, Fe, aluminosilicates, and silica is not surprising. During the calcination process prior to 3013

Table 1. Sample characteristics

Sample	[3]Actinide Content/ (wt Percent)	ρ(g/cm^3)	[1]Phases Identified by XRD	[4]Moisture (wt Percent)	Surface Area/(m^2/g)	[2]Storage Atmosphere
R600885	86.42	11.56	PuO_2, $NiCr_2O_4$	0.05	0.94	89 percent He, 10 percent N_2, 0.1 percent O_2, trace H_2, trace CO_2
R601722	84.25	11.00	PuO_2, $NiCr_2O_4$, NiO, Cr_2O_3, AgCl	0.04	0.58	82 percent He, 16 percent N_2 less than 0.1 percent O_2, trace H_2
R601957	87.48	11.32	PuO_2, $NiCr_2O_4$, NiO, $(Fe,Mg)(Cr,Fe)_2O_4$	0.04	0.47	86 percent He, 12 percent N_2, trace H_2, trace CO_2
R600719	86.24	10.62	PuO_2, Al_2O_3, NiO, $NiCr_2O_4$	0.04	0.82	80 percent He, 18 percent N_2, trace H_2, trace CO_2
R610735	53.35	4.28	PuO_2, KCl, NaCl, NiO, MgO, Fe_3O_4, $Na_{0.1}K_{0.9}Cl$, PbO_2, $Na_{0.68}Fe_{0.68}Si_{0.32}O_2$	0.19	0.58	76 percent He, 19 percent N_2, trace H_2, 0.2 percent CO_2
R610697	69.76	5.88	PuO_2, KCl, NaCl, NiO, $Na_{0.1}K_{0.9}Cl$	0.14	0.58	81 percent He, 19 percent N_2, trace H_2, trace CO_2, trace CH_4
R601285	85.84	10.95	PuO_2	0.10	0.99	75 percent He, 24 percent N_2, trace H_2, trace CO_2, less than 0.1 percent CH_4
R602731	97.433	9.42	PuO_2, U_3O_8	0.03	0.26	81 percent He, 19 percent N_2
R601318	83.62	10.41	PuO_2, $NiCr_2O_4$	0.02	0.75	88 percent He, 11 percent N_2
H000898	77.68	9.15	PuO_2, $NiCr_2O_4$, SiO_2(Q), SiO_2(Cr), Cr_2O_3, Fe/Ni Alloy, Graphite	0.04	0.25	76 percent He, 23 percent N_2
R610327	80.763	7.24	PuO_2, $U_{13}O_{34}$, UO_2, (U,Pu)O(2 x), $KCaF_3$	0.04	1.01	78 percent He, 20 percent N_2
R610298	64.83	6.03	PuO_2, NiO, KCl, NaCl, $Na_{0.1}K_{0.9}Cl$, $NiCr_2O_4$	0.14	0.31	79 percent He, 18 percent N_2
R610324	71.55	6.69	PuO_2, KCl, NaCl, NiO	0.10	0.58	79 percent He, 21 percent N_2
H001992	52.30	6.89	PuO_2, Fe_2O_3, NiO, $NiCr_2O_4$, SiO_2(Cr), ThO_2	0.03	0.45	54 percent He, 43 percent N_2
H003157	84.98	10.96	PuO_2, NiO, $NiCr_2O_4$	0.10	1.98	52 percent He, 46 percent N_2, 1.6 percent O_2
R610584	71.35	8.54	PuO_2, SiO_2(Q)	0.07	0.21	81 percent He, 18 percent N_2, 0.6 percent CO_2
R610578	64.70	7.22	PuO_2, NaCl, $CaWO_4$, $Ca_2Ta_2O_7$	0.19	0.56	78 percent He, 21 percent N_2
H001916	34.26	4.96	PuO_2, Fe_2O_3, $NiCr_2O_4$, $Ca_2Ta_2O_7$, WO_3, $Mg_2Si_5Al_4O_8$, $WNiO_4$, $Ta1_6W1_8O_{94}$, $K_6NiW_9O_{31}$, $Na_{0.5}Cr_{0.5}WO_4$, SiO_2(Cr)	0.07	0.28	52 percent He, 49 percent N_2
H002088	86.74	11.07	PuO_2, $NiCr_2O_4$	0.18	2.02	57 percent He, 44 percent N_2
H003409	73.96	6.97	PuO_2, NaCl, KCl	0.24	1.05	46 percent He, 38 percent N_2, 18 percent H_2
H002573	74.27	7.17	PuO_2, KCl, NaCl	0.33	1.26	41 percent He, 35 percent N_2, 29 percent H_2
H002534	70.49	6.96	PuO_2, KCl, NaCl, $NiCr_2O_4$	0.19	1.15	40 percent He, 29 percent N_2, 30 percent H_2, 2.6 percent CO_2
R610679	70.35	9.06	PuO_2, C, $KFe(WO_4)_2$, (W,Fe)(O,OH)$_2$, CaF_2	0.03	0.45	66 percent He, 31 percent N_2, 2.8 percent CO_2

[1] (Cr) – cristobalite, (Q) – quartz

[2] Composition in volume percent.

[3] Composition estimated from gamma counting. The uncertainty in the measurement of U by this technique is quite large because U-235 has only a single gamma which can be utilized.

[4] Moisture of sample taken from 3013 can, when can was initially opened

Table 1. (cont.) Sample characteristics

Sample	[3]Actinide Content/ (wt Percent)	ρ(g/cm³)	[1]Phases Identified by XRD	[4]Moisture ()wt Percent)	Surface Area/(m^2/g)	[2]Storage Atmosphere
H002750	69.63	8.06	PuO_2, $NiCr_2O_4$, $Na_{0.35}Fe_{0.65}Ti_{3.34}O_8$, $NaAlSiO_4$, (K,Na)$AlSiO_4$	0.07	0.59	59 percent He, 41 percent N_2
H004099	78.88	10.12	PuO_2, $NiCr_2O_4$, Fe_2O_3, MgO	0.03	0.46	41 percent He, 55 percent N_2, 0.19 percent O_2, trace H_2, 0.34 percent CO_2, trace CO, 1.3 percent N_2O
H004111	71.75	7.13	PuO_2, NiO, NaCl, KCl, $NiCr_2O_4$	0.26	1.00	32 percent He, 48 percent N_2, less than 0.1 percent O_2, 20 percent H_2, trace CO_2, trace CO, less than 0.1 percent N_2O
H002554	70.59	6.76	PuO_2, $NiCr_2O_4$, NaCl, KCl	0.22	1.07	Pressure too low to measure gas composition

[1] (Cr) – cristobalite, (Q) – quartz
[2] Composition in volume percent.
[3] Composition estimated from gamma counting. The uncertainty in the measurement of U by this technique is quite large because U-235 has only a single gamma which can be utilized.
[4] Moisture of sample taken from 3013 can, when can was initially opened

loading, all of these materials were heated in air at 750°C or 950°C. Generally, the material was contained in an Inconel™ or Hastelloy® tray during the calcination process. While these alloys are designed to be corrosion resistant, some corrosion, in the form of surface oxidation, is common. The thin oxide coating can spall from the tray and contaminate the Pu-bearing material, and is often found as thin flakes of bluish-hued material. The silicon-containing phases found in these materials, such as silica and aluminosilicates, are probably contaminants that spall from the furnace lining (the refractory furnace lining is often fabricated from mullite, $Al_6Si_2O_{13}$, and/or a silica-containing composite material).

A portion of each as-received sample was subjected to SEM and XRD analyses. Generally the XRD results show that the low-purity samples contain halide salts while the results from high-purity samples show no reflections that appear to result from halide-containing phases; the only exception to this behavior is H001992, for which the XRD results show numerous oxide phases, but no halide phases. While the phase characteristics of these samples are interesting, these results are qualitative in nature, and do not necessarily shed light on the quantitative chemical composition of the materials.

SEM analyses were performed to provide a preliminary elemental analysis of these materials. Energy dispersive spectra were collected on samples selected during visual inspection of the material. The spectrometry results for each sample were compared to pre-surveillance data to corroborate the most abundant metal present in the materials. These data were particularly useful for items that contained both U and Pu, since the SEM results could verify the presence of both actinides.

'If Required' Samples

'If required' samples were taken on a few occasions. In some of these cases, the IR sample contained elements and phases that suggest they were spalled oxide from the Inconel™ or Hastelloy® tray used in the calcination process. In the remainder of the cases, the IR sample appeared to be spalled refractory insulation from the calcination furnace. These conclusions are based primarily on the SEM analysis.

Density Measurements

As previously stated, both bulk and pycnometry density measurements were performed and values are shown in Table 2. In an attempt to evaluate the reasonability of the pycnometer data, these results were plotted versus the actinide fraction for each sample, as taken from the Pre-Surveillance Data Report (a compendium of information on each item which includes the results of any analyses performed on the material before, during, or after packaging). The line on Figure 3, extending from 2.2 g/mL (the approximate density of KCl and NaCl) to 11.46 g/mL (the theoretical density of pure PuO_2), is included as an evaluation tool. As shown on the plot, most of the values fall close to the line, as would be expected if it is assumed the density of a mixture of PuO_2 and the chloride salts is a linear combination of the phases involved. There is one clearly discordant point (at 97.43 wt percent, 9.42 g/mL). The uncertainty in the actinide content of this sample, R602731 ([U]=41.48 percent, from ICP-MS results), could be as great as 30 percent because the pre-surveillance actinide content was computed from a γ assay of the material and this sample is high in uranium (^{235}U has a weak γ, thus the high uncertainty in the assay).

Table 2. Bulk and pycnometer densities for 3013 representative samples

Sample	Bulk ρ(g/mL)	Pycnometer ρ/(g/mL)	Bulk ρ/ Pycnometer ρ
R600885	2.1	11.56	0.18
R601722	2.4	11.00	0.22
R601957	4.3	11.34	0.38
R600719	2.8	10.62	0.26
R610735	2.4	4.5	0.53
R610697	2.4	5.95	0.40
R601285	2.4	10.95	0.22
R602731	2.2	9.42	0.23
R601318	2.4	10.41	0.23
H000898	3.0	9.15	0.33
R610327	2.6	7.24	0.36
R610298	2.6	6.03	0.43
R610324	2.4	6.69	0.36
H001992	2.3	6.89	0.33
H003157	2.5	10.96	0.23
R610584	2.6	8.54	0.30
R610578	2.2	7.22	0.30
H001916	1.7	4.69	0.36
H002088	2.5	11.07	0.23
H003409	2.3	6.97	0.33
H002573	2.5	7.17	0.35
H002534	2.4	6.96	0.34
R610679	2.3	9.06	0.25
H002750	2.4	8.06	0.30
H004099	2.4	10.09	0.24
H004111	2.4	7.13	0.34
H002554	2.3	6.76	0.34
H001941	2.2	7.80	0.28
R600885	2.1	11.56	0.18

Dissolutions

To perform elemental analyses on solids, it is generally necessary to digest the solids to produce a liquid sample. The common practice when dissolving materials containing refractory oxides, especially materials that contain high-fired PuO_2, is to use a highly concentrated strong acid, such as HNO_3 to digest the material, accompanied by a complexant, such as $[F^-]$[3], to stabilize the aqueous Pu species in solution and drive the dissolution reaction to completion (per Le Chatelier's principle).[4] When $[F^-]$ is used as the Pu complexant, this approach sometimes leads to dissolution of the oxide followed by precipitation of PuF_4. In an attempt to combat "post-dissolution precipitation," a second complexant is added after the initial dissolution process is completed to compete for the anionic complexant (in this case $[F^-]$).

Figure 3. Experimentally measured sample density plotted as a function of pre-surveillance data report actinide content.

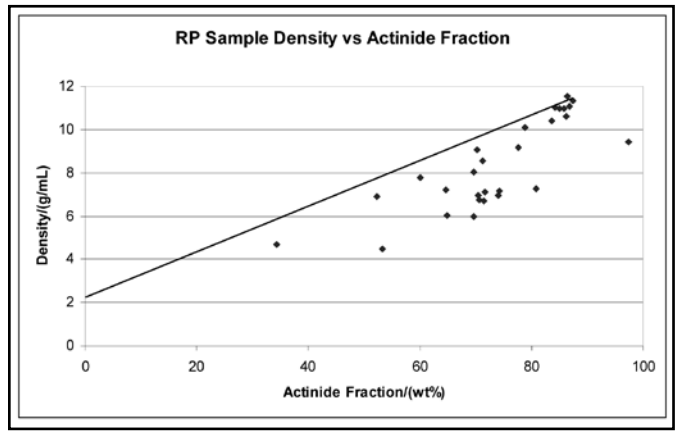

During the present study, we utilized two dissolution flowsheets for each sample. Both employed 12M HNO_3-0.2 M HF for sample digestion; however, boric acid was added to the dissolver product of one dissolution (hereafter referred to as the complexed dissolution) before allowing the solution to cool. The residues recovered from the dissolution testing indicate that the complexed dissolution provides a more thorough mechanism for solubilizing the samples of interest (as shown in Table 3); consequently, most of the discussion of the experimental results shall address the results from the complexed dissolutions.

Twenty-eight samples were subjected to the complexed dissolution method; of those, only nine showed Pu-bearing phases in the insoluble solids. In seven of those cases with recovered solids, the only Pu-bearing phase was a fluoride, suggesting the dissolution process had successfully digested the PuO_2 (all of the starting materials showed Pu present as PuO_2), but that Pu-bearing phases subsequently precipitated from the solution due to the high ionic strength and $[F^-]$ of the solution. In only two cases, H002573 and H002554, did the Pu-bearing phase(s) in the insoluble solids include PuO_2, and in both of those cases, the insoluble solids accounted for less than 10 percent of the initial sample mass. Based on these results, it is concluded that the solutions produced by the complexed dissolution scheme give a reasonable representation of the chemical composition of the solid samples.

Another result of interest is related to the graphite present in H000898 (Table 1) and R610584 (Table 3). It is believed that the graphite in these samples is a result of material processing performed prior to these materials being selected for 3013 storage. Graphite is often used as a mold material during the casting of Pu, so it is likely that the graphite in these two materials was a result of mold material that accompanied the material through the casting and oxidation processes. If the pieces of graphite were large enough, it is possible that they were not completely oxidized

Table 3. Dissolution residues

Sample ID	Uncomplexed Dissolution, Percent Insoluble	Insoluble Phases Identified by XRD, Uncomplexed Dissolution	Complexed Dissolution, Percent Insoluble	Insoluble Phases Identified by XRD, Complexed Dissolution
R600885		PuO_2, $Pu_3F_{12}\cdot H_2O$		$Pu_3F_{12}\cdot H_2O$*
R601722		$Pu_3F_{12}\cdot H_2O$**		None
R601957		None*		$Pu_3F_{12}\cdot H_2O$*
R600719		$Pu_3F_{12}\cdot H_2O$*		None*
R610735		$NiCr_2O_4$, NaCl, $MgWO_4$, NiO		NiO
R610697		$Pu_3F_{12}\cdot H_2O$*		$Pu_3F_{12}\cdot H_2O$*
R610285		PuO_2, $Pu_3F_{12}\cdot H_2O$		None
R602731	58.7	PuO_2, $Pu_3F_{12}\cdot H_2O$	0	None*
R601318	0	None*	1.4	None*
H000898	25.8	$Pu_3F_{12}\cdot H_2O$	4.8	None*
R610327	6.4	None*	2.7	None
R610298	59.1	PuF_4, $PuF_4(H_2O)_{1.6}$	3.1	$PuF_4(H_2O)_{1.6}$
R610324	26.9	PuO_2, PuF_4, $PuF_4(H_2O)_{1.6}$	2.7	PuO_2, PuF_4, $PuF_4(H_2O)_{1.6}$*
H001992	68.3	$Pu_3F_{12}\cdot H_2O$, $(Fe,Mg)(Cr,Fe)_2O_4$	26.1	$(Fe,Mg)(Cr,Fe)_2O_4$, NiO
H003157	54.0	$Pu_3F_{12}\cdot H_2O$	0	None*
R610584	27.7	$Pu_3F_{12}\cdot H_2O$	4.6	$KNiCrF_6$, graphite, $MgCrF_6$, SiC
R610578	41.2	$Pu_3F_{12}\cdot H_2O$, $WO_3\cdot H_2O$	25.0	$Pu_3F_{12}\cdot H_2O$, $WO_3\cdot H_2O$, PuO_2
H001916	11.5	Fe_2O_3, SiO_2, $NiCr_2O_4$, $(Na,Ca,U)_2(Nb,Ta)_2(OH,F)O_6$*	21.8	Fe_2O_3, SiO_2(Q), $MgWO_4$, $NiCr_2O_4$, $a,Ca,U)_2(Nb,Ta)_2O_6(OH,F)$, $NaTi_{0.2}Nb_{0.8}O_{2.9}$
H002088	61.2	$Pu_3F_{12}\cdot H_2O$	0.4	None*
R610700	36.3	$Pu_3F_{12}\cdot H_2O$	0.1	$Pu_3F_{12}\cdot H_2O$, $WO_3\cdot H_2O$, PuO_2*
H002573	38.7	$PuF_4(H_2O)_{1.6}$, PuF_4	9.6	Trace $PuF_4(H_2O)_{1.6}$, PuF_4 and PuO_2
H002534	37.8	$PuF_4(H_2O)_{1.6}$, PuF_4	0.8	$NiCr_2O_2$, NiO, Cr_2O_2
R610679	67.8	$Pu_3F_{12}\cdot H_2O$	6.8	TaO_2, Ta_2O_5
H002750	52.3	$Pu_3F_{12}\cdot H_2O$	7.1	Fe_2O_3, $NiCr_2O_4$ I
H004099	88.2	$PuF_4(H_2O)_{1.6}$	2.2	NiO, $NiCr_2O_4$, Fe_2O_3
H004111	73.0	$PuF_4(H_2O)_{1.6}$,PuF_4 ,K_3NiF_6	4.5	$WO_3\cdot H_2O$*
H002554	46.3	$Pu_3F_{12}\cdot H_2O$, $(K,Na)_2(Mg,Fe)_2Si_3$. I $Al_{0.9}O_{10}(OH)_2$	4.4	PuO_2, PuF_4*
H001941	62.1	NiO, Cr_2O_3, $NiCr_2O_4$, $Pu_3F_{12}\cdot H_2O$, $Na_2UO_2W_2O_8$, $CaWO_4$	21.6	NiO, Cr_2O_3, $NiCr_2O_4$, $SrCa_{0.5}W_{0.5}O_3$

** Polytetrafluoroethylene and SiO_2, constituents of the filter media, were detected.*
*** Polytetrafluoroethylene, a constituent of the filter media, was detected.*
[I] Unidentified material, face-centered cubic, a.=3.94 Å.

during the numerous heat treatments to which these materials were subjected; consequently, they were transferred to the 3013 container along with the Pu-bearing materials.

Table 4. IC anion results from aqueous leach solutions

Sample	F^-/(µg/gsample)	Cl^-/(µg/gsample)	NO_3^-/(µg/gsample)	PO_4^{3-}/(µg/gsample)	SO_4^{2-}/(µg/gsample)
R600885	555	118	875	<1400	134
R601722	498	355	785	<1250	225
R601957	<500	<500	890	1250	<500
R600719	<500	<500	825	1250	<1250
R610735	166	200000	469	930	831
R610697	<600	100000	530	515	655
R601285	<600	316	928	600	<600
R602731	<438	<438	638	<1090	<438
R601318	<465	<465	656	<1160	<465
H000898	393	<451	535	<1130	<451
R610327	339	518	<369	<747	763
R610298	<303	98000	<303	<758	712
R610324	<300	76000	<300	<749	<488
H001992	3650	322	<304	<761	795
H003157	<161	<161	850	<161	220
R610584	361	1860	180	<150	1410
R610578	<157	41000	187	<157	4380
H001916	<175	301	<159	849	434
H002088	<150	150	975	<150	225
H003409	<150	52000	209	<150	388
H002573	<157	67000	1080	<157	376
H002534	<152	64000	286	<152	646
R610679	300	<151	300	<151	330
H002750	814	1720	256	<302	783
H004099	<157	<157	313	376	250
H004111	<150	58100	210	<150	436
H002554	<151	65600	21-	No Result	480
H001941	6220	516	212	167	1320

Chemical Analyses

The aqueous leach solutions were analyzed by IC (Table 4) and ICP-ES (Table 5).

The dissolution samples were analyzed by ICP-ES, ICP-MS, and radiochemical methods, α and γ spectroscopy; the results of these analyses are shown in the Table 6 and Table 7.

In addition to the previously-mentioned analyses, the early aqueous leach solutions were also analyzed to detect any leaching of Pu- and/or U-bearing solids. The results of the analyses of these solutions confirmed the concentrations of Pu and U were at background levels, so these analyses were discontinued and will not be discussed further.

ICP-ES Analysis of Dissolution and Aqueous Leach Solutions

The ICP-ES results were used to identify the major, non-radioactive cations present in the dissolved solids. The major metallic contaminants generally included the alkali metals Na and K, the alkaline earth metals Ca and Mg, and the d-transition elements Ni, Fe, and Cr. In addition, one of the samples, R610327 contained 1 wt percent Be, while two others (R610584 and R610578) each contained more than 0.1 wt percent Be. All other cations detected were generally below 0.1 wt percent (1000 ppm). It was recognized that the high ionic strength of the acidic solutions might impede the dissolution of water-soluble ionic compounds, such as KCl and NaCl, so aliquots of each solid were also subjected to aqueous leaching and the resulting solutions were also subjected to cationic analysis by ICP-ES.

For elements that are expected to be present as oxides, such as Fe, Cr, and Ni, the acid dissolutions resulted in solutions with higher concentrations than those from the aqueous leaches. For elements expected to be present as halides, Na and K, the aqueous leaching results in solutions of higher concentrations than those from the acid digestions. In all cases for which there were high concentrations of Na and K, the [Cl^-] content was always adequate to account for the Na and K concentrations from the aqueous leach (assuming an alkali to halide ratio of 1:1).

Ion Chromatography of Aqueous Leach Solutions

Ion chromatographic analyses were performed only on the aqueous leach samples (Table 4). It was not possible to identify the anions of interest in the complexed dissolution samples because the high ionic strength of the solutions (12 M in NO_3^-) required that the samples be diluted to levels that resulted in [F^-] and [Cl^-] below the detection limit of the analytical method (and the fact that the digestion solutions contained [F^-], one of the anions of interest).

All of the IC samples had nitrate concentrations below 1100 ppm, and all but three, R601285, H002088, and H002573, had levels below 900 ppm. These low values are indicative of the processing of these materials. These materials were calcined in air, at either 750°C or 950°C, for at least two hours or until the mass loss during heating was less than 0.5 percent.[1] Under these conditions, essentially all the nitrate salts present in these materials would most likely be converted to oxides. The few instances in which the nitrate concentration approached 0.1 wt percent (1000 ppm) are most likely a result of a single factor, contamination, that occurred either during the aqueous leach process or while the solutions were handled subsequent to the leaching activities.

The generally low levels of phosphate are to be expected as well. The chemical processes associated with the 3013 materials, both at the production facilities where they were initially packaged and SRS, do not generally involve phosphates, so the low levels observed for the majority of the samples (less than 1000 ppm) are expected. For the few cases where the phosphate con-

Table 5. ICP-ES cation results from aqueous leach

Cation Concentrations/($\mu g/g_{sample}$)													
Sample	Ag	Al	Ba	Be	Ca	Cd	Cr	Fe	K	Mg	Na	Ni	Pb
R600885	< 10.6	< 11.3	6.1	< 0.1	265	< 1.4	13.4	< 3.1	< 53.2	13	< 56.5	14	< 9.2
R601722	< 11.3	24.7	<1.3	12.9	114.6	<1.1	< 2.3	< 3.3	128.5	153.0	403.5	76.2	< 9.7
R601957	< 3.6	< 12.7	3.5	< 0.14	227	< 1.0	< 1.3	< 2.0	< 59.9	33.6	59.3	38.8	< 10.3
R600719	<3.4	<12	<0.74	0.6	22.7	<13.4	<13.5	<13.8	<37.4	18.7	164.5	19.1	<17.2
R610735	28.4	ND	5.4	1.3	428	<3.8	17	<8.5	76200	7160	47400	584	<25.3
R610697	< 25.7	ND	< 1.63	< 0.30	< 31.1	< 3.23	6.7	< 7.46	60900	5180	37100	30.4	< 22.1
R601285	< 31.2	< 42.7	< 2.0	< 0.8	< 32.1	< 4	< 3.4	< 9.1	< 156	< 31.7	376.5	21.9	< 26.9
R602731	<1.23	ND	<0.668	0.2335	4.285	<0.795	<0.878	<1.36	<51.6	1.965	12.4	10.9	<4.52
R601318	36.25	ND	0.9955	0.0771	253.5	<0.845	<0.934	<1.44	<54.8	90.4	48.7	20.8	<5.00
H000898	<1.09	ND	<1.04	<0.065	462.5	<1.48	<0.907	<1.34	<53.2	53.6	46.25	18.55	<4.86
R610327	<0.723	ND	<0.687	50.35	322.5	<0.543	<0.600	<0.926	77.45	22.1	51.3	54.8	<3.22
R610298	2.385	ND	2.62	0.236	467.5	<1.38	<1.73	<2.35	49650	2045	30400	1995	43.95
R610324	<1.81	ND	<1.72	<0.0474	<2.33	<1.36	26.75	<2.32	41150	3150	24800	8.83	<8.07
H001992	3.47	ND	<1.16	8.37	109.5	<1.38	8.29	<2.35	640.5	767	3060	8.63	<8.17
H003157	<1.56	ND	<0.985	<0.0930	71.75	<1.17	<1.37	<2.00	<76.0	25.7	47.45	207.5	<6.94
R610584	<1.45	ND	4.815	46.15	1265	<1.09	<1.20	<1.86	137.5	106	204	65.9	<6.45
R610578	<3.78	ND	7.885	<0.300	19200	<2.84	92.3	<4.85	4675	304	2820	9.065	<16.8
H001916	<1.53	ND	<1.46	<0.0916	8.065	<1.15	254	<1.97	<74.9	294	2780	<14.1	<6.83
H002088	<1.45	ND	<0.690	<0.433	30.1	<0.698	<0.603	4.5	<35.4	22.95	90.35	42.7	<3.23
H003409	<1.45	ND	<0.916	<0.865	175	<0.379	24.6	<1.38	26099.5	1670	15300	<13.3	<6.45
H002573	<12.5	ND	<0.954	<3.79	2.545	<1.45	27.6	<1.44	33300	1510	20050	<13.9	<6.72
H002534	<5.95	ND	<0.924	<1.21	73.45	<1.10	17.3	<1.60	33850	1830	19050	<13.4	<6.40
R610679	<3.03	ND	5.52	3.505	211	<0.624	<1.79	<0.429	<52.4	30.75	44.65	184.5	<6.32
H002750	<1.68	ND	0.719	<0.928	41.05	<12.1	1610	<0.704	8270	151.5	2090	<121	<6.32
H004099	<1.74	ND	<0.655	<0.937	248.95	<0.463	16.2	<0.443	71.75	277.5	135.5	<8.13	<6.53
H004111	<1.67	ND	<0.629	<0.0920	499.5	<0.347	169	<0.425	30150	840	18100	519	<6.27
H002554	<1.67	ND	<1.20	<0.900	4.29	<0.444	31.65	<0.425	35900	1460	20900	<7.80	<6.27
H001941	<12.2	ND	<0.312	59.8	14.1	<0.629	48.5	<1.29	1300	46.8	4735	98.75	<6.37

centrations might be above this level by IC (see Table 4), it should be noted that these results are related to "less than values" above 1000 ppm, so the high value is just an upper limit of the concentration and ought not be taken as a measured value due to the high detection limit associate with these measurements.

The generally low levels of sulfate are to be expected as well. The chemical processes associated with the 3013 materials, both at the production facilities where they were initially packaged and SRS, do not generally involve sulfates, so the low levels observed for the majority of the samples (less than 1000 ppm) are expected. For the few cases where levels above this value were detected, R610584 (1410 ppm), R610578 (4380 ppm), and H001941 (5100 ppm), the carbon-sulfur analyses of these three materials showed sulfur contents of 650 ppm, 1700 ppm, and 5100 ppm, respectively, indicating that the sulfate was probably present in the as-received material. It is likely that any differences between the IC and carbon-sulfur values for sulfur are related to sample heterogeneity.

The remaining two anions, [F^-] and [Cl^-], are often present in these materials because of the utilization of halide salts in the high temperature processing of these materials.[2] The [F^-] in two samples, H001941 (6220 ppm) and H001992 (3650 ppm), were above 1000 ppm; for these two samples [F^-] was the most abundant anion detected. The alkali metal contents of these two samples (as based on the ICP-ES results) are more than adequate to account for this much fluoride. In addition, the pre-surveillance prompt γ results (Table 7) for these two samples indicate that there should be considerable fluorine present. It is not surprising

Table 6. ICP-ES cation results from complexed dissolution

Cation Concentrations/($\mu g/g_{sample}$)													
Sample	Ag	Al	Ba	Be	Ca	Cd	Cr	Fe	K	Mg	Na	Ni	Pb
R600885	<0.163	<0.652	<163	<12.2	779	<163	170	1120	<706	<163	<326	804	<85.2
R601722	<318	<636	<159	<159	1179.5	<159	<159	1095	<689	399	958	2180	<83.1
R601957	<164	<328	<164	<12.3	576.5	<164	<164	<492	<711	<164	343.5	627.5	<164
R600719	<163	<326	<55.0	<163	<163	<163	<163	953.5	<542	<163	<542	969.5	<163
R610735	<159	<1.59e3	<159	2010	621.5	<159	921.5	3755	72550	17600	46050	9000	<159
R610697	<198	<2015	<54.7	<5.22	<163	<96.2	707.5	948.5	44400	11000	27900	9660	<111
R601285	<164	<684	<55.4	<164	<165	<97.4	<328	781.5	<545	<16.4	443.5	575	<164
R602731	<22.8	<66.8	<18.0	<11.3	<16.1	<18.2	<15.8	299	<925	<7.00	<85.7	345	<84.4
R601318	<240	2440	<18.4	<48.5	5170	<18.6	<160	2490	<943	1260	<87.3	911	<86.0
H000898	<191	2900	<17.9	<47.3	13300	<18.1	<312	3590	<919	3380	<312	1080	<83.9
R610327	<780	<780	<156	10000	4680	<18.1	446	7420	<1500	462	<690	1210	<156
R610298	<159	<1590	<12.1	<159	544	<14.4	769	4330	40800	8890	26000	5850	717
R610324	<322	<1720	<12.3	<11.6	154	<18.7	245	765	41600	8820	26600	8080	<86.6
H001992	<166	3590	<166	<166	6330	<166	439	12500	1530	27900	10500	11000	<332
H003157	<178	<2810	<178	<178	218	<178	<178	2160	<255	<356	368	2160	<178
R610584	<19.9	2670	<165	3480	12900	<165	418	6710	<972	2580	946	1050	<825
R610578	<180	<900	<180	1830	45000	<20.9	461	3580	3610	5480	3480	4300	<180
H001916	<1708	23500	62.3	49.2	2050	<170	4110	23600	1610	26300	25700	4950	<170
H002088	<167	<334	<167	<167	232	<8.61	<163	590	<239	<167	311	415	<167
H003409	<165	<330	<165	<16.5	815	<16.5	144	1020	29900	6940	18200	1930	<86.2
H002573	<168	<1260	<12.8	<50.9	137	<19.5	39.4	1230	28600	4380	18400	4300	<90.3
H002534	<78,5	<1570	<12.0	<15.7	381	<14.3	1090	5980	29900	7920	17900	17600	<84.4
R610679	<330	<3300	<165	<165	10200	<8.50	676	3030	<715	776	<629	3190	<86.2
H002750	<161	11000	106	195	1520	<161	2890	11800	9780	3710	8360	8280	119
H004099	<165	<825	<320	<12.4	1230	<165	802	7600	<715	4220	<330	2660	<165
H004111	<163	<326	<163	<163	1220	<163	1070	1950	26800	6060	17100	8840	<85.2
H002554	<159	<398	<159	<11.9	<159	<159	1210	4030	34400	6660	20700	15900	<83.1
H001941	52	5940	<163	111	2040	<163	280	546	2790	1330	7680	9490	1690

that the IC results for fluoride show concentrations lower than might be expected (Table 4). The primary reason for the low-biased [F^-] is related not to the analytical technique, but to the generally low solubility of fluoride salts, especially the alkaline earth salts, as compared to the chloride analogues.

Numerous samples—R610735, R610697, R610298, R610324, R610578, H003409, H002573, H002534, H002750, H004111, and H002554 exhibited high [Cl^-]. In each of these cases, the prompt γ data from the PSDR and the cation results from the ICP-ES analyses supported the high [Cl^-] result. It should be noted that the IC aqueous leaching results for [Cl^-] are more reliable than those for [F^-]. In general, the solubility of fluoride salts of alkali and alkaline earth metals (especially those in the upper half of the family) tend to be less soluble than the corresponding [Cl^-] salts because the fluoride ion has a greater charge density; therefore, the fraction of the fluoride sample dissolved during the leaching process is lower than that for the chloride salts.

ICP-MS and Radiochemical Results for Complexed Dissolution Samples

All of the complexed dissolution samples were subjected to both radiochemical analyses (alpha and gamma spectroscopy) and ICP-MS. In general, it is expected that the radiochemical analyses (with uncertainties of +10 percent in the resulting values) give superior results for Pu because of the high specific activities of the Pu isotopes, while the ICP MS method (with uncertainties of

Table 7. Pu concentrations from ICP-MS, radiochemical analyses (γ and α scans) of complexed dissolution products, and PSDR; ^{241}Am concentrations from radiochemical analyses (γ and α scans) of complexed dissolution products and PSDR

Sample	[Pu]/(wt percent)			Pu Isotopic Fractions/(isotopic percent)					[^{241}Am]/(wt percent)	
				^{238}Pu	^{239}Pu	^{240}Pu		^{241}Pu		
	ICP-MS	γ and α scan	PSDR	γ scan	γ scan	γ scan	PSDR	γ scan	γ scan	PSDR
R600885	57.68	57.20	86.42	0.01	93.80	6.07	5.92	0.13	0.18	0.16
R601722[1]	59.53	66.51	84.05	0.01	93.70	6.12	5.75	0.12	0.17	0.16
R601957	55.18	67.98	87.48	0.01	94.40	5.43	5.74	0.12	0.15	0.13
R600719[2]	56.24	79.52	84.93	0.01	94.50	5.31	5.68	0.13	0.14	0.16
R610735	47.06	50.19	53.35	0.01	93.30	6.56	6.05	0.09	0.11	0.11
R610697	68.27	77.93	69.76	0.01	94.10	5.83	6.04	0.08	0.10	0.09
R601285	84.97	86.43	85.84	0.02	94.10	5.72	6.10	0.14	0.22	0.18
R602731[3]	73.17	65.08	55.86	0.01	93.90	5.94	5.68	0.10	0.21	0.09
R601318	72.69	84.11	83.46	0.01	93.70	6.15	5.56	0.12	0.18	0.16
H000898	71.96	79.73	77.52	0.01	93.80	6.02	6.05	0.12	0.20	0.17
R610327[4]	11.56	12.71	14.73	0.01	94.30	5.53	6.32	0.10	0.03	0.03
R610298	57.27	58.31	64.71	0.01	93.90	5.97	5.94	0.09	0.12	0.12
R610324	70.44	80.06	71.45	0.01	94.10	5.75	5.89	0.07	0.11	0.10
H001992	45.30	35.97	52.30	0.02	93.00	6.82	6.57	0.12	0.17	0.21
H003157	35.77	67.04	81.06	0.31	75.90	21.40	22.21	0.97	3.68	3.92
R610584	70.98	68.63	71.21	0.01	93.70	6.16	6.60	0.12	0.16	0.14
R610578	42.78	54.44	64.54	0.01	93.70	6.17	5.76	0.11	0.12	0.16
H001916	34.80	32.52	34.07	0.01	94.30	5.58	5.68	0.10	0.09	0.09
H002088	77.27	71.39	81.29	0.53	80.40	16.50	17.47	1.33	5.37	5.46
H003409	67.96	83.69	73.84	0.01	94.30	5.61	5.78	0.07	0.0001	0.12
H002573	72.81	65.18	74.19	0.01	94.50	5.19	5.52	0.06	0.08	0.08
H002534	54.00	78.32	70.40	0.01	94.30	5.66	5.78	0.06	0.10	0.10
R610679[5]	58.68	75.47	59.86	0.01	94.40	5.48	6.03	0.12	0.15	0.14
H002750	65.16	85.28	69.63	0.01	93.80	5.97	6.15	0.15	0.22	0.20
H004099	68.14	83.41	78.60	0.02	93.60	6.11	5.94	0.22	1.00	0.28
H004111	64.44	71.88	71.64	0.01	94.50	5.45	5.74	0.07	0.11	0.11

1 [U]=0.20 percent (93.12 percent ^{235}U)
2 [U]=1.31 percent (93.15 percent ^{235}U)
3 [U]=41.48 percent (92.80 percent ^{235}U)
4 [U]=66.01 percent (93.16 percent ^{235}U)
5 [U]=10.35 percent (93.16 percent ^{235}U)

+20 percent in the resulting values) produced superior results for ^{235}U, which is more difficult to quantify by radiochemical methods due to its low specific activity. Variations of the present results, as compared to the PSDR results, are not surprising since the present results are the result of analyses performed on a small portion of the can contents, and the homogeneity of the samples cannot be verified. In general, the ICP-MS and radiochemical results from the present work were in agreement. There were inconsistencies between the ICP-MS and radiochemical analyses (particularly for samples R600719, H003157, and H002534); however, these discrepancies are random in nature, and they are probably related to sample handling errors, such as contamination, loss of material, and volume measurement errors.

Surface Area Analysis

The surface area of each sample was determined utilizing the Brunauer, Emmett, and Teller (BET) method with nitrogen as the adsorbate. The analyzed materials were taken from the RP

sample from each 3013 container. For each RP sample, two subsamples were analyzed, and the surface area was taken to be the mean of the two values. The results show variation in surface area from a low of 0.21 m^2/g to a high of 2.02 m^2/g.

This wide variation of surface area is probably a reflection of the material properties of the samples. These materials were all calcined prior to being placed in the 3013 containers; however, the calcination temperatures were variable. Some materials were calcined at 750°C, some at 950°C, and two at undocumented temperatures. In addition, these materials are of variable composition, and it is not clear what impact the contaminants have on the measured surface areas. There appears to be little correlation of the observed surface area with any compositional or processing parameter other than calcination temperature, as can be seen on the plot of BET surface area versus calcination temperature (Figure 4). This plot does show surprising behavior of two samples, H003157 and H002088, which exhibit surface areas that are discordant with the rest of the set. The stabilization temperature for H003157 and H002088 are unknown, but the high surface areas suggest they may have been stabilized at a lower temperature than the remaining items. The high surface areas are not the only unique characteristics of these two materials. These two samples (H003157 and H002088) do not have a weapons grade Pu isotopic mixture; they have compositions that suggest they are reactor grade and fuel grade materials, respectively.

Figure 4. Plot of BET surface area versus calcination temperature for selected items

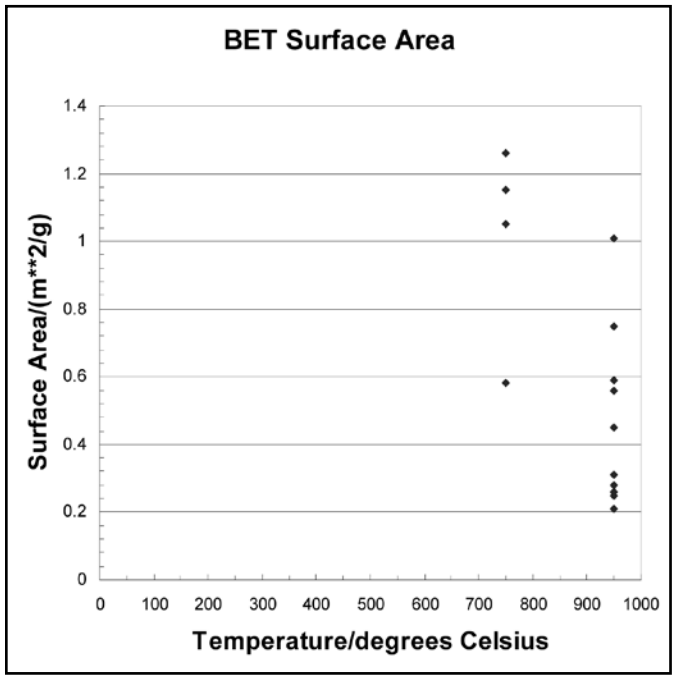

Comparison of Results to Pre-surveillance Data

Upon completion of the surveillance analyses, the experimental results are evaluated as to their reasonability. The most logical method of evaluation is to compare the present results to the data collected before the materials were packaged, and to any nondestructive evaluations performed on the packages. Probably the greatest single source of uncertainty in the measurements is sample homogeneity, or lack thereof. A wide range of materials are stored in 3013 containers, ranging from nearly pure PuO_2 to materials that are less than 50 percent PuO_2. Sampling of the mixtures has been performed in an attempt to choose "representative" samples of the stored materials, but it is not possible to determine how representative these samples are of the bulk material. Consequently, it is likely that the pre-surveillance results may be quite different than the present results for no reason other than the samples analyzed were not representative of the bulk materials. With these considerations in mind, an attempt to evaluate the agreement of the pre-surveillance and present measurements is presented.

Actinide Content

The most abundant actinide in the majority of these materials was Pu. In Table 7, the ICP-MS, radiochemistry, and pre-surveillance results for Pu are presented. In general, it appears that the ICP-MS under-estimates the actinide content, as compared to both the radiochemical and pre-surveillance results. This discrepancy is especially obvious in the first four items on the list. The radiochemical and pre-surveillance results appear to be in relatively good agreement for most of the items investigated, with the exception of H003157 and H002088 (as previously discussed in the Results and Discussion section).

One factor that can contribute to low Pu results is the sparingly small solubility of fluorides, specifically PuF_4 (and the related hydrated Pu-F phases). It is difficult to keep Pu in solution in the presence of fluoride. This inability to keep fluorides in solution is the reason why the most successful acid digestion technique applied during this investigation included the addition of H_3BO_3, a fluoride complexant, to the hot dissolver solution. However, even with the addition of the complexant, the presence of other solutes in the solution will reduce the solubility due to the fact that there is a limited amount of solute that can be dissolved in water. In addition, the presence of soluble chlorides will reduce the effectiveness of the complexant for keeping fluorides in solution by competing with the fluoride for the complexing species.

Overall, it appears that the radiochemical techniques utilized for this work produce results for Pu that are in good agreement with the pre-surveillance data with the exception of materials containing concentrations of ^{241}Pu at or above 1 weight percent.

Chemical Composition

Aqueous leaching and acid digestions were performed to produce aqueous solutions that can be used to assist in the determina-

tion of the composition of as-received materials. The resulting solutions were analyzed and the results of the analyses were compared to the pre-surveillance and in-situ non-destructive analysis results. In Table 8 the prompt gamma results for Al, Be, Cl, F, Mg, and Na are presented for comparison with the IC (for F and Cl) and ICP-ES (for Al, Be, Mg, and Na) results. The detection limit for the IC and ICP analyses are in the 100 ppm range, while the prompt gamma detection limit is about 10 times less sensitive; however, in general, the results for Al and Be are in fairly good agreement. The Cl and Na results generally agree to within an order of magnitude, with the prompt gamma values generally higher than the ICP-ES. The results for F and Mg show very poor agreement. This disagreement is due to one significant factor, the generally poor solubility of fluorides, and the specifically poor solubility of MgF_2.

Moisture Content

An in-depth discussion of the moisture results for these materials is addressed in detail elsewhere in this issue;[5] however, some general comments regarding how the TGA-MS moisture measurements performed at Savannah River National Laboratory compare to the prepackaged moisture data are appropriate. The present moisture measurements were performed by monitoring m/z 17 and 18 signals as the sample temperature is increased from ambient temperature to 1,000°C; essentially all of the pre-surveillance values were based on mass-loss measurement of the samples when heated to 1,000°C. The present measurement are, in all but a few instances, lower than the pre-surveillance values: however, it is believed that this discrepancy is most likely a function of the over-estimation of the moisture levels during the pre-surveillance measurements (as any evaporating species, included halide salts, were included in the mass loss attributed to moisture loss).

Conclusions

Twenty-eight samples were received and analyzed at SRNL in support of the 3013 DE Surveillance program. The samples were subjected to a battery of analyses in an attempt to characterize the phase and chemical character of the materials. Characterization techniques included: density determination; dissolution/leaching studies; ICP-MS, ICP-ES, and radiochemical analyses of dissolution products; IC and ICP-ES analyses of aqueous leachates; moisture content determination; surface area determination; and phase and elemental characterization by XRD and SEM, respectively.

The prepackaging treatment regimen was designed to remove liquids and other volatile reactive substances (such as excessive moisture) that might lead to degradation of the 3013 container during the fifty-year design life. The purpose of the present investigation was to perform analyses to characterize the stored materials so that it will be possible to understand materials interactions involving the stored materials and the containers, and how the materials interactions impact the storage conditions. The purpose of the selected analyses was to characterize the chemical and phase composition of the stored materials. Radiochemical analyses used in tandem with ICP-MS provide a reliable approach to determining actinide content in these materials. The measured density of each item is in reasonable agreement with the density that is calculated from the linear combination of the "theoretical densities" of PuO_2 and NaCl or KCl. The digestion method utilized was generally successful for dissolving the actinide-bearing materials, facilitating the use of standard analytical techniques to determine the cation content of these materials; however, for samples containing larger concentrations of halides, PuF_4 sometimes precipitated from the digested samples upon cooling. The precipitation of Pu-bearing phases impacts all of the wet chemistry results as the resulting solution does not provide a faithful representation of the solids (due to the loss of material through precipitation). The utilization of aqueous leaching facilitated the use of IC to determine the most important anion (Cl-) expected to be present in these materials. Knowledge about the chloride content of these materials is important since it is likely that any corrosion of the 3013 containers will be related to the presence of chloride salts. The present results do not provide a reasonable estimate of fluoride content of these materials. These poor results are primarily a result of the low solubility of fluorides in general, as compared to chlorides, and specifically the low solubility of CaF_2 and MgF_2. Development of a technique for digestion of fluoride salts is presently under consideration to remedy this shortcoming.

Glen F. Kessinger is a fellow scientist at Savannah River National Laboratory. He has a Ph.D. in physical chemistry from the University of Kansas and a B.A. in chemistry from the University of Northern Colorado.

Philip M. Almond is a senior scientist at Savannah River National Laboratory. He has a B.S. and a Ph.D. in chemistry from Auburn University.

Nick J. Bridges is a senior scientist at Savannah River National Laboratory. He has a Ph.D. in chemistry from the University of Alabama and a B.S. in chemistry from Tennessee Technological University.

Mike G. Bronikowski is a principal scientist at Savannah River National Laboratory. He has a Ph.D. in chemistry from Purdue University and a B.S. in chemistry from Marquette University.

Mark L. Crowder is a principal engineer at Savannah River National Laboratory. He has a Ph.D. and an M.S. in chemical engineering from Clemson University and a B.S. in chemical engineering from Rose-Hulman Institute of Technology.

Jonathan M. Duffey is a principal scientist at Savannah River National Laboratory. He has a Ph.D. and M.S. in inorganic chemistry from the University of Tennessee and a B.S. in chemistry from Union University.

Art R. Jurgensen is an advisory scientist (retired) at Savannah River National Laboratory. He has a Ph.D. and a B.S. in chemistry from the University of Florida.

Ronald R. Livingston is a continuous improvement expert at Savannah River Nuclear Solutions. He has a B.S. in chemistry from Augusta College.

Acknowledgements

This work was performed at the Savannah River Site and Savannah River National Laboratory. Savannah River National Laboratory is operated by Savannah River Nuclear Solutions for the U.S. Department of Energy under contract DE-AC09-08SR22470.

References

1. *Stabilization, Packaging, and Storage of Plutonium-bearing Materials.* 2004. DOE-STD-3013-2004. U.S. Department of Energy: Washington, D.C.
2. Clark, D. L., S. S. Hecker, G. D. Jarvinen, and M. P. Neu. 2006. *Chapter 7 – Plutonium in Volume 2, The Chemistry of the Actinide and Transactinide Elements,* Third Edition. L. R. Morse, N. M. Edelstein, and J. Fuger, editors. Springer, Dordrecht, The Netherlands, p. 865.
3. Hussain, N., K. A Shahid, I. H. Khan, and S. Raman. 2005. Oxidation of High-temperature Alloys (superalloys) at Elevated Temperatures in Air: I. *Oxidation of Metals,* 41(3&4), p.251.
4. Tallent, O. K. 1976. *Method for Dissolving Plutonium Dioxide.* United States, The United States of America as represented by the United States Energy patent # 3976775.
5. Berg, J. M., M. L. Crowder, and P. M. Almond. 2010. Relationship between Reported, As-Packaged Moisture and Moisture Measurements Made during Surveillance of 3013 Containers, *Journal of Nuclear Materials Management* Vol. 38, No. 3.

Evaluation of Plutonium Oxide Destructive Chemical Analyses for Validity of Original 3013 Container Binning

James W. McClard
Savannah River Nuclear Solutions, Aiken, South Carolina USA

Glen F. Kessinger
Savannah River National Laboratory, Aiken, South Carolina USA

Abstract

The surveillance program for 3013 containers is based, in part, on the separation of containers into various bins related to potential container failure mechanisms. The containers are assigned to bins based on moisture content and pre-storage estimates of content chemistry. While moisture content is measured during the packaging of each container, chemistry estimates are made by using a combination of process knowledge, packaging data and prompt gamma analyses to establish the moisture and chloride/fluoride content of the materials. Packages with high moisture and chloride/fluoride contents receive more detailed surveillances than packages with less chloride/fluoride and/or moisture. Moisture verification measurements and chemical analyses performed during the surveillance program provided an opportunity to validate the binning process. Validation results demonstrated that the binning effort was generally successful in placing the containers in the appropriate bin for surveillance and analysis.

Introduction

The termination of nuclear weapons production activities in the early 1990s left large quantities of surplus plutonium-bearing materials within the U.S. Department of Energy (DOE) complex. Some of the plutonium was in various stages of the manufacturing process, and the remainder was material in storage awaiting use or plutonium recovery. A DOE Technical Standard, DOE-STD-3013,[1] was developed to specify the long-term requirements for storage of these materials for a period of time that could be as long as fifty years. The 3013 standard specifies stabilization, packaging and surveillance requirements to assure that these plutonium-bearing materials can be safely stored until final disposition. Because of the large number of containers that are to be stored, a statistically-based surveillance program was implemented to assure safety, while minimizing the risks and costs associated with storage and surveillance activities. The surveillance program included the "binning" of various 3013 packages according to the chemistry of the plutonium bearing materials stored in the package. The package chemistry used for binning process was based on the best available knowledge of the impurity composition. However, the surveillance activities included chemical analyses of the contents of selected packages and thus provided an opportunity to determine the validity of the package binning process. The validity determination is the subject of this paper.

Background

The Plutonium-bearing Materials

At the beginning of the stabilization and packaging effort, there was a broad range of plutonium-bearing materials that required stabilization and packaging prior to long-term storage. These materials exhibited a wide range of chemical characteristics. At one compositional extreme was pure plutonium metal that was in the process of being manufactured into weapons components; at the other compositional extreme was a variety of impure scrap materials from processing and experimental programs that had been stored in vaults for decades awaiting plutonium recovery. In some cases, the only information available on the scrap material was the quantity of nuclear material present and the site of origin, which could be a DOE or commercial nuclear site involved in processing or research and development. In other cases, there are varying levels of "process knowledge" that describe how the material was generated and what possible impurities might be present. Chemical compositions of the material were very rarely available. However, the anticipated behavior of the package during storage depends on the chemistry of the plutonium bearing materials. The potential for corrosion depends on the presence of moisture, chloride salts and other materials variables as does the potential for pressure generation inside the sealed packages. Furthermore, the surveillance requirements for packages will vary with the potential for corrosion and/or pressurization. Therefore, process knowledge, site origin and other material information were used to evaluate the material chemistry and bin the various packages according to the estimated potential for corrosion and/or pressurization during long-term storage.

The Standard

The 3013 Standard took a one-size-fits-all approach. The Standard specifies robust stabilization and packaging requirements

that, based on the best available knowledge, are adequate for the highest risk material to be safely packaged and stored. This approach resulted in very robust stabilization and packaging requirements while eliminating the huge costs associated with analyzing and characterizing the chemistry of each of the thousands of containers of material prior to packaging. There was no experience storing such a wide variety of plutonium-bearing materials for up to fifty years in welded containers, so to bridge this experience gap, the 3013 Standard requires a surveillance program for the stored 3013 containers. The Standard encourages the use of a statistical selection approach so that a high level of confidence can be obtained while minimizing the risks and costs associated with surveillance activities. The statistical approach being used by the surveillance program is discussed in detail in Reference 2.

Binning by Failure Mode

The 3013 containers are welded, corrosion resistant stainless steel vessels. The outer container is a qualified pressure vessel with a design pressure of 4920 kPa (699 psig).[1] Only two credible failure mechanisms have been identified for these containers: corrosion or over-pressurization. To set up an effective statistically based surveillance program, the inventory of 3013 containers was split into three population groups or bins. The first bin is the Innocuous Bin (I), which includes items that are believed to present a minimum likelihood of container failure. The I Bin containers are those whose contents are plutonium metal and high purity plutonium oxide with minimum adsorbed moisture. The second bin is the Pressure Bin (P), which include containers that have the potential for gas generation with associated container pressurization. The P Bin containers are those whose contents are impure oxides with no chloride or fluoride content, as well as pure oxide containers whose moisture content are above a specified low threshold (but still below the maximum 0.5 wt % specified by the 3013 Standard). The third bin is the Pressure and Corrosion Bin (P&C), which includes containers believed to have the potential for both corrosion of the stainless steel container as well as gas generation and the associated container pressurization. The P&C Bin containers are those whose contents include chloride- and/or fluoride-contaminated plutonium oxides.

The data necessary to assign the containers to the appropriate bins are: plutonium oxide purity, moisture content, chloride content, and fluoride content. Actinide content is measured for each of the containers to establish the amount of special nuclear materials (in this case U, Np, Pu, and Am) in each container. Since the mass of the oxide is known, the purity of the plutonium (wt % Pu) can be calculated for each container. The 3013 Standard requires that measurements be made to assure that the moisture content of each 3013 container is below 0.5 wt %. Because of the uncertainties associated with measuring moisture content, a conservative moisture content is assigned to each container. Since the content of each 3013 container was not sampled and analyzed for chloride and fluoride content, Prompt Gamma (PG)[3] analyses were performed on the impure oxide containers after packaging. This nondestructive technique can be utilized to detect chloride and fluoride content in the 3013 containers; however, the minimum detection limit for chloride (approximately 8000 ppm) is above the concentration that could potentially cause corrosion. The method is more sensitive for fluoride determination as the PG detection limit for fluoride is approximately 900 ppm. For these reasons, PG is used in combination with process knowledge to identify whether chloride and/or fluoride may be present in the container. The most recent binning results are documented in Reference 4.

The surveillance approaches for the three bins are different. Pressurization can be detected during non-destructive examination (NDE) by radiographing the inner container and measuring lid deflection. Internal corrosion can only be detected by performing destructive examination (DE). For this reason, NDE is appropriate for I and P Bin containers while DE is necessary for characterization of items from the P&C Bin. DE was also performed on a sampling of containers from the P Bin as a method to baseline the NDE process.

A conservative approach was taken during the binning process.[2] Since the most extensive examination is performed on containers in the P&C Bin, if either process history information or PG analysis indicated that chloride or high fluoride content may be present, the container was placed in the P&C Bin. Likewise, only containers with the purest oxide and lowest moisture content were placed in the I Bin. The binning of containers is routinely re-evaluated as additional containers are generated and based on results from surveillances that may affect the binning of specific containers.

Destructive Examination

A portion of the destructive examination program involves sampling the contents of the 3013 packages to characterize the chemical composition of the stored materials. Specific protocols were developed for sampling and analysis of the can contents.

Sampling

The 3013 packages were opened in a glovebox at the Savannah River Site (SRS) K Area Material Storage Facility. An initial solid sample was taken immediately after opening each convenience can (the inner-most container in the 3013 package). This sample, referred to as the initial moisture (IM) sample, was immediately placed in an air-tight stainless steel ampoule (B-vial) and was subsequently analyzed by thermogravimetric analysis -mass spectrometry (TGA-MS) to determine the moisture content of the material (which is assumed to be representative of the condition of the solid when it was in the 3013 package). This analysis produces two results, the total mass loss from TGA as the sample is heated from ambient temperature to 1,000°C, and the fraction of the mass loss that is due to moisture as determined from the

Table 1. Characteristics of DE samples

Sample	Actinide Content/ (wt%)	Bin	Baseline Moisture (wt%)	Baseline Moisture Method	DE TGA Mass Loss (wt%)	DE TGA-MS Moisture (wt%)	Cl Concentration (ppm)			F Concentration (ppm)		
							Baseline PG	Surveillance PG	Surveillance IC*	Baseline PG	Surveillance PG	Surveillance IC*
R600885	86.4	P	0.11	LOI	0.04	0.05	ND	ND	118	ND	ND	555
R601722	84.3	P	0.18	LOI	0.16	0.04	ND	ND	355	2800	2700	498
R601318	83.6	P	0.17	LOI	0.08	0.02	ND	ND	<465	7100	6700	<465
H002088	86.7	P	0.22	TGA	0.23	0.23	ND	ND	150	ND	ND	<150
H003119	70.8	P	0.18	TGA	0.41	0.09	ND	34000	37500	5100	1300	230
H001916	34.3	P	0.06	TGA	0.06	0.06	ND	ND	301	3800	3200	<175
R601957	87.5	P&C	0.03	LOI	0.03	0.04	ND	ND	<500	ND	ND	<500
R600719	86.2	P&C	0.10	LOI	0.03	0.04	ND	ND	<500	ND	ND	<500
R610735	53.4	P&C	0.24	FTIR	4.10	0.19	85000	84000	168000	ND	500	166
R610697	69.8	P&C	0.12	FTIR	0.44	0.06	91000	85000	105000	ND	ND	<600
R601285	85.8	P&C	0.15	LOI	0.06	0.10	5000	ND	316	ND	ND	<600
R602731	97.4	P&C	0.07	LOI	0.10	0.03	ND	ND	<438	ND	ND	<438
H000898	77.7	P&C	0.14	TGA	0.19	0.04	ND	ND	<451	10000	4200	393
R610327	80.8	P&C	0.39	TGA	1.31	0.04	No Data	ND	518	No Data	ND	339
R610298	64.8	P&C	0.16	TGA	0.20	0.14	91000	82000	98000	ND	300	<303
R610324	71.6	P&C	0.07	TGA	0.17	0.10	100000	80000	76000	ND	ND	<300
H001992	52.3	P&C	0.37	TGA	0.27	0.05	ND	ND	322	17000	23000	3650
H003157	85.0	P&C	0.19	TGA	0.21	0.10	ND	ND	<161	10900	ND	<161
R610584	71.4	P&C	0.15	FTIR	1.05	0.07	ND	ND	1860	7600	7400	361
R610578	64.7	P&C	0.04	TGA	0.19	0.19	53000	50000	41000	12000	10000	<157
H003409	74.0	P&C	0.29	TGA	0.49	0.29	68000	62000	52000	ND	800	<150
H002573	74.3	P&C	0.37	TGA	0.56	0.33	74000	57000	67000	ND	ND	<157
H002534	70.5	P&C	0.35	TGA	0.55	0.19	73000	63000	64000	ND	ND	<152
R610679	70.4	P&C	0.26	TGA	0.30	0.03	ND	ND	<151	8200	7600	300
H002750	69.6	P&C	0.07	TGA	0.16	0.07	3800	ND	1720	1600	1300	814
H004099	78.9	P&C	0.23	TGA	0.09	0.03	58000	ND	<157	ND	2800	<157
H004111	71.8	P&C	0.40	TGA	0.55	0.26	85000	63000	58100	ND	ND	<150
H002554	70.6	P&C	0.32	TGA	0.37	0.22	81000	60000	65600	ND	ND	<151
H001941	60.1	P&C	0.06	TGA	0.17	0.02	ND	ND	516	6000	6600	6220
R602498	81.6	P&C	0.26	LOI	0.17	0.13	20000	12000	7450	ND	ND	150
H002509	70.7	P&C	0.39	TGA	0.65	0.26	62000	64000	58400	ND	ND	<151
H002565	70.1	P&C	0.39	TGA	0.38	0.25	93000	69000	75500	ND	800	<150
H002657	77.4	P&C	0.23	TGA	0.28	0.22	13000	33000	29400	ND	ND	<150
R611398	70.8	P&C	0.29	FTIR	0.02	0.02	ND	ND	151	4700	5000	151
H002200	71.1	P&C	0.22	TGA	0.33	0.03	ND	ND	151	21000	20000	1060
H002667	72.4	P&C	0.23	TGA	0.46	0.19	90000	64000	72500	ND	ND	<150
H002715	70.3	P&C	0.38	TGA	0.68	0.28	87000	68000	77600	ND	ND	<151
R610700	65.4	P&C	0.23	TGA	0.37	0.03	ND	ND	<150	10000	8800	160
R610764	62.6	P&C	0.06	TGA	0.28	0.05	61000	54000	74000	ND	ND	<618
R610573	63.5	P&C	0.25	TGA	0.63	0.22	46000	50000	34200	3400	28000	150
R610558	87.9	P&C	0.04	TGA	0.05	0.01	ND	ND	<151	9600	8600	<151
R610806	76.7	P&C	0.28	TGA	0.75	0.27	39000	30000	20300	9300	7500	<151
H002195	84.2	P&C	0.11	TGA	0.15	0.01	20000	ND	<151	ND	ND	<151

* *IC results are from ion chromatography of aqueous leach solution from the sample. Only water soluble species are detected.*

MS data. These results can subsequently be compared to the baseline result reported by the packaging site.

The remaining solid was then removed from the convenience can and poured into a rectangular tray and spread out to cover the entire surface of the tray; an aliquot was taken from each of four quadrants of the tray, and the four aliquots were combined to make a single sample. It was from this sample that a sub-sample (hereafter referenced as the representative or "RP" sample) was selected. The RP sample is loaded into a uniquely-numbered B-vial and transferred to Savannah River National Laboratory (SRNL) for analysis. While the material was in the tray, it was visually inspected. If there were items present in the tray that were unique, such as pieces of oddly colored or shaped material, some portion of the unique material, referred to as the, "if required" (IR) sample, was collected and loaded into a uniquely numbered B-vial and sent to SRNL for analysis.

Moisture Measurement

A three gram (nominally) sample is removed from the sealed ampoule, placed in a high-fired alumina crucible, and introduced to the TGA-MS. After purging the sample furnace with high purity Ar gas (a carrier gas), for approximately 10 minutes, the crucible and sample are heated from room temperature to 1,000°C at a rate of 15°C per minute. The mass loss is continuously measured as a function of time and temperature. The gas generated is sent through the MS and m/z 17 and 18 signals are measured as a function of temperature. These results, along with calibration data collected on samples of known moisture content, allow the use of the MS data to quantify the amount of water lost by the sample, which is assumed to be the moisture content of the sample.

Chloride and Fluoride Content Measurement

The PG analyses of the packaged materials provide an estimate for the fluoride and chloride contents of the solids in the package. To characterize the water-soluble chloride and fluoride content of the solids, aqueous leaching at 90°C for 3 hours was utilized to solublize the water-soluble fraction of the sample. Two aliquots of 1-gram each of the RP sample were leached in de-ionized water. Each sample to be leached was transferred to a flat-bottomed, screw lid 60-mL polypropylene reaction tube. Each tube was placed in a thermostated hot block heater capable of containing six reaction tubes. During each run, the hot block contained the two reaction tubes, a blank, and a "dummy" tube containing water into which a thermocouple was inserted (for an independent temperature measurement to which the thermostated hot block controller could be compared). A small watch glass (filled with water to condense the water vapor evaporating from the solution) was placed over the lid of the tube, and the temperature was ramped up to ~90°C over a period of 60 to 90 minutes. After temperature stabilization, the temperature was held constant for 3 hours. After the hot block had returned to ambient temperature, the volume of each leaching tube was checked and the solution volumes were adjusted, as necessary, to 30 mL using deionized water. The solid-solution mixtures were filtered through a 0.45 µm filter in 10 mL increments, and the resulting solutions were subjected to Ion Chromatography (IC) and Inductively Coupled Plasma-Emission Spectroscopy (ICP-ES) analyses to determine the concentrations of the aqueous species of interest. Since most chloride salts have a high solubility in water, this technique is expected to accurately measure the total chloride content in the sample. But since many fluoride compounds have low solubility in water, these results are expected to under-report the total fluoride content of the sample.

Results and Discussion

Destructive Examinations

Moisture Content

Moisture content is analyzed by TGA-MS. Table 1 shows the moisture results reported by the packaging site and the moisture results from SRNL DE measurements (IM samples). The packaging sites utilized one of four experimental methods to determine moisture contents of the packages material: loss-on-ignition (LOI); TGA; Fourier Transform-Infrared Spectroscopy (FTIR) in tandem with TGA (TGA-FTIR); and TGA-MS. The goal of the packaging site moisture analysis was to assure that 0.5 wt % was not exceeded and as such, some of the recorded values are over-estimates of the actual moisture content. Loss-on-ignition (LOI) and TGA can significantly over-report water content since these techniques report all mass loss as water, while neglecting the fact that some of the chloride salts present in these materials have considerable vapor pressures at 1000°C. Since TGA-FTIR and TGA-MS measure the amount of water driven off of the sample, results using these techniques most accurately reflect the true moisture content of the sample. The SRNL DE analyses utilized TGA-MS to measure the moisture content of the surveillance samples. As shown in Table 1, the packaging site-measured moisture content of each package surveilled falls below 0.5% by mass. As expected, the SRNL moisture values are either the same (within measurement uncertainties) or lower than the values reported by the packaging sites.

Chloride and Fluoride Content

Table 1 summarizes the chloride and fluoride results from SRNL IC analyses. DE results from forty-three containers were available for this review. For forty of the containers, the chloride results are consistent with the baseline PG estimates. For two containers, significant levels of chloride (58,000 ppm and 20,000 ppm) were reported in the baseline PGs but chloride was not detected in either the surveillance PGs or the chemical analyses. For one container, no chloride was reported in the baseline PG, but chloride was detected in both the surveillance PG (34,000 ppm) and chemical analyses (37,500 ppm).

Because of the low solubility of fluorides in water, the fluoride results in general are significantly below those indicated by PG. There were no cases where significant fluoride was found in any P Bin containers.

Summary and Conclusions

The DOE Technical Standard, DOE-STD-3013[1] was developed to specify stabilization, packaging and surveillance requirements to assure that the excess plutonium can be safely stored until final disposition. The standard was written to address storage for a period of time which was assumed to be up to fifty years; however, there was insufficient historical experience available to predict the behavior of these materials in hermetically sealed packages for such a long time interval, so a surveillance program was developed to investigate the behavior of the stored materials, and the material-package interactions. Because of the large number of containers that are to be stored, a statistically-based surveillance program was implemented to assure safety, while minimizing the risks and costs associated with surveillance activities. The data collected during destructive surveillance activities have been compared to the known process history for the oxide in the containers and non-destructive measurements performed on the containers.

DE results for forty-three containers were available for this review. For forty of the containers, the results show that the binning effort successfully assigned the correct surveillance bin. There were three containers that were not assigned to the correct bin. Two containers had been assigned to the P&C Bin, but DE results show that corrosive impurities were not present. One container was assigned to the P Bin, but DE results show the presence of a significant concentration of chloride impurities. In all three of these cases, the PG performed during surveillance

showed chloride and fluoride concentrations that were consistent with the DE sample results. It appears that there was an error in the reported baseline PG for these three containers. The results indicate that if the baseline PG is correct, the containers will be binned appropriately, however, there is the potential for the data packages to include incorrect baseline PGs.

The binning of containers is routinely reassessed and the results from surveillance activities are incorporated in the reassessments. For example, since these surveillances show that the three containers were in the incorrect bin, the containers are no longer valid containers for their former bin samples. As a result, the next re-binning will select additional, replacement containers for the bins. In addition, during the next re-binning, all baseline PGs will be reevaluated for possible errors.

DE of selected P&C Bin containers is currently scheduled to continue through FY2017. The results from the surveillances will be used to establish future surveillance requirements for containers in the P&C Bin. The surveillances of the initial sampling of P Bin and I Bin containers was completed in 2009. Those results are being evaluated to determine what level of surveillance will be needed for those bins in the future to evaluate longer term aging effects in containers that are basically free of chlorides. The results of these determinations will also be applied to new, chloride/fluoride free, P Bin and I Bin containers that are generated during future packaging operations.

James W. McClard is a fellow technical advisor at Savannah River Nuclear Solutions. He has a B.S. in chemical engineering from Clemson University.

Glen F. Kessinger is a fellow scientist at Savannah River National Laboratory. He has a Ph.D. in physical chemistry from the University of Kansas and a B.A. in chemistry from the University of Northern Colorado.

Acknowledgements

This work was performed at the Savannah River Site and Savannah River National Laboratory. Savannah River National Laboratory is operated by Savannah River Nuclear Solutions for the U.S. Department of Energy under contract DE-AC09-08SR22470.

References

1. *Stabilization, Packaging, and Storage of Plutonium-bearing Materials.* 2004. DOE-STD-3013-2004. U.S. Department of Energy: Washington, D.C.
2. Kelly, E. J., L. G. Peppers, L. A. Worl, and J. W. McClard. 2010. Sampling Approach to Validate the Safe Storage of Plutonium-Bearing Materials. *Journal of Nuclear Materials Management* Vol. 38, No. 2.
3. Narlesky, E. J., L. A. Foster, E. J. Kelly, and R. E. Murray. 2009. *A Calibration to Predict the Concentrations of Impurities in Plutonium Oxide by Prompt Gamma Analysis: Revision* 1, Los Alamos National Laboratory, LA-14411.
4. Peppers, L. G., E. J. Kelly, J. W. McClard, G. P. Friday, T. J. Venetz, and J. E. Stakebake. 2009. Selection of 3013 Containers for Field Surveillance: LA-14310, Revision 1, Los Alamos National Laboratory, LA-14395.

Relationship Between Reported, As-Packaged Moisture, and Moisture Measurements Made During Surveillance of 3013 Containers

John M. Berg
Los Alamos National Laboratory, Los Alamos, New Mexico USA

Mark L. Crowder and Philip M. Almond
Savannah River National Laboratory, Aiken, South Carolina USA

Abstract

Criteria for stabilizing plutonium-bearing materials, detailed in DOE-STD-3013-2004,[1] require verification that moisture content is less than 0.5 wt. percent at the time of packaging. This value limits the potential for H_2 gas generation from moisture decomposition to levels that are within the design pressure of the 3013 storage container. Ongoing container surveillance and shelf-life studies have confirmed that plutonium oxide containing salt impurities and moisture can generate H_2 gas inside sealed containers. The observed levels of H_2 inside containers stored for five years have not approached the limiting case of complete conversion of measured moisture to H_2 gas. To understand these observations, the reliability of the reported moisture content is one factor that must be considered. The moisture measuring protocols were inherently biased toward reporting higher than actual moisture content. This was recognized at the time the protocols were selected but was seen as desirable for assuring that reported values were conservative in assuring that packaging criteria were met. Other error sources such as those due to differences in the handling of the moisture analysis sample after removal from the parent batch can also be presumed to bias towards over-estimating the actual moisture content because the greater surface exposure and the relatively smaller ratio of sample mass to moisture in the glovebox atmosphere. Ongoing surveillance of containers in storage at Savannah River Site includes opening multiple containers per year and measuring the moisture on the contained material. In this paper we compare these surveillance data with the reported moisture on the materials in the same containers at the time of packaging. This comparison is used to better understand the errors and biases in both the pre-packaging and the surveillance data.

Introduction

Accepted approaches for the preparation and packaging of plutonium oxide for safe long-term storage in U.S. Department of Energy (DOE) facilities are based in part on the premise that the hydrogen component of any residual moisture in the material could be completely converted to hydrogen gas within the container during storage.[1] To preclude exceeding the design pressure of approved containers, and to minimize the potential for container corrosion, stabilization requirements dictate drying the material and verifying that it contains less than 0.5 wt. percent moisture at the time of packaging.

As part of an ongoing surveillance and monitoring program for 3013 containers stored at DOE facilities, approximately forty containers have now been destructively examined at the DOE Savannah River Site after five or more years of storage. Some H_2 gas has been found inside these containers, though it has not approached the limiting case of complete conversion of reported moisture. Shelf-life study results had led to anticipating the general result that much less than full conversion to H_2 would be observed during surveillance.[2] Shelf-life results have also led to quantitative prediction of H_2 pressure as a function of time, material characteristics, and moisture content. Accurate moisture content information is a critical link in this predictive approach. Moisture content is also important for assessing relative risks of corrosion inside containers. This paper describes the moisture measurements on existing containers after approximately five years of storage, discusses the measurement limitations, and considers whether more accurate estimates could be extracted from the data underlying the original pre-packaging moisture determinations.

The techniques and procedures that were approved to verify post-stabilization moisture content were deliberately chosen to be conservative and robust, at the expense of accuracy. Most packaging activities have used either loss-on-ignition or thermogravimetric analysis to measure moisture. Both techniques measure mass loss by a sample upon heating it to some temperature deemed high enough to volatilize any credible form of moisture in the material. A peak heating temperature of 1,000°C was used in all measurements considered in this paper. The differences between the techniques have to do with whether the sample mass loss is monitored and recorded throughout the heating cycle, as

Figure 1. Plot of sample mass vs. temperature during thermogravimetric analysis of samples from two batches of material prior to packaging. In the upper curve, more than half of the overall mass loss occurs at high temperature and is likely due to volatilization of alkali halide salts. In the lower curve, most of the mass loss occurs over a lower temperature range that is characteristic of moisture loss.

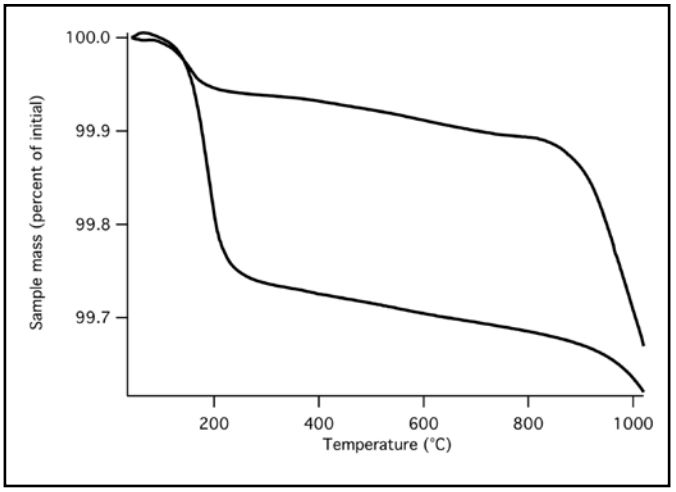

Figure 2. Plot of final vs. initial surveillance sample TGA-MS determinations of moisture. The best-fit line through the data is also shown and has a slope of 1.25. The correlation coefficient is 0.87. The dashed line with a slope of 1.0 and an intercept of 0.0 is included for reference to highlight deviations from equal initial and final measurements.

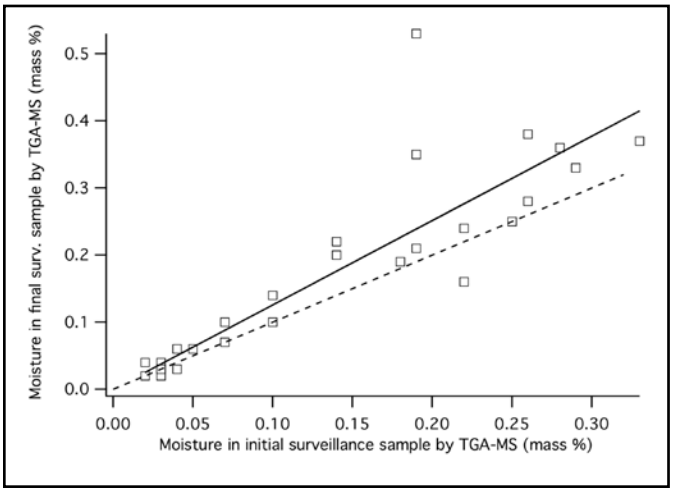

in thermogravimetric analysis (TGA), or only as an overall difference recorded after cool-down as in loss-on-ignition (LOI) measurement. Neither of these techniques directly distinguish between mass loss due to moisture and mass loss due to other volatile constituents or constituents that decompose to volatile products below 1,000°C. If any other components of the material are volatile below 1,000°C, both of these techniques will indicate an apparent moisture content that is higher than the actual moisture content of the sample. Many batches of packaged material contain substantial quantities of NaCl and KCl, both of which have significant vapor pressures at 1,000°C and therefore contribute mass losses that are attributed to moisture.

Where TGA was used, it is possible to examine the raw data in the form of sample mass as a function of temperature and distinguish the NaCl and KCl contribution to the overall mass loss based on the appearance of an accelerating mass loss above 800°C. This mass loss is generally well separated in temperature from the lower temperature mass loss events that are typical of moisture. This phenomenon is evident to different degrees in Figure 1, which shows evidence for high moisture and low salts in the lower curve, and less moisture and more salt in the upper curve.

Though the overall mass loss by TGA heating to 1,000°C was used almost exclusively for officially reported moisture verification, full TGA mass vs. temperature traces such as shown in Figure 1 are available for most packaged material having substantial impurities. We have examined most of these data and catalogued the mass loss up to 650°C as an alternative, probably more accurate measure of the moisture in the each sample. The choice of 650°C is a compromise between improving accuracy over the 1,000°C value and preserving some conservative bias.

The stabilization and packaging campaigns at Rocky Flats, Hanford, and Savannah River Sites measured many samples with alternative moisture measurement instrumentation that augmented TGA with either infrared absorption spectrometry (TGA-FTIR) or mass spectrometry (TGA-MS) interrogation of the volatile fraction as it flowed out of the furnace. The use of these techniques for moisture measurement was tested and validated prior to use.[3] The data from those instruments were collected and stored during packaging campaigns, though the data were usually analyzed to determine moisture content only in cases where the total TGA mass loss for the sample approached 0.5 percent or was somehow problematic. Where available, we have catalogued the sample moisture indicated by those data for comparison with the TGA results.

It must be emphasized that the biases toward reporting higher than actual moisture content due to the use of total TGA mass loss were recognized and viewed as beneficial as long as the goal was simply to assure that packaging criteria were met, and as long as there was a low frequency of measurements appearing to exceed the 0.5 percent limit. The principal potential drawback was that high false failure rates, had they occurred, would have led to increased time and expense in the stabilization and packaging effort. This proved not to be a major problem in packaging campaigns at DOE sites. However, there is now interest in improving the accuracy of moisture content estimates for existing containers in order to better assess the relative risks to long-term safe storage. By focusing on comparisons with the much more extensive data now becoming available as containers are destructively examined in the surveillance program at Savannah River Site, this paper explores how greater moisture accuracy might be obtained from existing pre-packaging data.

Figure 3. Moisture determination by total mass loss on heating of the sample taken before packaging vs. TGA-MS determination of moisture on the initial surveillance sample from the same container.

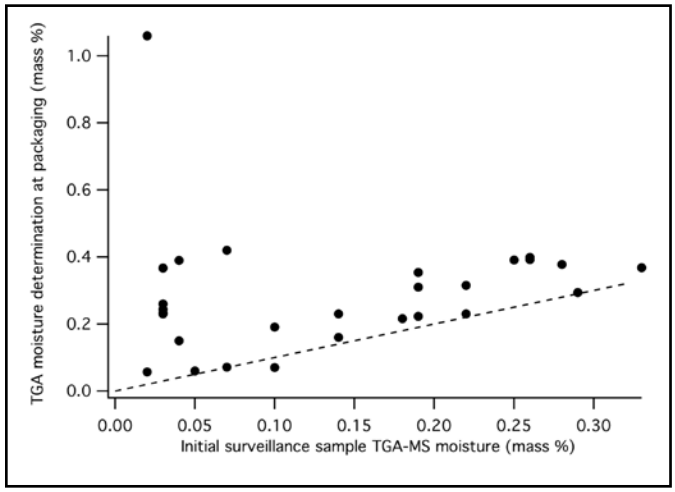

Results and Discussion

Surveillance Data Available for Comparison with Pre-packaging Data

As of this writing, moisture measurements have been made on samples of material from 38 containers that were opened for surveillance after having been in storage for at least five years. We focus on a subset of twenty-eight for which the pre-packaging moisture measurement was made by TGA, TGA-MS, or TGA-FTIR. Immediately prior to packaging, a single sample was collected from the material destined for each 3013 container and measured for moisture by one of the approved techniques. Later, during surveillance activities two samples were collected from each container and analyzed for moisture by TGA-MS. The first sample was collected from the top of the material bed immediately after opening the container, and we refer to this as the initial surveillance sample in the following discussions. The second sample, which we refer to as the final surveillance sample, was collected at the end of the surveillance activities to capture any moisture gain or loss that might have occurred during exposure of the material to ambient air in the surveillance glovebox. Each sample was split and measured twice. The average results for the replicates by TGA-MS are shown in Table 1 along with the total TGA mass loss to 1,000°C from the pre-packaging sample and the TGA mass loss to an intermediate temperature of 650°C for all samples.

Pair-wise Comparisons and Correlations

In this section we compare the results for individual containers obtained from different samples and different data analysis methods in order to highlight broad trends.

There is a reasonably good linear correlation between the TGA-MS determinations of moisture on the initial and final surveillance samples, as seen in Figure 2. The linear fit (solid line) has a correlation coefficient of r=0.87.[4] The fit slope of 1.25 indicates an average tendency for the final sample from each opened container to contain more moisture than the initial sample. A comparison between the data and a line with a slope of 1.0 (dashed line in Figure 2) highlights that there was either insignificant change or a moisture increase in all but one case. The increases are presumably due to absorption from the ambient humidity in the glovebox atmosphere during surveillance-related handling of the material between initial and final sample collection.

The moisture content of the samples collected prior to packaging as determined by total mass loss (LOI or TGA) are poorly correlated with the TGA-MS results on the surveillance samples, with correlation coefficients r=0.12 between packaging and first surveillance sample and r=0.10 between packaging and the second surveillance sample. As discussed above, equating moisture with the total mass loss in the TGA measurement guarantees a bias towards over-estimating moisture. The manifestation of this bias evident in Figure 3, where positive deviations from the dashed 1:1 line show that the TGA almost universally produced higher moisture estimates at the time of packaging than the more accurate TGA-MS on the same material after the container was opened for surveillance. A few containers showed substantial pre-packaging TGA mass loss but little or no appreciable moisture by TGA-MS in the corresponding surveillance samples. This would be expected of material that contained substantial NaCl and KCl but little moisture. The packaging samples outside this sub-population show better correlation with surveillance measurements (r=0.86), though there remains a tendency for the pre packaging TGA to over-estimate the moisture content by an average factor of about 1.4 relative to the TGA-MS of the initial surveillance sample.

The apparent poor accuracy of TGA confirmed by the comparison in Figure 3 does not undermine its use as a conservative measure of moisture to support packaging to meet DOE-STD-3013-2004 requirements. However to assess relative risk of both pressurization and corrosion during storage, it would be useful to have more accurate moisture content estimates. We find that it is possible to obtain significantly better moisture estimates by re-analyzing the raw TGA or TGA-FTIR data from the pre packaging samples to partially or completely exclude signal from other volatile components. Where only TGA data are available, as is the case for twenty-one of the twenty-seven containers considered here, the re-analysis is fairly simple. We extract the mass loss up to 650°C from the full data set and assume that value is a more accurate representation of the true moisture because it excludes all mass loss from KCl and NaCl. Some other volatiles such as CO_2 and NO_x cannot be separated from moisture by this method, but we make that compromise because a lower temperature cut-off would risk excluding some moisture. The utility of this approach in yielding improved sample moisture estimates is evident in Figure 4, which compares the agreement of TGA-MS moisture values with the TGA mass losses up to 650°C and 1,000°C for the initial surveillance samples. The lower-temperature TGA mass losses are clearly in much better

Figure 4. Plot of mass losses to 650 (solid triangles) and 1,000°C (open circles with crosses) versus total moisture determined by TGA-MS in the same initial surveillance samples. The dashed line passes through the origin with a slope of one, representing where data points would fall if the agreement between TGA and TGA-MS was perfect.

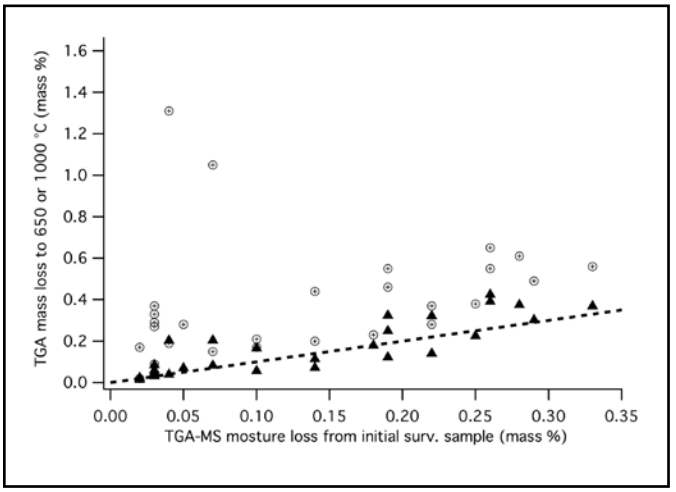

Figure 5. Moisture determination in the packaging samples obtained by re-analyzing TGA data vs. TGA-MS determination of moisture in the initial surveillance sample. The best linear fit under the constraint of passing through the origin is shown as a solid line. For reference, a line with a slope of 1 is also shown (dashed line).

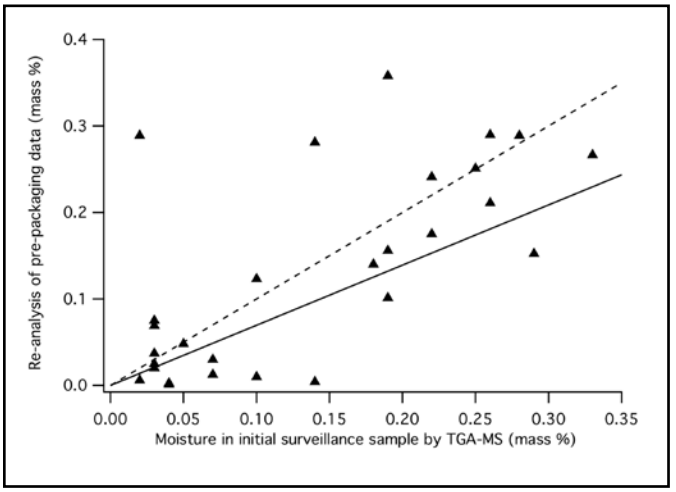

overall agreement with the TGA-MS moisture values and are therefore a source of more accurate moisture estimates than the TGA to 1,000°C. However, it should be noted that the existence of some points below the 1:1 dashed line suggests that, unlike the 1,000°C values, the TGA to 650°C cannot be relied upon to always be a conservative moisture measure.

Where pre-packaging TGA-FTIR data are available, we use the integrated intensity of the moisture-specific FTIR signal as the best pre-packaging moisture estimate. Calibration of this signal using data from Rocky Flats moisture standards is more problematic than calibration of the mass loss. Nonetheless, the overall accuracy of the moisture estimate from the FTIR data should be better than that from the mass loss alone because it excludes contributions from other volatile components across the full measurement temperature range.

The correlation between the re-analyzed pre-packaging data and the TGA-MS results for the initial surveillance samples are shown in Figure 5. The linear correlation coefficient is r=0.69 with a slope of 0.90. The correlation is far from perfect, but overall the residuals are smaller and the slope of the linear fit is closer to 1 than is the case for the comparison to pre-packaging TGA to 1,000°C (Figure 3). Furthermore, the deviations are in both directions indicating that the systematic bias in the pre-packaging results is considerably less than in the original analysis of the data. Notably, most of the poorly correlated sub-population in the upper left quadrant in Figure 3 is in much better agreement in Figure 5.

Though we have already argued that the total mass loss in TGA to 1,000°C is not as accurate as other measures of moisture, it is instructive to compare these measurement results between pairs of samples from individual containers for possible insight into sampling variability. Two such comparisons are shown in Figure 6. The comparison between the results on the initial and final surveillance samples (open circles), if the three outliers on the right are excluded from the fit, shows reasonably good correlation (r=0.95) and a slope of 1.1. The positive slope is probably due to the tendency of the material to absorb moisture from the atmosphere between collection of surveillance samples, as noted in the discussion of Figure 2. The outliers may simply indicate random sampling variability due to material inhomogeneity,

Figure 6. Total mass loss during TGA to 1,000°C by pre-packaging samples (closed triangles) and final surveillance samples (open circles) plotted against the result from the initial surveillance sample from the same container. A dashed line with a slope of 1 is shown as an indicator of where points would fall on the plot if all samples from a container gave the same result.

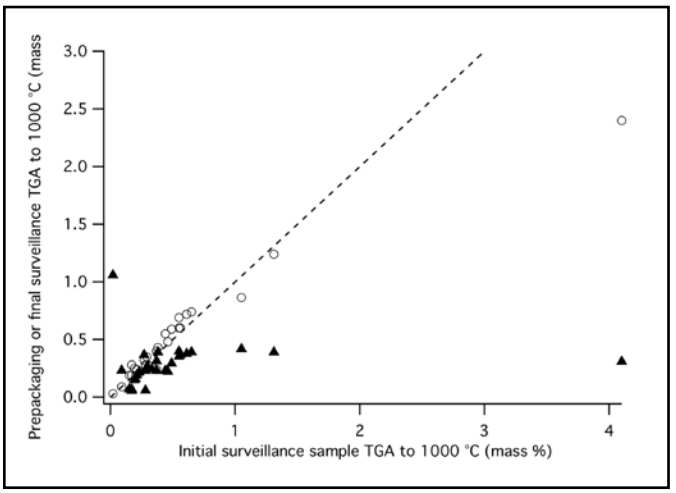

Figure 7. Histogram of mass loss values from pre-packaging TGA analyses conducted at Hanford site from materials stabilized in a dry glovebox atmosphere. The bin populations for mass losses up to 650°C are shown as dark, narrow bars and up to 1,000°C as lighter-shaded, wide bars. Almost all of the samples initially reported to contain more than 0.1 percent moisture using the 1,000°C TGA value showed minimal mass loss below 650°C, indicating minimal true moisture content.

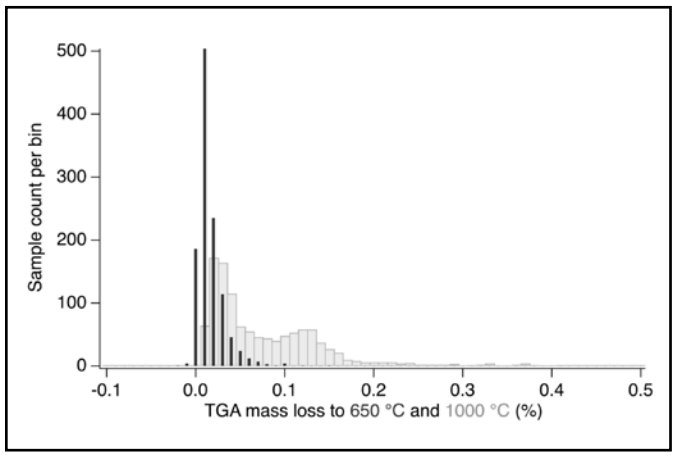

though the fact that the initial sample gave a higher result in all three cases suggests that consistent differences in the manner in which the initial and final surveillance samples are collected may play a role. Whatever the cause, it seems to have much more effect on the non-moisture volatile components than on the moisture determination.

The comparison between the results on the pre-packaging sample and the initial surveillance sample (solid triangles in Figure 6) shows much poorer agreement. The linear correlation coefficient is surprisingly poor (r=0.09), though this is heavily influenced by the four dramatic outlier points. If these are removed the linear correlation coefficient improves substantially (r=0.75), but both the scatter and the deviation from a slope of one remain clearly much greater than in the comparison between the two surveillance samples. There is a notable tendency for the measured mass loss of the surveillance sample to exceed that of the pre-packaging sample from the same container, even if the outliers are ignored. The lack of randomness in the direction of this deviation bears further investigation for what it may reveal about the effects of differences in the sampling or measurement protocols between pre-packaging and surveillance measurements.

Re-analysis of Pre-packaging Data from Other Containers

As mentioned above, raw TGA data and in some cases TGA-MS or TGA-FTIR are available for all pre-packaging samples taken from material with significant impurity content. We had previously examined these data and presented, in preliminary reports, what we believe to be better estimates of true moisture content than the initially reported values.[5] The initially reported values

Figure 8. Histogram of mass loss values from pre-packaging TGA analyses conducted at Hanford site from materials stabilized in a humid glovebox atmosphere. The bin populations for mass losses up to 650°C are shown as dark, narrow bars and up to 1,000°C as lighter-shaded, wide bars.

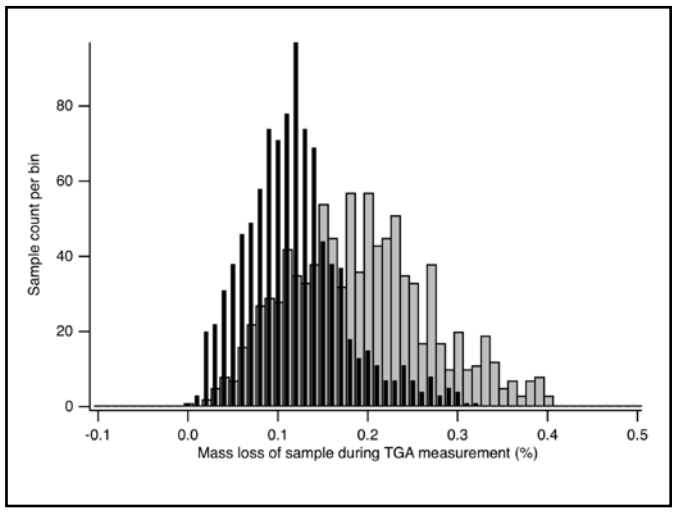

Figure 9. Histograms of TGA and TGA-FTIR determinations of moisture in prepackaging samples taken after material stabilization at Rocky Flats. Shaded bars show the distribution of mass losses measured in TGA analyses to 1000°C. The narrower, darker bars show the moisture released from the samples in the same analyses as determined by integrated water-specific FTIR signal of the released gases.

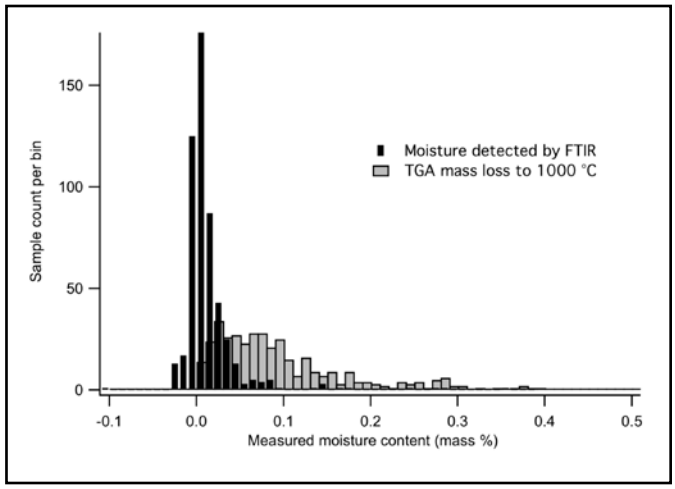

were based on mass loss in the TGA to 1,000°C. Our values are based on mass loss in the TGA to 650°C, or on integration of the FTIR moisture signal in the volatilized fraction. The comparison between the distributions initially reported moisture values and the distributions obtained by re-examining the data are shown in Figures 7 through 9, segregated by the particular glovebox line used for the stabilization and packaging. In all cases, the re-examination of the data produces a distribution of moisture estimates shifted significantly to lower values. The shifts are most

Table 1. Comparison of various moisture content measurements from material in containers subjected to surveillance

Container	Pre-packaging Sample Moisture (mass percent)		First Surveillance Moisture (mass percent)		Second Surveillance Moisture (mass percent)	
	TGA loss to 1,000°C	TGA loss to 650°C, except as noted	TGA-MS H_2O	TGA loss to 650°C	TGA-MS H_2O	TGA loss to 650°C
07-5	0.31[a]	0.36[b]	0.19	0.123	0.53	0.465
07-6	0.23[a]	0.28[b]	0.14	0.114	0.22	0.189
08-3	0.15	0.00[b]	0.04	0.039	0.03	0.037
08-4	0.39	0.00[b]	0.04	0.203	0.06	0.237
08-5	0.16	0.00[b]	0.14	0.072	0.20	0.078
08-6	0.07	0.01[b]	0.10	0.056	0.14	0.116
08-7	0.37	0.08	0.03	0.084	0.03	0.091
08-8	0.19	0.12	0.10	0.166	0.10	0.190
08-9	0.42	0.03	0.07	0.204	0.07	0.209
08-12	0.22	0.14	0.18	0.179	0.19	0.162
08-13	0.29	0.15	0.29	0.302	0.33	0.410
08-14	0.37	0.27	0.33	0.369	0.37	0.412
08-15	0.35	0.10	0.19	0.324	0.35	0.464
08-16	0.26	0.04	0.03	0.045	0.03	0.038
08-17	0.07	0.01	0.07	0.082	0.10	0.121
09-1	0.23	0.07	0.03	0.046	0.04	0.043
09-2	0.40	0.21	0.26	0.425	0.28	0.322
09-3	0.32	0.24	0.22	0.322	0.24	0.289
09-4	0.06	0.01	0.02	0.022	0.02	0.026
09-6	0.39	0.29	0.26	0.391	0.38	0.438
09-7	0.39	0.25	0.25	0.225	0.25	0.276
09-8	0.23	0.18	0.22	0.141	0.16	0.133
09-9	1.06	0.29[b]	0.02	0.014	0.04	0.022
09-10	0.24	0.02	0.03	0.059	0.02	0.055
09-11	0.22	0.16	0.19	0.249	0.21	0.277
09-12	0.38	0.29	0.28	0.375	0.36	0.481
09-13	0.23	0.03	0.03	0.032	0.03	0.032
09-14	0.06	0.05	0.05	0.070	0.06	0.082

[a] These TGA mass loss values are artificially low due to artifacts in the data.
[b] Value determined by integration of FTIR H_2O signal.

dramatic for material packaged in the dry-atmosphere glovebox lines at Hanford and Rocky Flats, where it would be surprising to find significant true moisture content on the material. But there is a significant shift of the distribution to lower moisture even for material packaged in the relatively humid glovebox line at Hanford. Using these results should allow better prediction of moisture-dependent material behavior in storage, such as the rate and ultimate amount of H_2 gas generation and the potential for corrosion.

Conclusions

Measurement of the moisture content of material stored in 3013 containers prior to packaging is mandated in order to constrain the total possible H_2 gas generation after long periods in storage. The approved moisture measuring protocols were chosen to be simple to interpret and inherently conservative, i.e., biased toward reporting higher than actual moisture content. It was deemed an acceptable accuracy would be somewhat compromised as a result of these choices. The results presented in this paper serve to confirm the conservative nature of the pre-packaging measurements

and to broadly quantify the errors introduced by those measurement choices. They also support the use of proposed alternate methods of re-evaluating the pre-packaging data to improve the accuracy of moisture estimates for containers that remain in storage. The re-evaluated results will no longer be conservative upper limits, but would be more useful for assessing relative risk for both H_2 generation and internal corrosion tendencies.

John M. Berg is a staff scientist at Los Alamos National Laboratory. He has a Ph.D. in chemistry from Princeton University and a B.A. in chemistry from St. John's University.

Mark L. Crowder is a principal engineer at Savannah River National Laboratory. He has a Ph.D. and an M.S. degree in chemical engineering from Clemson University and a B.S. chemical engineering from Rose-Hulman Institute of Technology.

Philip M. Almond is a senior scientist at Savannah River National Laboratory. He has a B.S. and Ph.D. in chemistry from Auburn University.

Acknowledgements

The authors would like to thank Mark Brugh and Yvonne Mazza of the former Rocky Flats Site, and Ted Venetz and G. Scott Barney of the Hanford Site for accessing the original pre-packaging data and for extensive discussions, and James Laurinat of Savannah River National Laboratory for computational assistance with surveillance measurements. Funding for this work was provided by the Surveillance and Monitoring Program, U.S. Department of Energy Office of Environmental Management. This work was conducted at Savannah River National Laboratory operated by Savannah River Nuclear Solutions for U.S. Department of Energy under contract DE-AC09-08SR22470 and at Los Alamos National Laboratory operated by Los Alamos National Security, LLC under contract DE-AC52-06NA25396.

References

1. *Stabilization, Packaging, and Storage of Plutonium-bearing Materials.* 2004. DOE-STD-3013-2004. U.S. Department of Energy: Washington, D.C.
2. Duffey, J. M., D. K. Veirs, R. R. Livingston, and J. M. Berg. 2010. Pressure Development in Sealed Packages Containing Plutonium-Bearing Materials. *Journal of Nuclear Materials Management* Vol. 37, No. 3.
3. Morales, L., U. Gallegos, L. Bustos, S. Lemarchand, E. Post, A. Schranner, K. Imrich, A. Jurgensen, Y. Mazza, M. Brugh, and S. Barney. 2002. *Certification of Thermal Gravimetric Analysis with Moisture Detection Systems for Water Determinations on 3013 Materials;* LA-UR-02-2233. Los Alamos National Laboratory.
4. Bevington, P. R., and D. K. Robinson. 1992. *Data Reduction and Error Analysis for the Physical Sciences.* 2nd ed. Boston, MA: McGraw-Hill.
5. Berg, J. M. 2005. *Re-Analysis of RFETS PuSPS TGA-FTIR Moisture Measurement Data.* LA-UR-05-7395. Los Alamos National Laboratory, Los Alamos, N.M.

International Safeguards in Nuclear Weapon States and a Look at the Future

Caroline Jorant
AREVA, Paris, France

Abstract

This paper shall reveiw the framework for applying international safeguards in the five nuclear weapon states and give an overview of their implementation.

It, shall then discuss some reasons for an evolution of those states and the International Atomic Energy Agency's (IAEA) commitments to apply its safeguards and suggest some ideas for the heightened but efficient involvement of the IAEA in those states fully taking into account the specificities of those states within the State-level Approach.

Introduction

International safeguards on nuclear materials were initially devised within the scope of the statute of the International Atomic Energy Agency (IAEA) in 1956 and under the Treaty Establishing the European Atomic Energy Community (Euratom Treaty) signed in 1957, that is with the early development of the civil application of nuclear energy. However, today general implementation of IAEA safeguards derives mainly from commitments required under the Treaty on the Nonproliferation of Nuclear Weapons (NPT). Under NPT Article 3, all Non-Nuclear Weapon States (NNWS) are obliged to accept safeguards on all nuclear materials for all nuclear activities on their territory. An often made criticism of the non-proliferation regime relates to discrimination regarding the absence of "guarantees" on the civil uses of facilities and materials in Nuclear-Weapon States (NWS). Is this criticism still valid or exaggerated? Does it hold for all weapon states countries? What are the obligations of nuclear-weapon states, and what is their situation with regards to the implementation of safeguards? How might or should this situation evolve in the future? These are the questions to be tackled hereunder.

Same Status, Different Obligations and Situations with Regard to International Safeguards

Same Status

The well-known and often criticized Nonproliferation Treaty (NPT) is based on a differentiation of status between nuclear-weapon states and non-nuclear-weapon states.

Without going into the historical details and context it can be said very pragmatically that the NPT fathers tried to achieve a universal treaty that was as attractive and balanced as possible to ensure its success. They took into account the situation of states in relation to the possession of nuclear weapons at the time of signature and considered separately the rights and duties of the five nuclear-weapon states (the United States, today's Russia that inherited the status of the USSR, China, the United Kingdom, and France).

These five states are party to the NPT although they did not all adhere at the outset. The U.S., Russia, and the UK signed in July 1968 and ratified in 1970 (the United States, Russia) and in November 1968 (the UK), while France and China only signed the NPT in 1992 and ratified it the same year.

Under the NPT there is no safeguards obligation imposed on weapon states and none of them had to enter into a safeguards agreement because of their mere adhesion to the NPT. In this respect it is interesting to note that the United States signed its first safeguards agreement as early as 1962 to allow the IAEA to test its safeguards tools and schemes on three research reactors and on one power reactor.[1] This agreement was superseded by another agreement in 1964 which was replaced by today's Voluntary Offer Agreement (VOA) that entered into force in 1980. It is also interesting to note that both Chinese and French safeguards agreements signed respectively in 1988 and in 1978 well preceded the adhesion of both countries to the NPT (in 1992). The UK signed such a VOA in 1973, while Russia entered into such an agreement only in 1985.

The five NWS are all members of the Nuclear Suppliers Group (NSG), with China being the last to join in 2005. This group adopted what are known as the "NSG guidelines," which describe the conditions the supplier countries agree to impose on recipient countries when exporting specifically listed nuclear material and items.

Under the NSG guidelines, no specific safeguards obligations are foreseen for supplying nuclear goods, services or technology to nuclear-weapon states.

The IAEA statute that came into force as early as 1957 also preceded any definition of nuclear-weapon states as opposed to non-nuclear-weapon states and does not impose any specific safeguards obligations on any states but foresees the means of implementing safeguards if so requested by a member state.

To summarize, the status of weapon states stems from the NPT and is reflected in the NSG, while no mention was made for obvious reasons in the IAEA statute before the NPT came

into force but no later amendments to the statute introduced any distinction between NNWS and NWS.

Different Commitments

Aside from general political goodwill, or the desire to set an example, NWS have accepted international safeguards on different grounds. In this respect two situations should be distinguished and clarified if one wants to understand the reality of the implementation of international safeguards in NWS.

Bilateral Commitments on Nuclear Material and Facilities

Safeguards on Nuclear Materials

Major uranium suppliers, such as Australia and Canada, which together represent two-thirds of the world's uranium supply have adopted as a national policy to subject exports of materials extracted from their mines to conditions and commitments described in intergovernmental agreements.

In this respect, both countries demand that material be subject to IAEA safeguards, regardless of whether the material comes from NWS or not.

For instance, Australia[2] has signed a bilateral agreement with the United States (1981) and with France (1981) including a peaceful use provision that is to be *verified* through the implementation of the United States/IAEA and the France/Euratom/IAEA safeguards agreements.

In 1990, Australia signed a limited scope agreement with Russia to allow front end processing (conversion, enrichment, and fabrication) for the benefit of third country customers, and to require that any remaining material be under the IAEA/Russia agreement. Since then, in 2007, they signed a regular agreement allowing the use of Australian origin material in facilities included in the Eligible Facilities List and to be agreed upon between both States. Such materials are subject to IAEA safeguards under the Russian/IAEA agreement. However this agreement is pending ratification and currently Russia cannot use Australian origin nuclear materials in its power plants.

An Australia/China agreement of the same type as the 2007 agreement with Russia is already in force and allows the transfer of Australian material into mutually determined facilities and provided the acceptance of IAEA safeguards on the material.

The same policy is being implemented by the United States that requires an IAEA safeguards commitment applied through the VOA of other weapon states. This commitment applies to any uranium mined in the United States as well as to any material processed or merely used for fabrication purposes on United States territory and then exported. Since the United States has agreements with all other weapon states but not with Russia, material of United States origin cannot today be transferred to Russia. However, an agreement that had been negotiated under the Bush administration was frozen in September 2008 as a consequence of the Russia/Georgia conflict.

This draft agreement called for IAEA safeguards on the material delivered pursuant to the VOA without imposing any restrictions as to the facilities of destination.

Apart from uranium supplier countries, customer states may be viewed as another category of suppliers of nuclear material imposing for instance to have their fuel under IAEA safeguards while being processed in NWS.

This is the case with Japanese or Swiss fuel reprocessed in the UK or France, under specific bilateral agreements.

This situation often results in multi-layers of bilateral commitments on the same material. For example if Australian-mined uranium, enriched and used to fabricate fuel in the United States, is then used in a Japanese reactor and sent to La Hague to be reprocessed, it will result in being subject to France/Australia, Euratom/Australia, U.S./Euratom, France/Japan, and now also Euratom/Japan agreements that all require this material to be subject to IAEA safeguards in France.

These few examples illustrate the fact that because of bilateral commitments, NWS have indeed accepted to submit nuclear materials to IAEA safeguards under specific agreements with NNWS suppliers but also with NWS supplier states (as with the United States). However there are some differences and some agreements may be more limited in scope.

Because of the subject of this paper, we will not provide a full description of the different types of bilateral agreements but it is worth having in mind that some agreements do take full account of the NWS status and, while requiring a peaceful use commitment, do not call for any verification mechanisms.

Safeguards Applied to Technology Transfers

Under the NPT or the NSG, no specific safeguards obligation is to be imposed on NWS in relation to a technology transfer. However, it is to be noted that, because this was a requirement of the technology transferor, there are some examples of NWS having accepted to submit facilities built upon foreign technology to IAEA safeguards. Sometimes, going beyond the mere commitment to add facilities to the list of their VOA, they are also committed to actively seeking to have the IAEA select their facility. This kind of situation arose in relation to enrichment, which are "sensitive technology" facilities.

The first case involves two NWS, Russia and China in relation to the Shaanxi enrichment plant.

A second case involves two NNWS (Germany and the Netherlands) and a NWS (UK) as the supplier countries and a NWS (France) as the recipient. Resulting from those three Euratom states requirement, France has actively pleaded for the designation by IAEA of its new Georges Besse 2 centrifuge enrichment plant at Tricastin.

As a result, Georges Besse 2 was designated by the IAEA in September 2009 for the implementation of its safeguards activities.

A third example will concern in the future enrichment plants under construction or to be built in the United States on the former URENCO and now ETC centrifuge technology. A re-

quirement to submit these future facilities to IAEA safeguards is contained in the so-called "Washington Treaty" between the UK, Germany, the Netherlands and the U.S. and shall be reproduced in the agreement to be negotiated between those countries plus France.

Multilateral Commitments

The two European NWS, historically France and the UK, belong to the European Atomic Energy Community through a treaty that entered into force in 1958. The commonly called "Euratom Treaty" is legally binding upon its members and enforced through a number of secondary legally binding texts, called Directives and Regulations. While Directives set the objectives to be attained by all members states on different matters—leaving to each member state the choice of the tools to achieve the goal—European regulations are of direct application.

Chapter seven of the Euratom Treaty is titled *"Contrôle de sécurité"* or "Safeguards" and provides for the verification by Euratom and its inspectors, of the appropriate use and location of all nuclear materials that are declared to be devoted to "peaceful uses." In addition the Euratom controls are to check that obligations subscribed under the supply agreement between Euratom and a supplier state are respected. Since Euratom has entered into bilateral supply agreements, it has agreed for instance to have Canadian, Australian, and U.S. origin material subjected to IAEA safeguards, irrespective of the European country where the material is to be transferred, be it a NNWS or one of the two European nuclear weapon states.

Hence, according to the Euratom Treaty and the safeguards regulation, which has been revised in 2005, all peaceful nuclear activities are under strict Euratom control in all civil facilities on EU territory.

The implementation of Euratom safeguards has developed and evolved in parallel with the IAEA safeguards, using the same basic principles, methods, and equipments.

Altogether in the UK and France the inspection effort of Euratom was greater than in all NNWS of the EU.

Safeguards Implementation

The implementation of safeguards in the NWS is very different in scope and application, with the two European states being *de facto* under international safeguards for all their civil activities while no IAEA routine inspections are being implemented in Russia, as of now.

Voluntary Offers Agreements

Excluded from general safeguards requirements stemming from their NPT membership, the five NWS countries have concluded what are known as Voluntary Offer Agreements with IAEA.

The United States signed its first safeguards agreement in 1962 that was replaced by INFCIRC 57 in 1964 and then by the VOA signed in November 1977, entered into force in December 1980, and published as INFCIRC 288.

The first UK safeguards agreement signed in 1973 was replaced by the trilateral agreement, including Euratom when the UK joined the EU. Signed in 1976 this agreement was published as INFCIRC 263 and entered into force in August 1978.

The other trilateral agreement involving the IAEA, France and Euratom was signed in July 1978 and entered into force in September 1981 (INFCIRC 290).

Russia (at that time the USSR) did not rely on any imports of nuclear material for a long period of time and only signed its VOA in February 1985. This agreement entered into force in June of the same year (INFCIRC 327).

Lastly, China's VOA was signed in September 1988 and entered into force in September 1989 (INFCIRC 369).

All five NWS have also concluded Additional Protocols that are by nature different from those of NNWS, but whereby NWS accept to give additional information and access to the IAEA.

These VOAs are based on a **similar structure and principles but are different in their implementation.**

Basically, the VOAs reflect the INFCIRC 153 model. A first part describes the scope and recalls the general approach and main principles, while the second part describes in some detail the procedures to be followed. In addition "subsidiary arrangements" (that are not published) go into more implementation details, rights and duties. By contrast with the NNWS, the VOAs apply to a list of facilities proposed solely by NWS, and that can be changed as they wish, of course in relation with its other bilateral commitments as seen above.

Likewise, once the IAEA receives the list of "eligible facilities" that are offered to be safeguarded, it is the IAEA's responsibility to select such and such facility (or none). No bilateral agreement involving a NWS may be binding on the IAEA to effectively implement verification activities in such or such facility.

The same language about the procedures to be followed by the IAEA is used in Russian and U.S. VOAs. It is indicated that those procedures should be the same as those applied to similar material and similar facilities in NNWS. If the term procedure is to be understood as including quantity and timeliness goals, this could seem to somehow restrict the possibility for the IAEA to adopt a state-level approach for those two states. By contrast, in the Chinese and in both European NWS trilateral agreements, there are no such provisions and the IAEA should in principle have more flexibility in the way it may implement its safeguards. However this legal nuance has had no real impact up to now.

Independent from the selection of specific facilities, the VOAs provide for the transmission of accountancy information on materials subject to IAEA safeguards.

In the case of France and UK this information encompasses both the global inventory of materials to be subjected to IAEA safeguards and, transferred by Euratom, very detailed accountancy reports of materials in some facilities (today fifteen in France).

The facilities under IAEA inspection as published on the IAEA Web site are:

China — Qin Shan (power plant), Nankou HTGR (research), and Shaanxi (enrichment);

UK — Urenco Capenhurst (enrichment), Sellafield, Thorp (storage facilities);

United States — (Savannah River, Hanford, Oak Ridge (plutonium storage offered as excess weapons materials facilities), BWXT, (Lynchburg down blending HEU facility); and

France — UP2, UP3, La Hague (Plutonium storage).

NB: although not in this list, the French Melox fabrication plant is also subject to inspections in relation to the export of MOX fuels to NNWS, and now the French Georges Besse 2 enrichment plant should also be listed.

Russia is not mentioned since no Russian facility has been selected by the IAEA for its regular inspection activities.

Practical Implementation

As far as the implementation of safeguards in the selected facilities is concerned, the same principles, tools and methods as in NNWS are used.

The basic dogma is that the IAEA must draw independent safeguards conclusions and it makes use of the usual array of measures, although making some use of other existing information and to some extent, of Euratom safeguards. These measures include the verification and regular reverification of the design information of the facilities, confinement and surveillance systems by means of cameras, detectors and seals, sampling and analysis of material, some environmental sampling, and physical inventories. All these measures are being based on a stringent accountancy control.

In some states like France the accountancy related to the materials in the list of all eligible facilities is transferred, while in the United States, for instance, the accountancy reports are transmitted only in relation with materials in facilities designated for IAEA inspections.

Evolution of Safeguards in NWS, in the Twenty-first Century

The nuclear safeguards system has evolved in the past to respond to the evolution of technology but also to respond to the need for a global nonproliferation regime that reacted and still has to adapt to new challenges and critical situations. In this broader context, some reflections and proposals are described hereunder to promote a more balanced but pragmatic approach to implementing international safeguards in NWS in the twenty-first century.

Safeguarding Civil Sensitive Facilities (Enrichment and Reprocessing)

The IAEA should not refuse to apply an effective and efficient system to the sensitive facilities that would be offered to safeguards in NWS.

A series of meetings launched in 2004 under the leadership of the former IAEA Deputy Director General Bruno Pellaud was devoted to international approaches to the nuclear fuel cycle, which resulted in a document reflecting the views of the IAEA in favor of multi-national approaches to the nuclear fuel cycle, often referred to as MNA. A parallel reflection was led by the United States and resulted in 2006 in the Global Nuclear Energy Partnership (GNEP) initiative that was launched under the Bush administration.

Whatever the fate of these proposals or names, what is important is the gradual and currently rather large consensus about the fact that it makes sense from a non-proliferation point of view, to try and limit worldwide, on a voluntary basis, the number of fuel cycle sensitive facilities such as enrichment and reprocessing facilities.

Without entering into too long a debate, and although such existing facilities can be properly safeguarded on a technical ground, the fewer the number of new countries developing such facilities, the lower the risk one takes that such countries might break away from all their non-proliferation commitments. In addition, avoiding the deployment of too many such facilities in new NNWS would allow for a better allocation of scarce IAEA resources.

This limitation principle can only be adopted by countries developing nuclear energy together with very strong commitments from the supplier states as to the assurance of supply. In addition, it would be legitimate for those countries to rely on an international verification mechanism ensuring that their materials are not contributing to the possible increase of weapons in such NWS (vertical proliferation).

Hence, as a complement to its MNA proposal, the IAEA should be tasked to permanently implement safeguards in sensitive civilian facilities operating in NWS but with the participation of or for the benefit (service) of NNWS.

How Would This be Handled?

Legally, since the VOAs allow the NWS the possibility of adding or withdrawing any facility from the list of facilities offered to safeguards, it is likely that either an amendment to the safeguards agreement or a complementary offer agreement to put such facilities **permanently** under IAEA safeguards would be needed.

For legitimate budgetary reasons and given the prospects of a nuclear expansion worldwide, the IAEA is currently reluctant to select for inspection, any new facility in the NWS. The selection of the new French enrichment plant (George Besse 2 plant) required a long discussion process. Such a long process is prejudicial to the overall efficiency of the safeguards scheme. This situation should not be duplicated in the future. **The IAEA should have no choice but to select such a sensitive facility.**

This could be reflected in the aforementioned complementary agreement or protocol. Alternately, a generic resolution of the

Board of Governors applying to multinational fuel cycle facilities should impose IAEA's conduct.

Who Would Pay?

The IAEA regular budget should be increased to take into account such new tasks.

It would be completely abnormal, or discriminatory if only NWS and, or even worse, the nuclear industry in NWS were to bear the cost of IAEA safeguards efforts. Indeed this scheme would be of benefit to all, avoiding spending even more resources to safeguard new facilities in new countries. In addition it would echo many countries' call for a "non-discriminatory" regime.

Differentiation is Not Discrimination

A specific state-level approach should be developed to apply IAEA safeguards in NWS. This would pave the way for a verifiable cut-off treaty that is regularly debated before NPT review conferences. This of course should equally apply to any such sensitive facility in non-NPT states.

In relation to the above proposal, but also integrating the evolution of the safeguards approach to NNWS, a specific state approach regarding NWS should be devised.

In short, the idea here would be to recognize that there would be no purpose for NWS that are allowed to produce nuclear material for their military program, to try to divert small or large quantities of materials that would not be equivalent in quality to what they have been using to build up their arsenals and stocks of materials.

Although it might be of interest for a NNWS to try to proliferate nuclear explosive devices with relatively limited impact and no reliability, the diversion of certain materials usable for "weapon or explosive devices" as opposed to direct weapon use material would be objectively of low gain and would constitute a high-risk strategy for the NWS. Ultimately, it would be of a negligible practical significance. Hence the objective of safeguarding the sensitive facilities in NWS would be to verify that the facilities as such are not used to produce direct weapon use material. This would mean in practice that the objective of the verification for an enrichment plant would be to confirm that there is no enrichment of Uranium above a 20 percent U235 level. As far as reprocessing is concerned, the objective should be to verify that only high burn-up fuel is being processed in the plant. Indeed, plutonium contained in high burn-up fuels is unfit to contribute to a vertical proliferation effort that is, to be used to increase the number of nuclear weapons comparable to those weapons held by NWS.

However, this would not prevent the integration of measurement devices or a close follow-up of the material in case a low burn-up fuel would have to be processed.

In other words this path would mean taking into consideration attractiveness criteria, adapted to NWS, in the proliferation scenario. Making full use of the state-level approach applied to NWS could be adopted smoothly avoiding changing some wordings in the current VOAs. (E.g., Article 3c of INCIRC 288).

Making Full Use of Euratom Safeguards

This point is of a more general nature but is worth discussing in the context of this paper since two out of the five NWS are concerned. This may have an important and positive impact on the issue of resources.

As mentioned earlier, both the IAEA and Euratom consider that they have to draw their "independent safeguards conclusions."

Fortunately there is some cooperation between both organisms when they both carry out inspection activities at a site but a more integrated approach could be devised. For instance, were the proposals above to be adopted as confidence building measures, the safeguards activities led by Euratom could be verified and quality controlled by the agency, and serve as part of the IAEA safeguards activities in NWS. Since Euratom carries out its safeguards activities in all civil facilities of both European NWS, with similar tools and approaches as the IAEA does, the IAEA could reduce its efforts and costs, by checking Euratom's activities and even devising the safeguards plan with Euratom, while preserving its legal rights to intervene without prior notification (short notice or unannounced inspections) in any facility on the list of "eligible facilities."

Conclusion

As in all other industrial sectors, nuclear energy has developed thanks to an increased interdependency between the different nations of the world. The nonproliferation regime and safeguards systems have undergone profound adaptations. Nuclear weapon states have progressively accepted from their suppliers or from their customers, and have imposed even on their peers, not only peaceful-use commitments but also safeguards obligations. Today in the perspective of a further expansion of nuclear energy, there is a broad consensus on the benefit on nonproliferation grounds, of a limitation of the number of countries with sensitive nuclear facilities. The acceptance of this approach will be facilitated if NWS that host most of these facilities would accept international safeguards and if the IAEA would indeed perform its activities in such facilities that should be subject to safeguards in perpetuity. This move will entail additional costs to the agency and to the IAEA community but those costs could be reduced through a better definition of the scope of the safeguards, applying a state-level approach, and thanks to a less dogmatic approach towards regional, and in particular Euratom safeguards.

Revisiting the issue of safeguards in NWS in a pragmatic spirit, appears to be very timely as part of a new reflection on the role of the IAEA, and not only in the context of a recommended globalization of the nuclear industry but also in the perspective of the political discussions over a Fissile Material Production Cut-off Treaty and of the next NPT Review Conference.

References

1. Sanborn, J., 2007. D. Lockwood, L. Hilliard, B. Moran, S. Pepper, J. W. Tape. The Evolution of IAEA Safeguards: U.S. Perspectives. *Journal of Nuclear Materials Management* Vol. 35, No. 4.
2. Carlson, J. F. M. Last, and J. S. Smith. 2006. The Role of Bilateral Nuclear Safeguards Agreements, *Trust and Verify*, VERTIC's Journal, Issue 122.

Author Submission Guidelines

The Journal of Nuclear Materials Management is the official journal of the Institute of Nuclear Materials Management. It is a peer-reviewed, multidisciplinary journal that publishes articles on new developments, innovations, and trends in safeguards and management of nuclear materials. Specific areas of interest include international safeguards, materials control and accountability, nonproliferation and arms control, packaging and transportation, physical protection, and waste management JNMM also publishes book reviews, letters to the editor, and editorials.

Submission of Manuscripts: JNMM reviews papers for publication with the understanding that the work was not previously published and is not being reviewed for publication elsewhere. Papers may be of any length. All papers must include an abstract.

The Journal of Nuclear Materials Management is an English-language publication. We encourage all authors to have their papers reviewed by editors or professional translators for proper English usage prior to submission.

Papers should be submitted as Word or ASCII text files only. Graphic elements must be sent in TIFF, JPEG or GIF formats as separate electronic files and must be readable in black and white.

Submissions may be made via e-mail to Managing Editor Patricia Sullivan at psullivan@inmm.org. Submissions may also be made via by regular mail. Include one hardcopy and a CD with all files. These submissions should be directed to:

Patricia Sullivan
Managing Editor
Journal of Nuclear Materials Management
111 Deer Lake Road, Suite 100
Deerfield, IL 60015 USA

Papers are acknowledged upon receipt and are submitted promptly for review and evaluation. Generally, the author(s) is notified within ninety days of submission of the original paper whether the paper is accepted, rejected, or subject to revision.

Format: All papers must include:

- Author(s)' complete name, telephone and fax numbers, and e-mail address
- Name and address of the organization where the work was performed
- Abstract
- Camera-ready tables, figures, and photographs in TIFF, JPEG, or GIF formats. Black and white only.
- Numbered references in the following format:
  1. Jones, F.T. and L. K. Chang. 1980. Article Title. Journal 47(No. 2): 112–118. 2. Jones, F.T. 1976. Title of Book, New York: McMillan Publishing.
- Author(s) biography

Peer Review: Each paper is reviewed by at least one associate editor and by two or more reviewers. Papers are evaluated according to their relevance and significance to nuclear materials safeguards, degree to which they advance knowledge, quality of presentation, soundness of methodology, and appropriateness of conclusions.

Author Review: Accepted manuscripts become the permanent property of INMM and may not be published elsewhere without permission from the managing editor. Authors are responsible for all statements made in their work.

Reprints: Reprints may be ordered at the request and expense of the author. Contact Patricia Sullivan at psullivan@inmm.org or +1-847-480-9573 to request a reprint.

April 11–16, 2010
Northwest International Conference on Global Nuclear Security: The Decade Ahead
Portland, OR USA
Sponsors: Pacific Northwest Chapter of INMM and Eastern Washington Section of ANS
Contact: Carrie Mathews
Pacific Northwest National Laboratory
+1-509-375-6783
E-mail: carrie.mathews@pnl.gov
Web site: http://pnwcgs.pnl.gov/PNIC/PNIC.stm

June 6–11, 2010
INMM International Workshop on Containment & Surveillance: Concepts for the 21st Century
Oak Ridge National Laboratory
Oak Ridge, Tennessee USA
Contact: Peggy York, yorkpj@ornl.gov
Sponsored by: The NNSA Office of Nonproliferation Research & Development

July 11–15, 2010
51st INMM Annual Meeting
Marriott Waterfront Baltimore Hotel
Baltimore, MD USA
Sponsor: Institute of Nuclear Materials Management
Contact: INMM
+1-847-480-9573
Fax: +1-847-480-9282
E-mail: inmm@inmm.org
Web Site: http://www.inmm.org/meetings

October 3–8, 2010
PATRAM 2010
16th International Symposium on the Packaging and Transport of Radioactive Materials
IMO Headquarters
London, UK
Hosted by: Department for Transport of the United Kingdom, in cooperation with the International Atomic Energy Agency, the International Maritime Organization and the World Nuclear Transport Institute
E-mail: admin@patram2010.org
Web site: http://www.patram2010.org

INMM Membership Application

MEMBERSHIP

All information should be printed or typewritten.

Name _____ Date _____

Employer _____ Title _____

Address

Address _____

City _____ State/Province _____ Country _____ Zip _____

Telephone _____ Fax_____ E-mail _____

If you would like your INMM mail sent to an alternative address, please indicate preferred mailing address:

Address _____

City _____ State/Province _____ Country _____ Zip _____

Occupation

❑ Commercial Utility ❑ Government Contractor ❑ Nuclear Material Processing
❑ Equipment Manufacturer ❑ Government or International Agency ❑ Research or Consulting
❑ Other (describe): _____

Field(s)/Subject(s) of expertise _____

Total number of years work experience in nuclear materials management field(s) _____

Education (If you are applying for a student membership, indicate the year that you anticipate receiving your degree)

College/University Major/Degree Year Degree Obtained/Expected

1. _____

2. _____

3. _____

If you are applying for a student membership, provide contact information for a faculty advisor to verify your full-time status:

Name _____ Telephone _____ E-mail _____

Membership Type Desired

❑ Student $20
❑ Regular $50

Sustaining:
❑ 0 – 19 employees $250
❑ 20 – 49 employees $500
❑ 50 or more employees $750

From the categories listed below, please indicate your top 3 areas of interest within INMM (1 being the greatest interest):

___ International Safeguards
___ Materials Control and Accountability
___ Nonproliferation & Arms Control
___ Packaging & Transportation
___ Physical Protection
___ Waste Management

Membership in Other Scientific and Technical Societies (Attach additional sheet if necessary)

Society Names and Membership Grades _____

Signature _____
PAID BY: ❑ Check ❑ MasterCard ❑ VISA ❑ American Express ❑ Diners Club

Card No. _____ Exp. Date _____

Complete the application (keep a copy for your records) and mail or fax it with membership dues to:

INSTITUTE OF NUCLEAR MATERIALS MANAGEMENT
111 Deer Lake Road, Suite 100 • Deerfield, Illinois 60015 USA
+1-847-480-9573, Fax: +1-847-480-9282
E-mail: inmm@inmm.org • Website: www.inmm.org

INMM
INSTITUTE OF NUCLEAR MATERIALS MANAGEMENT

SRNL
SAVANNAH RIVER NATIONAL LABORATORY
TM

We Put Science To Work™

...creating applied solutions in Security, Energy and Environmental Management

Nuclear materials management initiatives at the U.S. Department of Energy's Savannah River National Laboratory are focused on homeland and global security and legacy materials disposition.

SRNL provides applied science and technology critical to:

- **Nuclear Materials Package Development**
- **Nuclear Materials Transportation, Storage and Disposition**
- **Safeguards and Monitoring Technologies**

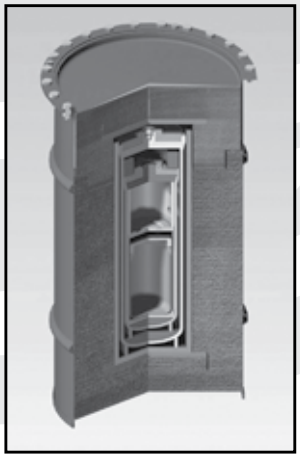

09T01494

Visit us on the web at http://srnl.doe.gov

The NEW ORTEC Micro-trans-SPEC: tailored to your application.

The Lightweight and Compact Solution for Heavyweight Spectroscopic Problems

- All-in-one ultra-light HPGe Spectrometer: No LN_2 required.
- High Sensitivity — 50 mm Ø x 30 mm HPGe detector.
- Tough — Enclosure, Display, and all connections sealed against moisture and dust. Water spray resistant.
- Amazingly light: 15 lb (6.8 kg).
- Digitally Stable electronics.
- High Visibility display.
- Removable data storage on SD card.
- Multiple choice of power sources.

Smart MCA Software — Onboard ROI-based Nuclide ID and activity calculation.

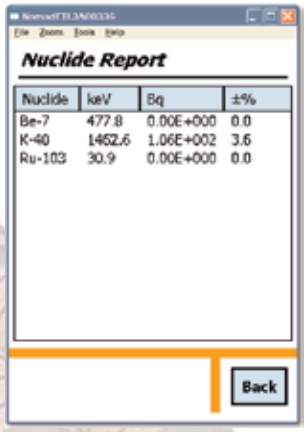

And NOW: available with Custom Software Applications

Application Example: Simpler UF6 Cylinder assays.

Enrichment Meter Application, Built IN.

No need for an associated computer.

The ORTEC Micro-trans-SPEC is a great NDA platform for HPGe applications. It is light, rugged, reliable, compact, and available now. Contact us with your application needs and we will work with you on implementation.

801 South Illinois Ave., Oak Ridge, TN 37831-0895 U.S.A. • (865) 482-4411 • Fax (865) 483-0396 • ortec.info@ametek.com
For International Office Locations, Visit Our Website

ORTEC® www.ortec-online.com AMETEK ADVANCED MEASUREMENT TECHNOLOGY